

AN INVESTIGATION OF THE  
USE OF DENDRIMER-BASED  
CARRIER TO CROSS CELLULAR  
BARRIERS

By  
HUEY MINN TEOW

A thesis submitted to the University of Central Lancashire in  
partial fulfilment of the requirements for the degree of  
Doctor of Philosophy

October 2010

## TABLE OF CONTENTS

---

---

<b>TABLE OF CONTENTS.....</b>	<b>2</b>
<b>LIST OF FIGURES .....</b>	<b>8</b>
<b>LIST OF TABLES .....</b>	<b>12</b>
<b>ABSTRACT .....</b>	<b>13</b>
<b>DECLARATION.....</b>	<b>16</b>
<b>COPYRIGHT STATEMENT.....</b>	<b>17</b>
<b>ACKNOWLEDGEMENTS.....</b>	<b>18</b>
<b>ABBREVIATIONS .....</b>	<b>19</b>
<b>CHAPTER 1: INTRODUCTION .....</b>	<b>21</b>
<b>1.1 DRUG DELIVERY ACROSS CELLULAR BARRIERS .....</b>	<b>22</b>
<b>1.2 MECHANISM OF INTESTINAL BARRIER ABSORPTION .....</b>	<b>23</b>
1.2.1 Transcellular pathway .....	25
1.2.1.1 Passive transcellular diffusion.....	25
1.2.1.2 Carrier-mediated transport .....	26
1.2.1.3 Endocytosis/ Vesicular transport.....	27
1.2.2 Paracellular pathway .....	27
<b>1.3 TRANSPORT ACROSS THE BLOOD-BRAIN BARRIER .....</b>	<b>28</b>
1.3.1 The blood-brain barrier .....	29
1.3.1.1 Tight junctions .....	32
1.3.2 Therapeutic pathways across the blood-brain barrier .....	34
1.3.2.1 Transcellular lipophilic pathway .....	35
1.3.2.2 Carrier-mediated transport .....	36
1.3.2.2.1 P-glycoprotein efflux transporter .....	37

1.3.2.2.2	Multidrug resistance-associated proteins .....	39
1.3.2.2.3	Breast cancer resistance protein .....	40
1.3.2.3	Receptor mediated transcytosis.....	41
1.3.2.3.1	Transferrin receptor.....	41
1.3.2.3.2	Insulin receptor.....	42
1.3.2.3.3	Lipoprotein receptor.....	43
1.3.2.4	Adsorptive-mediated transcytosis .....	44
1.3.3	Therapeutic delivery across cellular barriers .....	44
<b>1.4</b>	<b>DENDRIMERS.....</b>	<b>45</b>
1.4.1	Synthesis of dendrimers .....	46
1.4.1.1	Divergent synthesis .....	46
1.4.1.2	Convergent synthesis .....	47
1.4.2	Pharmaceutical applications of dendrimers .....	49
<b>1.5</b>	<b>POLYAMIDOAMINE (PAMAM) DENDRIMERS.....</b>	<b>49</b>
1.5.1	Synthesis of PAMAM dendrimers .....	49
1.5.2	Physicochemical properties of PAMAM dendrimers .....	50
1.5.3	PAMAM dendrimers as drug carriers.....	51
1.5.3.1	Drug encapsulation.....	52
1.5.3.2	PAMAM-drug conjugates.....	54
<b>1.6</b>	<b>CHARACTERISATION TECHNIQUES .....</b>	<b>58</b>
1.6.1	Thin layer chromatography (TLC).....	58
1.6.2	Nuclear magnetic resonance (NMR) spectroscopy.....	59
1.6.3	Mass spectrometry (MS).....	60
1.6.4	High performance liquid chromatography (HPLC).....	61
<b>1.7</b>	<b>CELL LINES AND CELL CULTURE .....</b>	<b>62</b>
1.7.1	Intestinal barriers <i>in vitro</i> cell model .....	62
1.7.2	Blood-brain barrier <i>in vitro</i> cell lines and cell culture models.....	62
1.7.2.1	Immortalised brain endothelial cell lines.....	63
1.7.2.2	Primary brain endothelial cultures .....	63
1.7.2.2.1	Porcine Brain Endothelial Cells (PBECS).....	64
<b>1.8</b>	<b>AIMS AND OBJECTIVES .....</b>	<b>65</b>

**CHAPTER 2: SYNTHESIS AND CHARACTERISATION OF G3 PAMAM DENDRIMER AND DRUG CONJUGATES..... 66**

<b>2.1</b>	<b>INTRODUCTION .....</b>	<b>67</b>
<b>2.2</b>	<b>MATERIALS AND METHODS .....</b>	<b>69</b>
2.2.1	Materials.....	69
2.2.2	Synthesis of lauryl-G3 PAMAM dendrimers .....	69
2.2.2.1	Synthesis of lauryl 4-nitrophenyl carbonate .....	70
2.2.2.2	Synthesis of G3L3, G3L6 and G3L9 conjugates .....	71
2.2.3	Synthesis of G3-glutarate-paclitaxel/lauryl-G3-glutarate-paclitaxel conjugates.....	73
2.2.3.1	Synthesis of 2'-glutaryl-paclitaxel .....	73
2.2.3.2	Synthesis of pac-glu-NHS ester .....	76
2.2.3.3	Synthesis of G3-glu-pac/ lauryl-G3-glu-pac .....	78
2.2.4	Synthesis of FITC-labelled G3 PAMAM dendrimer and conjugates .....	80
2.2.5	Chemical stability of G3 PAMAM dendrimer conjugates.....	82
2.2.6	Statistical analysis of data .....	82
<b>2.3</b>	<b>RESULTS AND DISCUSSION .....</b>	<b>83</b>
2.3.1	Synthesis and characterisation of lauryl-G3 PAMAM dendrimer conjugates.....	83
2.3.1.1	Synthesis of lauryl 4-nitrophenyl carbonate .....	83
2.3.1.2	Conjugation of lauryl alcohol with G3 PAMAM dendrimers .....	84
2.3.2	Synthesis and characterisation of G3-glu-pac/lauryl-G3-glu-pac conjugates.....	88
2.3.2.1	Conjugation of linker (glutaric anhydride) to paclitaxel.....	88
2.3.2.2	Synthesis of pac-glu-NHS active ester.....	94
2.3.2.3	Conjugation of pac-glu to G3/ lauryl-G3 PAMAM dendrimers.....	96
2.3.3	Synthesis and characterisation of FITC-labelled G3 PAMAM dendrimer and conjugates .....	98
2.3.4	Chemical stability of G3 PAMAM dendrimer conjugates.....	103
<b>2.4</b>	<b>CONCLUSIONS .....</b>	<b>104</b>

**CHAPTER 3: BIOLOGICAL EVALUATION OF G3 PAMAM  
DENDRIMER AND DRUG CONJUGATES WITH CACO-2  
CELLS .....** **105**

<b>3.1</b>	<b>INTRODUCTION .....</b>	<b>106</b>
------------	---------------------------	------------

<b>3.2</b>	<b>MATERIALS AND METHODS .....</b>	<b>108</b>
3.2.1	Materials.....	108
3.2.2	Caco-2 cell culture techniques .....	108
3.2.2.1	Maintenance and optimisation of growth conditions.....	108
3.2.2.2	Reviving cell stocks .....	109
3.2.2.3	Passaging cells .....	109
3.2.2.4	Viable cell number counting by trypan blue assay .....	109
3.2.2.5	Cryopreserving cells .....	110
3.2.3	Measurement of <i>in vitro</i> cytotoxicity of G3 PAMAM dendrimers and paclitaxel conjugates using Caco-2 cells.....	110
3.2.3.1	Lactate dehydrogenase release assay .....	110
3.2.3.2	Optimal cell concentration determination.....	111
3.2.3.3	Cytotoxicity studies.....	112
3.2.4	Transepithelial transport studies across Caco-2 cell monolayers .....	113
3.2.4.1	Caco-2 cell monolayer integrity.....	113
3.2.4.2	Permeability studies .....	114
3.2.5	Statistical analysis of data .....	115
<b>3.3</b>	<b>RESULTS AND DISCUSSION.....</b>	<b>116</b>
3.3.1	Cytotoxicity studies of G3 PAMAM dendrimer and drug conjugates using Caco-2 cells .....	116
3.3.1.1	Optimal cell concentration determination using LDH assay .....	116
3.3.1.2	The effect of G3 PAMAM dendrimer and drug conjugates on Caco-2 cell viability .....	117
3.3.2	Permeability studies of G3 PAMAM and conjugates on Caco-2 cells .....	120
3.3.2.1	Permeation of G3 PAMAM dendrimer and drug conjugates across Caco-2 cell monolayers.....	120
3.3.2.2	The effect of G3 PAMAM dendrimer and drug conjugates on Caco-2 cell monolayers integrity .....	122
<b>3.4</b>	<b>CONCLUSIONS.....</b>	<b>125</b>
<b>CHAPTER 4: BIOLOGICAL EVALUATION OF G3 PAMAM DENDRIMER AND DRUG CONJUGATES WITH PORCINE BRAIN ENDOTHELIAL CELLS .....</b>		<b>126</b>

<b>4.1</b>	<b>INTRODUCTION .....</b>	<b>127</b>
<b>4.2</b>	<b>MATERIALS AND METHODS .....</b>	<b>129</b>
4.2.1	Materials.....	129
4.2.2	PBECs cell culture techniques .....	130
4.2.2.1	Preparation of lab-made rat tail collagen .....	130
4.2.2.2	Plating cell culture medium .....	131
4.2.2.3	Maintenance and optimisation of growth conditions.....	131
4.2.2.4	Thawing cells .....	131
4.2.2.5	Coating with rat tail collagen and fibronectin.....	132
4.2.2.6	Passaging cells .....	132
4.2.3	Examination of PBECs morphology.....	133
4.2.4	Measurement of <i>in vitro</i> cytotoxicity of G3 PAMAM dendrimer and paclitaxel conjugates using PBECs .....	133
4.2.4.1	Optimal cell concentration determination.....	133
4.2.4.2	Cytotoxicity studies.....	134
4.2.5	Transendothelial transport studies across PBEC monolayers.....	135
4.2.5.1	Passaging cells onto a Transwell® insert.....	135
4.2.5.2	Treatment with cAMP and RO-20-1724.....	135
4.2.5.3	Transendothelial electrical resistance (TEER) measurement with PBECs .....	136
4.2.5.4	Permeability studies .....	136
4.2.6	Statistical analysis of data .....	137
<b>4.3</b>	<b>RESULTS AND DISCUSSION .....</b>	<b>138</b>
4.3.1	Morphology of the PBEC monolayer .....	138
4.3.2	Effect of cell culture conditions on PBECs growth .....	138
4.3.2.1	Rat tail collagen and fibronectin .....	138
4.3.2.2	Growth medium .....	140
4.3.3	Cytotoxicity studies of G3 PAMAM dendrimer and drug conjugates on PBECs .....	142
4.3.3.1	Optimal cell concentration.....	142
4.3.3.2	The effect of G3 PAMAM and drug conjugates on PBECs viability .....	143
4.3.4	Permeability studies of G3 and drug conjugates on PBECs .....	146
4.3.4.1	TEER measurement of PBEC monolayers .....	146

4.3.4.2	Permeation of G3 PAMAM dendrimer and drug conjugates across PBEC monolayers .....	148
4.3.4.3	The effect of G3 PAMAM dendrimer and drug conjugates on PBEC monolayers integrity .....	151
<b>4.4</b>	<b>CONCLUSIONS .....</b>	<b>154</b>
<b>CHAPTER 5: CONCLUSIONS AND FUTURE WORK .....</b>		<b>155</b>
<b>5.1</b>	<b>CONCLUSIONS .....</b>	<b>156</b>
<b>5.2</b>	<b>FUTURE WORK .....</b>	<b>157</b>
<b>CHAPTER 6: APPENDICES .....</b>		<b>158</b>
<b>APPENDIX I: HPLC CHROMATOGRAMS OF PACLITAXEL, PAC-GLU, G3 PAMAM DENDRIMERS AND CONJUGATES .....</b>		<b>159</b>
<b>APPENDIX II: HPLC ASSAY CALIBRATION CURVES OF PACLITAXEL AND PAC-GLU .....</b>		<b>162</b>
<b>APPENDIX III: SPECTROFLUOROMETRIC ASSAY CALIBRATION CURVES OF FITC-LABELLED G3 PAMAM DENDRIMERS AND CONJUGATES .....</b>		<b>163</b>
<b>APPENDIX IV: PUBLICATIONS, CONFERENCE PRESENTATIONS AND AWARDS .....</b>		<b>166</b>
<b>CHAPTER 7: REFERENCES .....</b>		<b>167</b>

## LIST OF FIGURES

---

---

Figure 1-1: Structure of the cell membrane .....	24
Figure 1-2: Mechanism of intestinal absorption. (a) passive transcellular transport, (b) paracellular transport, (c) vesicular endocytosis/endocytosis, (d) carrier mediated transport, and (e) P-gp mediated efflux transport.....	24
Figure 1-3: Schematic diagram of a cerebral capillary .....	30
Figure 1-4: Cellular components of the blood-brain barrier .....	31
Figure 1-5: A schematic diagram of the tight junction and adherens junction of the blood-brain barrier .....	33
Figure 1-6: Transport mechanisms across the blood-brain barrier .....	35
Figure 1-7: Generic structure of a dendrimer molecule .....	46
Figure 1-8: Divergent and convergent syntheses of dendrimers.....	48
Figure 1-9: Synthesis of PAMAM dendrimers .....	50
Figure 1-10: A dimensionally scaled comparison of a series of PAMAM dendrimers (G4 – G7) with a variety of proteins, a typical lipid bilayer membrane and DNA, indicating the closely matched size and contours of important proteins and bioassemblies. ....	52
Figure 1-11: Schematic diagram of TLC and measurement of $R_f$ .....	59
Figure 1-12: A simplified schematic of a mass spectrometer.....	60
Figure 1-13: Schematic diagram of HPLC instrumentation .....	61
Figure 2-1: Schematic diagram showing the synthesis of lauryl 4-nitrophenyl carbonate. ....	70
Figure 2-2: Schematic diagram showing the conjugation of lauryl to G3 PAMAM dendrimer. ....	72
Figure 2-3: Schematic diagram showing the synthesis of 2'-glutaryl-paclitaxel.....	74
Figure 2-4: Schematic diagram showing the synthesis of pac-glu-NHS ester.....	77
Figure 2-5: Schematic diagram showing the synthesis of lauryl-G3-glu-pac.....	79
Figure 2-6: Schematic diagram showing the labelling of G3 PAMAM dendrimer with FITC.....	81
Figure 2-7: Chemical structure of lauryl 4-nitrophenyl carbonate.....	83
Figure 2-8: $^1\text{H}$ NMR spectrum of lauryl 4-nitrophenyl carbonate.....	84

Figure 2-9: Chemical structure of G3 PAMAM dendrimer.....	85
Figure 2-10: A branch of G3 PAMAM dendrimer with a lauryl chain attached via a carbamate bond.....	85
Figure 2-11: <sup>1</sup> H NMR spectrum of G3 PAMAM dendrimer.....	86
Figure 2-12: Schematic diagram of G3 PAMAM dendrimer with a lauryl chain attached.....	86
Figure 2-13: <sup>1</sup> H NMR spectra of lauryl-G3 dendrimer conjugates (a) G3L3 (b) G3L6 and (c) G3L9.....	87
Figure 2-14: Chemical structure of paclitaxel with numbered carbons.....	90
Figure 2-15: <sup>1</sup> H NMR spectrum of paclitaxel.....	90
Figure 2-16: <sup>13</sup> C NMR spectrum of paclitaxel.....	91
Figure 2-17: Chemical structure of 2'-glutaryl-paclitaxel with numbered carbons.....	91
Figure 2-18: <sup>1</sup> H NMR spectrum of 2'-glutaryl-paclitaxel.....	92
Figure 2-19: <sup>13</sup> C NMR spectrum of 2'-glutaryl-paclitaxel.....	92
Figure 2-20: Electrospray ionisation mass spectra (ESI-MS) of (a) paclitaxel, and (b) 2'-glutaryl-paclitaxel.....	93
Figure 2-21: Chemical structure of pac-glu-NHS ester with numbered carbons.....	94
Figure 2-22: <sup>1</sup> H NMR spectrum of pac-glu-NHS.....	95
Figure 2-23: <sup>13</sup> C NMR spectrum of pac-glu-NHS.....	95
Figure 2-24: Chemical structure of L-G3-glu-pac conjugate.....	96
Figure 2-25: <sup>1</sup> H NMR spectra of (a) G3-glu-pac, (b) L3-G3-glu-pac, and (c) L6-G3-glu-pac.....	97
Figure 2-26: <sup>1</sup> H NMR spectrum of FITC-G3 PAMAM dendrimer.....	99
Figure 2-27: Size distribution of (a) FITC-labelled G3, (b) FITC-labelled G3L3, and (c) FITC-labelled G3L6, (mean ± SD, n = 10 of triplicate experiments).....	101
Figure 2-28: Size distribution of (a) FITC-labelled G3-glu-pac, (b) FITC-labelled G3L3-glu-pac, and (c) FITC-labelled G3L6-glu-pac, (mean ± SD, n = 10 of triplicate experiments).....	102
Figure 3-1: Reaction scheme of LDH assay enzyme activity.....	111
Figure 3-2: A diagram of cell monolayer cultured on a Transwell® insert.....	113
Figure 3-3: The absorbance of Caco-2 cell seeding densities incubated with assay medium (low control) or Triton X-100 1% (high control) for optimal concentration determination, (mean ± SD, n = 3 of triplicate experiments).....	117

Figure 3-4: The cytotoxicity effect of G3 PAMAM dendrimer, free paclitaxel and conjugates on the Caco-2 cells (mean $\pm$ SD, n = 4 of triplicate experiments). * indicates a significant difference ( $p < 0.05$ ) from other conjugates.....	119
Figure 3-5: The A $\rightarrow$ B (■) and B $\rightarrow$ A (■) permeability of G3 PAMAM dendrimer, free paclitaxel and conjugates across the Caco-2 cell monolayers after 3 h incubation at 37°C (mean $\pm$ SD, n = 3 of triplicate experiments). * $p < 0.05$ .....	121
Figure 3-6: The effect of G3 PAMAM dendrimer, free paclitaxel and conjugates on the TEER of Caco-2 cell monolayers after (A) apical and (B) basolateral incubation at 37°C (mean $\pm$ SD, n = 3 of triplicate experiments).....	124
Figure 4-1: Phase contract microscopy of primary cultured PBECs on culture day 3 (a1 and a2) and day 7 (b1 and b2). Arrows indicating cells undergoing proliferation and differentiation (a1 and b1 original magnification 10x, a2 and b2 original magnification 40x).....	139
Figure 4-2: Phase contrast microscopy of primary cultured PBECs on culture day 3. Arrows indicating dead contaminant cells (original magnification 10x).....	141
Figure 4-3: Phase contrast microscopy of primary cultured PBECs on culture day 7 (original magnification 10x). .....	141
Figure 4-4: The absorbance of PBECs seeding densities incubated with assay medium (low control) or Triton X-100 1% (high control) for optimal concentration determination (mean $\pm$ SD, n = 3 of triplicate experiments).....	143
Figure 4-5: The cytotoxicity effect of G3 PAMAM dendrimer, free paclitaxel and conjugates on the PBECs (mean $\pm$ SD, n = 3 of triplicate experiments). * indicates a significant difference ( $p < 0.05$ ) from other conjugates.....	145
Figure 4-6: Transendothelial electrical resistance values of PBEC monolayers on various days in culture (mean $\pm$ SD, n = 3).....	148
Figure 4-7: The A $\rightarrow$ B (■) and B $\rightarrow$ A (■) permeability of G3 PAMAM dendrimer, free paclitaxel and conjugates across the PBEC monolayers after 3 h incubation at 37°C (mean $\pm$ SD, n = 3 of triplicate experiments). * indicates a significant difference ( $p < 0.05$ ) from other conjugates. ** indicates a significant difference ( $p < 0.05$ ) for B $\rightarrow$ A compared to A $\rightarrow$ B. ....	150
Figure 4-8: The effect of free G3 PAMAM dendrimer, free paclitaxel and conjugates on the TEER of PBEC monolayers after (A) apical and (B) basolateral incubation (mean $\pm$ SD, n = 3).....	153

Figure 6-1: HPLC chromatogram of pac and internal standard.....	159
Figure 6-2: HPLC chromatogram of pac-glu and internal standard. ....	159
Figure 6-3: HPLC chromatogram of G3 PAMAM dendrimer and paclitaxel. ....	160
Figure 6-4: HPLC chromatogram of FITC-G3 and paclitaxel.....	160
Figure 6-5: HPLC chromatogram of FITC-G3L6-glu-pac. ....	161
Figure 6-6: HPLC chromatogram of FITC-G3L6-glu-pac collected after crossing PBEC monolayers during permeability studies. ....	161
Figure 6-7: Calibration curve of paclitaxel in methanol, $R^2 = 0.9974$ (mean $\pm$ SD, n = 3). ....	162
Figure 6-8: Calibration curve of pac-glu in methanol, $R^2 = 0.9991$ (mean $\pm$ SD, n = 3). ....	162
Figure 6-9: Calibration curve of FITC-G3 in transport medium, $R^2 = 0.9974$ (mean $\pm$ SD, n = 3). ....	163
Figure 6-10: Calibration curve of FITC-G3L3 in transport medium, $R^2 = 0.9824$ (mean $\pm$ SD, n = 3). ....	163
Figure 6-11: Calibration curve of FITC-G3L6 in transport medium, $R^2 = 0.9947$ (mean $\pm$ SD, n = 3). ....	164
Figure 6-12: Calibration curve of FITC-G3-glu-pac in transport medium, $R^2 =$ $0.9986$ (mean $\pm$ SD, n = 3). ....	164
Figure 6-13: Calibration curve of FITC-G3L3-glu-pac in transport medium, $R^2 =$ $0.9904$ (mean $\pm$ SD, n = 3). ....	165
Figure 6-14: Calibration curve of FITC-G3L6-glu-pac in transport medium, $R^2 =$ $0.9969$ (mean $\pm$ SD, n = 3). ....	165

## LIST OF TABLES

---

---

Table 2-1: Assignment of peaks and chemical shifts for G3 PAMAM dendrimer.....	86
Table 2-2: Molar ratios of lauryl chains conjugated to G3 PAMAM dendrimer by comparison of relative peak integrals from the <sup>1</sup> H NMR spectra.....	88
Table 2-3: Molar ratio of pac-glu conjugated to G3 and lauryl-G3 PAMAM dendrimers determined by comparison of relative peak integral from the <sup>1</sup> H NMR spectra.....	98
Table 2-4: Hydrodynamic diameter of FITC-labelled G3 PAMAM dendrimer and dendrimer conjugates in HBSS at 37°C (mean ± SD, n = 10 of triplicate experiments). * indicates significant difference ( <i>p</i> < 0.05) compared to other conjugates.....	100
Table 2-5 Chemical stability of FITC-G3L3-glu-pac incubated at pH 1.2, 7.4 and 8.5 (37°C). (mean ± SD, n = 3 of triplicate experiments). * indicates a significant difference ( <i>p</i> < 0.05) from 48 h.....	103
Table 3-1: The cytotoxicity effect of G3 PAMAM dendrimer and drug conjugates on the Caco-2 cells as determined by IC <sub>50</sub> (mean ± SD, n = 3 of triplicate experiments). * indicates a significant difference ( <i>p</i> < 0.05) from other conjugates.....	118
Table 4-1: The cytotoxicity effect of G3 PAMAM dendrimer and conjugates on the PBECs as determined by IC <sub>50</sub> (mean ± SD, n = 3 of triplicate experiments). * indicates a significant difference ( <i>p</i> < 0.05) from other conjugates.....	144

## ABSTRACT

---

---

Dendrimers are a novel class of highly branched polymers with a high degree of uniformity and monodispersity. As a result of the unique properties and characteristics of dendrimers, they have found a wide range of pharmaceutical applications. This study investigated the ability of polyamidoamine (PAMAM) dendrimer-based drug delivery systems to enhance the permeability of a drug that is a substrate of P-glycoprotein (P-gp) efflux transporter with low water solubility. This thesis described the syntheses, characterisations and biological evaluations of the dendrimer-based drug delivery system to overcome the cellular barriers.

G3 PAMAM dendrimers were conjugated with lauryl chains via a carbamate bond. Paclitaxel, a low water solubility P-gp substrate and anti-tumour drug, was conjugated to G3 and/or lauryl-G3 PAMAM dendrimer conjugates via a glutaric anhydride linker. Unmodified G3 PAMAM dendrimer and all the dendrimer conjugates (lauryl-G3 and G3-drug conjugates) were labelled with fluorescein isothiocyanate (FITC) for quantitative detection by spectrofluorimetry in permeability studies. These conjugates were characterised using various techniques including thin layer chromatography,  $^1\text{H}$  and  $^{13}\text{C}$  NMR, ESI-MS and dynamic light scattering. Chemical stability studies showed that the tested dendrimer conjugate (FITC-G3L6-glu-pac) was stable at all test pHs (1.2, 7.4, and 8.5) after 48 h of incubation at  $37^\circ\text{C}$ . The ester bond of the conjugate was stable under several chemical conditions after 10 days of incubation.

Biological evaluation of the dendrimer conjugates was initially conducted using Caco-2 cells. Lactate dehydrogenase (LDH) release assay showed that conjugation of lauryl chains and paclitaxel molecules on the surface of G3 PAMAM dendrimer significantly ( $p < 0.05$ ) increased the cytotoxicity in Caco-2 cells. The permeation of G3 PAMAM dendrimer and drug conjugates was investigated by measuring the apparent permeability coefficient ( $P_{\text{app}}$ ) in both apical to basolateral  $\text{A} \rightarrow \text{B}$  and  $\text{B} \rightarrow \text{A}$  directions across Caco-2 cell monolayers at  $37^\circ\text{C}$ . The  $\text{B} \rightarrow \text{A}$   $P_{\text{app}}$  of paclitaxel was found to be significantly ( $p < 0.05$ ) higher than the  $\text{A} \rightarrow \text{B}$   $P_{\text{app}}$ , indicating active function of P-gp efflux transporter system in the cell model. Covalent conjugation of paclitaxel to G3 PAMAM dendrimer

via a glutaric anhydride linker significantly ( $p < 0.05$ ) increased its  $A \rightarrow B$   $P_{app}$  through Caco-2 cell monolayers. A more pronounced increase of paclitaxel permeation was observed when surface modified G3 PAMAM dendrimers with six lauryl chains were used as the carrier. L6-G3-glu-pac was found with highest permeability across the Caco-2 cell monolayers. The results suggested that G3 PAMAM dendrimer-based drug delivery systems enhance the permeability of paclitaxel and bypass P-gp efflux transporter system in Caco-2 cell monolayers, thereby overcoming the intestinal barrier.

Further biological evaluation was carried out using porcine brain endothelial cells (PBECS) as a blood-brain barrier (BBB) cell model to examine the potential of G3 PAMAM dendrimer as a carrier for paclitaxel (P-gp substrate) to bypass the BBB. Cell culture conditions of PBECS were monitored and examined to establish optimal conditions for cell growth. PBECS were successfully cultured with characteristic elongated spindle-like morphology. Integrity of the cell monolayers was evaluated by measuring the transendothelial electrical resistance (TEER) across the cell monolayers. Successfully cultured cell monolayers that achieved TEER values of higher than 200  $\Omega \cdot \text{cm}^2$  were used for permeability studies. Elevation of TEER was observed when PBEC monolayers were cultured in the serum-free medium with hydrocortisone and treated with the cAMP/RO-20-1724 solution mixture.

G3 PAMAM dendrimer was found to be relatively non-toxic to PBECS compared to all other conjugates. Conjugation of lauryl chains and paclitaxel molecules on the surface of G3 PAMAM dendrimer significantly ( $p < 0.05$ ) increased the cytotoxicity in PBECS, as assessed by LDH assay. Permeability studies of paclitaxel across the PBEC monolayers showed a similar transport profile to that of Caco-2 cell. The significant higher  $B \rightarrow A$   $P_{app}$  of paclitaxel compared to the  $A \rightarrow B$   $P_{app}$  indicated active function of P-gp efflux transporter system in the cell model. The  $A \rightarrow B$   $P_{app}$  of L6-G3-glu-pac was found to be approximately 12 fold greater than that of free paclitaxel across the PBEC monolayers, where lauryl chains were acting as permeability enhancer. The cytotoxicity and permeability results using PBECS were found to be in good agreement with the findings when Caco-2 cells were used as the cellular barrier cell model.

From these studies, it can be concluded that G3 PAMAM dendrimers-based drug delivery systems are potential nanocarriers for low solubility and P-gp substrate drug to bypass the P-gp efflux transporter system and overcome cellular barriers.

## DECLARATION

---

---

I declare that while registered as a candidate for this degree I have not been registered as a candidate for any other award from an academic institution. No portion of the work referred to in this thesis has been submitted in support of an application for another degree or qualification of this or any other university or institute of learning.

Signed

Huey Minn Teow

## **COPYRIGHT STATEMENT**

---

---

Copyright in text of this thesis rests with the Author. Copies (by any process) either in full, or of extracts, may be made only in accordance with instructions given by the Author and lodged in the UCLan library. Details may be obtained from the Librarian. This page must form part of any such copies made. Further copies (by any process) of copies made in accordance with such instructions may not be made without the permission (in writing) of the Author.

The ownership of any intellectual property rights which may be described in this thesis is vested in the University of Central Lancashire subject to any prior agreement to the contrary, and may not be made available for use by third parties without the written permission of the University, which will prescribe the terms and conditions of any such agreement.

Further information on the conditions under which disclosures and exploitation may take place is available from the Head of School of Pharmacy and Biomedical Sciences.

## ACKNOWLEDGEMENTS

---

---

I would like to express my utmost gratitude to my supervisors, Prof. Antony D'Emanuele, Dr. Zhengyuan Zhou and Dr. Mohammad Najlah who have wisely guided me throughout the course of this study with their valuable advice, support and encouragement.

Thank you to Prof. N. Joan Abbott and Miss Siti Yusof from the Blood-Brain Barrier Group, King College London, for the supply of porcine brain endothelial cells and the cell culture techniques.

Thanks also to all the colleagues and members in the many labs (Darwin and Maudland building) that I have worked in, Dr. Julie Shorrocks, Dr. Rahima Patel, Dr. Sarah Dennison, Sal, Tony, Basel, Jim, Tamar, Martin, and Sujata for their help, support and friendship.

Special thanks to my great friends Khai, Sheve, Natalie and Arati for their valuable friendship, encouragement, support and entertainment throughout especially during my writing up period!

I would like to express my deepest respect and most sincere gratitude to my parents for their endless encouragement, support and love, never holding me back from achieving my dreams through out my life.

A very special thanks and appreciation are due to my dear husband, Yingren, for his sacrifice, patience, understanding, encouragement and wise advices through out all these years of study. Thank you.

Huey Minn Teow

## ABBREVIATIONS

---

A	Apical
ABC	Adenosine triphosphate binding cassette
ATP	Adenosine triphosphate
B	Basolateral
BBB	Blood-brain barrier
BCEC	Brain capillary endothelial cell
BCRP	Breast cancer resistance protein
Caco-2	Human Caucasian colon adenocarcinoma
cAMP	3', 5'-cyclic monophosphate sodium salt
Da	Dalton
DCM	Dichloromethane
DMEM	Dulbecco's Modified Eagle's Medium
DMF	Dimethylformamide
DMSO	Dimethyl sulfoxide
DNA	Deoxyribonucleic acid
DPC	Diphenyl phosphoryl chloride
EDA	Ethylenediamine
EDTA	Ethylenediaminetetraacetic acid
ESI-MS	Electrospray ionisation-mass spectrometry
EtOAc	Ethyl acetate
FITC	Fluorescein isothiocyanate
FBS	Foetal bovine serum
G	Generation
G3-Lx/ Lx-G3	G3 PAMAM-lauryl conjugates/ lauroyl-G3 PAMAM conjugates
G3-glu-pac	G3-glutarate-paclitaxel
GI	Gastrointestinal
glu	Glutarate
GLUT1	Glucose transporter 1
HBSS	Hank's Balanced Salt Solution
HEPES	4-(2-hydroxyethyl)-1-piperazineethanesulfonic acid

HIV	Human immunodeficiency virus
L	Lauroyl chain
Lx-G3-glu-pac	Lauryl-G3-glutarate-paclitaxel
LDH	Lactate dehydrogenase
[M <sup>+</sup> ]	Mass of positive ion
mAb	Monoclonal antibody
MDR	Multidrug resistance
MRP	Multidrug resistance-associated protein
MW	Molecular weight
NHS	N-hydroxysuccinimide
NMR	Nuclear magnetic resonance
pac	Paclitaxel
PAMAM	Polyamidoamine
P <sub>app</sub>	Apparent permeability coefficient
PBS	Phosphate buffer saline
PEG	Poly (ethylene glycol)
P-gp	P-glycoprotein
PBEC	Porcine brain endothelial cell
R <sub>f</sub>	Retention factor
RP-HPLC	Reverse-phase high performance liquid chromatography
rpm	Revolutions per minute
SDPP	N-hydroxysuccinimide diphenyl phosphate
TEA	Triethylamine
TEER	Transepithelial/ transendothelial electrical resistance
THF	Tetrahydrofuran
TLC	Thin layer chromatography
TFA	Trifluoroacetic acid
Tf	Transferrin
TfR	Transferrin receptor
TMS	Tetramethylsilane
UV	Ultraviolet
δ	Chemical shift
λ	Wavelength
Ω	Ohm

## **CHAPTER 1:INTRODUCTION**

---

## 1.1 Drug delivery across cellular barriers

The development of an effective drug delivery system to overcome cellular barriers remains a major challenge for pharmaceutical scientist. Cellular barriers such as the intestinal and the blood-brain barriers are generally responsible of maintaining the cell environment for the optimal activity of organs, regulating the trafficking of essential nutrients and xenobiotics across the cells and providing protection from circulating toxins (1, 2). Apart from providing protection from potential harmful xenobiotics, these cellular barriers also significantly limit the entry of many therapeutic drugs from reaching the targeted site of effect. For example, it was reported that the blood-brain barrier prevented approximately more than 95% of drugs to brain exposure (3).

Many attempts have been made to develop drug carrier systems that bypass cellular barriers to enhance the therapeutic efficacy of drugs. The general properties of efficient drug carrier systems are the ability to enhance solubility hence the bioavailability of the drugs, enhanced absorption, *in vivo* stability, biodegradable, and selective delivery to the target site. This should be accompanied by minimal toxicity and immunogenicity. In addition, during the selection and design of drug carrier systems, it is desirable to obtain an optimal balance of lipophilicity and hydrophilicity. Adequate lipophilicity can enable rapid and easy entry of the system across the lipid membrane; yet the system can still be soluble in the aqueous site and less able to diffuse back due to the hydrophilicity (1, 4-6). Trafficking across the intestinal and the blood-brain barriers is not only governed by the nature of physical barrier, but also controlled by numerous biological transport systems (1, 6). Therefore, the ability of carriers to utilise transport systems as delivery pathways and to circumvent the efflux pump systems needs to be taken into consideration during the design of efficient drug delivery systems.

Drug carriers such as antibodies (7), liposomes (8), nanoparticles, and polymers prodrugs (9) have been widely investigated. Classical polymers (e.g. linear, branched and random coiled polymers) have received significant attention in the development of drug carrier systems but their applications may be limited due to issues such as high polydispersity (10). A new class of polymer, namely dendrimers, have emerged as a popular drug carrier candidate. Dendrimers, with their monodispersity and well-defined

structures, allow precise control of size and shape. The terminal groups are amenable for specific functionality. With their unique properties, dendrimers have been recently investigated as drug carriers to overcome cellular barriers (11).

In general, chemical and biological characteristics of drug carriers together with the understanding of transport mechanisms across the cellular barriers such as the intestinal barrier and the blood–brain barrier (BBB) are vital to the successful development of new and effective drug delivery systems.

## **1.2 Mechanism of intestinal barrier absorption**

The absorption of both nutrients and therapeutics from the intestinal tract is mainly controlled by the physical and biochemical barrier factors of the intestinal membrane. The cell membrane, which is a physical selective permeable barrier, mainly consists of lipid bilayers of phospholipids with inter-dispersed carbohydrates, integral membrane proteins and cholesterol components (12) (Figure 1-1). The lipid bilayer membrane exhibits the characteristics of a lipoidal semi permeable sieve which allows high permeation for lipophilic molecules and low permeation for hydrophilic molecules. The cholesterol component helps to maintain the lipid membrane fluidity and prevents close packing of fatty acid chains, hence enhancing the permeation of lipid-soluble molecules. Water and small hydrophilic molecules are able to permeate across the cell membrane through numerous protein channels formed by the integral membrane protein (12). The tight junctions which are located at the apical site of the cell membrane restrict the permeation of molecules across the membrane through the aqueous pores between the cells (13). The biochemical barrier factors include a number of transport mechanisms and transporter proteins which require energy to selectively transport molecules back and forth across the membrane. In general, nutrients and therapeutics can be transported across the membrane barrier via transcellular pathway (across the cells) and paracellular pathway (between the cells) (12). A summary of the membrane transport mechanisms is illustrated in Figure 1-2.

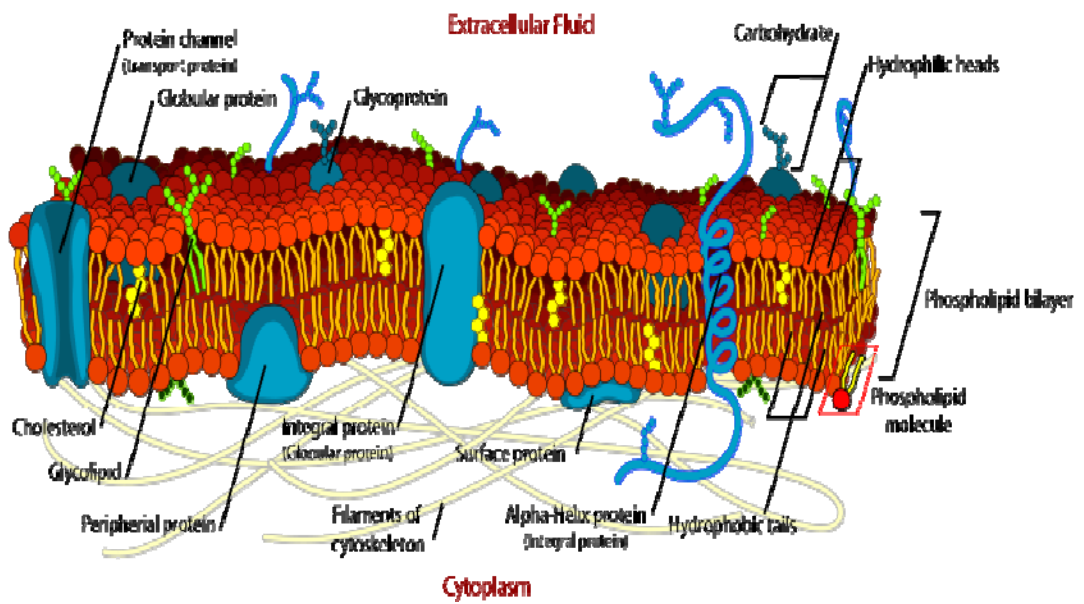


Figure 1-1: Structure of the cell membrane [taken from (14)].

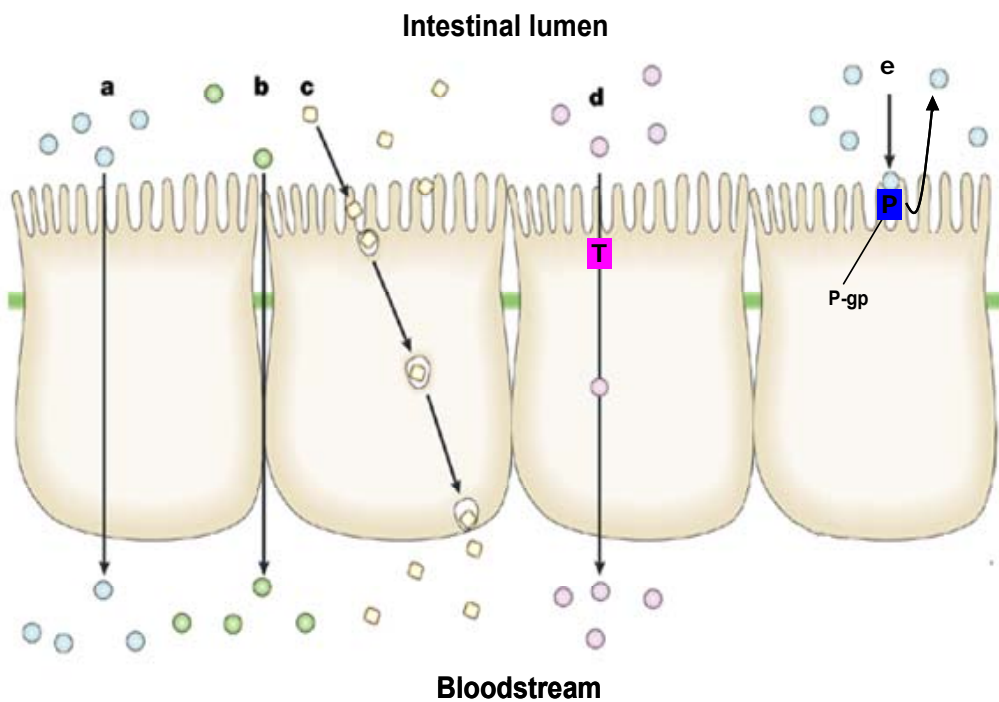


Figure 1-2: Mechanism of intestinal absorption. (a) passive transcellular transport, (b) paracellular transport, (c) vesicular endocytosis/endocytosis, (d) carrier mediated transport, and (e) P-gp mediated efflux transport [modified from (6)].

## 1.2.1 Transcellular pathway

Transcellular pathway is a general route for non-ionic and lipophilic molecules to be transported across cells. It can be further divided into simple passive transcellular diffusion, carrier-mediated transport and endocytosis which will be further discussed in the following sections.

### 1.2.1.1 Passive transcellular diffusion

Low molecular weight and lipophilic molecules and drugs generally prefer to cross the intestinal epithelium transcellularly via passive diffusion. In this non-energy dependent process, molecules or drugs will undergo a partitioning process between the gastrointestinal aqueous fluid and the lipoidal-like membrane of the intestinal epithelium. Diffusion then occurs across the lipid bilayer membrane, the molecules and drugs will be absorbed from a high concentration region in the lumen to a relatively low concentration region in the blood. The rate of absorption can be described mathematically by Fick's first law of diffusion:

$$dC/dt = k(C_1 - C_2)$$

in which the rate of diffusion across a membrane ( $dC/dt$ ) is proportional to the difference in concentration on each side of the membrane ( $C_1 - C_2$ ), and  $k$  is a proportionality constant (12).

The solubility characteristics of a drug have an important role in its absorption. Due to the oleaginous nature of the membrane, a minimum level of lipophilicity is needed for molecules or drugs in order to partition into epithelial cell membranes and to be absorbed transcellularly through passive diffusion (15). In general, the absorption rate is determined by the physicochemical properties of the drug, the nature of the membrane and the concentration gradient of the drug across the membrane (12).

### 1.2.1.2 Carrier-mediated transport

Carrier-mediated transport involves carrier or membrane protein transporters which are located at the apical cell membrane to transport the substances across the epithelial membrane. There are two main types of transport: active transport and facilitated diffusion. Active transport involves transportation of a substrate against a concentration gradient across the cell membrane thus energy is required in this process. The energy sources for active transport may either derive from the hydrolysis of ATP or from the transmembrane ion gradients (mostly  $\text{Na}^+$ ,  $\text{Ca}^{2+}$ , and  $\text{H}^+$  gradients) and/or electrical potential. Unlike active transport, facilitated diffusion cannot work against concentration gradient; it does not require energy input and transport substrate from a high concentration region to a low concentration region across the cell membrane (12).

Carrier systems with specific membrane protein transporters are concentrated at different segments of the GI tract and provide transportation for electrolytes, amino acids, dipeptides, saccharides, lipids, carboxylic acids, organic cations, phosphates nucleosides, and water soluble vitamins. Each transporter will interact with the substrate according to its specific chemical structure, forming a transporter-substrate complex. However, some transporters have broader specificity, allowing drugs with a chemical structure similar to natural substances to be transported via this mechanism (12, 16). For example, studies show that the human peptide transporter 1 (hPepT1) is involved in transporting various peptide-like drugs such as cephalosporins, angiotensin-converting enzyme (ACE) inhibitors, and 5'-amino acid ester prodrugs of antiviral nucleosides, acyclovir and azidothymidine (AZT) (17-19). At a high concentration, the rate of absorption will remain constant as the carrier system is saturated. Thus, competition between two substrates with similar chemical structure for the same transport mechanism will result in inhibition (12).

Apart from facilitating the intestinal drug absorption process, transporters are also crucial in limiting drug uptake by eliminating/effluxing substances from the cell to the intestinal lumen. Efflux transporters from the ATP binding cassette (ABC) superfamily include the multidrug resistance protein (MDR), P-glycoprotein (P-gp), and multidrug resistance-associated protein (MRP) family. P-glycoprotein (also called ABCB1, MDR1 and PGY1) is a prominent energy-dependent efflux pump located at the apical

membrane of biological barriers. P-gp has very broad substrate specificity and was reported to limit the uptake of anticancer drugs (anthracyclins (20), etoposide (21), vinblastine (22) and paclitaxel (23, 24)), peptides (cyclosporine), and cardiac glycoside (digoxin) (12, 16, 25). However, calcium channel blocker such as nifedipine and verapamil (22) are found to inhibit the P-gp action thus may improve the bioavailability of other substrate drugs.

### 1.2.1.3 Endocytosis/ Vesicular transport

Endocytosis is a general term for a group of processes that transport macromolecules, large particles and organisms into the cells (12). There are mainly three types of endocytosis: phagocytosis, pinocytosis (fluid-phase endocytosis) and receptor-mediated endocytosis. In all these three processes, the plasma membrane invaginates around the absorbed molecules, forming small pockets which then deepen and become intracellular membrane-bound vesicles. This vesicle separates from the plasma membrane and migrates with its contents to the cell's interior. Phagocytosis involves engulfment of particles larger than 500 nm. While pinocytosis or fluid-phase endocytosis is the engulfment of small droplets of extracellular fluid such as fat soluble vitamins A, D, E and K. Receptor mediated endocytosis occurs when molecules with suitable ligands are bound to the receptors at the cell surface. The ligand-receptor complexes are then progressively internalised and delivered to early endosomes. The ligands usually dissociate from their receptors within the endosomes and many of the receptors are then recycled to the plasma membrane (12). Frequently, the dissociated ligands and solutes will be delivered for degradation in lysosomes. Occasionally, ligands that gain access to a vesicle targeted to the basolateral membrane for release can bypass lysosomes, transport across the cells via transcytosis and secrete in a non-degraded form on the opposite site of the cells (12, 26).

### 1.2.2 Paracellular pathway

Differing from all other absorption pathways, paracellular pathway can be considered as an aqueous route where substances are transported through the intercellular space

between adjacent cells. The cells are joined together via closely fitting junctional complexes at the apical side of the cells which consist of (a) tight junctions or zonula occludens, (b) zonula adherens, and (c) desmosome or macula adherens. Tight junctions (TJs) primarily regulate paracellular permeability by selectively allowing the passage of small hydrophilic compounds, forming an intermembrane diffusion barrier by maintaining enterocyte polarity and excluding potentially toxic molecules (12, 27). The aqueous nature of the paracellular pathway allows absorption of ions (calcium, sodium and potassium), sugars, amino acids and peptides through passive diffusion (12). Small hydrophilic and charged drugs with molecular mass less than 200 Da cross the cell membrane via the paracellular pathway, although higher molecular mass drugs (more than 200 Da) have been reported to be absorbed via this route (12). The use of paracellular permeation enhancers such as calcium chelators (EDTA), medium chain fatty acids, medium chain glycerides, chitosan (28), and some drugs such as verapamil (29) have been reported to be able to disrupt the TJs structure, hence enhancing the absorption via the paracellular pathway.

The total area of the paracellular pathway, relative to the transcellular route, has been reported to represent about 0.1% (12, 30) of the total surface area of the intestinal epithelium, which is 2,000,000 cm<sup>2</sup> (31). The corresponding value of the paracellular surface area theoretically will be about 2000 cm<sup>2</sup>, which should not be underestimated since even the absorption of minute quantities of a potent therapeutic drug may be sufficient to exert a biological effect (31).

### **1.3 Transport across the blood-brain barrier**

The central nervous system (CNS) requires a perfectly regulated environment in order to maintain a level of homeostasis for optimal activity. Protection from circulating toxins is especially important for the brain compared to most other tissues of the body. Thus, the maintenance of homeostasis and prevention of unrestricted exchange of substances between the CNS and the blood is crucial and is mainly regulated by the gate keeper, the blood-brain barrier (32, 33).

However, apart from protection from circulating toxins, the blood-brain barrier also significantly limits the penetration and entry of many drugs and prevents them from reaching therapeutic targets within the brain. For this reason, it is important to understand the physiology and pharmacological role of the blood-brain barrier (BBB) for the development of drug delivery and targeting strategies that can enhance the transport of therapeutics across the BBB for the management of CNS diseases (4, 33).

### 1.3.1 The blood-brain barrier

The existence of a barrier between the blood and the brain was first reported by Ehrlich following the observation that the barrier prevented entry of a xenobiotic into the CNS (34). The blood-brain barrier is generally a selective barrier which encompasses three main aspects of barrier function including physical, transport and metabolic aspects.

#### *Physical barrier*

The physical barrier is mainly formed by brain capillary endothelial cells, surrounded by basal lamina and astrocyte end-feet, with pericytes embedded within the basal lamina membrane (35, 36). Brain capillary endothelial cells are distinct from the endothelial cells in most other tissues, characterised by the presence of complex tight junctions and lack of pinocytotic vacuoles (33). The endothelial cells are closely packed to each other, forming complex tight junctions. This hinders the paracellular transport of most hydrophilic molecules through the junctions and forces most molecular traffic to take the transcellular pathway across the BBB. Small gaseous and lipophilic molecules such as O<sub>2</sub>, CO<sub>2</sub>, alcohol, caffeine, nicotine and anaesthetics can pass the plasma membrane by passive diffusion (37). Lipophilic drugs such as barbiturates and ethanol can also diffuse through the lipid membrane via this route (36). Figure 1-3 shows a schematic diagram of a cerebral capillary which encompasses endothelial cells that build up the capillary surrounding by pericytes and astrocyte end-feet. The cross section of the capillary is illustrated in Figure 1-4.

Astrocytes and pericytes, located at the close vicinity around capillary endothelial cells, play an important role in the formation and functions of the BBB. Astrocytes end-feet

are closely attached to the blood microvessel wall on one side and to the neurons on the other. It forms a specific relay station between the neurons and the blood (33) which provides the cellular link to the neurons (36). Astrocytes are involved in inducing and maintaining brain intercellular signalling, neuronal metabolism, and discharge of used substrates, which have crucial effect on the BBB stability and normal function (38). Cell culture studies strongly indicate that astrocytes can upregulate many BBB features which include tighter tight junctions, expression and polarised localisation of transporter such as P-gp and glucose transporter 1 (GLUT1), and specialised enzyme systems (2, 39-41). Pericytes embedded within the basal lamina membrane surrounding the BBB play a key role in angiogenesis, structural integrity and differentiation of the vessel and formation of endothelial TJs (35). Pericytes are also known to be responsible for the regulation of endothelial activity, mediation of inflammation and control of capillary-like structure formation and capillary diameter (33).

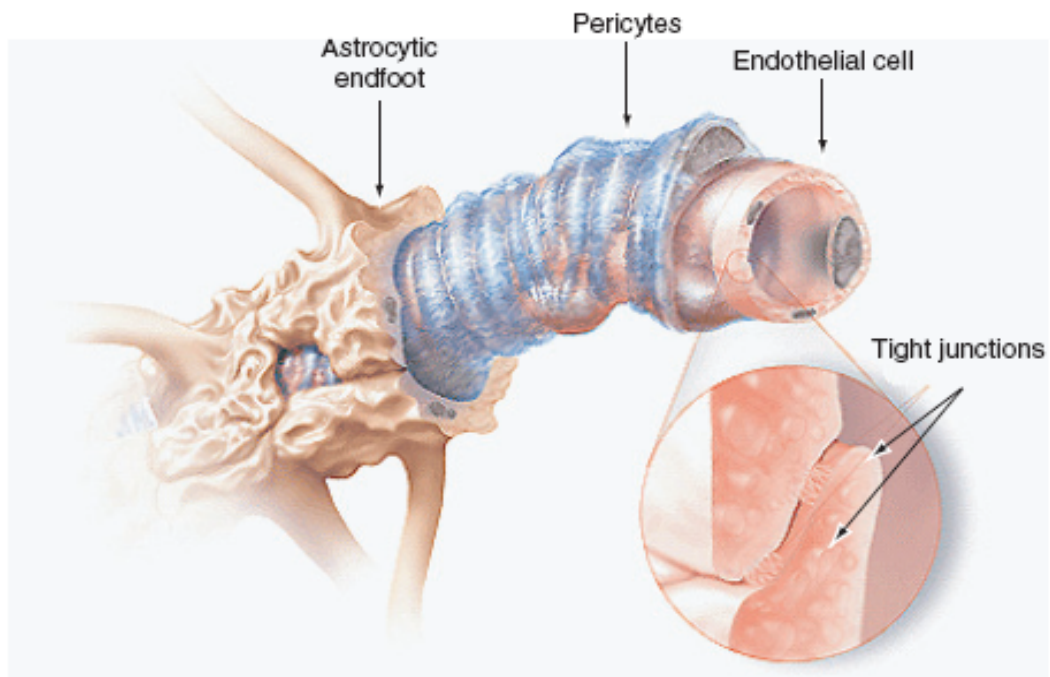


**Figure 1-3: Schematic diagram of a cerebral capillary [taken from (42)].**

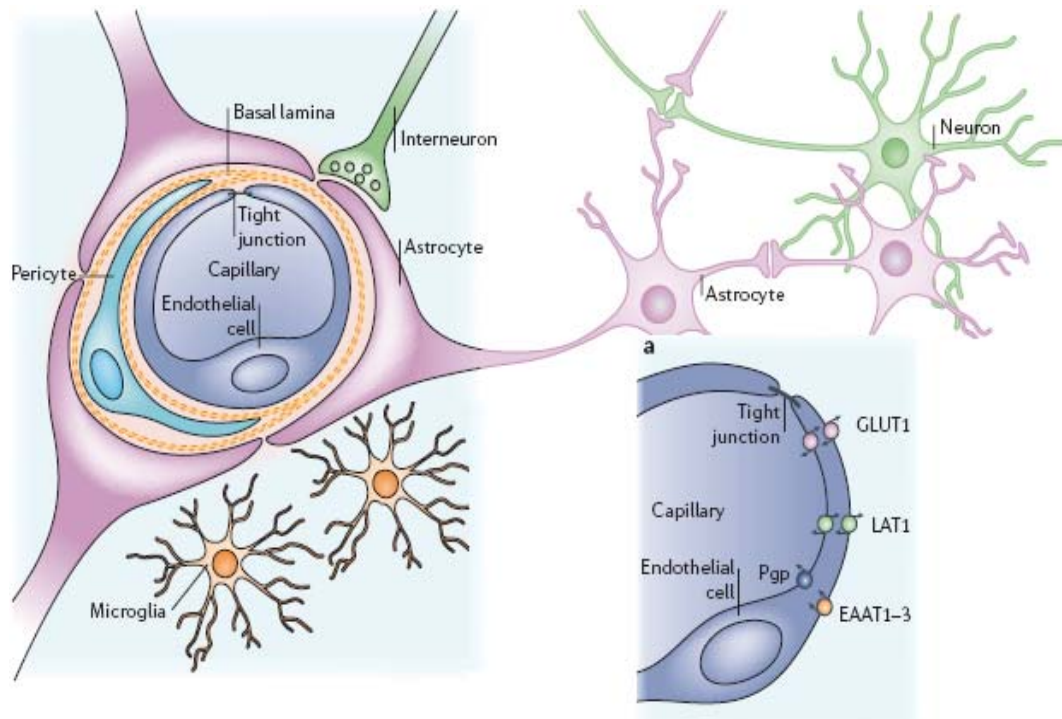


**Figure 1-4: Cellular components of the blood-brain barrier [modified from (36)].**

### *Transport barrier*

Specific transport systems existing at the luminal (blood) and abluminal (brain) membrane act as selective ‘transport barriers’. Ionic and small hydrophilic molecules are only able to cross the barrier through special membrane transporters, thus allowing required nutrients to reach the brain and limiting the entry of potentially harmful compounds (36, 43).

### *Metabolic barrier*

Apart from specific transport systems, enzymatic activity in cerebral endothelium cells provides a ‘metabolic barrier’ which prevents unwanted toxic compounds, including drugs, from entering the brain. Extracellular enzymes such as peptidases and nucleotidases regulate the metabolism of peptides and ATP, respectively, while intracellular enzymes such as monoamine oxidase and cytochrome P450 can inactivate many neuroactive and toxic compounds (4, 36).

### 1.3.1.1 Tight junctions

The presence of complex tight junctions is one of the specific characteristics that distinguish cerebral endothelial cells from the peripheral endothelial cells. Tight junctions formed within the cerebral endothelial cells are characterised by extremely high transepithelial electrical resistance (TEER) of 1500 to 2000  $\Omega\cdot\text{cm}^2$  (33, 44) compared to those of peripheral capillaries (TEER of 2-20  $\Omega\cdot\text{cm}^2$ ), and those within the epithelial cells in the colon (TEER of 150 – 400  $\Omega\cdot\text{cm}^2$ ). The unique characteristic of the complex tight junction (or zonula occludens) structure is due to the existence and interaction of numerous plasma membrane proteins that tightly seal the paracellular pathway. Among those identified as main contributors to the tight junctions are the transmembrane proteins claudin and occludin, and the adherens junction (AJs) molecules (33, 35, 36, 45).

Occludin and claudin are proteins with four transmembrane domains and two extracellular hoops. Occludin was found to interact with zonula occludens protein 1 (ZO-1) and is responsible for stabilising the tight junction. Claudin 1/3, 5 and 12 expressed in the BBB appear to contribute to the high TEER. Junctional adhesion molecules (JAMs) are involved in the formation and maintenance of tight junctions. JAM-A, JAM-B and JAM-C were found to be present in brain endothelial cells and may play a role in cell adhesion and monocyte migration through the BBB. Identified cytoplasmic proteins including zonula occludens protein 1 (ZO-1), ZO-2 and cingulin were shown to link the transmembrane proteins (occludin and claudin) to actin, a primary cytoskeleton protein which maintains the structural and functional integrity of the endothelium (Figure 1-5). The interaction of these plasma membrane proteins regulates and allows paracellular transport to be modulated in response to different stimuli. In epithelial cells, tight junctions and adherens junctions are strictly separated from each other, but these junctions are intermingled in endothelial cells (33, 35, 36, 45). Adherens junctions contribute to the second component in stabilising and tightening endothelial cell structure. The transmembrane protein cadherins are linked to the actin cytoskeleton by catenins to form adhesive contacts between cells. Cadherins on the surface of adjacent cells interact homotypically in the presence of calcium ions (Figure

1-5). Both tight and adherens junctions contribute to the human BBB. It was reported with evidence that ZO-1 and catenin interact with each other, suggesting that TJs and AJs function together to maintain the integrity (46).

Tight junctions are important in regulating paracellular permeability across the cerebral endothelia cells. The functions of various numbers of plasma membrane proteins and the negative charges on the endothelial membrane contribute to the size and charge selectivity properties. Furthermore, tight junctions also segregate the luminal and abluminal membrane domains, preserving a polarised cell membrane (33, 35, 36, 45, 47).

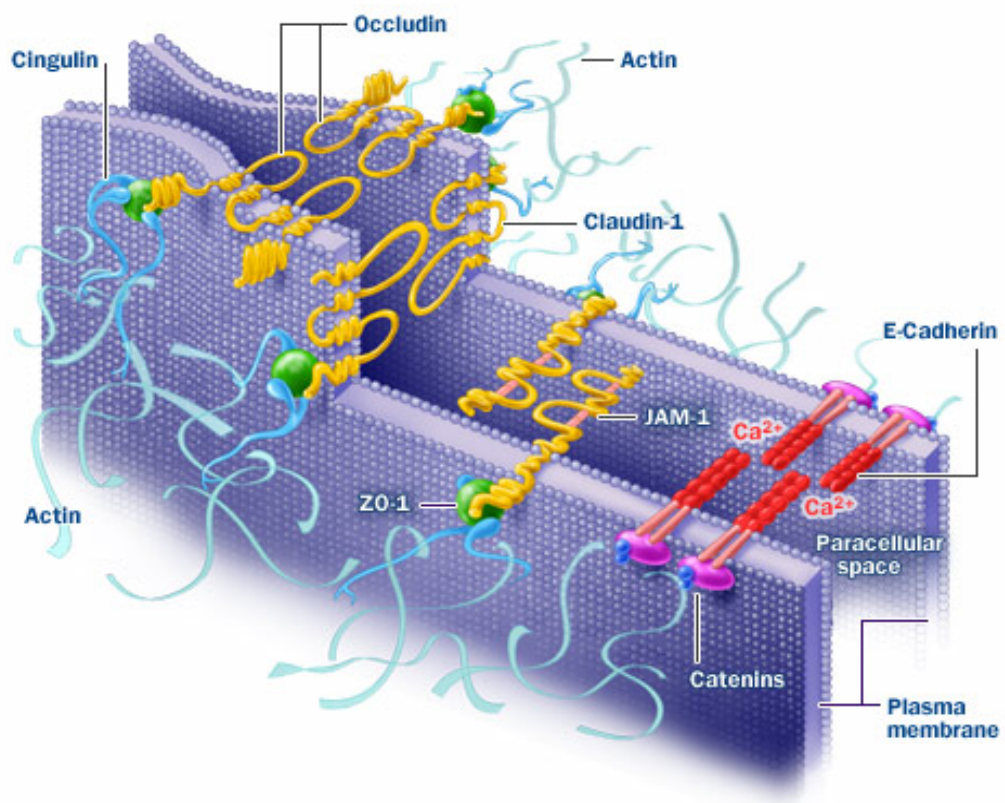


**Figure 1-5: A schematic diagram of the tight junction and adherens junction of the blood-brain barrier [taken from (48)].**

### 1.3.2 Therapeutic pathways across the blood-brain barrier

The existence of the blood brain barrier tight junctions, together with numerous functions of complex cell membrane domains almost seal off the paracellular pathway. As a result, the trafficking of essential nutrients, blood gases as well as removal of neurotoxic or xenobiotic molecules between blood and brain is predominantly via transcellular routes. Many transcellular transport systems have been discovered to play important roles not only in maintaining the blood-brain barrier integrity and homeostasis; but also in influencing drug delivery to the brain. Diffusion of most hydrophobic drugs across the blood-brain barrier via the paracellular aqueous pathway is almost negligible. However, enhanced delivery can be achieved via opening/disruption/shrinking of tight junctions which has been proven to be a more aggressive approach (43). It has been reported in numerous studies that by improving strategies such as chemical modification, the transport of drugs across the barrier via the transcellular route can be adapted and improved. The transcellular routes across the blood-brain barrier are (a) transcellular lipophilic pathway (or transcellular passive diffusion/partitioning pathway), (b) carrier-mediated transport (or solute carriers/transporters pathway), (c) receptor mediated transcytosis, and (d) adsorptive-mediated transcytosis (4, 36, 43, 47). A summary of the transport mechanism across the blood-brain barrier is shown in Figure 1-6 below.

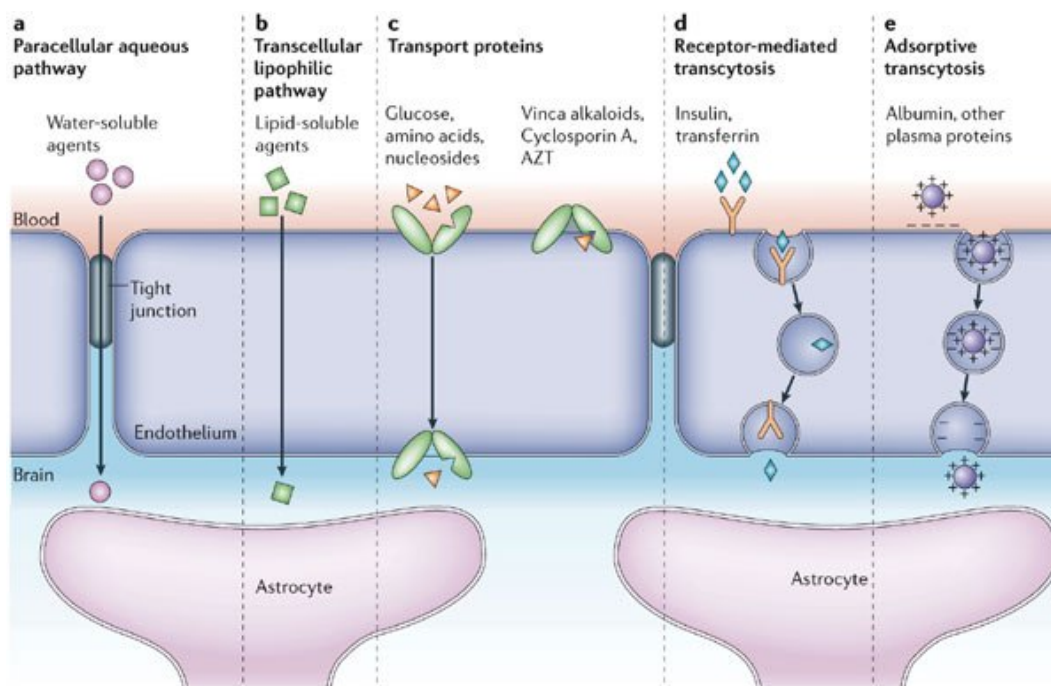


**Figure 1-6: Transport mechanisms across the blood-brain barrier [taken from (36)].**

### 1.3.2.1 Transcellular lipophilic pathway

As indicated by the route's term, transcellular lipophilic pathway or passive diffusion/partitioning generally transport lipid-soluble molecules across the barrier. The rate of diffusion depends on the lipophilicity and molecular weight of the solute. Studies indicate that the rate at which a solute enters the CNS correlates with its lipid solubility (4, 43, 47). There are others factors that restrict the penetration of solutes across the barrier, e.g. high polar surface area or charge of the solutes or drugs, the tendency to form more than six hydrogen bonds when penetrating the membrane, a molecular weight of less than 450 Da and the presence of rotatable bonds in the molecule. However, there are still many examples of effective CNS active drugs in clinical use which do not comply with these molecular and physicochemical factors for the blood-brain barrier penetration, thus these general rules are not always an absolute indication for the brain permeation.

Compared to negatively charged acids, positively charged bases are thought to have a better permeation due to their cationic nature which can interact with the negatively charged glycocalyx and phospholipids head groups. Supply of oxygen and carbon dioxide to the brain is through passive diffusion across the barrier with their concentration gradient and the rate is blood-flow dependent. The permeation of therapeutic drugs across the barrier via lipophilic pathway could be enhanced by the addition of hydrophobic groups. It was reported that the consecutive addition of methyl groups to a series of barbiturate homologues increased the lipophilicity and brain penetration, leading to increased hypnotic activity *in vivo* (4).

### 1.3.2.2 Carrier-mediated transport

Numerous membrane transporters or solute carriers are localised on the luminal and abluminal membranes in the brain capillary endothelial cells. These transporters/solute carriers, forming a functional carrier-mediated transport system, are responsible in regulating the transcellular transport of essential nutrients between the blood and brain, as well as effluxing the potential harmful substances.

Essential polar nutrients such as glucose and amino acids are transported across the barrier via the GLUT1 glucose carrier and several amino acid carriers (large neutral amino acid transporter (LAT1), L-system), respectively. More than 20 influx transporters/carriers including transporters for nucleosides, nucleobases, several organic anion and cation transporters are also found to be highly expressed on the brain endothelium (36, 49). GLUT1 and LAT1 are bidirectional; they can be present in both luminal and abluminal membranes, or predominantly in one. These transporters were found to be responsible for moving substrates against a concentration gradient (50). The utility of these transport systems for drug delivery to the brain has been explored. Glucose carrier has very limited usage for drug delivery as it has very restrictive substrate diversity and will only transport molecules closely resembling D-glucose. In contrast, the amino acid carrier L-system is less specific and drugs that closely mimic the substrate including baclofen (muscle relaxant) (51), gabapentin (anticonvulsant) (52), L-DOPA (treatment for Parkinson's Disease) (49) can be transported across the barrier via this carrier system. However, the brain delivery of these agents is limited due to low

transport affinity. Various strategies including substrate modifications were developed to enhance carrier binding and transport. The development of analogues of phenylalanine (a natural L-system substrate) – melphalan and d,l-2-amino-7-bis[(2-chloroethyl)-amino]-1, 2, 3, 4-tetrahydro-2-naphthoic acid (D,L-NAM) was reported to have greatly improved brain uptake (with increased uptake by more than 20 fold for the D,L-NAM). The enhanced affinity of these phenylalanine derivatives for the amino acid transporters were thought to be the result of interaction of the additional side chains with a hydrophobic-binding site on the carrier (53). Thus, it was suggested that the L-system amino acid carrier could enhance drug delivery to brain by drug modification with hydrophobic side chains (4).

Apart from carrier systems that facilitate the entry of nutrients across the barrier, efflux transporters from the ABC superfamily including P-glycoprotein (P-gp), the Multidrug Resistance-associated Protein (MRPs, ABCC1, 2, 4, 5 and possibly 3 and 6) and Breast Cancer Resistance Protein (BRCP, ABCG2) are of greatest significance for actively effluxing a diverse range of lipid-soluble compounds as well as limiting drug uptake by eliminating/extruding substances out of the brain capillary endothelium cells. Amongst these transporters, P-gp has gained the highest attention. The outstanding role of P-gp has attracted most interest and been an obvious target for therapeutic approaches to overcome the blood-brain barrier.

#### 1.3.2.2.1 P-glycoprotein efflux transporter

P-glycoprotein (also called ABCB1, MDR1 and PGY1) is an ATP energy-dependent efflux pump that is found predominantly in the apical membrane of numerous epithelial cell types in the body, including the luminal surface of the small intestine and colon, and the brain capillary endothelial cells that form the blood-brain barrier. In the blood-brain barrier, P-gp is highly concentrated on the luminal membrane (54). P-gp has been proven to prevent the cellular uptake and accumulation of many compounds, e.g. neurotoxic endogenous or xenobiotic molecules and a variety of drugs in the brain by efflux transport of these compounds from the brain back to the blood circulation (55).

P-gp has very broad substrate specificity and has been reported to limit the uptake of numerous types of drug with diverse chemical structures and sizes. The reported substrate drugs include: antineoplastic agents anthracyclines (daunorubicin and doxorubicin), vinca alkaloids (vincristine and vinblastine), taxanes (paclitaxel and docetaxel), immunosuppressive agents (cyclosporine A), antibiotics (erythromycin and actinomycin), cardiac glycosides (digoxin) and several human immunodeficiency virus (HIV) protease inhibitors (indinavir and saquinavir) (56-58). P-gp is not only localised in the brain capillary endothelia cells, but is also highly expressed in multi-drug resistant tumour cells. It pumps out therapeutic drugs back to the blood thus limiting the CNS therapeutic effect of the administered drug.

Several strategies to overcome the barrier and to circumvent the P-gp efflux pump have been explored. There are drugs that act as inhibitors of P-gp, such as verapamil and cyclosporine A which might help in improving bioavailability of other P-gp substrates. PSC-833 (Valspodar), which is a derivative of cyclosporine A, has demonstrated increased CNS levels of paclitaxel and decreased tumour volume of a paclitaxel-sensitive orthotopic transplanted human glioblastoma in nude mice by 90% when co-administrated with paclitaxel. No significant effect on the tumour volume was observed with paclitaxel alone as well as when the combination of drug and inhibitor were administered to a non-paclitaxel sensitive implanted U-87 MG tumour. It was suggested that direct inhibition of P-gp transporters may enhance the brain uptake of drugs which are substrate to the efflux transporter. However, reservations on the chronic administration of inhibition agents remains, given the protective role of the efflux transporter in the blood-brain barrier (59). Another strategy reported was encapsulation of substrate drugs to bypass P-gp efflux pumps. P-gp substrates have been shown to be delivered efficiently via receptor-mediated endocytosis to the brain by encapsulation in immunoliposomes (60, 61). Similar delivery method was reported with liposomes coupled to cationised albumin (62). The exploitation of nanoparticles in overcoming P-gp efflux pumps via the endocytosis route has also been demonstrated successfully for the delivery of several substrate drugs into the brain in chemotherapy treatment of brain tumours (63).

The quantity structure-activity relationship (QSAR) for the P-gp efflux transporter were studied to provide more understanding on the well defined structural features

responsible for the substrates and inhibitory activities. There are suggestions that explain that the hydrophobic and amphipathic nature of P-gp substrates probably relates to the mechanism of drug translocation by P-gp, which may depend on the ability of the drug to insert into one hemileaflet of the membrane lipid bilayer (64). Stouch and Gudmundsson (57) later found that the affinity of compounds to P-gp depended on two important characteristics: high lipophilicity and hydrogen bonding capability.

#### 1.3.2.2.2 Multidrug resistance-associated proteins

Multidrug resistance-associated proteins (MRPs) are the second efflux transport protein subfamily which also belongs to the ABC protein superfamily. Apart from P-gp efflux transporter, MRPs also play a significant role in multidrug resistance. To date, 9 proteins (MRP1-9) for the mammalian MRP family have been reported (65). MRPs were found expressed in both luminal and abluminal sides of the brain endothelial cell membrane, in contrast to P-gp which is found located generally at the luminal site. However, it has been suggested that only luminal localisation confers in the restriction of substrate penetration and protective efflux activity (66). MRPs were found to primarily transport organic anions, and were also able to transport neutral organic drugs across the endothelium (33).

MRP1 and 2 are the best characterised family members. MRP1 have been reported to mediate resistance to a number of anti-tumour agents including vincristine and daunorubicin when it is overexpressed (67). In some studies, the transport of phenytoin was found to be restricted by MRP2 expression (68). MRP roles in the protection against toxic compounds were demonstrated by experiments with MRP inhibitors (e.g., probenecid, MK-571). Drugs efflux was inhibited from isolated endothelial cells and enhanced drug penetration into the brain was observed after the inhibitor was applied (68). Leggas and co-workers (69) investigated the role of MRP4 and found that the transport of topotecan was limited by the expression of MRP4 in *Mrp4* knock-out mice. It was suggested that MRP4 not only acted to inhibit the penetration of toxic anionic compounds to the brain, but also extruded therapeutic organic anions and transported metabolites from the brain.

### 1.3.2.2.3 Breast cancer resistance protein

Breast cancer resistance protein (BCRP) (also called ABCG2 or mitoxantrone resistance protein, MRP) is another member of the ABC superfamily and is reported to have a significant efflux function at the BBB. BCRP was primarily discovered in a chemotherapy-resistant breast cancer cell line for high resistance to mitoxantrone, hence how the name of the transporter was derived. Similar to P-gp, BCRP was found to be expressed in the luminal membrane of the blood-brain barrier. The similar localisation of BCRP with P-gp implies its possible functions in efflux transporting of xenobiotics which plays an important role in multi-drug resistance for brain protection. It was reported that BCRP was likely to serve as a cellular defense mechanism in response to mitoxantrone and anthracycline exposure (33, 45, 47, 70). Initial *in vitro* studies carried out by Eisenblätter and co-workers (71) demonstrated active extrusion of daunorubicin from porcine brain endothelial cells mediated mainly by BCRP (or ABCG2) compared to P-gp, suggesting an important role of BCRP in the efflux transport of xenobiotics from the brain.

Numerous influx and efflux transporters in the blood-brain barrier are important in protecting and maintaining the normal functions of the brain by transporting essential nutrients and metabolites as well as limiting entry of neurotoxic and harmful substances into the brain. However, it is still a major impediment to the transport and delivery of therapeutic drugs to the brain. Although it has been shown that the brain uptake of drug substrates can be enhanced with the use of inhibitors of ABC transporters, toxic substrates might gain unrestricted entry to the brain due to the down regulated efflux transport activity. Therefore, a drug delivery system which can overcome these barriers is needed. Important characteristics such as: i) better lipid solubility, ii) ability to perform biochemical opening of tight junctions, and iii) ability to bypass the efflux transporters need to be considered during the design of delivery systems for the efflux transporters substrate and low solubility drugs (59).

### 1.3.2.3 Receptor mediated transcytosis

Macromolecules including peptides, proteins and genes are able to enter the brain endothelial cells following uptake into endosomal vesicles and exocytosis via receptor-mediated transcytosis and adsorptive-mediated transcytosis (in section 1.3.2.4). Receptor-mediated transcytosis occurs when macromolecules with suitable ligand bind to specific receptor on the cell surface. This triggers an endocytotic process where the receptor-ligand complexes are internalised at the luminal (blood) side, by forming a caveolus (about 50-80 nm in diameter) which is pinched into vesicles. These internalised vesicles are progressively moved through the endothelium cytoplasm in which the macromolecules with ligand are dissociated from the receptor and exocytosed at the abluminal (brain) side of the brain capillary endothelium cells (5, 43, 47). However, to avoid degradation of the molecules, the vesicles are required to transport across the cell by routing the primary endosomes and its contents away from the lysosomal acidic degradation compartment. Thus, the application of a lysosomal escape mechanism is significant to ensure intact transcytosis of macromolecules such as essential peptides/protein as well as specific delivery/ targeting of large drug molecules or drug- carrier across the blood-brain barrier endothelia cells via receptor-mediate transcytosis route (43, 47). Examples of receptor involved in receptor-mediated transcytosis are the transferrin receptor, insulin receptor and lipoprotein receptor (43).

#### 1.3.2.3.1 Transferrin receptor

The transferrin receptor (TfR) is a transmembrane receptor consisting of two 90kDa subunits linked by a disulfide bridge where each of the subunits can form a bond with one transferrin molecule. The transferrin receptor is found to be expressed on the brain endothelial cells (both luminal and abluminal membrane with greater abundance on the luminal membrane) as well as on other cells (hepatocytes, erythrocytes, intestinal cells and monocytes) with the main function of mediating the cellular uptake of iron bound to transferrin (72).

Endogenous ligand transferrin had been shown to achieve drug targeting to the transferrin receptor in drug delivery. Visser *et al.* (8) reported targeted delivery to the

bovine brain endothelial cells *in vitro* using PEGylated liposomes which were loaded with protein or peptide drugs and tagged with transferrin. The binding studies showed that the transferrin-tagged liposomes displayed a significant higher binding to the brain capillary cells compare to untagged liposomes. It was also found that liposomes released some of their content within the BBB, making targeting of transferrin-tagged liposomes to the transferrin receptors on BCEC an attractive approach for brain drug delivery.

Another approach that was found to be effective in drug targeting to the transferrin receptor was by the use of monoclonal antibodies directed against the rat transferrin receptor (OX26; anti-rat TfR). The OX26 antibody can be linked to a drug or peptide/protein, serving as a vector for preferential delivery to the blood-brain barrier. It was thought that the binding of OX26 antibody to the transferrin receptor appeared to trigger endocytosis followed by transcytosis of the whole construct across the cell. It was reported that vasoactive intestinal polypeptide, nerve growth factor, glial-derived neurotrophic factor, and brain derived neurotrophic factor can be delivered successfully to the central nervous system by using an OX26 antibody vector (7, 73).

#### 1.3.2.3.2 Insulin receptor

Another classical and widely characterised receptor-mediated transcytosis system for targeted drug delivery to the brain is the insulin receptor. It is a 300 kDa heterotetramer protein consisting of two extracellular- $\alpha$  and two transmembrane- $\beta$  subunits. The  $\alpha$  and  $\beta$  subunits are linked by disulfide bonds, forming a cylindrical structure. Upon binding of insulin, the shape and conformation of the receptor change into a tunnel, allowing entry of molecules into the cells. After internalisation into endosomes, receptors are generally recycled to the cell surface or endocytosis of the insulin receptor might occur to remove insulin from the cell allowing time-limited response of target cell to the hormone (74).

Studies to target drug delivery to the brain via the insulin receptor have been reported. Murine 83-14 monoclonal antibody (mAb) that binds to the human insulin receptor was used for drug or gene delivery in rhesus monkeys. By using this mAb, radiolabelled

amyloid- $\beta$  peptide<sup>1-40</sup> serving as a diagnostic probe for Alzheimer's disease and PEGylated immunoliposomes containing plasmid DNA encoding for  $\beta$ -galactosidase were successfully synthesised by Pardridge and colleagues for delivery to the brain of primates. Unfortunately, immunogenic reactions were reported with 83-14 mAb thus ruling out its application in humans. Nevertheless, drug and gene delivery to the human brain via the insulin receptor can still be achieved with genetically engineered, effective forms of the mAb (73, 75).

#### 1.3.2.3.3 Lipoprotein receptor

The potential of lipoprotein receptors application in targeted drug delivery to the brain has been extensively explored during the past decades. Low density lipoprotein receptor-related protein 1 (LRP1) and LRP2 are among the lipoprotein family, that have been widely characterised. Both receptors are highly expressed at the blood-brain barrier and share a large number of substrates (76).

It was first reported by the group of Béliveau (76) that the transport of melanotransferrin (iron binding protein P97) across the blood-brain barrier was via transcytosis mediated by the LRP1 receptor. With this finding, Gabathuler *et al.* (77) conjugated doxorubicin (or adriamycin) to melanotransferrin and successfully delivered the drug to brain tumours in animal studies. This showed significant potential of melanotransferrin as an effective therapeutic drug targeting technology (NeuroTrans®) across the BBB. Another approach of protein-based drug delivery was also reported by Pan and co-workers (78) where receptor-associated protein (RAP) has been efficiently transferred across the blood–brain barrier by the LRP1 and LRP2 receptors.

In recent years, angiopep-2, (one of the 'angiopeps' of a series of 19 amino acid peptides) targeted to LRP1 receptor was developed by Demeule *et al.* (79, 80). Enhanced transcytosis across a brain endothelial monolayer system *in vitro* and improved brain uptake by *in situ* perfusion were demonstrated by angiopep-2. The research group of Béliveau (79, 80) conjugated 3 molecules of paclitaxel to angiopep-2 via cleavable ester linkages, yielding a drug-peptide conjugate namely ANG1005 which has been shown to have activity against subcutaneously implanted glioblastoma and

lung tumors, and to extend the survival of mice with intracerebral tumors (81). Further investigation by Thomas and co-workers (82) reported successful and significant increased uptake of paclitaxel in the form of ANG1005 into brain using *in situ* rat brain perfusion, which indicated the peptides vector, angiopep-2 as a promising drug delivery vehicle for the treatment of brain tumors.

#### 1.3.2.4 Adsorptive-mediated transcytosis

In adsorptive-mediated transcytosis, peptide/protein molecules with excess positive charges can bind to the negatively charged plasma membrane on the cell surface. The charge interaction between the molecules and the luminal cell surface of the endothelium cells directly induces endocytosis with the formation of vesicles and internalisation as in receptor-mediated transcytosis. Cationic peptides/proteins and cationised albumin that possess significant positive charges may be transcytosed via this pathway. The intactness of the molecules being transported generally depends on the lysosomal escape mechanism as described in section 1.3.2.3 (5, 43, 47).

#### 1.3.3 Therapeutic delivery across cellular barriers

Various approaches have been devised to enhance therapeutic delivery to cross the intestinal and the blood-brain barrier barriers. Chemical modification of drugs which involves either the addition of lipophilic moiety to increase the permeability across the lipid membrane via passive diffusion or the use of endogenous transport systems has shown enhanced delivery across the barriers. However, alteration of the drugs chemical structure might result in a decreased biological action. Thus, an improved understanding of transport mechanisms across these barriers certainly plays an important role in the design and development of drug delivery systems. In general, for an efficient drug delivery system to overcome cellular barriers, it must possess ideally most of the characteristics such as: (a) small molecular weight and hydrophilicity to passage via the paracellular diffusion pathway, (b) lipophilicity (balanced with optimal hydrophobicity for dissolution and to prevent back diffusion) for passive transcellular lipid pathway or passive diffusion, (c) ability to be transported via specific carrier-mediated mechanism,

(d) ability to circumvent efflux system, (e) ability to be transported via receptor or absorptive mechanism. Efficient drug delivery systems which involve drug carriers such as antibodies (7), liposomes (8), polymers (9) and dendrimers prodrugs (11, 83-87) have been widely investigated.

## 1.4 Dendrimers

The term dendrimer was coined in the early 1980s by Donald Tomalia from the Greek words 'dendron' which refers to tree and 'meros' which means parts, describing the tree-like branched structure of the macromolecules (88). As described, dendrimers are highly branched macromolecules which consist of three main components: (a) initiator core, (b) interior branches and (c) terminal groups with specific functionality (Figure 1-7). Interior cavities are formed due to the steric hindrance between the branches as well as the closely packed terminal groups (89).

Unlike classical linear and random coil polymers, dendrimers possess well defined architectures. Dendrimers are monodisperse macromolecules with large molecular weights and a high number of terminal groups. During the stepwise design of dendrimer, homo-structural layers are formed on the terminal groups starting from the core towards the outer periphery. Each homo-structural layer formed is termed as a generation. Thus, the initiator core is denoted generation 0 (G0), and a first generation (G1) dendrimer is synthesised after a homo-structural layer is formed on the terminal groups of the core (90). The size and shape of a dendrimer change with generation, for example, low generation polyamidoamine (PAMAM) dendrimers have a tertiary structure that is ellipsoidal while the structure of higher generation are spherical. Thus, distinct from linear polymers, dendrimers have a comparably lower hydrodynamic radius due to their spherical structure (91).

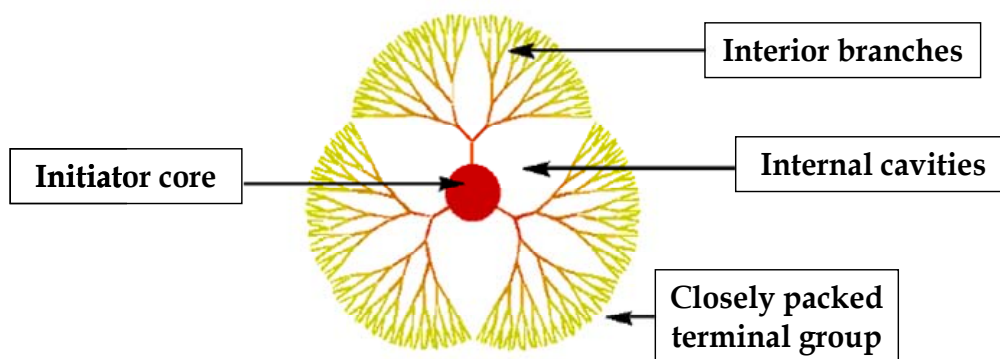


**Figure 1-7: Generic structure of a dendrimer molecule [taken from (92)].**

### 1.4.1 Synthesis of dendrimers

Dendrimers can be synthesised by two controlled stepwise approaches: (a) divergent synthesis and (b) convergent synthesis (Figure 1-8).

#### 1.4.1.1 Divergent synthesis

Divergent synthesis was first reported by Tomalia (88) and Newkome (93) in the 1980s. In this approach, the construction of the dendrimer originates from the initiator core in a stepwise manner and is built towards the outer periphery through a series of reaction and purification steps. The stepwise reactions are repeated for several generations until further reactions of the ends groups are prevented by steric hindrance (94). The dendrimer generation increases with each step, where each generation has its own individual properties, e.g. differences in size, shape, molecular weight and number of terminal functional groups.

This approach is relatively straight forward and is able to produce dendrimers with high molecular weight. However, synthesis of higher generations requires a higher number of reactions at each step. This is because more reaction sites are formed owing to the increasing number of terminal functional groups. At higher generations, synthesis problems such as intramolecular cyclisation and intermolecular coupling result in low

yield and imperfect structure (95). This leads to difficulties in purification and separation due to the similar properties and size of the dendrimer and its impurity (96). Polypropyleneimine (PPI) and PAMAM dendrimers are synthesised by this approach and are commercially available in the market.

#### 1.4.1.2 Convergent synthesis

In contrast to the divergent approach, convergent synthesis, reported by Fréchet and Hawker (97), starts from the periphery and builds towards the central core. Branching subunits (dendrons) are constructed and attached to the centre core by stepwise addition.

In the convergent approach, there are less reaction sites which reduce the number of side reactions. Hence the number of imperfect dendrimers is reduced, the purification and separation steps are simplified (96). Multifunctional dendrimers can be synthesised by attaching dendrons with different functional terminal groups to the dendrimer (97). A drawback of this approach is the limitation on the size and generation of dendrimers due to steric hindrance causing difficulties in final attachment (98).

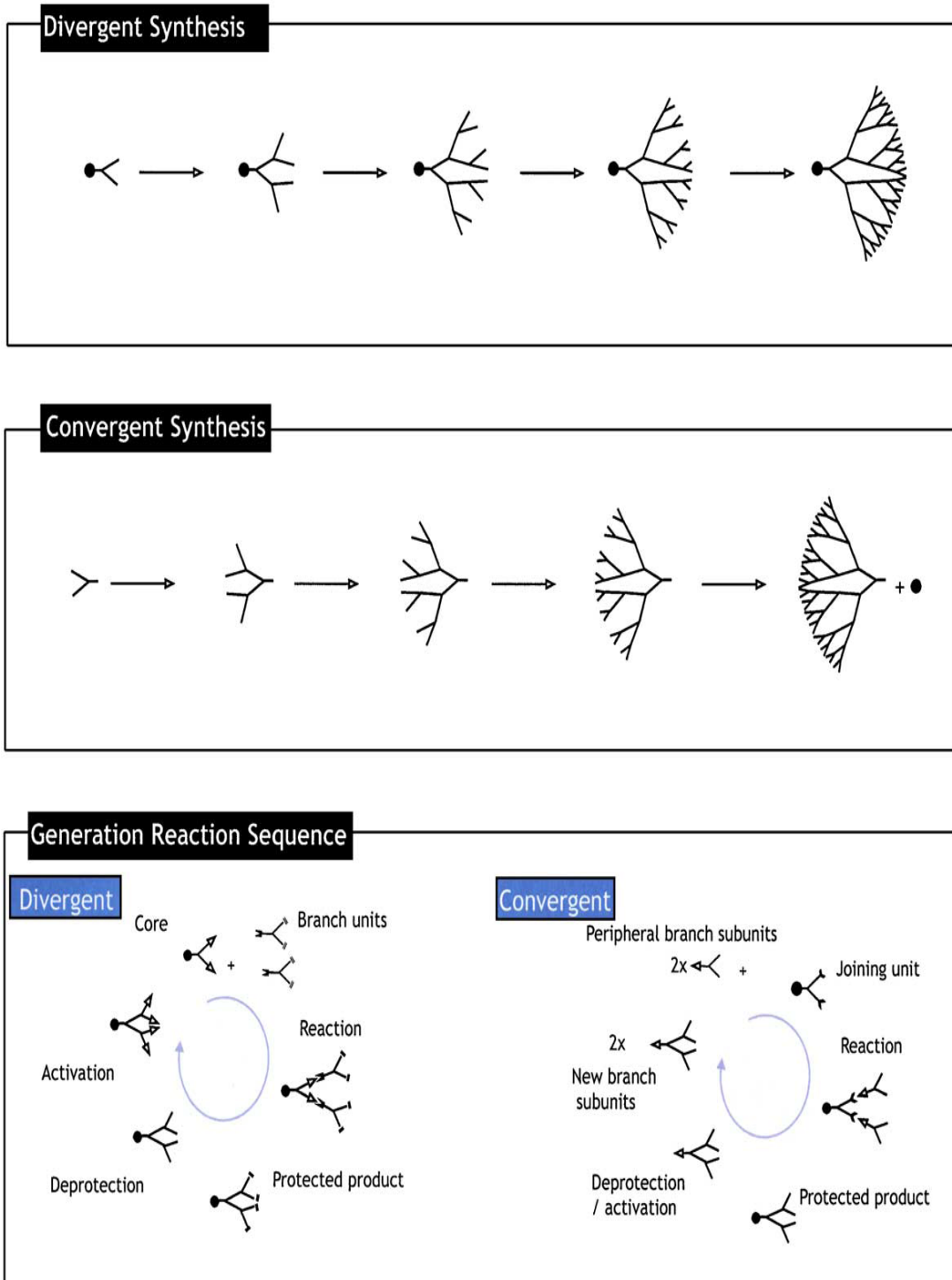


**Figure 1-8: Divergent and convergent syntheses of dendrimers [taken from (94)].**

## 1.4.2 Pharmaceutical applications of dendrimers

The potential pharmaceutical applications of dendrimers have been explored extensively due to their unique properties. Over the years, dendrimers have found use in many pharmaceutical applications such as enhancing drug solubility (99, 100), gene delivery (94, 101), drug encapsulation (88), magnetic resonance imaging (102), drug delivery system to enhance bioavailability (83, 86, 103) and targeted site delivery (104, 105).

With their spherical, three dimensional, highly uniform structure and low polydispersity, dendrimers have good stability and therefore should lead to predictable pharmacokinetic data, which are important parameters in the consideration of drug carriers (85, 86). The large number of surface groups which are amenable to different functionalities allow attachment of molecules which can enhance solubility (11, 84, 86, 87), enable target site delivery and lower cytotoxicity of a free drug (103, 106). Another attractive property is the high drug solubilisation capacity due to the availability of the terminal functional groups. Apart from the surface groups, the internal cavities created by the spherical dendritic structure allow encapsulation of drugs (10). More specific pharmaceutical applications of PAMAM dendrimers will be further discussed in detail in section 1.5.3.

## 1.5 Polyamidoamine (PAMAM) dendrimers

### 1.5.1 Synthesis of PAMAM dendrimers

PAMAM dendrimers are synthesised by the divergent approach, starting from an initiator core of ammonia or ethylenediamine (EDA). The synthesis follows a two-step reaction, as shown in Figure 1-9, firstly (a) a Michael addition of methyl acrylate to the amine group, which yields a half generation PAMAM with a carboxyl-terminated intermediate. This is followed by a second reaction (b) amidation of the carboxyl-terminated intermediate with EDA, which produces a full generation PAMAM (G0 – G10) (107).

In the synthesis of PAMAM, the divergent approach is favoured over the convergent approach due to self limiting growth of the dendrimers. At higher generations, steric

hindrance arises due to the high number of terminal groups; the reaction step of assembling the dendrons in a convergent approach becomes more difficult. Therefore, the divergent approach, which is able to yield higher generation number, is applied.

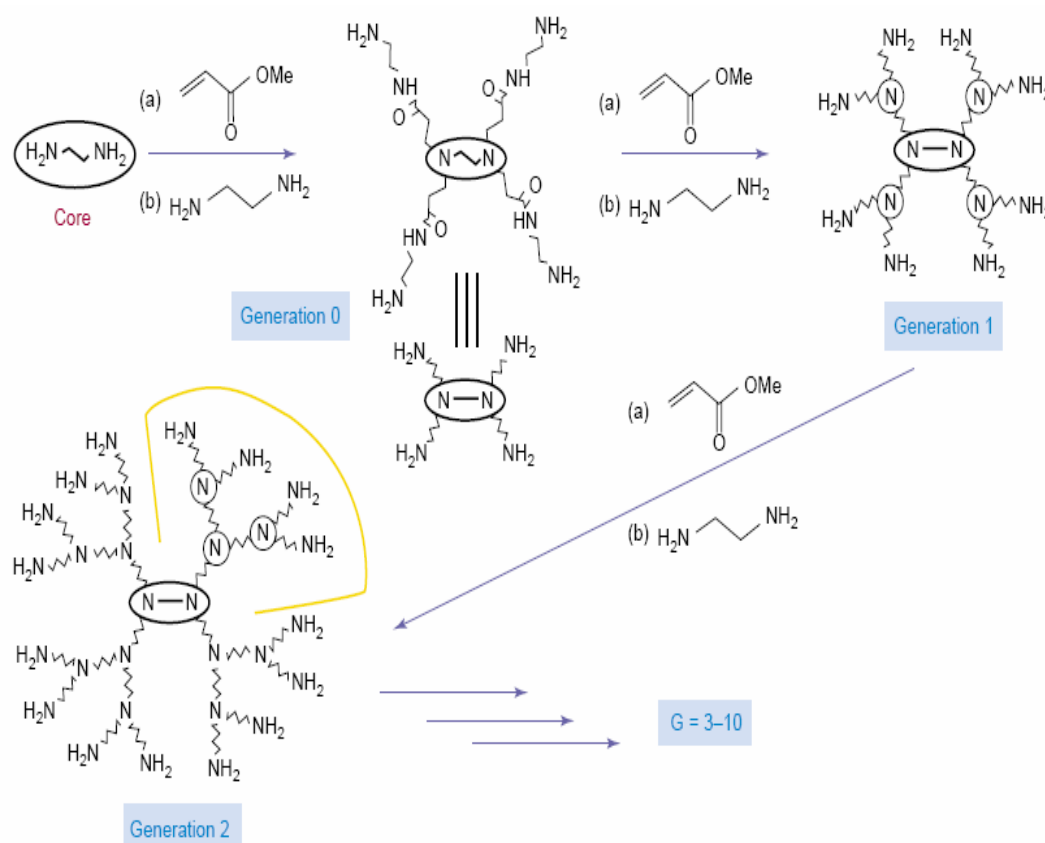


**Figure 1-9: Synthesis of PAMAM dendrimers [taken from (108)].**

### 1.5.2 Physicochemical properties of PAMAM dendrimers

As the generation of PAMAM dendrimers grows higher, the distinct features of the dendritic architecture and molecular properties become more obvious in terms of size, shape and molecular weight, number and functionality of surface terminal groups, density of the outer shell and internal cavities formed.

Computer-simulated modelling of the structure of PAMAM dendrimers showed that early generation (G0 – G3) PAMAM dendrimers have a range of open amorphous shapes and as the generation increases, PAMAM dendrimers grow to a more tangled spheroidal network, forming a globular shape for the higher generation of G4 – G7 (91). PAMAM dendrimers at the fourth generation and above are globular and the molecular dimension is comparable to a medium size protein. The internal cavities provide binding or encapsulating sites for free drug showing mimicry of liposome functionality in drug delivery application. Figure 1-10 shows a dimensionally scaled comparison of G4 – G7 PAMAM dendrimers with globular proteins and bio-assemblies (108).

The ionisable groups present on the surface and interior of PAMAM dendrimers result in pH driven conformation changes. Full generation PAMAM dendrimers were studied using computer simulation models. It was found that at low pH ( $\text{pH} \leq 4$ ), surface primary and interior tertiary amines were protonated, causing electrostatic repulsion between the positively charged ammonium groups which lead to an extended conformation. At neutral pH, hydrogen bonding occurred between the protonated surface primary amines and unprotonated tertiary amines; backfolding occurred leading to a denser dendrimer core. At higher pH ( $\text{pH} \geq 10$ ), as the charge of molecules becomes neutral, the dendrimer contracted and appeared in a more spherical structure with a loose compact network (109).

### 1.5.3 PAMAM dendrimers as drug carriers

PAMAM dendrimers have shown great potential as drug carriers due to their well-defined architecture. PAMAM dendrimers with amine (full generation) and carboxylic (half generation) as the surface functional groups can act as drug carriers by drug encapsulation within the internal cavities of the dendritic structure. Prodrugs can be synthesised by interacting free drugs or through linker molecules via electrostatic interaction or covalent bonds respectively, with the surface functional groups (10, 108).

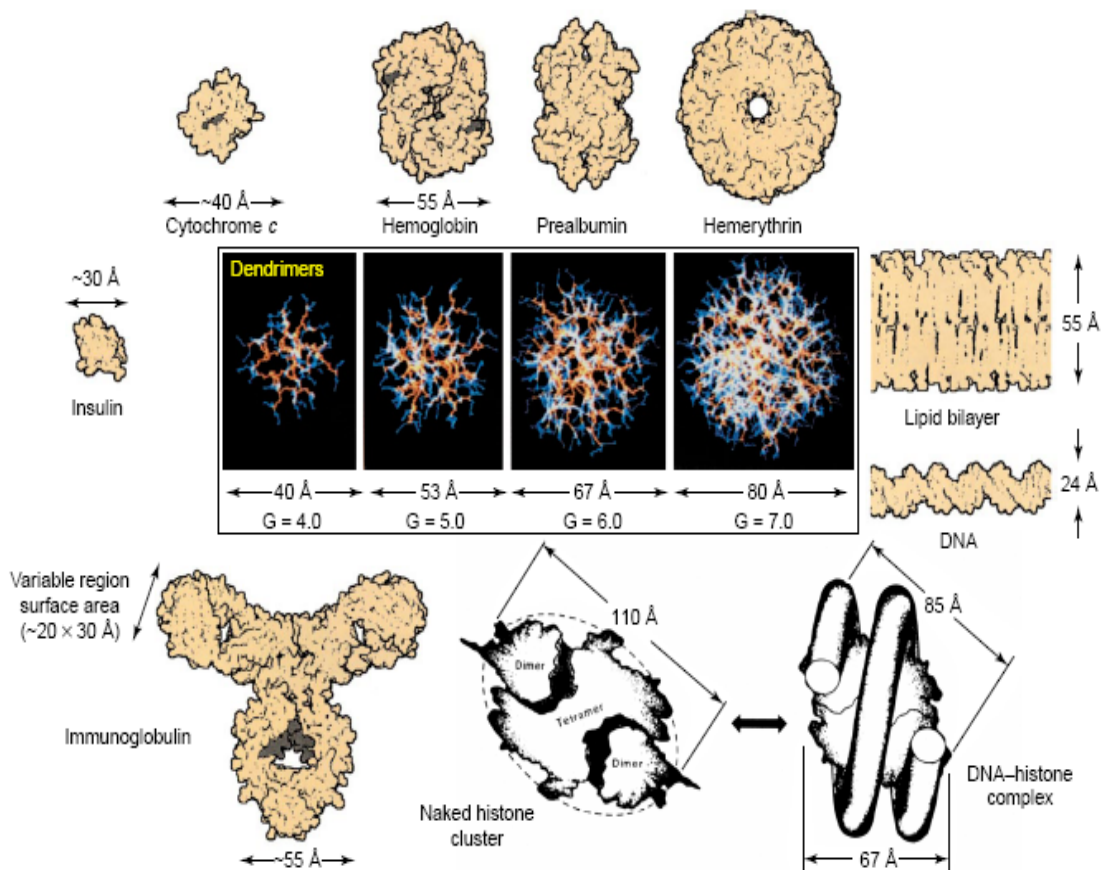


**Figure 1-10: A dimensionally scaled comparison of a series of PAMAM dendrimers (G4 – G7) with a variety of proteins, a typical lipid bilayer membrane and DNA, indicating the closely matched size and contours of important proteins and bioassemblies [taken from (108)].**

### 1.5.3.1 Drug encapsulation

PAMAM dendrimers, especially the higher generations (G3 – G5), have demonstrated the ability to encapsulate therapeutic agents in the internal cavities within the dendritic structure. The encapsulation ability is generally based on hydrophobic interactions, ionic interaction and physical entrapment (110). Successful non-covalent encapsulation of hydrophobic drugs into the PAMAM dendrimers has been established over the years.

PAMAM dendrimers have demonstrated the ability to enhance the solubility of low water insoluble drugs (107). Devarakonda and co-workers (111) studied the effect of G0

– G3 PAMAM dendrimers on the aqueous solubility of nifedipine, a low solubility calcium channel blocking agent. The solubility of nifedipine was found to be increased significantly when the drug was encapsulated and formed a complex with PAMAM dendrimers. The increasing order of drug solubility at pH 7 was  $G_{2.5} > G_3 > G_{1.5} > G_2 > G_{0.5} > G_1 > G_0$ , indicating that drug solubility depends on the size and type of surface functional groups. The greatest solubility increase of nifedipine was observed in the presence of half generation PAMAM dendrimer at pH 7 compared to pH 4 and pH 10. The dependence of nifedipine solubility on pH leads to a potential of pH dependant controlled-release drug delivery system design.

Further studies were carried out by Devarakonda *et al.* (112) to investigate the effect of PAMAM dendrimers on the aqueous solubility and *in vitro* cytotoxicity of a poorly soluble drug, paclitaxel. Up to 16 molecules of paclitaxel were successfully formed complexes with both G3 and G5 PAMAM dendrimers. The aqueous solubility of paclitaxel was found to increase significantly with increasing dendrimer concentration. The cytotoxicity of free paclitaxel and dendrimer-paclitaxel complexes was compared and studied using prostate cancer cells (PC-3M). A significantly higher percentage of cell death was observed with the cells treated with dendrimer-paclitaxel complexes. The enhanced cytotoxic effect of the complexes could be due to the increased solubility of the drug and/or cellular uptake of the complexes by the cancer cells.

Charge complexation and encapsulation of ibuprofen to PAMAM dendrimers has been reported by Milhem *et al.* (99), Kolhe *et al.* (113) and Kannan *et al.* (114). Milhem *et al.* (99) found that the solubility of the hydrophobic drug ibuprofen was significantly increased in PAMAM G4 dendrimer solutions. The solubility was directly proportional to dendrimer concentration. Kolhe *et al.* (113) suggested that formation of complex was due to the ionic interaction between the amine end groups of PAMAM dendrimer and carboxylic group of ibuprofen. Kannan *et al.* (114) found that the number of ibuprofen molecules forming ionic complexes with dendrimers was charge and size dependent of the dendrimers. Both Kolhe *et al.* (113) and Kannan *et al.* (114) studied the cellular entry of the dendrimer-ibuprofen complex into A549 human lung epithelial carcinoma cells. A higher and rapid cellular entry of the dendrimer-ibuprofen complex (more than 80%) into the A549 cells was obtained compared to the free ibuprofen (40%) within 1 h. The same group also reported high payloads of drug when complexed with PAMAM

dendrimers (up to 78 drug molecules), suggesting the PAMAM dendrimers can act as efficient drug carriers and facilitate rapid cellular entry of ibuprofen.

Ke and co-workers (115) successfully incorporated doxorubicin, a P-gp substrate and drug with poor bioavailability into G3 PAMAM dendrimers. The doxorubicin-PAMAM complex demonstrated time and concentration dependent cellular uptake by Caco-2 cells. Drug transport from the mucosal side to the serosal side in different segments of the small intestine of rats was significantly improved with the drug-dendrimer complex compared to the free drug. Higher bioavailability was obtained by doxorubicin-PAMAM complex indicating that drug-dendrimer complex may represent a potential oral delivery system.

### 1.5.3.2 PAMAM-drug conjugates

The potential of PAMAM dendrimers to act as a drug carrier has been further developed by direct covalent conjugation of drug molecules to the dendrimer surface or via biodegradable spacers/linkers. In addition, PAMAM dendrimers with the amenable terminal functional groups can be surface engineered for specific applications, e.g. enhancement of drug solubility and permeability, and targeted delivery.

Jevprasesphant *et al.* (103) found that the properties of PAMAM dendrimer such as solubility, cytotoxicity and permeation across Caco-2 cells, were changed significantly when surface engineered with lauroyl chains. Surface modified cationic PAMAM dendrimers (G2, G3 and G4) displayed reduced cytotoxicity and enhanced permeability across Caco-2 cell monolayers. It was reported that the transport of dendrimers and conjugates across Caco-2 cell monolayers involved both paracellular and transcellular pathways. Dendrimers provided better delivery as they not only enhanced transcellular transport but also enhanced paracellular transport by opening up the tight junctions (84, 103). These findings suggested that surface engineered PAMAM dendrimers can be used as effective drug delivery systems.

Studies were carried out by the same group (83) to develop a dendrimer based drug delivery system to enhance oral bioavailability. Propranolol (P), a low solubility and P-

glycoprotein (P-gp) efflux transporter substrate drug was conjugated covalently to surface modified and unmodified PAMAM dendrimers. The solubility of propranolol was increased by at least two orders of magnitude when conjugated to surface modified dendrimers. Propranolol conjugates with both surface modified and unmodified PAMAM dendrimers demonstrated the ability to bypass P-gp efflux in Caco-2 monolayers. Interestingly, propranolol conjugates with lauryl modified PAMAM dendrimers gives a higher apical (A) to basolateral (B) apparent permeability coefficient ( $P_{app}$ ) than the conjugates with unmodified dendrimers, with G3L6-P showing highest  $P_{app}$ . These findings demonstrate the potential application of dendrimer nanocarriers as a drug delivery system for low solubility and P-gp substrate drugs.

Khandare and co-workers (116) reported the conjugation of methylprednisolone to G4-OH PAMAM dendrimers via glutaric acid as a spacer. Methylprednisolone-glutaric acid was first prepared and subsequently conjugated to the PAMAM-OH dendrimers. A high payload dendrimer-drug conjugate (12 molecules of methylprednisolone per dendrimer) had been successfully synthesised due to lower steric hindrance at the dendrimer surface and higher stability and reactivity of methylprednisolone. In addition, the conjugates were fluorescently labelled with fluorescein isothiocyanate (FITC) for the dynamic studies on cellular entry using A549 human lung epithelial carcinoma cells. It was found that over the study period, the conjugates were localised primarily in the cytosol and showed comparable therapeutic activity to the free drug.

Khandare *et al.* (117) further reported the conjugation of the chemotherapeutic drug paclitaxel to G4-OH PAMAM dendrimers via a succinic acid spacer. *In vitro* cytotoxicity studies of the conjugates using A2780 human ovarian carcinoma cells showed a 10-fold increase in cytotoxicity by G4-OH-succinic acid-paclitaxel conjugates when compared with free drug. Applications of PAMAM dendrimers as drug carrier for paclitaxel were studied by several researcher groups. Majoros and co-workers (105) had synthesised a partially acetylated G5 PAMAM dendrimer conjugated with paclitaxel, folic acid and labelled with FITC. The function of the partial acetylation was to prevent nonspecific targeting interactions while conjugation of folic acid was for targeting the over-expressed folate receptors on specific cancer cells. *In vitro* targeted delivery of the dendrimer conjugates was investigated using KB cells (Human epidermoid carcinoma cells that over-express the folate receptor). Flow cytometry analysis found that only KB

cells with up-regulated folic acid receptors (KB+) treated with dendrimer conjugates showed green fluorescence and cytotoxicity study using XTT assay showed that only KB+ were sensitive to the cytotoxicity effect of the dendrimer conjugates at 100 nM. While KB cells with down-regulated folic acid receptors (KB-) remained viable and comparable to untreated cells. These results indicated uptake and specific delivery of the dendrimer conjugates. Bi *et al.* (118) also synthesised similar dendrimer conjugates as developed by Majoros *et al.* (105) and studied the stability of the conjugates. Two linkers, succinic acid and glutaric acid were employed to attach paclitaxel to dendrimer. The kinetic study of the hydrolysis of the dendrimer conjugates with succinic linker showed that paclitaxel was released through ester bond hydrolysis in a time-dependent manner with a 10 h half life in PBS buffer (pH 7.4) while no significant paclitaxel hydrolysis was observed for dendrimer conjugates with glutaric linker after 7 days.

Najlah *et al.* (85, 87) reported the synthesis and *in vitro* evaluation of dendrimer prodrugs for oral delivery. Naproxen (nap), a low aqueous solubility drug, was conjugated either directly to G0 PAMAM dendrimers or via a linker, L-lactic acid (lac) or diethylene glycol (deg). G0-nap prodrug formed by a direct amide covalent bond, demonstrated high stability in plasma and liver homogenate and was therefore unsuitable for prodrug development. The advantages of using a linker in the synthesis of prodrugs were observed with G0-lac-nap and G0-deg-nap prodrugs. G0-lac-nap prodrug has a high stability in plasma with slow hydrolysis in liver homogenate, suggesting potential application in controlled release systems. G0-deg-nap prodrug demonstrated high chemical stability but readily released drug in plasma and liver homogenate, thus a potential candidate for poorly soluble drugs (85). Cytotoxicity studies showed that G0 PAMAM dendrimers and conjugates were not toxic toward Caco-2 monolayers. From permeability studies, naproxen transport was shown to increase in both directions when the drug was conjugated to G0 dendrimer. When a lauryl chain was attached to the dendrimer surface, a higher increase in naproxen transport was observed. These results illustrated the potential of G0 PAMAM dendrimers as nanocarriers for enhancing oral bioavailability.

Further studies were carried out by Najlah *et al.* (86) who synthesised G1 PAMAM dendrimer prodrugs and assessed their enhancement of the cellular permeability of P-gp substrates. In this study, terfenadine (Ter), a water-insoluble P-gp substrate drug was

conjugated to G1 PAMAM dendrimers using biodegradable linkers, succinic acid (suc) and deg. G1–Ter conjugates with a covalent linkage displayed a significant increase of terfenadine transport across Caco-2 monolayers compared to the unchanged terfenadine transport profile in the presence of G1 PAMAM dendrimer in the transport medium. When G1 PAMAM dendrimers were modified with lauryl chains, a more pronounced increase in terfenadine transport was observed with the prodrugs. These findings are in agreement with previous work by the same group (85, 87, 103, 106).

Several other studies have been carried out to explore the potential of PAMAM dendrimers for gene delivery to the brain. Huang and co-workers (119) investigated the cellular and brain uptake of brain-targeting gene vector based on PAMAM dendrimers, *in vitro* and *in vivo*. PAMAM-PEG-Tf conjugate was synthesised by conjugating brain-targeting ligand, transferrin (Tf) to PAMAM via polyethylene glycol (PEG). Cellular uptake studies of the conjugate were reported to be concentration dependent and a 2.25 fold increase of brain uptake was observed when compared to PAMAM and PAMAM-PEG *in vivo*. The transfection efficiency of PAMAM-PEG-Tf/DNA complex was reported to be significantly higher than PAMAM/DNA and PAMAM-PEG/DNA complexes in brain capillary cells. The brain gene expression of the complex with Tf (PAMAM-PEG-Tf/DNA) was found to be 2 fold higher than those without Tf (PAMAM/DNA and PAMAM-PEG/DNA). Similar studies were conducted using the PAMAM-based conjugate synthesised with lactoferrin (Lf) as the brain-targeting ligand (120). It was found that Lf-conjugate/complex demonstrated significantly increased brain uptake, transfection efficiency, and brain gene expression compared to that of Tf-conjugate/complex. These results suggest that PAMAM-PEG conjugated with the Tf or Lf ligand offer a promising nonviral approach for gene delivery to brain via non-invasive administration. It can be concluded from these reviews that PAMAM dendrimers has the potential to act as nanocarriers for delivery across the cellular barriers.

## 1.6 Characterisation techniques

### 1.6.1 Thin layer chromatography (TLC)

Thin layer chromatography is a chromatographic technique widely used for organic compound separation. TLC is often used to monitor the progress of organic reactions and purity of products due to the simplicity and rapidity of the technique (121).

Thin-layer chromatography consists of a stationary phase, a mobile liquid phase, and a developing chamber. The stationary phase is a TLC plate of glass, metal or plastic coated with a thin layer of solid absorbent (usually silica or alumina). A small amount of the sample mixture, either liquid or dissolved in a volatile solvent, is deposited as a spot at 1-2 cm from the bottom of the TLC plate. The components of a sample can be identified by running standards with the unknown simultaneously. This plate is then placed in a developing chamber which contains a shallow pool of the mobile phase (comprising one or more miscible solvents) (121).

The mobile phase moves up the plate by capillary action. When the solvent front reaches about  $\frac{3}{4}$  distances up the plate, the plate is removed and dried. The separated spots are visualized with ultraviolet light or by placing the plate in iodine vapour (121). The different components in the mixture move up the plate at different rates due to differences in their partitioning behaviour between the mobile phase and the stationary phase. Figure 1-11 illustrated the TLC technique.

The retention factor ( $R_f$ ) is defined as the distance travelled by the compound ( $D_{\text{sample}}$ ) divided by the distance travelled by the solvent ( $D_{\text{mobile phase}}$ ).

$$R_f = D_{\text{sample}} / D_{\text{mobile phase}}$$

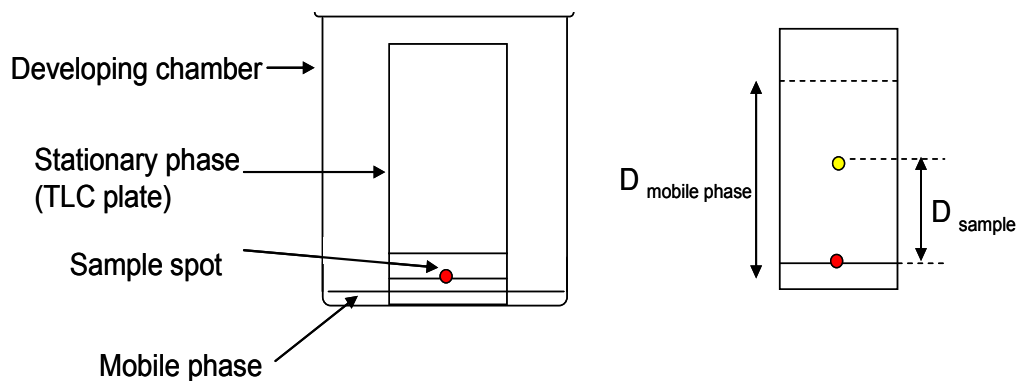


**Figure 1-11: Schematic diagram of TLC and measurement of  $R_f$ .**

### 1.6.2 Nuclear magnetic resonance (NMR) spectroscopy

Nuclear magnetic resonance (NMR) spectroscopy is a pre-eminent technique to determine the structure of organic and inorganic compounds. It is an absorption spectrometry based on the quantum mechanical magnetic properties of an atom's nucleus having a nuclear spin ( $I$ ) in the presence of an applied magnetic field (122).

In general, a sample is dissolved in a solvent which itself does not give rise to an NMR signal that can interfere with the signals of the sample in the spectrum, and then lowered into a sample chamber applied with a homogeneous magnetic field. When the frequencies of the nuclei, e.g.  $^1\text{H}$  and  $^{13}\text{C}$  (most commonly used), are in resonance with the applied radio frequency, the nuclear spin will be promoted from the low energy state (parallel to the field) to the high energy state (anti-parallel). A receiver records the changes in magnetic moment as the nuclei relax back to an equilibrium state. Fourier Transform of the data gives the different frequencies of the nuclei in different electrical environments in the sample. The spectrometer will then record and plot the spectrum as absorption against the frequency (122).

The frequencies are measured as a relative difference from an internal standard, usually tetramethylsilane (TMS). The position of the relative difference to TMS is called chemical shift ( $\delta$ ), and is measured in parts per million (ppm).

### 1.6.3 Mass spectrometry (MS)

Mass spectrometry is an analytical method used to identify a compound or sample chemical composition based on the mass-to-charge ( $m/z$ ) ratios of the charged particles generated by the spectrometer. A mass spectrometer can be separated into three fundamental parts: ionisation source, mass analyser, and detector (122).

Sample is introduced into the ionisation source of the instrument in the vapour phase. The sample molecules are ionised by accelerated electrons generated in the ionisation chamber. These ions are extracted into the mass analyser region where they are deflected and separated according to their  $m/z$  ratios. Lastly, the separated ions are detected; their relative abundances are recorded and plotted against their  $m/z$  values in the format of a  $m/z$  spectrum. There are many different types of ionisation sources, mass analysers and detectors that can be used for different mass spectrometers depending on the type of sample under investigation (122).

Figure 1-12 illustrates a simplified schematic of mass spectrometer with different available fundamental parts. The ionisation source, analyser and detector need to be maintained under high vacuum to allow the ions to travel from one end of the instrument to the other without any hindrance from air molecules.

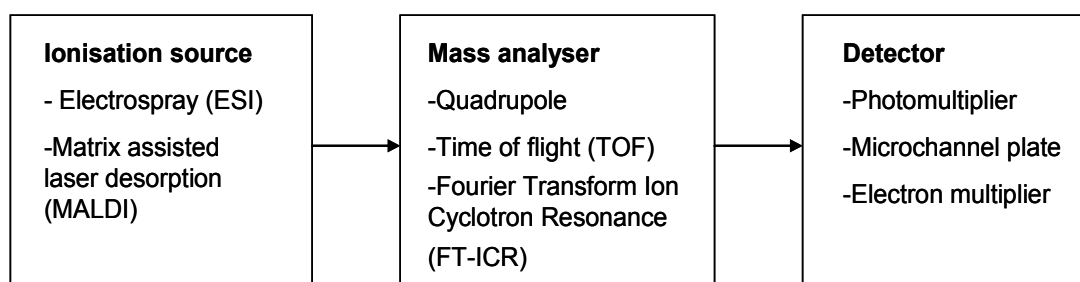


**Figure 1-12: A simplified schematic of a mass spectrometer.**

#### 1.6.4 High performance liquid chromatography (HPLC)

HPLC is a chromatographic technique that has been widely used to separate, identify, quantify and purify the individual components of a mixture of compounds (biological or chemical molecules). Separation of molecules is based on different distribution of size and charge and the interaction between the stationary and mobile phase in the system (123, 124).

The components of a basic HPLC system consist of a solvent reservoir, pump, injector, column, detector and waste reservoir (Figure 1-13). In general, solvent/eluent (mobile phase) is propelled by the high pressure generated by the pump through a densely packed column (stationary phase). In reverse-phase high performance liquid chromatography (RP-HPLC), a high polar mobile phase and a non-polar hydrocarbon stationary phase is used. The sample (analyte) is introduced by the injector into the continuously flowing mobile phase stream that carries the sample into the HPLC column. Individual components of the sample are separated during their migration through the stationary and mobile phase. Analytes eluted from the column will be analysed by the detector that provides a characteristic retention time. Analyte retention time varies with factors such as the strength of its interactions with the stationary phase, the type and the ratio/composition of solvent(s) used, and the flow rate of the mobile phase. The mobile phase that exits the detector will be sent to waste. The qualitative analysis is determined by the retention time while the quantitative analysis is determined by the peak area or height in comparison with reference standards (124).

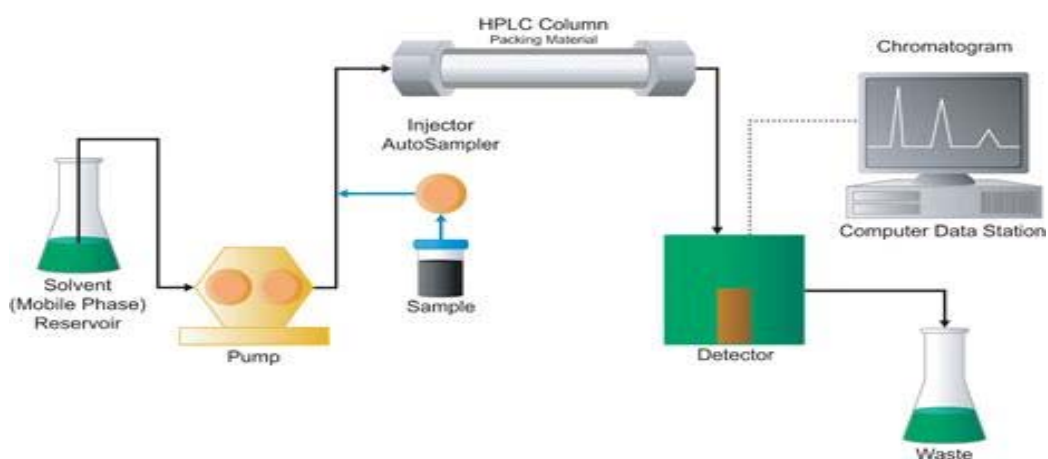


**Figure 1-13: Schematic diagram of HPLC instrumentation [taken from (125)].**

## 1.7 Cell lines and cell culture

### 1.7.1 Intestinal barriers *in vitro* cell model

For the investigation of *in vitro* drug absorption across intestinal cell barriers, morphological and functional properties similar to those of normal human small intestine are generally the main criteria for the selection of a cell culture model. In this study, Caco-2 cells were used as an *in vitro* cell culture model to investigate the transport of dendrimer-based drug carrier across the intestinal barrier as it has been commonly used as a cell model for dendrimer uptake (11, 83, 84, 86, 87, 103, 106).

Although Caco-2 cells are derived from the human colon carcinoma, the cells become differentiated and polarized such that their phenotype, morphologically and functionally, resembles the small intestine enterocytes when cultured under specific conditions (126). Caco-2 cells closely resemble small intestine enterocytes characteristic with the expression of tight junctions, microvillus, and a number of enzymes (peptidases, esterases) and transporters (P-glycoprotein, uptake transporters for amino acids, bile acids and carboxylic acids) (127-129). However, one of the limitations displayed by Caco-2 cells is its high TEER value which is similar to value in colon rather than that in the small intestine. This is due to their origin from colon carcinoma cells (126, 130). Despite this limitation, good correlation between the *in vitro* apparent permeability coefficient ( $P_{app}$ ) across Caco-2 monolayers and the *in vivo* fraction absorbed ( $f_a$ ) has been well established, thus making Caco-2 cell a widely used *in vitro* cell culture model for studies of intestinal drug absorption (131).

### 1.7.2 Blood-brain barrier *in vitro* cell lines and cell culture models

Numerous attempts have been made to develop well-characterised *in vitro* models that can be used to examine and to further understand the transport mechanisms across the blood-brain barrier (58). To date, *in vitro* endothelial cell culture models or cell lines have been the most useful model to study the BBB mechanisms at the cellular and molecular level (58). However, no specific *in vitro* BBB model has yet been accepted as an 'industrial standard'. The selection of cell culture model in experiments are usually a

compromise between the application, convenience, availability of resource, cost, time and how closely a model needs to resemble the *in vivo* conditions (32, 45). A variety of BBB *in vitro* cell models including immortalised cell lines and primary cultures have been developed and characterised to predict the BBB permeability (58, 132).

### 1.7.2.1 Immortalised brain endothelial cell lines

Immortalised brain endothelial cell lines were developed by transfection of pure brain endothelial cells. Rat and mouse brain, in particular, received most attention to be developed into cell lines due to their general application as small laboratory animals in many *in vivo* BBB studies. Therefore, rat brain endothelial (RBE) cell culture systems have been developed to provide more information for *in vitro* and *in vivo* correlation (133).

Immortalised BBB cell models such as transgenic rats TR-BBB (134) and RBE4 cell lines (133), have been developed and widely characterised. Immortalised cell lines are generally useful in examining transport mechanism and cell-cell interaction as they retain the expression of many typical endothelial markers (45). However, a great drawback found with characterisation studies of these immortalised BBB cell lines (e.g. TR-BBB cell lines) was that they generally form an insufficiently tight barrier for use in permeability studies (132-134).

### 1.7.2.2 Primary brain endothelial cultures

In general, bovine and porcine tissues have been utilised as source for primary brain endothelial cell cultures due to the brain size and availability. Primary cultures of microvessel endothelial cells from brain tissue have been generated by a series of cell isolation procedures which include enzymatic digestion, filtration, centrifugation, differential adhesion on different matrices, and techniques to kill contaminants in order to obtain maximum yield and purity and to eliminate fast-growing contaminating cells. Contaminating cells are mainly pericytes, fibroblast and smooth muscle cells (58).

Primary or low passage cell cultures were found to retain several morphological and biochemical properties of the BBB *in vivo* phenotype, including endothelial enzymes, transporters, receptors and complex tight junctions (45). Primary cultured bovine brain microvessel endothelial cells (BBMECs) and primary porcine brain microvessel endothelial cells (PBMECs) are among the most well established primary cultures.

#### 1.7.2.2.1 Porcine Brain Endothelial Cells (PBECs)

The use of primary porcine brain microvessel endothelial cells (PBMECs) has been assessed by several research groups (135-137) for *in vitro* permeability studies. It was suggested that the PBMEC model might provide a more restrictive paracellular pathway compared to the BBMEC model (135).

Recently, Zhang *et. al.* (132) have developed, characterised and evaluated the use of PBMECs as an *in vitro* model to predict the blood-brain barrier (BBB) permeability *in vivo*. It was reported that higher TEER values of 300 – 550  $\Omega\cdot\text{cm}^2$  were achieved than those of previously reported BBMVECs (80 – 140  $\Omega\cdot\text{cm}^2$ ) (138) and in-house observation TR-BBB (5 – 20  $\Omega\cdot\text{cm}^2$ ) (132). It has been showed that higher TEER values were achievable by brain endothelial cells when co-culturing with astrocyte-conditioned medium (36, 139-141). However, Zhang and co-workers (132) reported unchanged sucrose permeability across the PBMEC model. The expression of the mRNA of several BBB uptake and efflux transporters (GLUT1, LAT1, MRP1, MRP4, MRP5, P-gp, and BCRP) was observed with the cell cultured. Study of functional activity also suggested that P-gp was functionally active and was predominantly located on the apical membrane. Moreover, PBMEC model was reported to take shorter times (5 – 6 days) to reach confluency compared to BBMEC which needed 10 – 12 days.

PBMEC model maintains the complexities of the *in vivo* BBB and demonstrates strong and significant quantitative correlations between the *in vitro* and *in situ* permeability (132), indicating that the PBMEC model can be used as an effective *in vitro* model to study the BBB permeability.

## 1.8 Aims and objectives

Working hypothesis: Is it possible to develop dendrimer-based delivery to overcome cellular barriers during drug delivery?

The development of effective drug delivery system to overcome the cellular barriers has been a major challenge for oral drug delivery as well as drug delivery to the CNS for the management of many CNS diseases. One of the key problems encountered is limited drug entry, especially drugs that are P-gp substrates (e.g. paclitaxel) across the intestinal and blood-brain barriers. The main aim of this study was to develop dendrimer-based drug delivery systems to overcome these cellular barriers.

The specific objectives of study are:

- to synthesise and characterise dendrimer-based drug delivery systems using G3 PAMAM dendrimer to enhance cellular permeability of paclitaxel, a poorly soluble drug and substrate of P-gp efflux transporter.
- to determine the cytotoxicity of G3 PAMAM dendrimer-based drug delivery systems on Caco-2 cells using the LDH assay and determination of  $IC_{50}$  values.
- to examine the permeation of G3 PAMAM dendrimer-based drug delivery systems across the Caco-2 cell monolayers.
- to determine the cytotoxicity of G3 PAMAM dendrimer-based drug delivery systems on porcine brain endothelial cells (PBECS) using the LDH assay and determination of  $IC_{50}$  values.
- to investigate the potential of G3 PAMAM dendrimer to act as a drug carrier for paclitaxel to bypass P-gp transporters, using PBECS as the blood-brain barrier cell model.
- to examine the influence of surface modification of G3 PAMAM dendrimer with lauryl chains as permeability enhancer on the cytotoxicity and permeability of the resulting dendrimer-based drug delivery systems.

**CHAPTER 2: SYNTHESIS AND CHARACTERISATION OF G3  
PAMAM DENDRIMER AND DRUG CONJUGATES**

---

## 2.1 Introduction

Over the years, numerous attempts have been explored to devise therapeutic delivery systems able to cross the cellular barriers for efficient drug delivery (4). Problems encountered during drug delivery are normally associated with low solubility and permeability of therapeutic drugs (4). Efflux transporter systems (e.g. P-gp efflux transporter) actively function at cellular barriers and limit drugs which are substrates from transport across the barrier. Chemical modification is one of the strategies to enhance permeability and solubility of drugs for more efficient delivery. Addition of lipophilic components to drugs and conjugation of drugs to a carrier with high solubility or carrier which can bypass the P-gp system have been shown to demonstrate higher permeation across the cellular barriers (4).

In this study, paclitaxel was selected as the model drug and a P-gp substrate with poor water solubility. It represents a new class of antimicrotubule anticancer drugs which has been shown experimentally to have antitumor activity (142, 143). Paclitaxel has been reported to demonstrate remarkable efficacy against ovarian and breast cancer and more recently, against malignant gliomas and brain metastases (24). However, pharmaceutical applications of paclitaxel are greatly limited by its low solubility as well as low permeability across cellular barriers due to exclusion by the P-gp efflux transport system present in cellular barriers, e.g. the intestinal and the blood-brain barriers.

Dendrimers with their unique properties and characteristics have been of great interest for pharmaceutical applications for the encapsulation/ solubilisation of drugs and conjugation of drugs for transepithelial transport (83). They are highly branched polymers with a high degree of uniformity and monodispersity. The surface groups of dendrimers can be engineered to specific functionality. G3 PAMAM dendrimer was reported to bypass the P-gp efflux transporter and enhance permeability of P-gp substrate drug with low water solubility (e.g. propranolol and terfenadine) (83). Surface engineered PAMAM dendrimers with lauryl chains demonstrated enhanced permeability and lower cytotoxicity compared to unmodified dendrimers (103, 106).

In this chapter of the study, a third generation (G3) polyamidoamine (PAMAM) dendrimer-based drug delivery system to enhance the permeability of paclitaxel and to overcome the cellular barriers (e.g. the intestinal barrier and the blood-brain barrier) was synthesised and characterised. G3 PAMAM dendrimers were conjugated with lauryl chains at 1:3, 1:6 and 1:9 molar ratios. Paclitaxel was conjugated to G3 and/or lauryl-G3 dendrimer conjugates via a glutaric anhydride linker by using the N-hydroxysuccinimide (NHS) active ester method. Unmodified G3 PAMAM dendrimer and all the dendrimer conjugates (lauryl-G3 and G3-drug conjugates) were labelled with fluorescein isothiocyanate (FITC) for quantitative detection by spectrofluorimetry in permeability studies. These conjugates were characterised using various techniques including thin layer chromatography (TLC), proton ( $^1\text{H}$ ) and carbon ( $^{13}\text{C}$ ) nuclear magnetic resonance (NMR), electrospray ionisation-mass spectrometry (ESI-MS) and dynamic light scattering. Chemical stability of the dendrimer conjugate was studied in buffer at three different pHs: pH 1.2 (hydrochloric acid buffer), pH 7.4 (phosphate buffer), and pH 8.5 (borate buffer) at  $37^\circ\text{C}$ .

## 2.2 Materials and methods

### 2.2.1 Materials

G3 PAMAM dendrimer with an ethylenediamine core (20% w/w in methanol) was purchased from Dendritech Inc. 1-dodecanol, 4-nitrophenyl chloroformate, triethylamine (TEA), Sephadex LH20 (bead size: 40-120  $\mu\text{m}$ ), diphenyl phosphoryl chloride (DPC), N-hydroxysuccinimide (NHS), fluorescein isothiocyanate (FITC) 98%, dimethyl sulfoxide (DMSO), sodium chloride (NaCl), disodium hydrogen phosphate ( $\text{Na}_2\text{HPO}_4$ ), sodium dihydrogen phosphate ( $\text{NaH}_2\text{PO}_4$ ), glutaric anhydride, pyridine, magnesium sulphate ( $\text{MgSO}_4$ ), potassium chloride (KCl), hydrochloric acid (HCl), dipotassium hydrogen phosphate ( $\text{K}_2\text{HPO}_4$ ), potassium dihydrogen phosphate ( $\text{KH}_2\text{PO}_4$ ), sodium tetraborate decahydrate ( $\text{Na}_2\text{B}_4\text{O}_7 \cdot 10\text{H}_2\text{O}$ ), boric acid ( $\text{H}_3\text{BO}_3$ ), phenanthrene, and trifluoroacetic acid (TFA) were purchased from Sigma-Aldrich Co. Ltd. (Gillingham, Dorset, UK). Tetrahydrofuran (THF), hexane, dimethylformamide anhydrous (DMF), methanol, dialysis membrane (Spectra/Por® 7, 1000 Dalton molecular weight cut-off, MWCO), membrane filter (Millex pore size 0.45 $\mu\text{m}$ ), chloroform, ammonium hydroxide, dichloromethane (DCM), and ethyl acetate (EtOAc) were purchased from Fisher Scientific UK Ltd (Loughborough, UK). Paclitaxel was purchased from Advance Tech. & Ind. Co., Ltd. (Kln, Hong Kong). Diethyl ether and silica gel for flash chromatography were purchased from BDH Laboratory Supplies (Lutterworth, UK).

### 2.2.2 Synthesis of lauryl-G3 PAMAM dendrimers

G3 PAMAM dendrimers modified with lauryl chains were expressed as G3-L<sub>x</sub> with x being the average number of lauryl chains per dendrimer. Lauryl chains were attached covalently to the surface of G3 PAMAM dendrimers as described by Najlah *et al.* (86). The lauryl chain was activated to form lauryl 4-nitrophenyl carbonate, which was then reacted with the surface amine groups of G3 PAMAM dendrimers.

### 2.2.2.1 Synthesis of lauryl 4-nitrophenyl carbonate

Lauryl alcohol (1-dodecanol) (1.86 g, 10 mmol) was dissolved in anhydrous THF (5 ml) and TEA (2.02 g, 20 mmol) was added. The mixture was stirred for 10 min and 4-nitrophenyl chloroformate (4.03 g, 20 mmol) in THF (2 ml) was added portion wise over 4-5 h, followed by stirring for 24 h at room temperature under a nitrogen flow. Figure 2-1 showed the reaction scheme for the synthesis of lauryl 4-nitrophenyl carbonate.

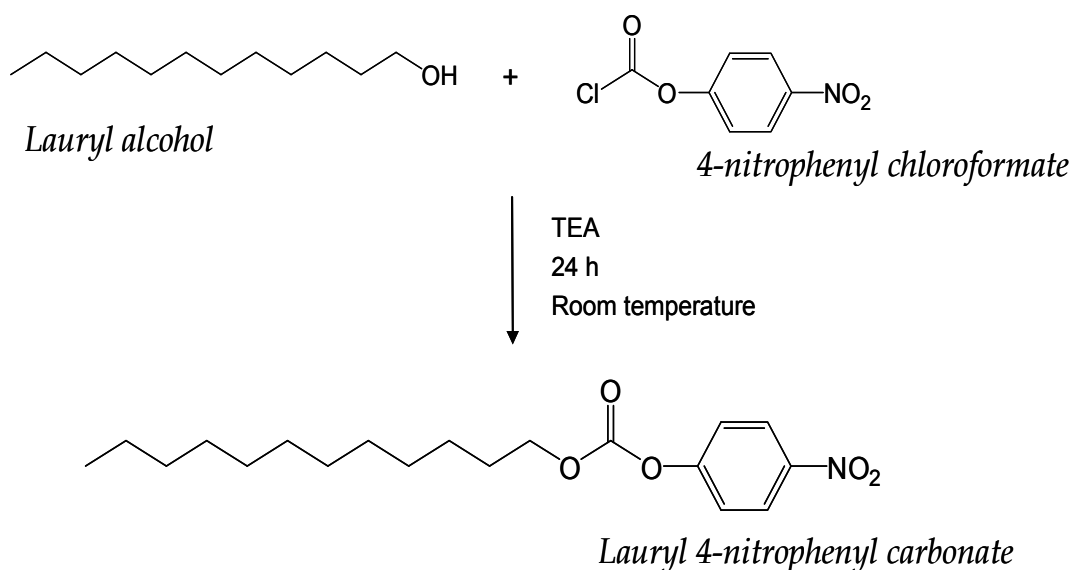


**Figure 2-1: Schematic diagram showing the synthesis of lauryl 4-nitrophenyl carbonate.**

#### *Purification of lauryl 4-nitrophenyl carbonate*

The yellowish reaction mixture was evaporated under vacuum (Buchi Rotavapor R-215, Switzerland) to remove THF. The residue was dissolved in hexane: EtOAc (90:10), filtered through a Whatman No. 1 filter paper and purified by silica gel column chromatography. The solvent ratio, hexane: EtOAc (90:10), was obtained by using thin layer chromatography (TLC) to give a value of  $R_f = 0.6$ . Silica gel particles were added to the sample in solution, mixed well before being evaporated under vacuum. The dried mixture was placed carefully at the top of a silica gel chromatography column with

hexane: EtOAc (90:10) as mobile phase. The column was eluted with the mobile phase at a flow rate of 2 ml/min, and portions of 5 ml eluents were collected and analysed by TLC to identify the purified compound. Evaporation of the combined eluents gave lauryl 4-nitrophenyl carbonate with a yield of 82%.

#### *Characterisation of lauryl 4-nitrophenyl carbonate*

The product was characterised by proton ( $^1\text{H}$ ) and carbon ( $^{13}\text{C}$ ) nuclear magnetic resonance spectroscopies (NMR).  $^{13}\text{C}$  and  $^1\text{H}$  NMR spectra were obtained using Bruker Avance 400, Bruker, Coventry, UK). Samples were dissolved in deuterated solvent with tetramethylsilane (TMS) as an internal standard. The Free Induction Decay (FID) files were converted to NMR spectra using MestRe-C software (Mestrelab Research, Spain).

$^1\text{H}$  NMR ( $\text{CDCl}_3$ ): 0.80 (3H, t,  $J = 6.9$ ,  $\text{CH}_3$ ), 1.30-1.10 (18H, m,  $9\times\text{-CH}_2\text{-}$ ), 1.68 (2H, pentet,  $J = 6.8$ ,  $\text{-CH}_2\text{-}$ ), 4.20 (2H, t,  $J=6.8$ ,  $\text{-CH}_2\text{-O-CO-}$ ), 7.35-7.25 (2H, m, Ar), 8.20-8.15 (2H, m, Ar).

$^{13}\text{C}$  NMR ( $\text{CDCl}_3$ ): 14.5 ( $\text{-CH}_3$ ), 23.1 ( $\text{-CH}_2\text{-}$ ), 26.0 ( $\text{-CH}_2\text{-}$ ), 30.0-28.9 ( $7\times\text{-CH}_2\text{-}$ ), 32.3 ( $\text{-CH}_2\text{-}$ ), 70.0 ( $\text{-CH}_2\text{-O-CO-}$ ), 122.1 ( $2\times\text{CH}$ , Ar), 125.6 ( $2\times\text{CH}$ , Ar), 145.7 (CH, Ar), 152.9 (CH, Ar), 156.0 ( $\text{-CO-}$ ).

#### 2.2.2.2 Synthesis of G3L3, G3L6 and G3L9 conjugates

G3 PAMAM dendrimer was reacted with 20% excess of the required amount of lauryl 4-nitrophenyl carbonate to yield the target molar ratios G3: lauryl of 1:3 (G3L3), 1:6 (G3L6) and 1:9 (G3L9). Lauryl 4-nitrophenyl carbonate for target ratios of 1:3 (91.0 mg, 0.259 mmol), 1:6 (182.2 mg, 0.518 mmol) and 1:9 (272.7 mg, 0.776 mmol) in DMF (2 ml) were added drop-wise to stirred solutions of G3 PAMAM dendrimer (500.0 mg, 0.072 mmol) in DMF (1 ml) over a period of 4-5 h. The reaction mixture was stirred for 5 days at room temperature under a nitrogen flow. Figure 2-2 represents the reaction scheme for the conjugation of lauryl chains to G3 PAMAM dendrimer.

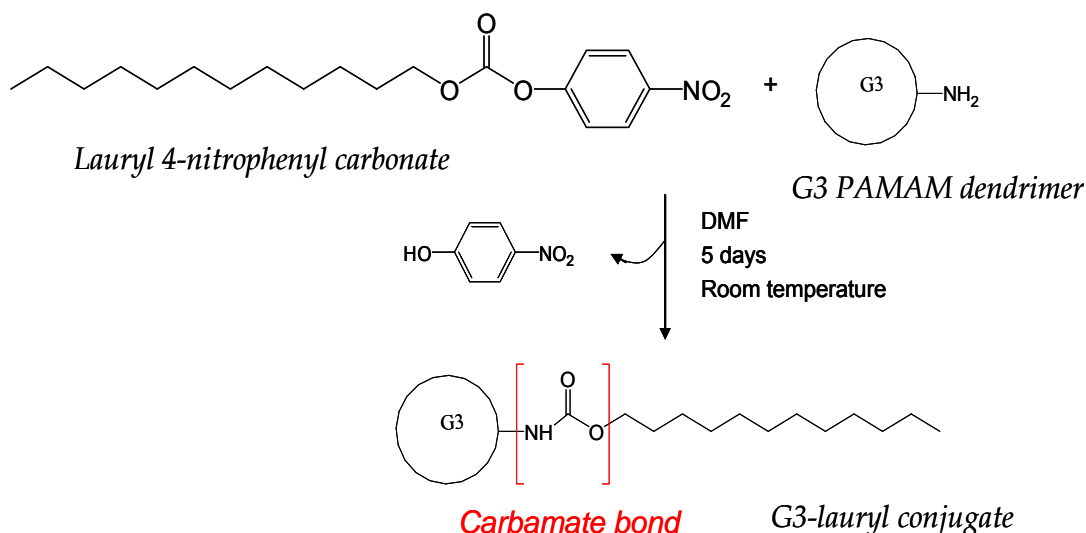


**Figure 2-2: Schematic diagram showing the conjugation of lauryl to G3 PAMAM dendrimer.**

#### *Purification and characterisation of G3-lauryl conjugates*

The reaction mixture was evaporated under vacuum and the resulting product was purified by size exclusion chromatography using Sephadex LH 20 as a stationary phase (column diameter 25 mm). The mobile phase was composed of methanol:water (85:15). The Sephadex LH20 particles were pre-swollen in methanol and left standing undisturbed for 24 hr before use. The dried reaction mixture was dissolved in methanol and was loaded carefully into the column. Portions of 1.5 ml eluents were collected and analysed by TLC to identify the purified compound. Evaporation of the combined eluents gave the G3-lauryl conjugates with a yield of 65% for G3L3, 61% for G3L6 and 68% for G3L9. The products were characterised by  $^1\text{H}$  NMR spectroscopy.

**G3L3:**  $^1\text{H}$  NMR ( $d_4$ -MeOD): 0.90 (9H, t,  $J = 6.9$ , 3 x  $\text{CH}_3$ , L3), 1.45-1.20 (54H, 3 x (9 x  $-\text{CH}_2-$ , L3), 1.70-1.54 (6H, pentet,  $J=9.7$ , 3 x  $-\text{CH}_2-$ , L3), 2.45-2.30 (120H, m, c-G3), 2.65-2.50 (60H, m, a-G3), 2.90-2.67 (178H, 2m, b-G3, f-G3), 4.04-3.96 (6H, t,  $J=7.4$ , 3 x  $-\text{CH}_2-$ , L3).

**G3L6:**  $^1\text{H}$  NMR ( $d_4$ -MeOD): 0.90 (18H, t,  $J = 7.1$ , 6 x  $\text{CH}_3$ , L6), 1.45-1.20 (108H, 6 x (9 x  $-\text{CH}_2-$ , L6), 1.70-1.55 (12H, pentet,  $J=6.6$ , 6 x  $-\text{CH}_2-$ , L6), 2.47-2.30 (120H, m, c-

G3), 2.67-2.50 (60H, m, a-G3), 2.93-2.70 (178H, 2m, b-G3, f-G3), 4.12-3.95 (12H, t, J=6.8, 6 x -CH<sub>2</sub>-, L6).

**G3L9:** <sup>1</sup>H NMR (d<sub>4</sub>-MeOD): 0.90 (27H, t, J = 6.9, 9 x CH<sub>3</sub>, L9), 1.45-1.25 (162H, 9 x (9 x -CH<sub>2</sub>-, L9), 1.70-1.55 (18H, pentet, J=6.5, 9 x -CH<sub>2</sub>-, L9), 2.48-2.32 (120H, m, c-G3), 2.62-2.52 (60H, m, a-G3), 2.90-2.71 (178H, 2m, b-G3, f-G3), 4.11-3.97 (18H, t, J=6.3, 9 x -CH<sub>2</sub>-, L9).

*(<sup>1</sup>H NMR peak assignments are shown in Figure 2-11 to Figure 2-13.)*

### 2.2.3 Synthesis of G3-glutarate-paclitaxel/lauryl-G3-glutarate-paclitaxel conjugates

Paclitaxel was conjugated to G3 and lauryl-G3 PAMAM dendrimer conjugates through glutaric anhydride as a linker using the NHS method (144). Firstly, paclitaxel was reacted with glutaric anhydride to yield 2'-glutaryl-paclitaxel (pac-glu). The drug-linker was converted to pac-glu-NHS ester, followed by covalent conjugation to G3 or lauryl-G3 PAMAM dendrimer conjugates.

#### 2.2.3.1 Synthesis of 2'-glutaryl-paclitaxel

Paclitaxel (100 mg, 0.12 mmol) and glutaric anhydride (16.4 mg, 0.14 mmol) were dissolved in DCM (6 ml) and stirred for 10min, followed by addition of dry pyridine (95  $\mu$ l, ~10x molar excess). The reaction mixture was stirred for 3 days at room temperature. Figure 2-3 showed the reaction scheme for the synthesis of 2'-glutaryl-paclitaxel.

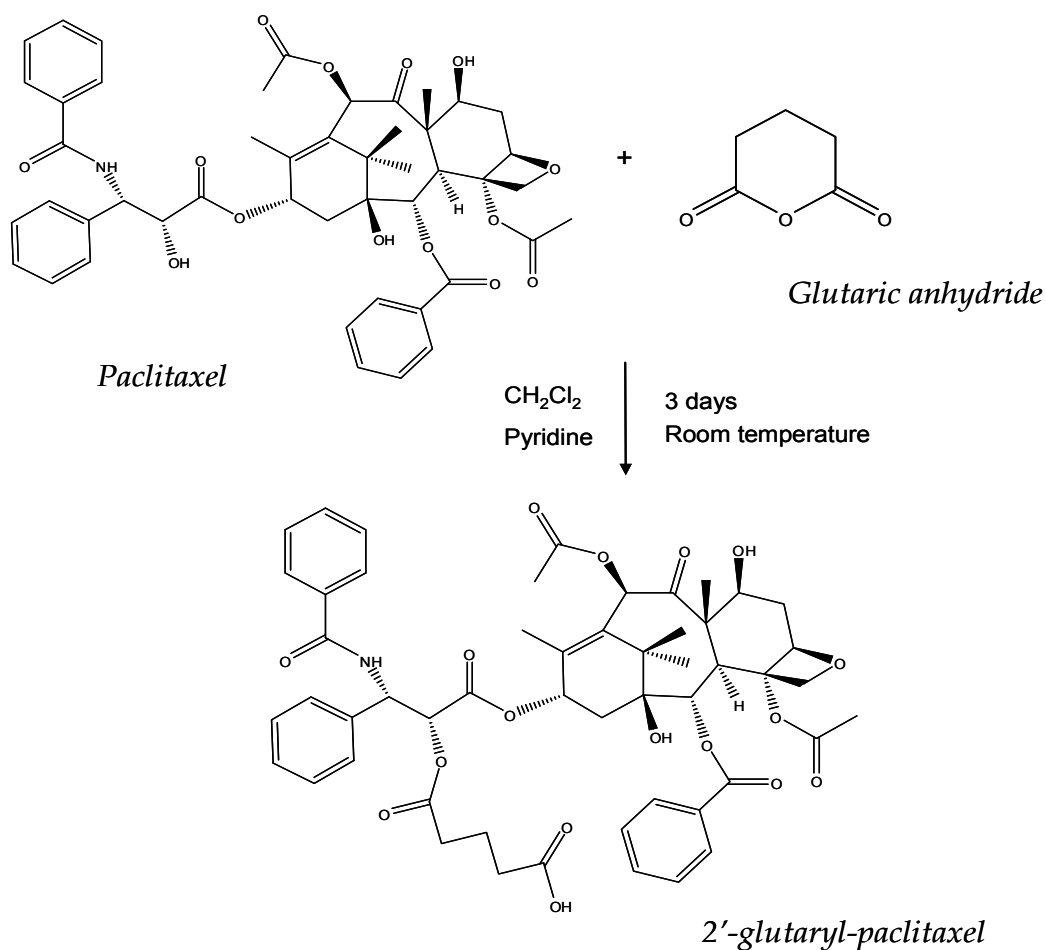


**Figure 2-3: Schematic diagram showing the synthesis of 2'-glutaryl-paclitaxel.**

*Purification and characterisation of pac-glu conjugates*

The reaction mixture was evaporated under vacuum to remove pyridine. The dried residue was re-crystallised from DCM, and the white crystals formed were separated by filtration. The product purity was determined by using TLC with methanol:chloroform (3:97) as eluent.

The crystalline product, pac-glu, with a yield of 78% ( $R_f = 0.3$ ) was characterised and verified by  $^1\text{H}$  and  $^{13}\text{C}$  NMR spectroscopies and electrospray ionisation mass spectrometry (ESI-MS). Electrospray ionisation mass spectra (ESI-MS) were obtained using Thermo Fisher Scientific Finnigan LCQ Advantage MAX (UK).

$^1\text{H}$  NMR ( $\text{CDCl}_3$ ): 1.35-1.0 (6H, m, 2 x  $\text{CH}_3$ ), 1.72-1.57 (3H, s,  $\text{CH}_3\text{CCHO}$ ), 1.98-1.72 (7H, m,  $\text{C-OH}$ ,  $\text{CH}_3\text{CCHOH}$ ,  $\text{COOCH}_2\text{CH}_2\text{CH}_2\text{COOH}$ ,  $\text{HOCHCHCHO}$ ), 2.64-2.10 (14H, m,  $\text{COOCH}_2\text{CH}_2\text{CH}_2\text{COOH}$ ,  $\text{CH-OH}$ ,  $\text{HOCHCHCHO}$ ,  $\text{CH}_3\text{COOCH}$ ,  $\text{CHOCH}_2\text{COH}$ ,  $\text{CH}_3\text{COOCHCO}$ ), 3.81 (1H, d,  $J=6.8$ ,  $\text{CHOCHCO}$ ), 4.18, 4.19 (2H, d,  $J=8.2$ ,  $\text{COCH}_2\text{OCH}$ ), 4.43 (1H, quartet,  $J=6.4$ ,  $\text{CH}_2\text{CHOH}$ ), 4.97 (1H, d,  $J=8.8$ ,  $\text{CH}_2\text{CH-O}$ ), 5.49 (1H, d,  $J=2.8$ ,  $\text{NHCHCHOCO}$ ), 5.68 (1H, d,  $J=6.8$ ,  $\text{COHCHOCO-Ar}$ ), 6.0 (1H, quartet,  $J=6.4$ ,  $\text{NHCHCHOCO}$ ), 6.26 (2H, m,  $\text{COCHOC(O)CH}_3$ ,  $\text{O-CHCH}_2$ ), 7.66-7.30 (11H, m, 11 x CH, Ar), 7.73 (2H, d,  $J=7.6$ , 2 x  $\text{CHCCNH}$ , Ar), 8.14 (2H, d,  $J=7.6$ , 2 x  $\text{CHCCOO}$ , Ar).  $^{13}\text{C}$  NMR ( $\text{CDCl}_3$ ): 9.65 ( $\text{CH}_3\text{CCHOH}$ ), 14.81 ( $\text{CH}_3\text{CCHO}$ ), 19.72 ( $\text{COOCH}_2\text{CH}_2\text{CH}_2\text{COOH}$ ), 20.86 ( $\text{CH}_3\text{COOCHCO}$ ), 22.18 ( $\text{CH}_3$ ), 22.71 ( $\text{CH}_3\text{COOCH}$ ), 26.83 ( $\text{CH}_3$ ), 29.72 ( $\text{CHOCH}_2\text{COH}$ ), 32.39 ( $\text{COOCH}_2\text{CH}_2\text{CH}_2\text{COOH}$ ), 32.70 ( $\text{COOCH}_2\text{CH}_2\text{CH}_2\text{COOH}$ ), 35.60 ( $\text{HOCHCH}_2\text{-CHO}$ ), 43.24 ( $\text{HOCC(CH}_3)_2$ ), 45.63 ( $\text{CHOCHCO}$ ), 52.84 ( $\text{NHCHCHOCO}$ ), 58.50 ( $\text{CH}_3\text{CCHOH}$ ), 71.96 ( $\text{CH}_2\text{CHOH}$ ), 72.10 ( $\text{OCHCH}_2$ ), 74.21 ( $\text{NHCHCHOCO}$ ), 75.17 ( $\text{COHCHOCO-Ar}$ ), 75.65 ( $\text{COCHOC(O)CH}_3$ ), 76.47 ( $\text{COCH}_2\text{OCH}$ ), 78.93 ( $\text{CH}_2\text{C(OH)CHO}$ ), 81.15 ( $\text{CHCOCH}_2\text{O}$ ), 84.47 ( $\text{CH}_2\text{CH-O}$ ), 126.58 (2 x  $\text{CH-CCNH}$ , Ar), 127.20 (2 x CH, Ar), 128.53 (CH, Ar), 128.72 (2 x CH, Ar), 128.77 (2 x CH, Ar), 129.12 (2 x CH, Ar), 129.29 (C, Ar), 130.27 (2 x CH, Ar), 132.07 (CH, Ar), 132.94 ( $\text{CH}_3\text{CCCHO}$ ), 133.62 (C, Ar), 133.69 (CH, Ar), 136.81 (C, Ar), 142.60 ( $\text{CH}_3\text{CCHO}$ ), 166.93 ( $\text{OCNHCH}$ ), 167.80 ( $\text{CHOCO-Ar}$ ), 168.22 ( $\text{CH}_3\text{COOCHCH}_2\text{O}$ ), 169.91 ( $\text{CH}_3\text{COOCHCO}$ ), 171.29 ( $\text{NHCHCHOCO}$ ), 171.98 ( $\text{COOCH}_2\text{CH}_2\text{CH}_2\text{COOH}$ ), 176.26 ( $\text{COOCH}_2\text{CH}_2\text{CH}_2\text{COOH}$ ), 203.81 ( $\text{COCOCCH}_3$ ). (+)-ESI-MS: 990.20 [ $\text{M}^+$  + Na], 968.20 [ $\text{M}^+$  + H]. (Theoretical: ( $\text{C}_{52}\text{H}_{57}\text{NO}_7$ ) 967.91 g/mol).

### 2.2.3.2 Synthesis of pac-glu-NHS ester

#### *Formation of N-hydroxysuccinimido diphenyl phosphate (SDPP)*

TEA (1.01 g, 10 mmol) in DCM (7 ml) was added slowly to the stirred mixture of DPC (2.69 g, 10 mmol) and NHS (1.15 g, 10 mmol). The mixture was stirred at room temperature for 30 min and dried under vacuum to obtain crude SDPP. Crude SDPP was triturated with diethyl ether and filtered. The residue was collected, dissolved in EtOAc, washed twice with water (10 ml) and dried with MgSO<sub>4</sub>. The mixture was filtered and dried under vacuum (yield of 89%). The purity of the resulting product was determined by TLC using methanol:chloroform (3:97) as eluent.

#### *Synthesis of pac-glu-NHS active ester*

TEA (62  $\mu$ l, 0.43 mmol) was added to a stirred solution of pac-glu (100 mg, 0.10 mmol) and SDPP (53.8 mg, 0.15 mmol) in acetonitrile (5 ml). The reaction mixture was stirred for 6 h at room temperature under a nitrogen flow. Figure 2-4 illustrated the reaction scheme for the synthesis of pac-glu-NHS ester.

#### *Purification and characterisation of pac-glu-NHS ester*

The reaction mixture was evaporated under vacuum to remove acetonitrile. The residue was dissolved in EtOAc:hexane (70:30) and purified using silica gel chromatography as described in section 2.2.2.1 with a yield of 52% ( $R_f = 0.4$ ).

The pac-glu-NHS ester was characterised and verified by <sup>1</sup>H and <sup>13</sup>C NMR spectroscopies.

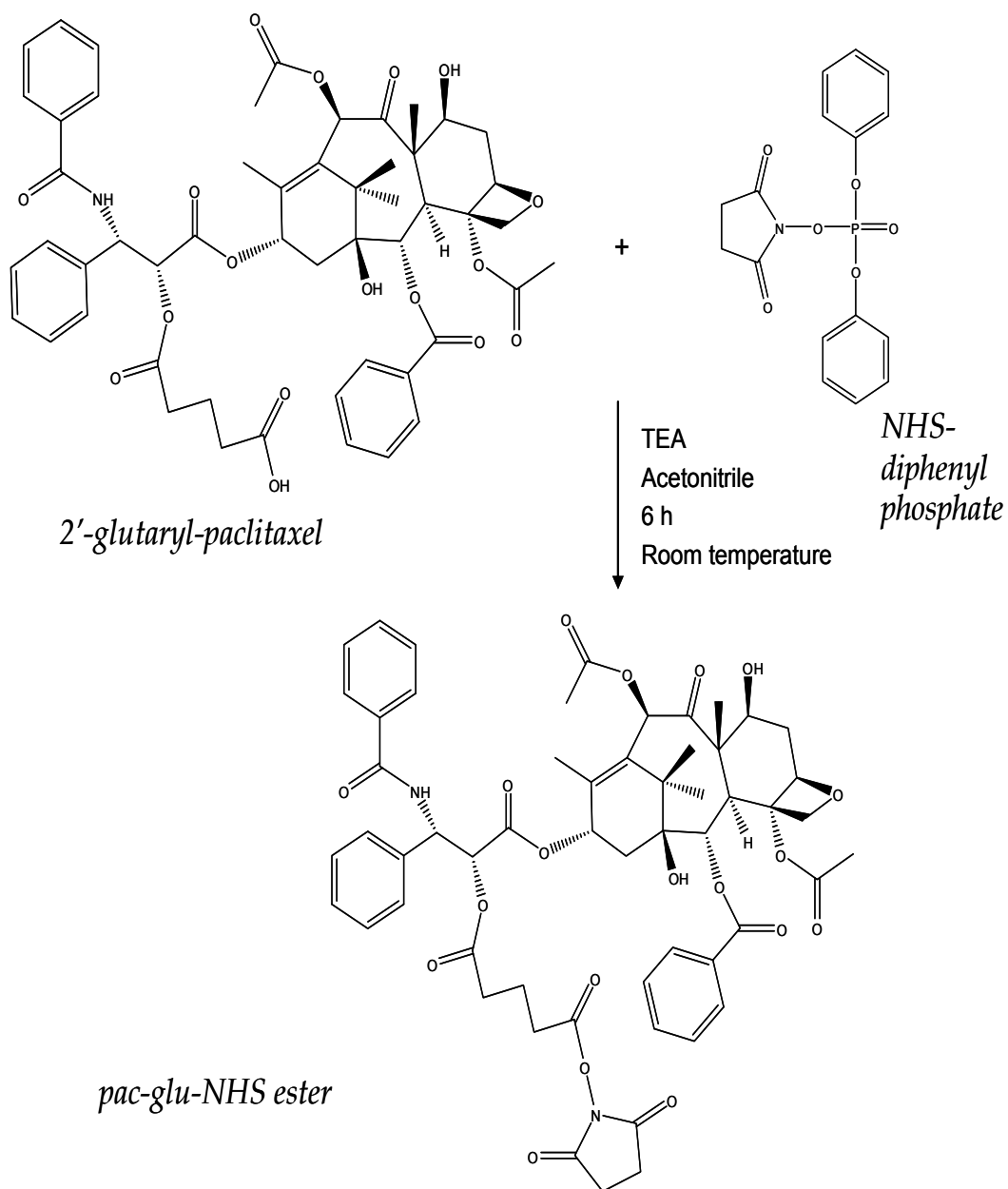


**Figure 2-4: Schematic diagram showing the synthesis of *pac-glu-NHS ester*.**

$^1\text{H}$  NMR ( $\text{CDCl}_3$ ): 1.35-1.0 (6H, m, 2 x  $\text{CH}_3$ ), 1.72-1.57 (3H, s,  $\text{CH}_3\text{CCHO}$ ), 2.30-1.72 (15H, m, C-OH,  $\text{CH}_3\text{CCHOH}$ ,  $\text{COOCH}_2\text{CH}_2\text{CH}_2\text{COON}$ ,  $\text{HOCHCHCHO}$ ,  $\text{NC(O)CH}_2\text{-CH}_2\text{C(O)}$ ), 2.95-2.30 (14H, m,  $\text{COOCH}_2\text{CH}_2\text{CH}_2\text{COON}$ , CH-OH,  $\text{HOCHCHCHO}$ ,  $\text{CH}_3\text{COOCH}$ ,  $\text{CHOCH}_2\text{COH}$ ,  $\text{CH}_3\text{COOCHCO}$ ), 3.81 (1H, d,  $J=11.2$ ,  $\text{CHOCHCO}$ ), 4.18, 4.29 (2H, d,  $J=8.8$ ,  $\text{COCH}_2\text{OCH}$ ), 4.43 (1H, br quartet,  $J=13.6$ ,  $\text{CH}_2\text{CHOH}$ ), 4.97 (1H, d,  $J=12.8$ ,  $\text{CH}_2\text{CH-O}$ ), 5.48 (1H, d,  $J=5.2$ ,  $\text{NHCHCHOCOO}$ ), 5.68 (1H, d,  $J=11.2$ ,  $\text{COHCHOCO-Ar}$ ), 6.0 (1H, quartet,  $J=10.4$ ,  $\text{NHCHCHOCOO}$ ), 6.27 (2H, m,  $\text{COCHOC(O)CH}_3$ , O- $\text{CHCH}_2$ ), 7.66-7.3 (11H, m, 11 x CH, Ar), 7.71 (2H, d,  $J=11.2$ , 2 x  $\text{CHCCNH}$ , Ar), 8.12 (2H, d,  $J=11.2$ , 2 x  $\text{CHCCOO}$ , Ar).  $^{13}\text{C}$  NMR ( $\text{CDCl}_3$ ): 9.60 ( $\text{CH}_3\text{CCHOH}$ ), 14.86 ( $\text{CH}_3\text{CCHO}$ ), 20.10 ( $\text{COOCH}_2\text{CH}_2\text{CH}_2\text{COON}$ ), 20.84 ( $\text{CH}_3\text{COOCHCO}$ ), 22.10 ( $\text{CH}_3$ ), 22.73 ( $\text{CH}_3\text{COOCH}$ ), 25.49 ( $\text{NC(O)CH}_2\text{-CH}_2\text{C(O)}$ ), 26.78( $\text{COOCH}_2\text{CH}_2\text{CH}_2\text{COON}$ ), 26.86 ( $\text{CH}_3$ ), 29.41 ( $\text{CHOCH}_2\text{COH}$ ), 32.02 ( $\text{COOCH}_2\text{CH}_2\text{CH}_2\text{COON}$ ), 35.56 ( $\text{HOCHCH}_2\text{-CHO}$ ), 43.14 ( $\text{HOCC(CH}_3)_2$ ), 45.60 ( $\text{CHOCHCO}$ ), 52.81 ( $\text{NHCHCHOCOO}$ ), 58.42 ( $\text{CH}_3\text{CCHOH}$ ), 71.85 ( $\text{CH}_2\text{CHOH}$ ), 72.07 ( $\text{OCHCH}_2$ ), 74.42 ( $\text{NHCHCHOCOO}$ ), 75.06 ( $\text{COHCHOCO-Ar}$ ), 75.59 ( $\text{COCHOC(O)CH}_3$ ), 76.40 ( $\text{COCH}_2\text{OCH}$ ), 78.96 ( $\text{CH}_2\text{C(OH)CHO}$ ), 80.98 ( $\text{CHCOCH}_2\text{O}$ ), 84.41 ( $\text{CH}_2\text{CH-O}$ ), 126.67 (2 x  $\text{CH-CCNH}$ , Ar), 127.26 (2 x CH, Ar), 128.46 (CH, Ar), 128.71 (2 x CH, Ar), 128.78 (2 x CH, Ar), 129.04 (2 x CH, Ar), 129.18 (C, Ar), 130.19 (2 x CH, Ar), 131.64 (CH, Ar), 132.76 ( $\text{CH}_3\text{CCCHO}$ ), 133.61 (C, Ar), 134.08 (CH, Ar), 136.93 (C, Ar), 142.66 ( $\text{CH}_3\text{CCHO}$ ), 166.87 ( $\text{OCNHCH}$ ), 167.58 ( $\text{CHOCO-Ar}$ ), 168.03 ( $\text{COOCH}_2\text{CH}_2\text{CH}_2\text{COON}$ ), 168.12 ( $\text{CH}_3\text{COOCHCH}_2\text{O}$ ), 169.27 ( $\text{OCNCO}$ ), 169.76 ( $\text{CH}_3\text{COOCHCO}$ ), 171.17 ( $\text{NHCHCHOCOO}$ ), 171.79 ( $\text{COOCH}_2\text{CH}_2\text{CH}_2\text{COOH}$ ), 203.83 ( $\text{COCOCCH}_3$ ).

### 2.2.3.3 Synthesis of G3-glu-pac/ lauryl-G3-glu-pac

Pac-glu-NHS was conjugated to G3, G3L3 and G3L6 conjugates at 1:1.2 molar ratio. For example, pac-glu-NHS (18.5 mg, 0.017 mmol) in DMF (2 ml) was added drop-wise to a stirred solution of G3 (100 mg, 0.014 mmol) in DMF (1 ml) over a period of 4-5 h. The reaction mixture was stirred for 5 days at room temperature under a nitrogen flow. Figure 2-5 showed the reaction scheme for the synthesis of L-G3-glu-pac.

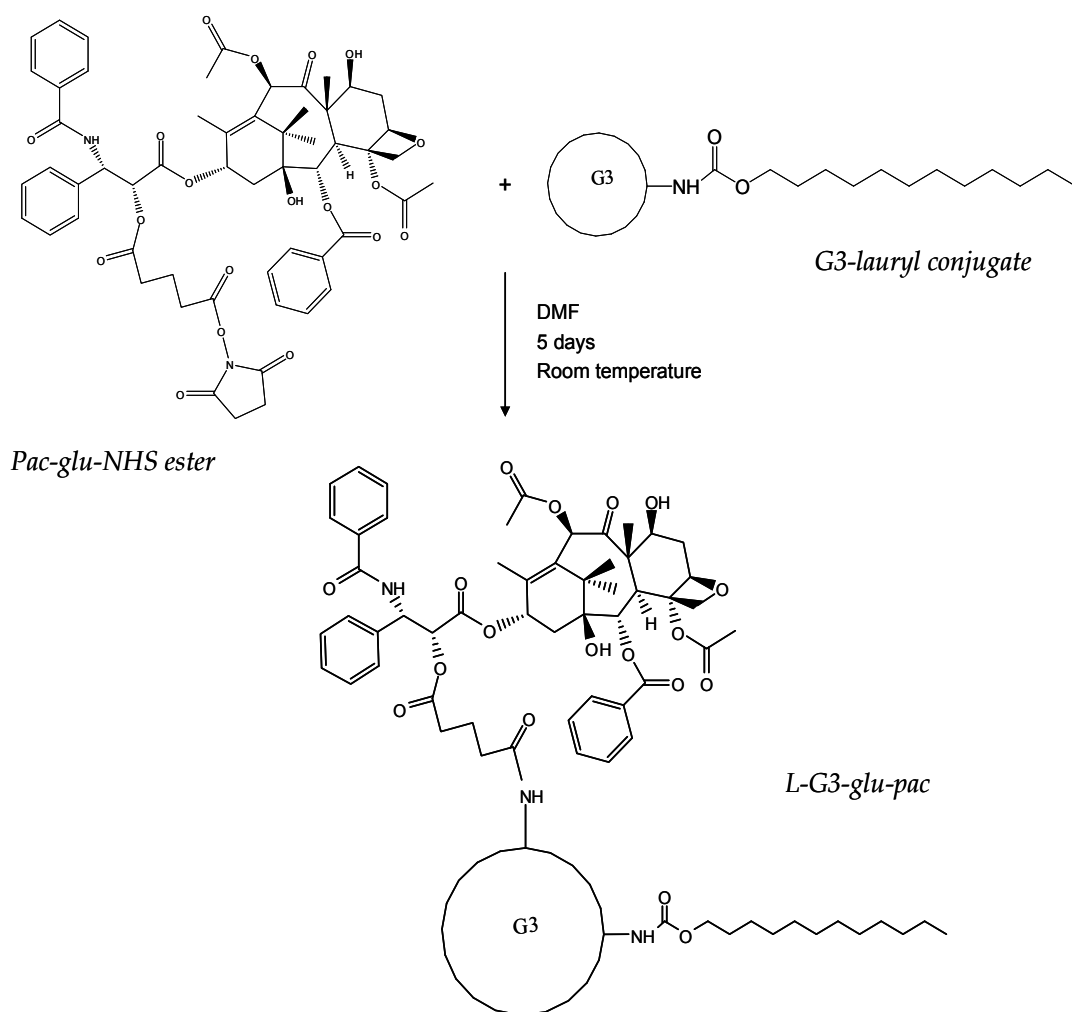


**Figure 2-5: Schematic diagram showing the synthesis of lauryl-G3-glu-pac.**

*Purification and characterisation of G3-glu-pac, L3-G3-glu-pac and L6-G3-glu-pac conjugates*

The reaction mixture was evaporated under vacuum and purified by size exclusion chromatography as described in section 2.2.2.2.

G3-glu-pac (54% yield), L3-G3-glu-pac (87% yield) and L6-G3-glu-pac (81% yield) conjugates were characterised and verified by  $^1\text{H}$  and  $^{13}\text{C}$  NMR spectroscopies.

## 2.2.4 Synthesis of FITC-labelled G3 PAMAM dendrimer and conjugates

Synthesis of FITC-labelled G3 PAMAM dendrimer and conjugates were carried out by two methods, previously described by Majoros *et al.* (105) and Jevprasesphant *et al.* (103).

### *Method I* (105)

FITC (4.7 mg, 0.012 mmol) dissolved in DMSO (2 ml) was added to dendrimer (69.1 mg, 0.01 mmol) in DMSO (2 ml). The reaction mixture was allowed to stir in the dark for 24 h under a nitrogen flow.

### *Method II* (103)

FITC (4.7 mg, 0.012 mmol) dissolved in methanol (2 ml) was added to dendrimer (69.1 mg, 0.01 mmol) in phosphate buffer saline (PBS) (2 ml). The reaction mixture was allowed to stir for 24 h in the dark under a nitrogen flow at room temperature. Figure 2-6 showed the reaction scheme for the synthesis of FITC labelled G3 PAMAM dendrimer.

### *Purification and characterisation of FITC labelled G3 PAMAM dendrimer*

The reaction mixture was dialysed against deionised water using dialysis membrane (1000 MWCO) to separate the non-reacted FITC until no free FITC was detected by TLC (mobile phase was composed of chloroform: methanol: ammonium hydroxide (50:40:10)). Further purification was carried out using size exclusion chromatography as described in section 2.2.2.2 with a mobile phase of chloroform:methanol:ammonia (5:4:1).

FITC-labelled G3 PAMAM dendrimer and conjugates were characterised and verified by  $^1\text{H}$  and  $^{13}\text{C}$  NMR spectroscopies. The particle size of all the FITC-labelled PAMAM dendrimer conjugates was measured using dynamic light scattering (Zetasizer Nano, Malvern Instruments, UK). The conjugates were dissolved in HBSS and filtered through a 0.22  $\mu\text{m}$  pore size PVDF filter into the scattering cell. All measurements were carried out at 37°C.

Syntheses of all products have been repeated more than 3 times. The conjugation of all the products have been characterised and confirmed by NMR after each synthesis.

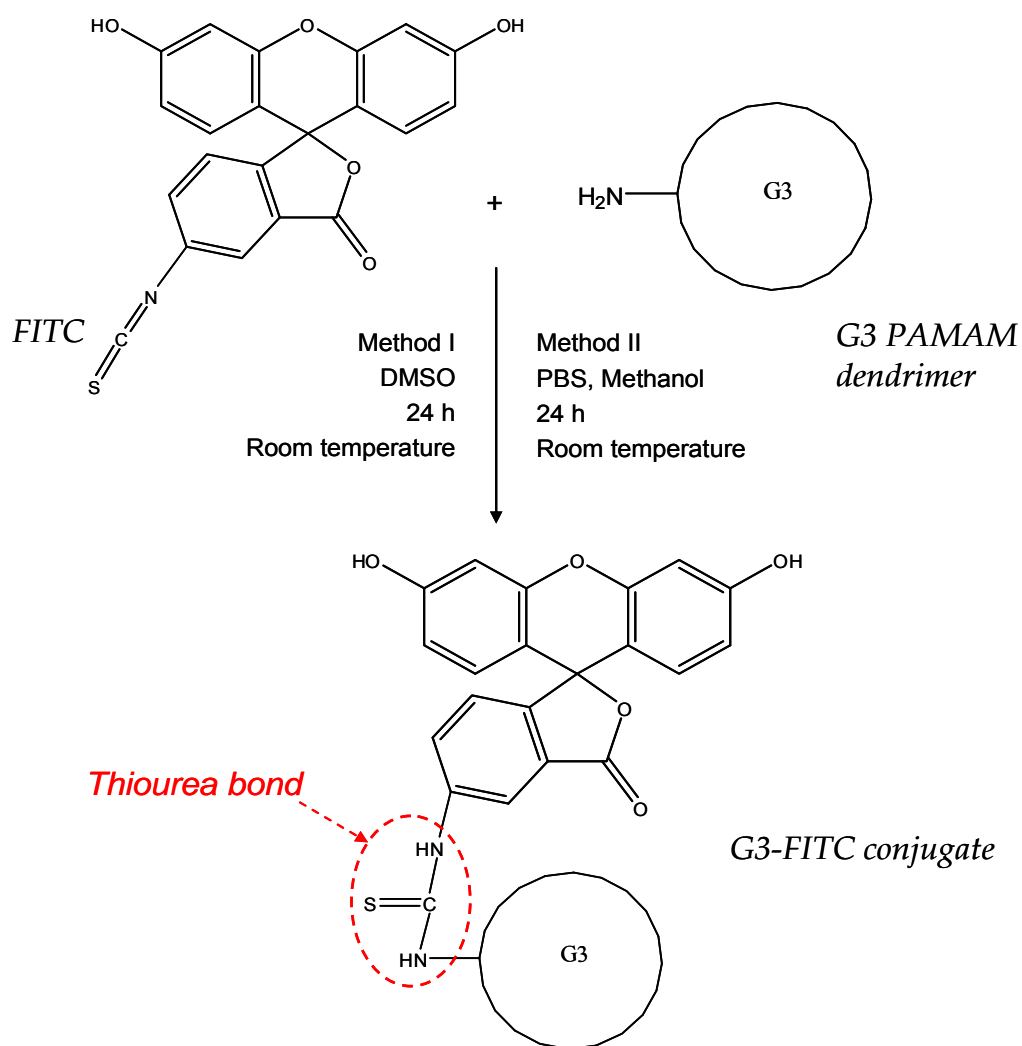


**Figure 2-6: Schematic diagram showing the labelling of G3 PAMAM dendrimer with FITC.**

### 2.2.5 Chemical stability of G3 PAMAM dendrimer conjugates

The hydrolysis of G3 PAMAM dendrimer conjugates was investigated in buffers at pH 1.2 (0.1 M hydrochloric acid buffer), 7.4 (0.1 M phosphate buffer) and 8.5 (0.2 M borate buffer). Conjugates with a concentration of 0.0002 M were prepared in a 5 ml preheated buffer solution using screw-capped test vials. The solutions were maintained at 37°C and 100 µl of samples were withdrawn at appropriate intervals over a period of 240 h. 100 µl of methanolic solution of phenanthrene was added and samples were analysed by HPLC. HPLC analyses were carried out using Agilent 1100 Series HPLC system (UK) equipped with a Luna 5 µm, C18 column (250 mm x 4.6 mm) (Phenomenex, Cheshire, UK). The solvent system used was MeOH:TFA (0.05% w/v) (80:20) for FITC-G3L6-glu-pac, with phenanthrene as an internal standard, the flow rate was 1.0 ml/min and UV detection was at  $\lambda = 230$  nm.

### 2.2.6 Statistical analysis of data

All data were expressed as mean values  $\pm$  standard deviation (mean  $\pm$  SD). Statistical analysis was carried out using the Student's t-test. Probability values of  $p < 0.05$  were considered to be statistically significant. In this study, the experiments were replicate of between 3-5 times for each synthesis. The syntheses of all products have been repeated more than three times. The conjugation of the products have been characterised and confirmed by NMR and ESI-MS after each synthesis.

## 2.3 Results and discussion

### 2.3.1 Synthesis and characterisation of lauryl-G3 PAMAM dendrimer conjugates

#### 2.3.1.1 Synthesis of lauryl 4-nitrophenyl carbonate

The results of this study have shown that lauryl alcohol was attached to the surface primary amine groups of the G3 dendrimer using 4-nitrophenyl chloroformate as the coupling agent. Lauryl alcohol demonstrated higher stability and provided more consistent yields (85) compared to lauroyl chloride used in the method described by Jevprasesphant *et al.*(103). In the method described by Najlah *et al.* (85), lauryl alcohol was reacted with 4-nitrophenyl chloroformate to obtain lauryl 4-nitrophenyl carbonate ( Figure 2-7) which was purified and characterised by TLC and <sup>1</sup>H NMR spectroscopy. The results from the <sup>1</sup>H NMR spectrum (Figure 2-8) confirmed that lauryl 4-nitrophenyl carbonate was successfully synthesised.

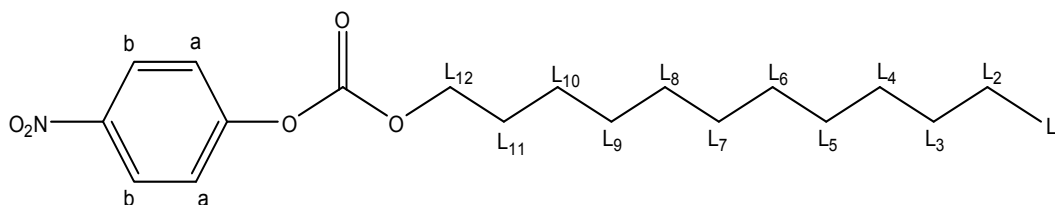


**Figure 2-7: Chemical structure of lauryl 4-nitrophenyl carbonate.**

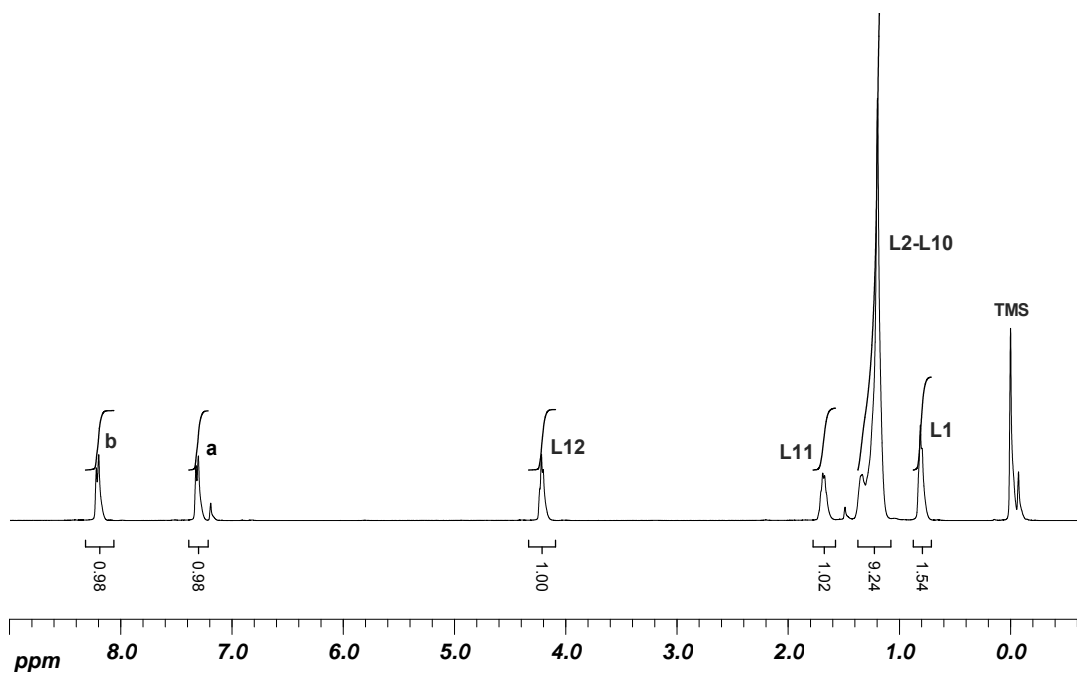


**Figure 2-8:  $^1\text{H}$  NMR spectrum of lauryl 4-nitrophenyl carbonate.**

### 2.3.1.2 Conjugation of lauryl alcohol with G3 PAMAM dendrimers

G3 PAMAM dendrimer (Figure 2-9) was reacted with lauryl 4-nitrophenyl carbonate at the appropriate molar ratios (1:3, 1:6 and 1:9) to yield lauryl-G3 PAMAM dendrimers (G3L3, G3L6 and G3L9). Lauryl chains were conjugated covalently to the surface primary amine groups of G3 PAMAM dendrimer via carbamate bonds. The G3 PAMAM dendrimer and the lauryl-G3 PAMAM dendrimers were analysed by TLC and  $^1\text{H}$  NMR spectroscopy.

The TLC chromatogram of the purified lauryl-G3 PAMAM dendrimers showed a single spot at the baseline with  $R_f = 0.0$ . The  $^1\text{H}$  NMR peaks in the G3 PAMAM dendrimers spectrum (Figure 2-11) were assigned accordingly to use as a comparison and reference for the spectra of lauryl-G3 PAMAM dendrimers (Figure 2-13). The chemical shifts of G3 PAMAM dendrimer were assigned as shown in Table 2-1. Figure 2-11 shows the peaks originating from G3 PAMAM dendrimer at chemical shifts between 2.35-3.33 ppm. The additional peaks at the chemical shifts at 0.90-1.70 ppm and 3.90-4.12 ppm found in Figure 2-13 confirmed the successful conjugation of lauryl chains to G3 PAMAM dendrimers.

The number of lauryl chains attached to dendrimer was determined by comparing the relative integrals of the  $^1\text{H}$  NMR peaks originating from the lauryl substituents to those of G3 dendrimers. By comparing the peak integrations of lauryl at chemical shift 0.90 ppm and G3 PAMAM dendrimer's at 2.57 ppm, the number of protons in each peak was calculated to determine the ratio of lauryl to G3 PAMAM dendrimer. 1:3, 1:6 and 1:9 molar ratios of G3 to lauryl were calculated and shown in Table 2-2.

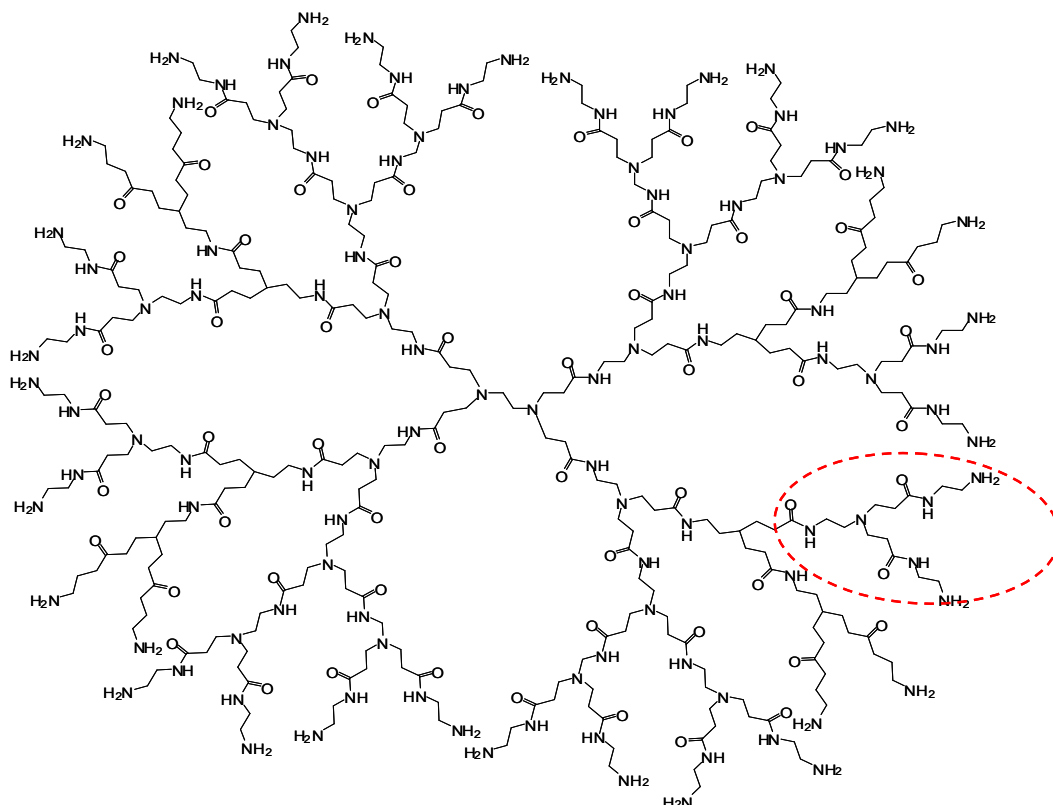


**Figure 2-9: Chemical structure of G3 PAMAM dendrimer.**

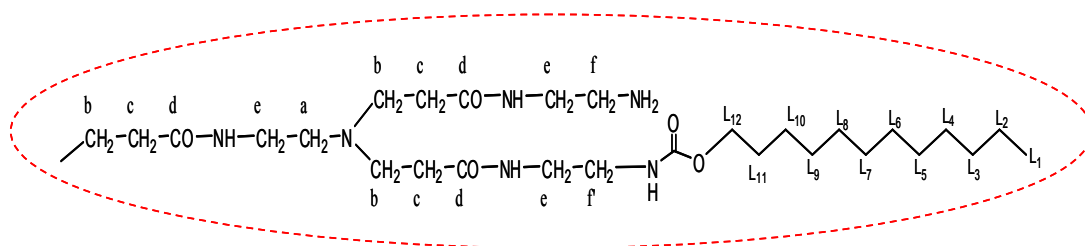


**Figure 2-10: A branch of G3 PAMAM dendrimer with a lauryl chain attached via a carbamate bond.**

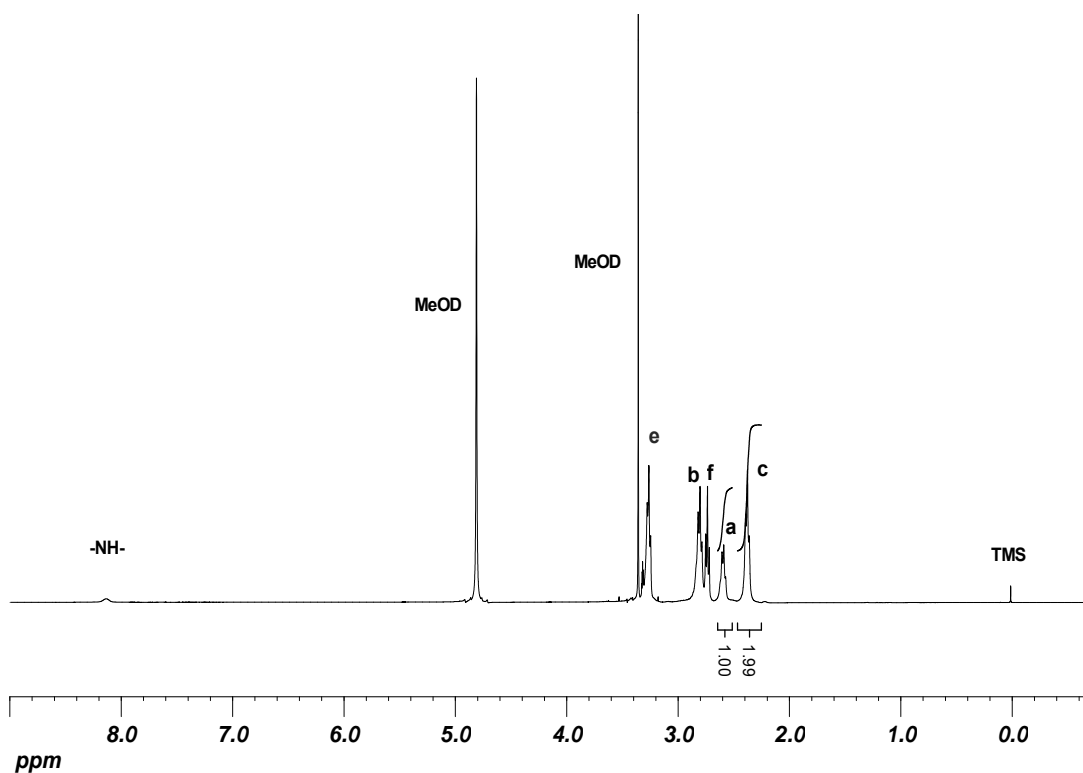


Figure 2-11:  $^1\text{H}$  NMR spectrum of G3 PAMAM dendrimer.

Dendrimer	c	a	f	b	e
G3	2.38	2.60	2.74	2.81	3.26

Table 2-1: Assignment of peaks and chemical shifts for G3 PAMAM dendrimer.

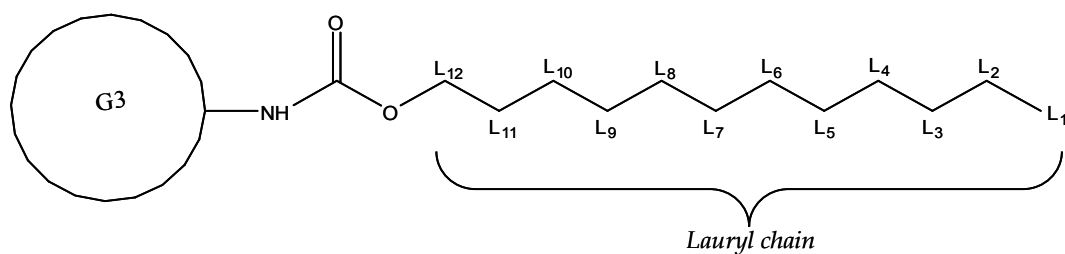


Figure 2-12: Schematic diagram of G3 PAMAM dendrimer with a lauryl chain attached.

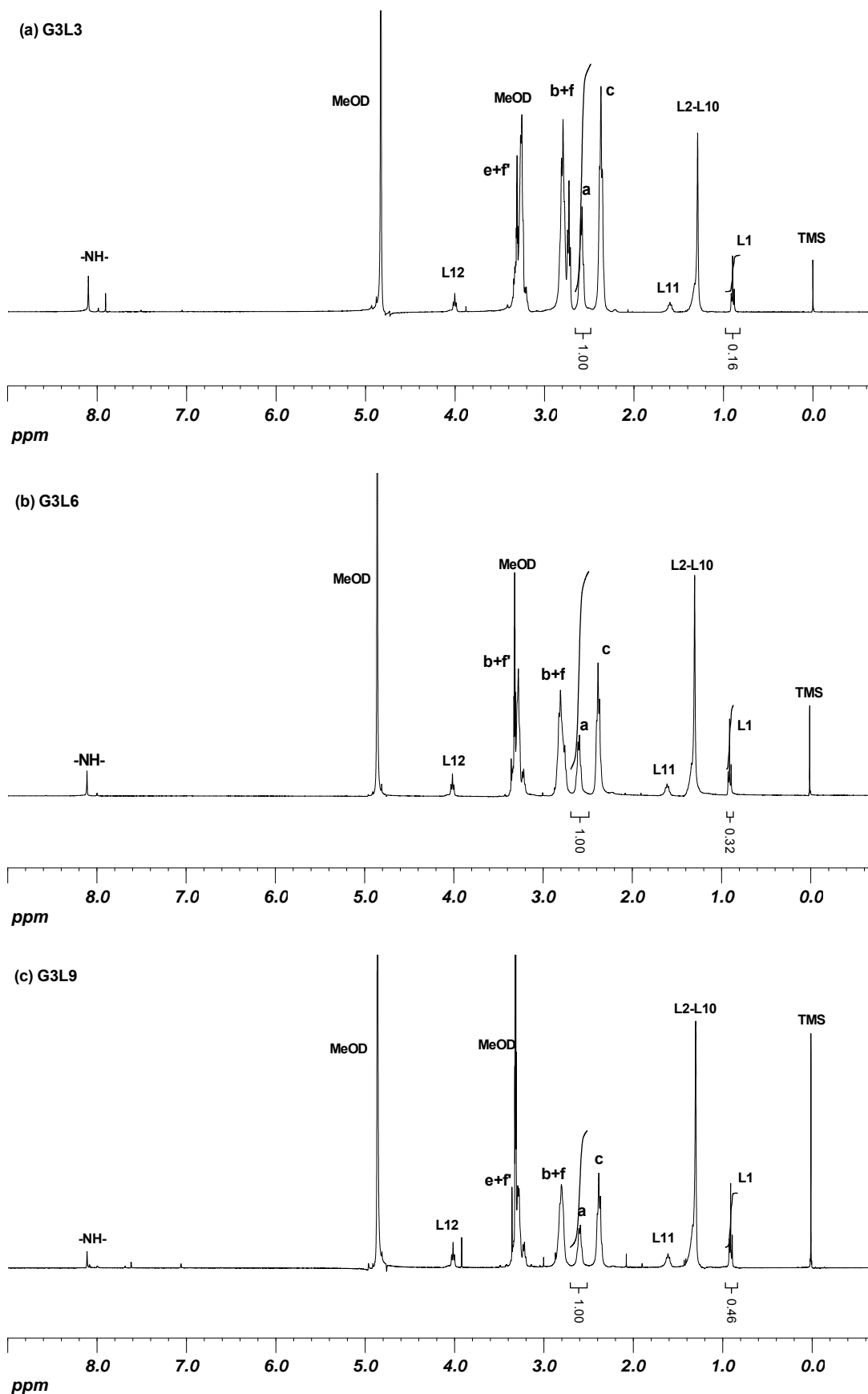


Figure 2-13:  $^1\text{H}$  NMR spectra of lauryl-G3 dendrimer conjugates (a) G3L3 (b) G3L6 and (c) G3L9.

<b>G3 conjugates</b>	<b>Conjugation ratio G3: lauryl</b>
G3L3	1: 3.19
G3L6	1: 6.39
G3L9	1: 9.18

**Table 2-2: Molar ratios of lauryl chains conjugated to G3 PAMAM dendrimer by comparison of relative peak integrals from the  $^1\text{H}$  NMR spectra.**

### 2.3.2 Synthesis and characterisation of G3-glu-pac/lauryl-G3-glu-pac conjugates

The dendrimer based drug delivery system consisting of the dendrimer – G3 PAMAM dendrimer, the permeability enhancer moieties – lauryl chains, the linkers – glutaric anhydride, and the drug – paclitaxel was synthesised and characterised.

#### 2.3.2.1 Conjugation of linker (glutaric anhydride) to paclitaxel

Paclitaxel was reacted with glutaric anhydride in an equimolar ratio to obtain 2'-glutaryl-paclitaxel (pac-glu). Paclitaxel was linked by its hydroxyl group at the C2' position with the carboxyl group in glutaric acid, forming an ester bond between the drug and linker (Figure 2-17). The successful formation of the ester bond between paclitaxel and glutaric acid was demonstrated by the upfield shift of the methine group (CH-O) from 4.78 ppm in the paclitaxel  $^1\text{H}$  NMR spectrum (Figure 2-15) to 5.49 ppm in the pac-glu spectrum (Figure 2-18). The upfield shift of the C3' proton was observed to change from 5.76 ppm in paclitaxel  $^1\text{H}$  NMR spectrum to 6.00 ppm in pac-glu  $^1\text{H}$  NMR spectrum due to the ester bond formed.

This ester bond formation at C2' position was further confirmed with  $^{13}\text{C}$  NMR. In the pac-glu  $^{13}\text{C}$  spectrum (Figure 2-19), the appearance of g2, g3, g4 and g5 peaks at 32.39, 19.72, 32.70 and 176.26 ppm, respectively, indicates the existence of glutaric acid in the product. A new ester carbonyl peak was also found at 171.98 ppm (C-COO) which

corresponded to the covalent bond between the drug and linker. Furthermore, the downfield shift of the C2' peak from 73.33 ppm in paclitaxel (Figure 2-16) to 74.21 ppm in pac-glu (Figure 2-19), and the upfield shift of C3' peak from 55.20 ppm to 52.84 ppm indicated successful ester bond formation at the C2' position in paclitaxel. Theoretically, there are 3 hydroxyl groups at C2', C1 and C7 in paclitaxel that can be used as reaction sites for the ester bond formation. It has been reported previously that C2' and C7 hydroxyl groups are the most suitable sites for structural conjugation in paclitaxel (117, 145). The primary C2' hydroxyl is a more reactive site than C7 hydroxyl due to less steric hindrance, hence esterification is more likely to occur at C2' position (146-148). However, there are possibilities that conjugates with more than one confirmation can be formed if reaction occurs at either these two sites. In this work, the peaks corresponding to C1 and C7 were observed to be unchanged in the  $^{13}\text{C}$  NMR spectrum of pac-glu (Figure 2-19) compared to the spectrum of non-reacted paclitaxel (Figure 2-16). Therefore, this confirmed that the ester bond was formed only at the C2' hydroxyl position of paclitaxel.

The conjugation of paclitaxel and glutaric anhydride was also confirmed by using electrospray mass spectrometry (ESI-MS). In Figure 2-20(a), two peaks of free paclitaxel were detected at a molecular weight of  $[\text{M}^+ + \text{H}]$  854.2 Da/e and  $[\text{M}^+ + \text{Na}]$  876.20 Da/e which is consistent with the theoretical molecular weight of paclitaxel ( $\text{C}_{47}\text{H}_{51}\text{NO}_4$ ) 853.91 g/mol. After the conjugation with glutaric anhydride, two peaks at molecular weight of  $[\text{M}^+ + \text{H}]$  968.20 Da/e and  $[\text{M}^+ + \text{Na}]$  990.20 Da/e were observed in Figure 2-20(b). The spectra results were consistent with the theoretical molecular weight of 2'-glutaryl-paclitaxel ( $\text{C}_{52}\text{H}_{57}\text{NO}_7$ ) (967.91 g/mol), indicating the successful synthesis of 2'-glutaryl-paclitaxel.

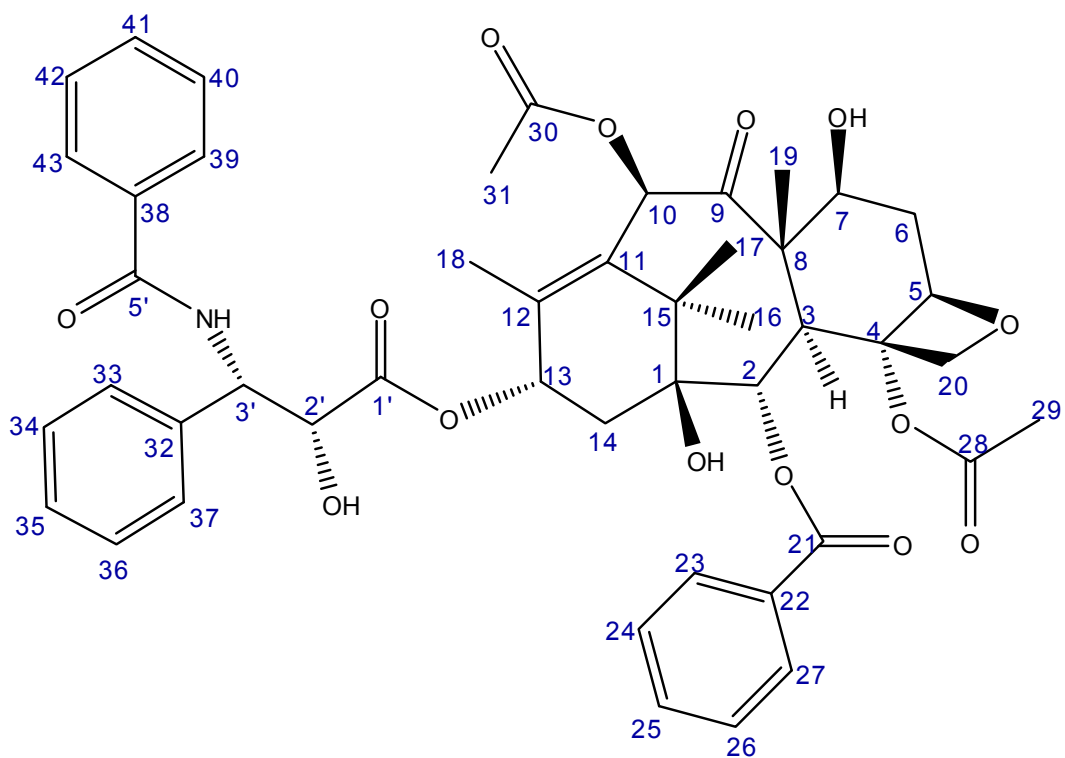


Figure 2-14: Chemical structure of paclitaxel with numbered carbons.

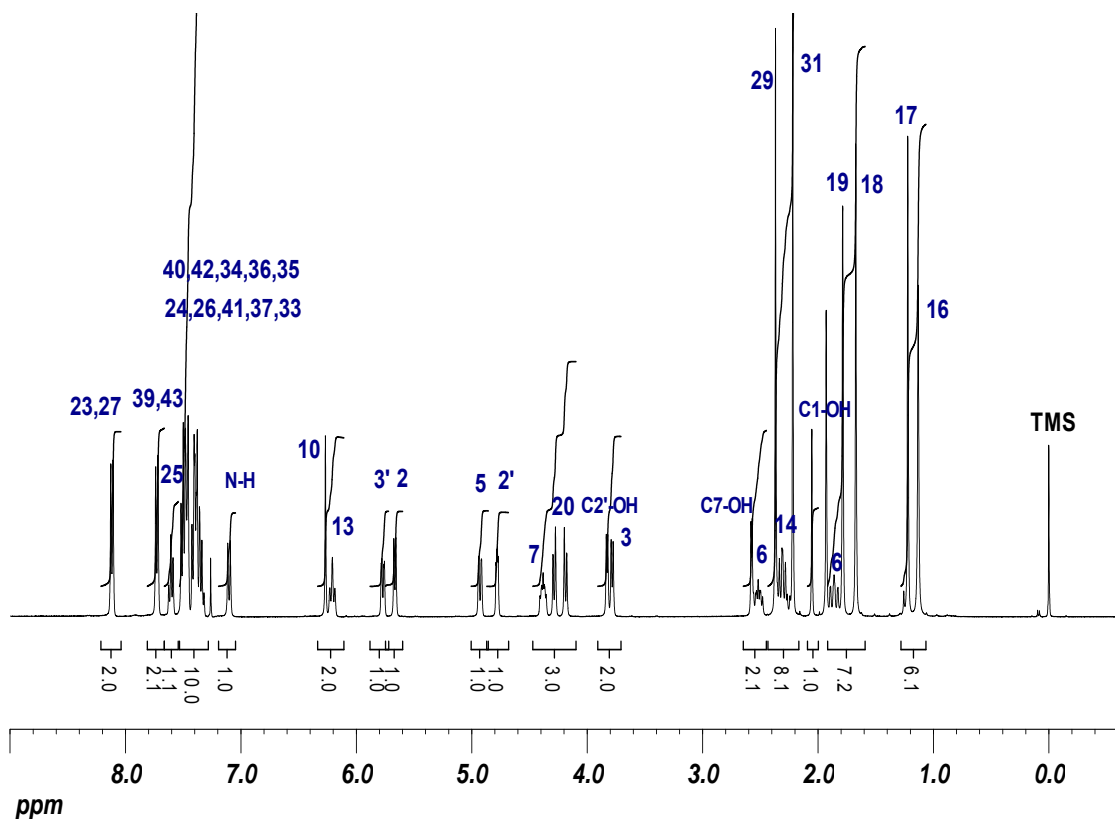


Figure 2-15:  $^1\text{H}$  NMR spectrum of paclitaxel.

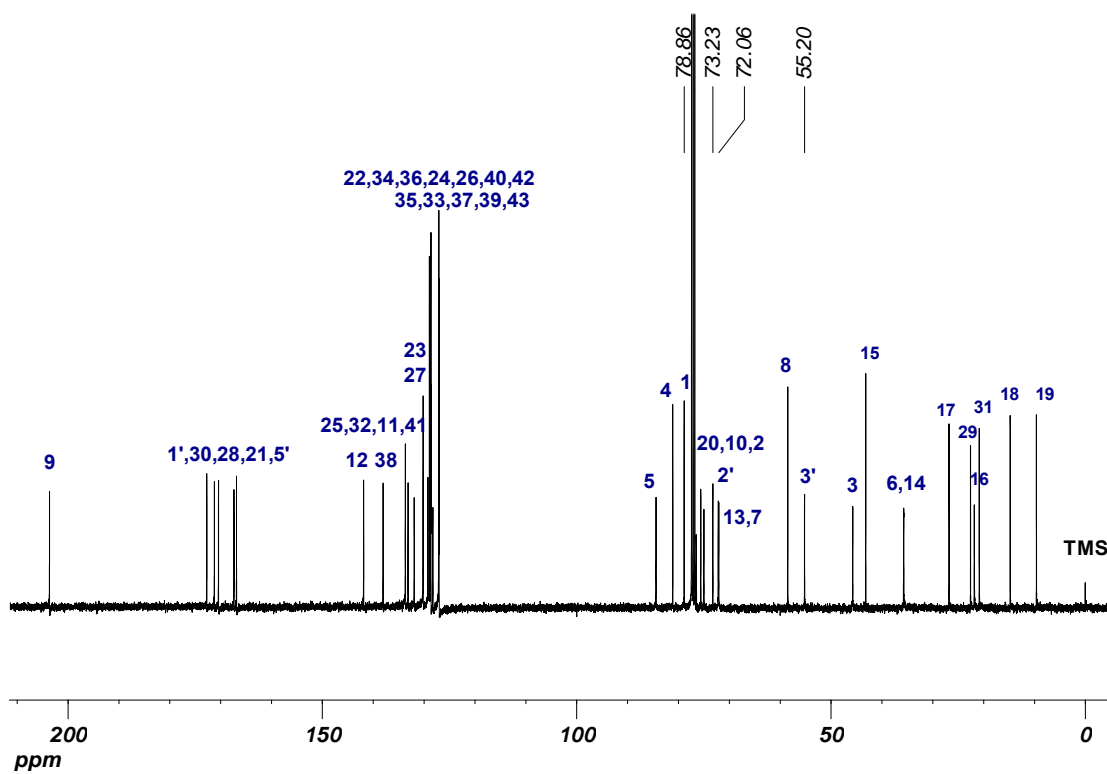


Figure 2-16:  $^{13}\text{C}$  NMR spectrum of paclitaxel.

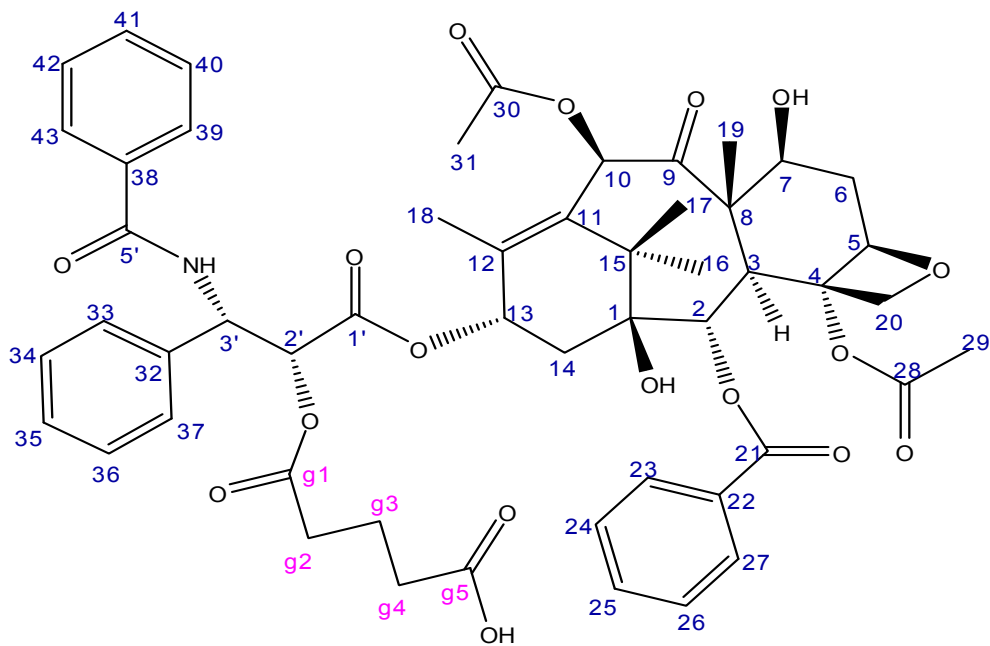


Figure 2-17: Chemical structure of 2'-glutaryl-paclitaxel with numbered carbons.

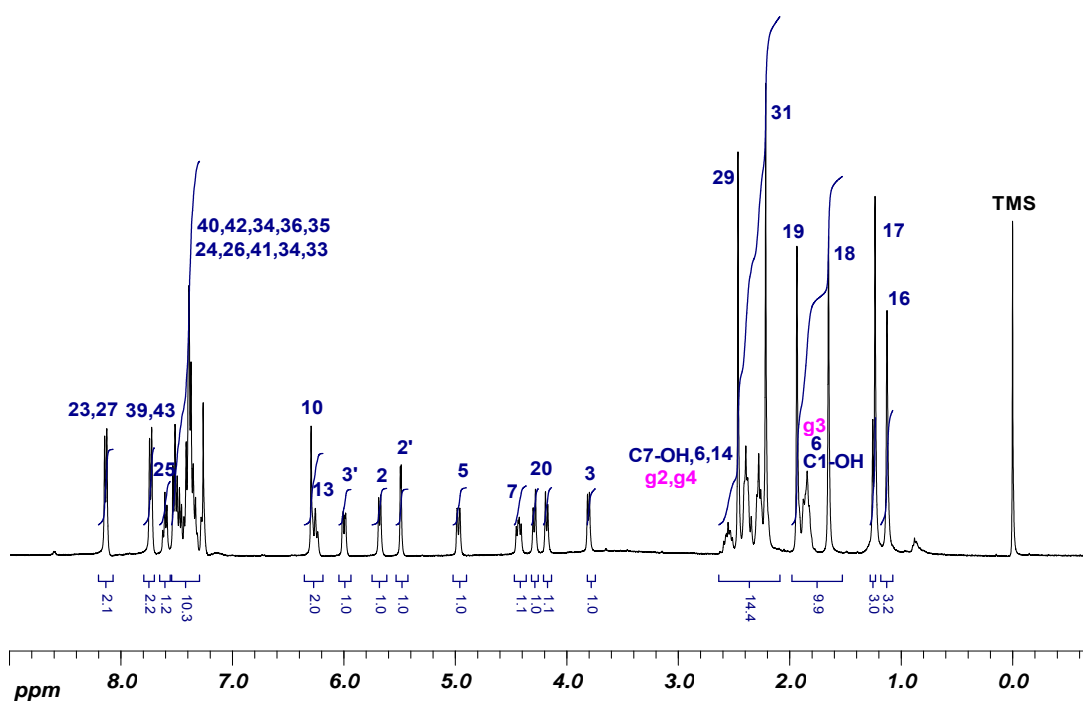


Figure 2-18: <sup>1</sup>H NMR spectrum of 2'-glutaryl-paclitaxel.

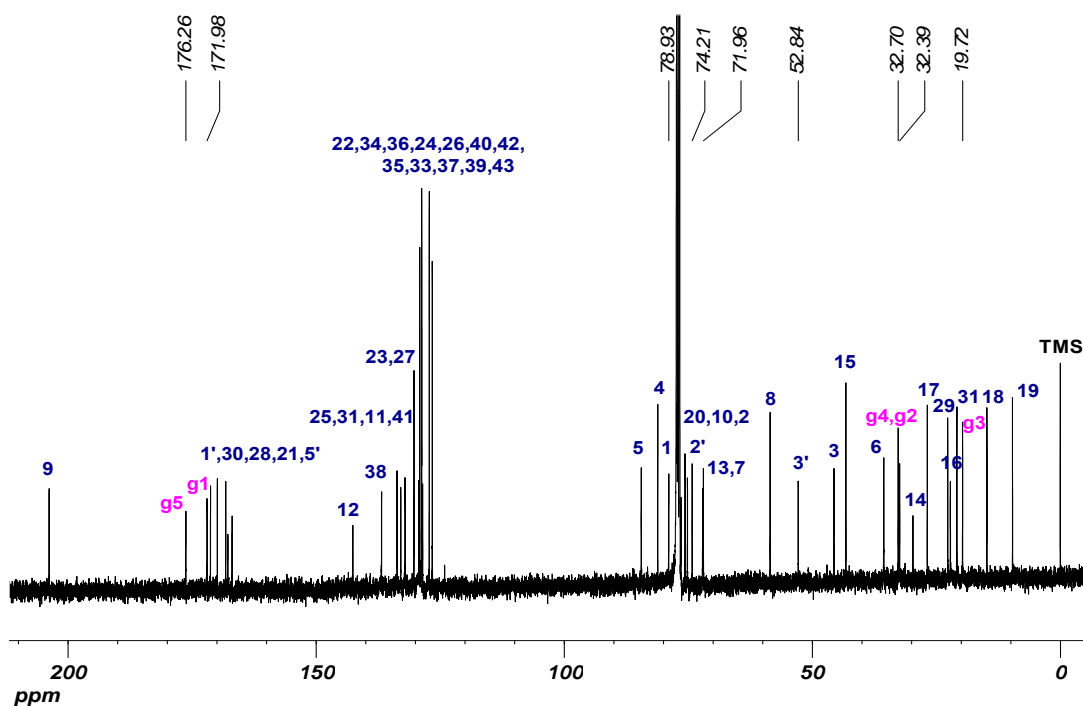
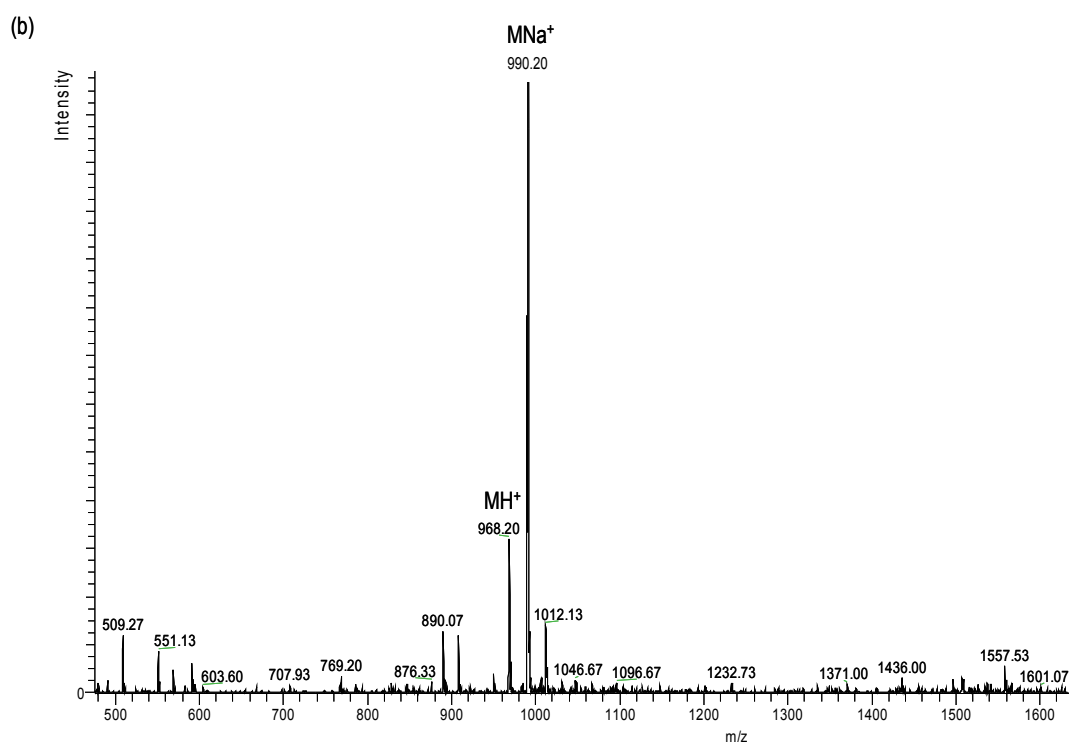
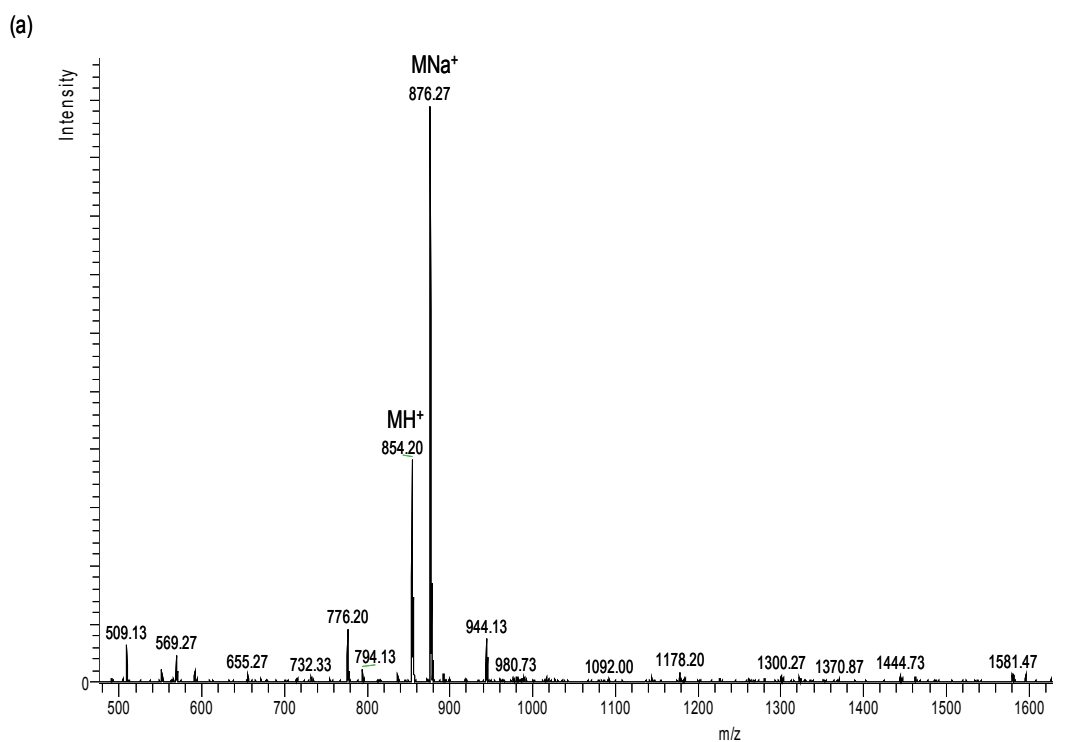


Figure 2-19: <sup>13</sup>C NMR spectrum of 2'-glutaryl-paclitaxel.



**Figure 2-20: Electrospray ionisation mass spectra (ESI-MS) of (a) paclitaxel, and (b) 2'-glutaryl-paclitaxel. Synthesis was repeated more than 3 times and products were characterised after each synthesis.**

### 2.3.2.2 Synthesis of pac-glu-NHS active ester

2'-glutaryl-paclitaxel (pac-glu) was reacted in an equimolar ratio with G3 and/or lauryl-G3 PAMAM dendrimers using the active ester NHS method (144). The active ester was prepared by using N-succinimidyl diphenylphosphate (SDPP) (synthesised in section 2.2.3.2) rather than the DCC method (149). Using the phosphate coupling agent, the NHS method was found to be more convenient and efficient than the DCC method. Pac-glu-NHS ester was characterised with  $^1\text{H}$  NMR and  $^{13}\text{C}$  NMR spectroscopies.

From the  $^1\text{H}$  NMR spectrum of pac-glu-NHS ester (Figure 2-22), four additional protons were observed from the peak integration at chemical shifts of 1.72 – 2.3 ppm. These four protons originate from n3 and n4 in the active ester (Figure 2-21) and indicate the existence of succinimide in the product. This was further confirmed by the appearance of two new peaks of  $-\text{CH}_2-$  at 169.27 and 25.49 ppm found in the  $^{13}\text{C}$  NMR spectrum of pac-glu-NHS (Figure 2-23). These two peaks correspond to n1, n2 and n3, n4 carbon molecules of the active ester. The successful conjugation between the carboxyl group of pac-glu and the succinimide was confirmed by the  $^{13}\text{C}$  NMR spectrum. The g5 carbon peak shifted upfield from 176.26 ppm in the  $^{13}\text{C}$  NMR spectrum of pac-glu to 168.03 ppm in pac-glu-NHS spectrum; where the g4 carbon peak shifted upfield from 32.70 ppm to 26.78 ppm, indicating the successful formation of covalent bond between the carboxyl group at the g5 and succinimide.

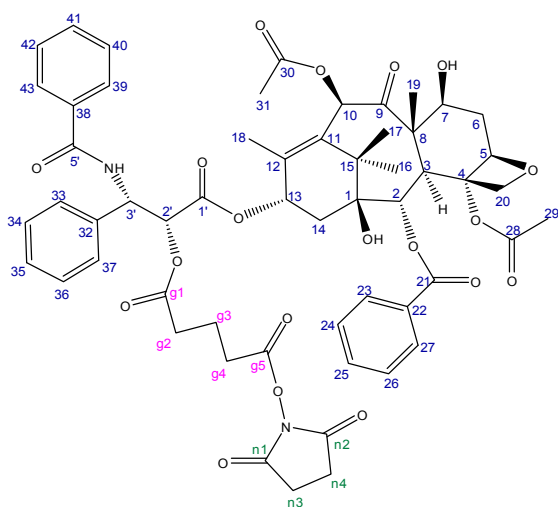


**Figure 2-21: Chemical structure of pac-glu-NHS ester with numbered carbons.**

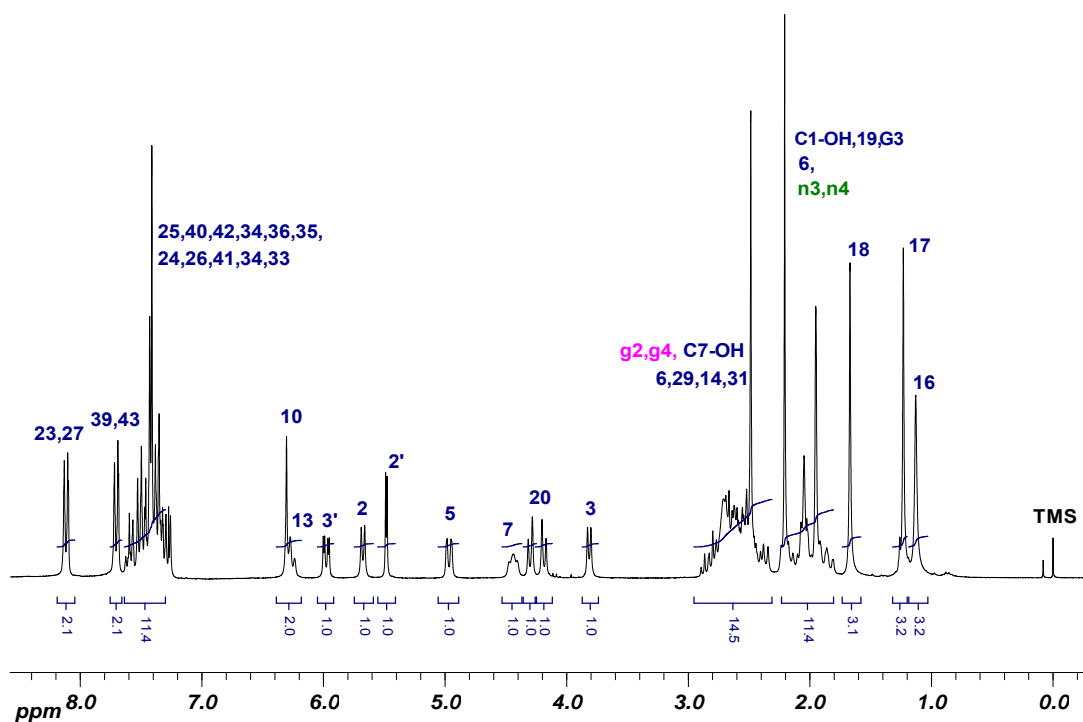


Figure 2-22: <sup>1</sup>H NMR spectrum of pac-glu-NHS.

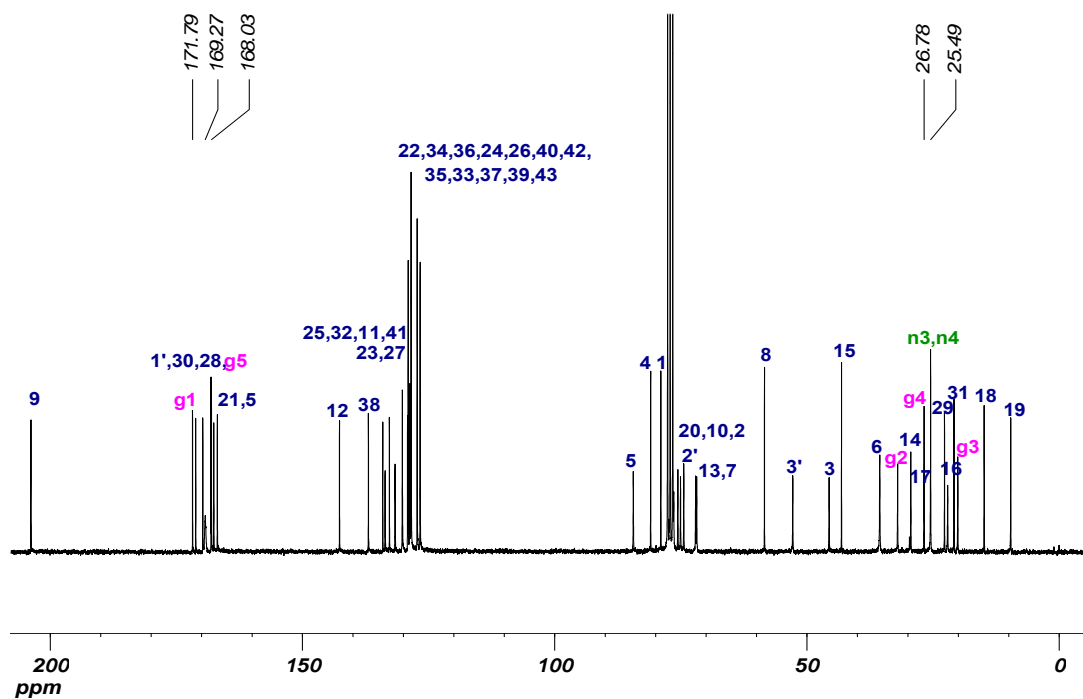
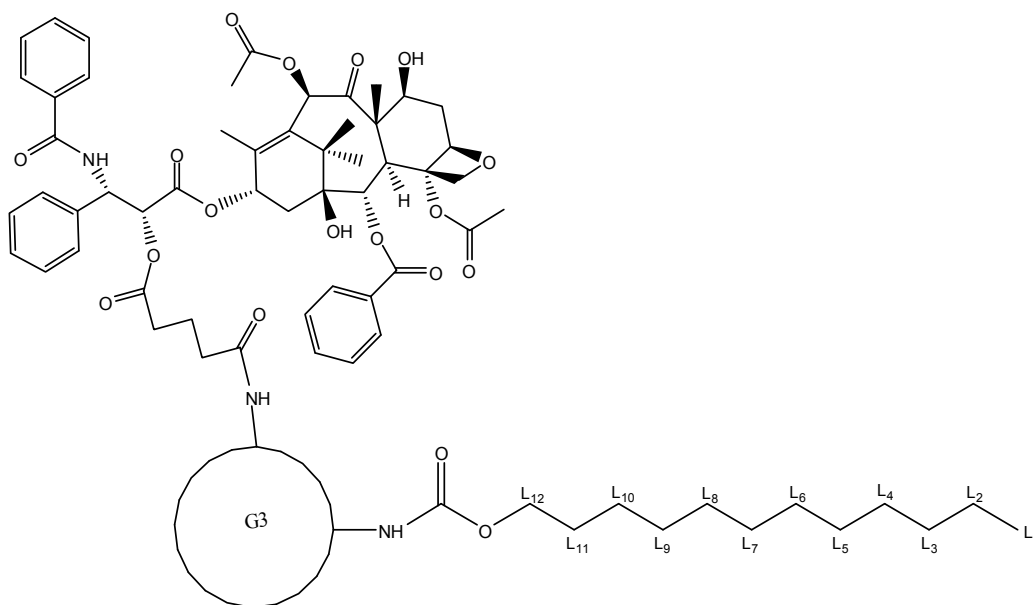


Figure 2-23: <sup>13</sup>C NMR spectrum of pac-glu-NHS.

### 2.3.2.3 Conjugation of pac-glu to G3/ lauryl-G3 PAMAM dendrimers

Pac-glu-NHS was conjugated to the surface amine group of G3 and/or lauryl-G3 PAMAM dendrimers via an amide bond. The dendrimer conjugates were purified by size exclusion chromatography and characterised with TLC and  $^1\text{H}$  NMR spectroscopy. The 1:1 molar ratio of dendrimer to paclitaxel was determined by comparing the peak integrals of the aromatic protons of paclitaxel (7.23 – 8.25 ppm) to those of G3 PAMAM dendrimers (Figure 2-25). The average number of pac-glu per G3 and/or lauryl-G3 PAMAM dendrimers was calculated and shown in Table 2-3.



**Figure 2-24: Chemical structure of L-G3-glu-pac conjugate.**

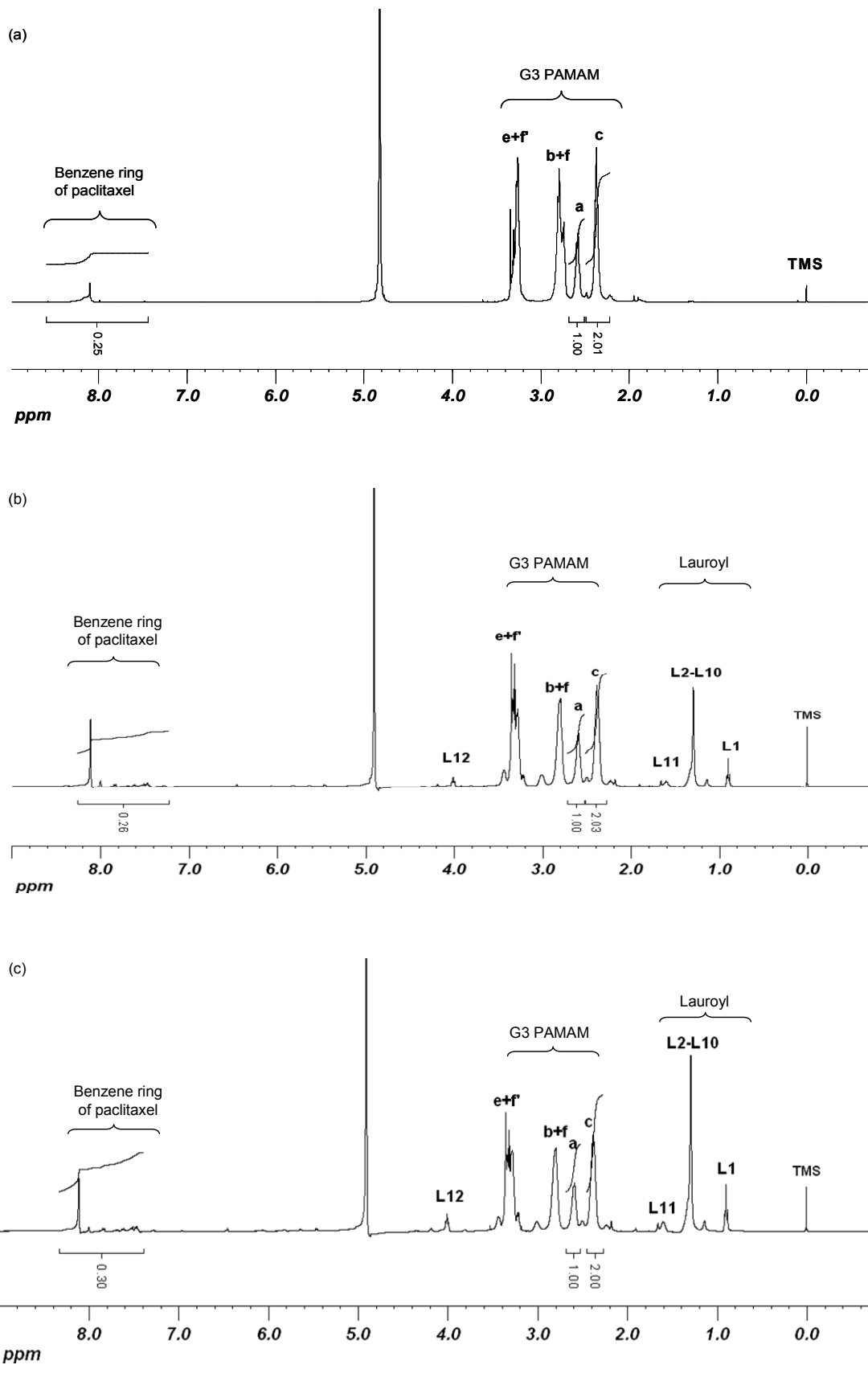


**Figure 2-25:  $^1\text{H}$  NMR spectra of (a) G3-glu-pac, (b) L3-G3-glu-pac, and (c) L6-G3-glu-pac.**

G3 conjugates	Conjugation ratio G3Lx: glu-pac
G3-glu-pac	1: 1.0
G3L3-glu-pac	1: 1.04
G3L6-glu-pac	1:1.20

**Table 2-3: Molar ratio of pac-glu conjugated to G3 and lauryl-G3 PAMAM dendrimers determined by comparison of relative peak integral from the  $^1\text{H}$  NMR spectra ( $n = 3$ ).**

### 2.3.3 Synthesis and characterisation of FITC-labelled G3 PAMAM dendrimer and conjugates

Fluorescein isothiocyanate (FITC) was conjugated to G3 dendrimer through a thiourea bond between the dendrimer surface amine group and the isothiocyanate group of FITC. Method II used by Jevprasesphant (103) was preferred due to difficulties in removing DMSO from the final product in method I. However, the dialysis purification method employed by both methods could not remove free FITC molecules efficiently. Free FITC traces were detected by TLC. Thus, purification of the FITC labelled dendrimer conjugates was conducted by using size exclusion chromatography. The absence of free FITC in the conjugates was confirmed by TLC. The final purified conjugates were characterised by  $^1\text{H}$  NMR spectroscopy.

Proton peaks corresponding to FITC occur in the chemical shift region of 6.50 – 8.02 ppm, whereas dendrimers demonstrated a group of peaks in the region of 2.00 – 3.40 ppm. The  $^1\text{H}$  NMR spectrum of the FITC-labelled G3 PAMAM dendrimer (Figure 2-26) showed peaks in both regions. The 1:1 molar ratio of the dendrimer and/or dendrimer conjugates to FITC can be determined by comparing the integrations of the  $^1\text{H}$  NMR peaks originating from the FITC substituents to those of G3 dendrimers. In the  $^1\text{H}$  NMR spectrum (Figure 2-26), peak *a* represents 60 protons from the G3 dendrimer whilst peak *b* represents 6 protons from FITC, giving a molar ratio of 1:1 for G3: FITC. TLC analysis was also conducted for an equimolar mixture of FITC and dendrimer

conjugates. The TLC results demonstrated isolation of FITC. This eliminated the possibility of an electrostatic interaction between FITC and dendrimer in the conjugates (150). Hence, the TLC and  $^1\text{H}$  NMR spectroscopy results confirmed the covalent conjugation.

Prior to use in biological studies, the chemical stability of the thiourea bond between the FITC and G3 dendrimer was examined by incubating the conjugates in HBSS (pH 7.4) at  $37^\circ\text{C}$  for 5 days. The TLC results with a single spot at the baseline ( $R_f = 0.0$ ) observed indicated that no free FITC was released. FITC-labelled G3 PAMAM dendrimer and conjugates were found to possess a stable thiourea linkage.

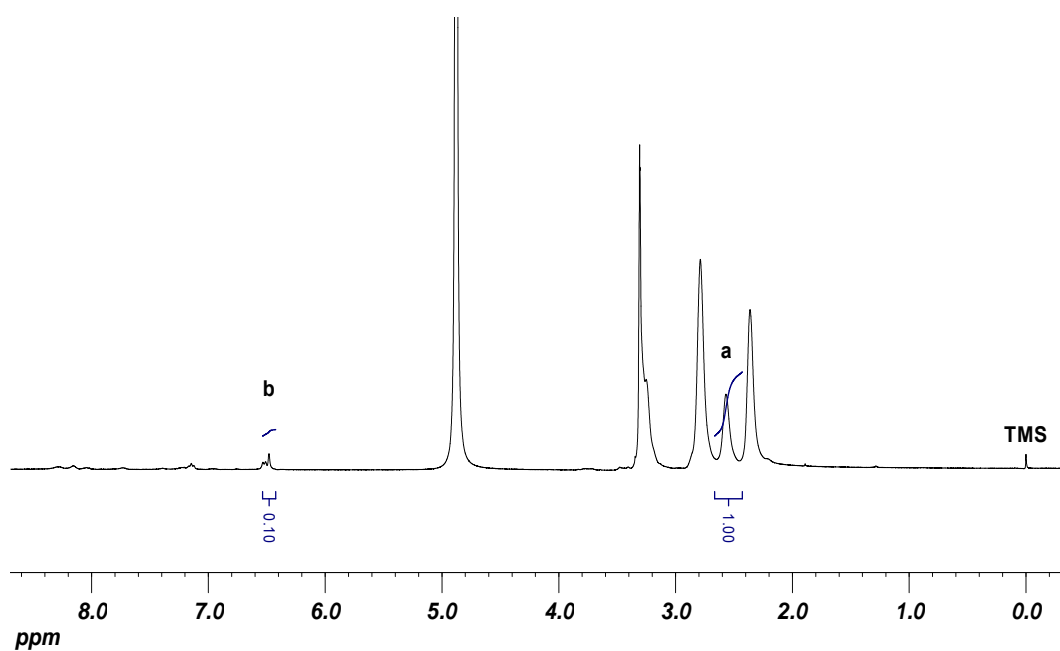


**Figure 2-26:  $^1\text{H}$  NMR spectrum of FITC-G3 PAMAM dendrimer.**

Analysis of size distribution of all the FITC-labelled PAMAM dendrimer conjugates was performed using dynamic light scattering. The light scattering study results were summarised in Table 2-4. As shown in the table, the diameters of FITC-labelled G3, -G3L3, -G3L6 conjugates are 6.72, 10.49 and 10.67 nm, respectively. After conjugation with drug, the diameter of the dendrimer conjugates was observed to increase

accordingly. The diameters of FITC-labelled G3-glu-pac, -G3L3-glu-pac and -G3L6-glu-pac were found to be 11.34, 13.62 and 13.66 nm. There is no significant aggregation or presence of large particles observed from the particle size measurements (Figure 2-27 and Figure 2-28).

<b>Dendrimer conjugates</b>	<b>Diameter (nm)</b>
FITC-G3	6.72 ± 1.35
FITC-G3L3	10.49 ± 0.19*
FITC-G3L6	10.67 ± 0.10*
FITC-G3-glu-pac	11.34 ± 0.73*
FITC-G3L3-glu-pac	13.62 ± 2.75*
FITC-G3L6-glu-pac	13.66 ± 1.25*

**Table 2-4: Hydrodynamic diameter of FITC-labelled G3 PAMAM dendrimer and dendrimer conjugates in HBSS at 37°C (mean ± SD, n = 10 of triplicate experiments). \* indicates a significant difference ( $p < 0.05$ ) for other conjugates compared to FITC-G3.**

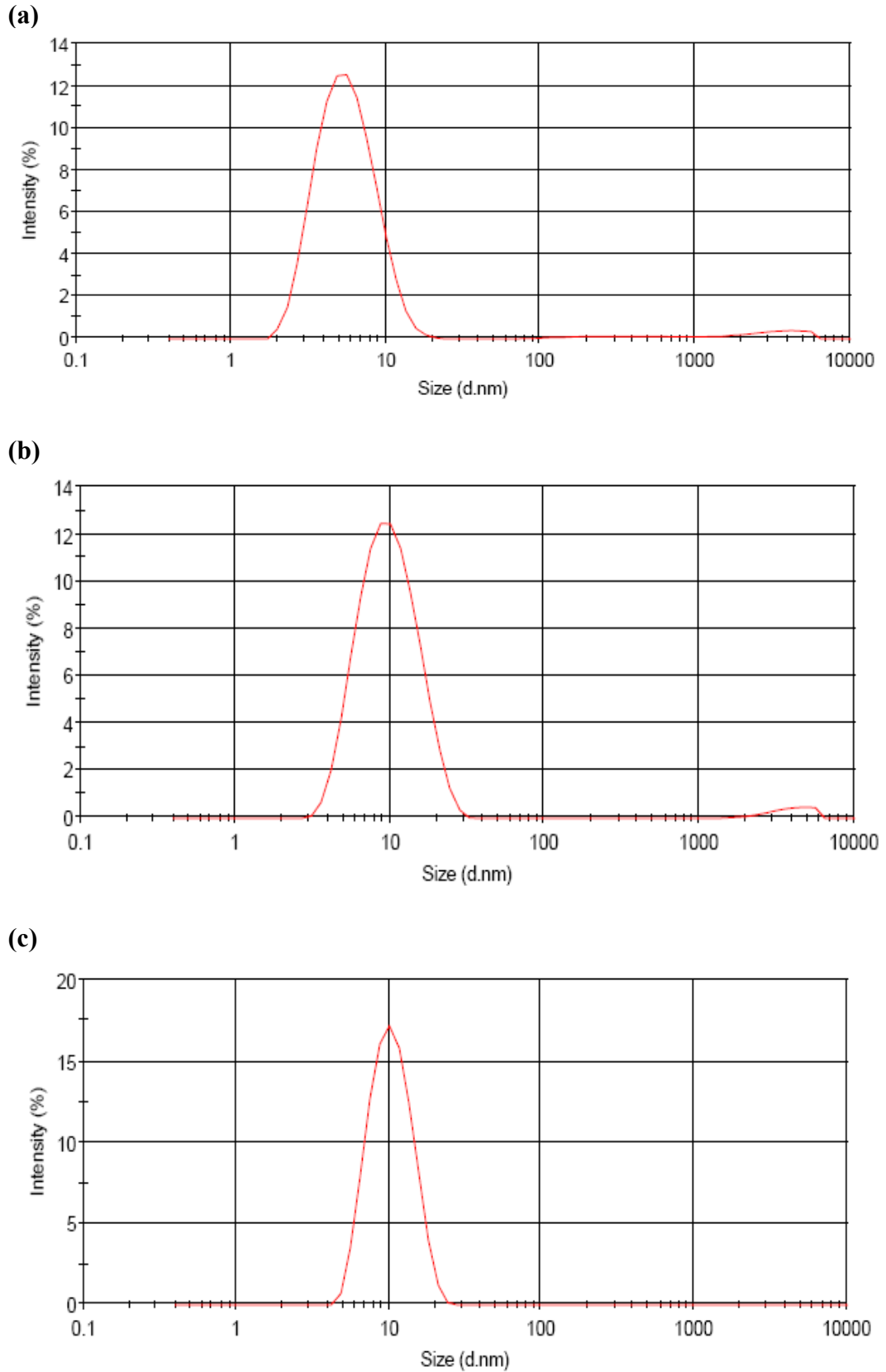
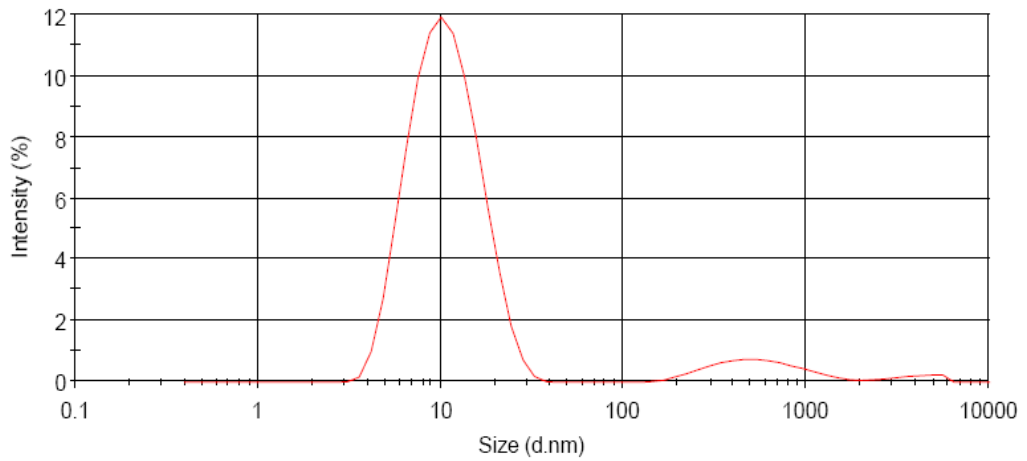
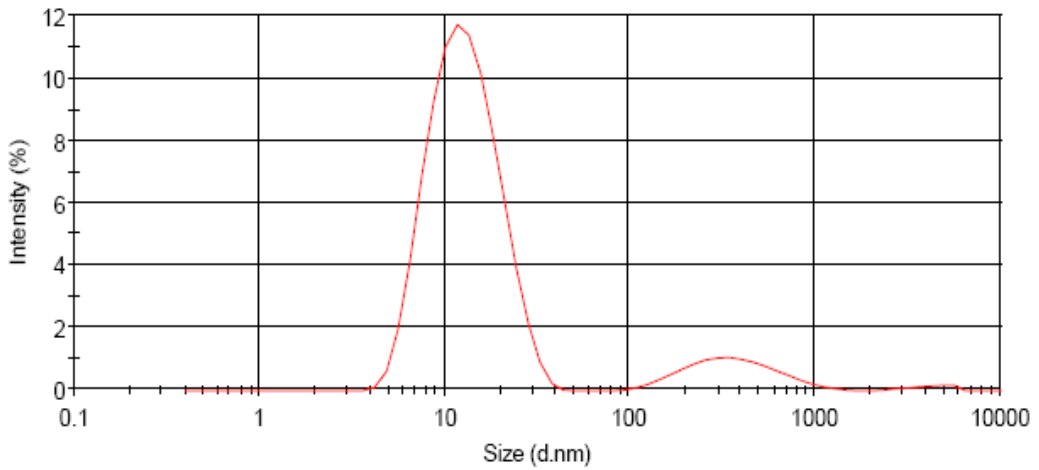


**Figure 2-27: Size distribution of (a) FITC-labelled G3, (b) FITC-labelled G3L3, and (c) FITC-labelled G3L6, (mean  $\pm$  SD, n = 10 of triplicate experiments).**

(a)



(b)



(c)

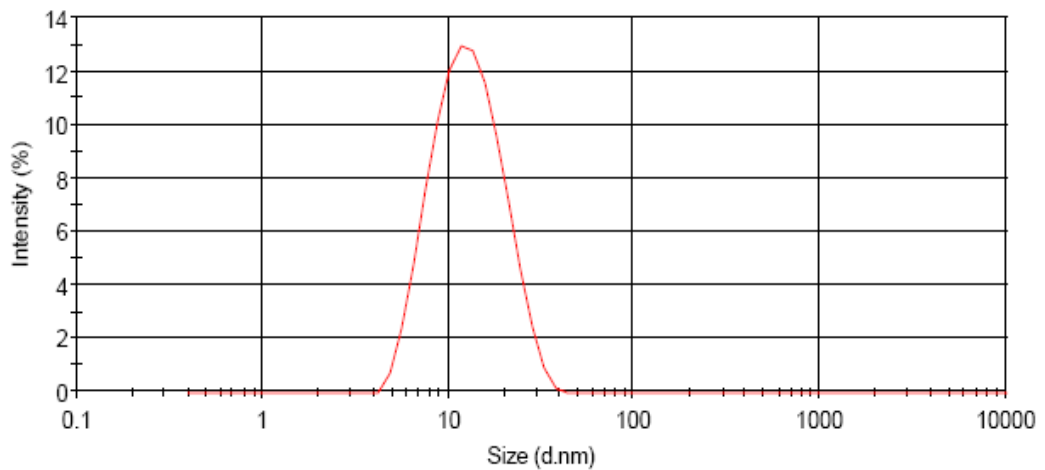


**Figure 2-28: Size distribution of (a) FITC-labelled G3-glu-pac, (b) FITC-labelled G3L3-glu-pac, and (c) FITC-labelled G3L6-glu-pac, (mean  $\pm$  SD, n = 10 of triplicate experiments).**

### 2.3.4 Chemical stability of G3 PAMAM dendrimer conjugates

Stability studies of the dendrimer conjugates were conducted at pH 1.2, 7.4 and 8.5. FITC-G3L6-glu-pac was chosen as the dendrimer conjugate for the studies. The percentage of conjugates remaining after hydrolysis of the ester bond is shown in Table 2-5. The results showed that the stability of dendrimer conjugates were high with more than 90% of conjugates remains intact at all pHs after 48 h of incubation at 37°C. At pH 1.2, approximately 84% and 69% of the conjugates were remained stable after 5 and 10 days. Stability of conjugates in the alkaline conditions (pH 8.5) was slightly higher than that at pH 1.2 with approximately 87% and 75% of conjugates remain intact after 5 and 10 days. The ester bond of the dendrimer conjugates showed good stability under physiological conditions (pH 7.4 and 37°C) with more than 85% of conjugates remain intact even after 10 days of incubation. It has been previously reported that paclitaxel can be released from various conjugates via hydrolysis of ester bond at different rates (118, 151-153). Stability assay reported by Bi and co-workers (118) showed that no significant release of free paclitaxel for the conjugates using glutaric acid linker after 7 days of incubation in PBS buffer (pH 7.4). Our results of stable ester bond of FITC-G3L6-glu-pac under similar chemical conditions are in agreement with their findings.

Time, h	% Conjugate remaining		
	pH = 1.2	pH = 7.4	pH = 8.5
48	96.20 ± 0.7	98.83 ± 1.0	93.85 ± 1.4
120	84.65 ± 1.2	96.43 ± 1.7	87.45 ± 2.3
240	69.51 ± 0.5*	87.05 ± 0.5*	75.24 ± 0.6*

**Table 2-5 Chemical stability of FITC-G3L3-glu-pac incubated at pH 1.2, 7.4 and 8.5 (37°C). (mean ± SD, n = 3 of triplicate experiments). \* indicates a significant difference ( $p < 0.05$ ) from 48 h compared to pH change at 240 h.**

## 2.4 Conclusions

Novel dendrimer-based drug delivery systems consisting of the dendrimer – G3 PAMAM, the permeability enhancer moieties – lauryl chains, the linker – glutaric anhydride and the drug – paclitaxel were successfully synthesised and characterised. Lauryl chains were conjugated covalently to the surface amine groups of G3 PAMAM dendrimer through carbamate bonds, giving dendrimer conjugates of G3L3, G3L6 and G3L9. The 1:3, 1:6 and 1:9 molar ratios of dendrimer to lauryl chains were determined by  $^1\text{H}$  NMR spectroscopy. Paclitaxel was attached to the dendrimer surface amine group via a glutaric anhydride linker using the active ester NHS method. The drug-linker (pac-glu) and the active ester (pac-glu-NHS) were characterised with  $^1\text{H}$  NMR,  $^{13}\text{C}$  NMR spectroscopies and ESI-MS. The active ester, pac-glu-NHS, was subsequently conjugated to the unmodified G3 and surface modified G3L3 and G3L6, giving G3-glu-pac, G3L3-glu-pac and G3L6-glu-pac conjugates. The number of drug-linker attached to the unmodified and surface modified G3 PAMAM dendrimer was determined from the relative integrals of the  $^1\text{H}$  NMR peaks of paclitaxel and G3 dendrimer conjugates. All the dendrimer conjugates were labelled with a fluorophore (namely FITC) at a molar ratio of 1:1, and characterised by TLC and  $^1\text{H}$  NMR. The average hydrodynamic diameter of FITC-labelled G3 PAMAM dendrimer (FITC-G3) was approximately 6.72 nm while the average diameters of FITC-labelled G3 PAMAM conjugates (FITC-G3L3, FITC-G3L6, FITC-G3-glu-pac, FITC-G3L3-glu-pac, and FITC-G3L6-glu-pac) were approximately 10 – 14 nm. Chemical stability studies showed that dendrimer conjugates were stable at all pHs after 48 h of incubation. Ester bond of the conjugates are stable in a range of pHs following 10 days of incubation. The FITC-labelled dendrimer conjugates were evaluated in quantitative permeability studies using Caco-2 and blood-brain barrier cell monolayers.

**CHAPTER 3: BIOLOGICAL EVALUATION OF G3 PAMAM  
DENDRIMER AND DRUG CONJUGATES WITH  
CACO-2 CELLS**

---

### 3.1 Introduction

The pharmaceutical applications of dendrimers have been extensively explored. The dendritic well-defined structure allows precise control of size, shape and surface group functionality (88, 91). More recently, dendrimer-based delivery systems have demonstrated effective intracellular transport of drugs across cellular barriers.

Previous work in our research group has shown the ability of PAMAM dendrimer conjugates to enhance drug solubility and bypass P-glycoprotein (P-gp) efflux transporters, therefore increasing drug bioavailability (83, 86, 87). G3 PAMAM dendrimer was reported as a potential drug carrier for propranolol, a P-gp substrate drug with low water solubility. Enhanced permeability and ability to bypass the P-gp efflux transporter were observed when propranolol was conjugated to surface modified G3 PAMAM dendrimer (83). Surface engineered PAMAM dendrimers with lauryl chains demonstrate enhanced permeability and lower cytotoxicity compared to unmodified dendrimers (103, 106). Conjugation of drugs to PAMAM dendrimers via biodegradable linker was assessed by Najlah *et. al.* (85-87). Diethylene glycol (deg) and succinic acid (suc) were used as linkers to conjugate drugs to PAMAM dendrimers. Enhanced solubility and permeability were found when naproxen was conjugated to G0 PAMAM dendrimer via a deg linker. Further studies were conducted with conjugates of terfenadine (a water-insoluble P-gp substrate drug) with a lauryl surface modified G1 PAMAM dendrimer via a double linker (suc-deg). The dendrimer prodrug demonstrated enhanced permeability and solubility, and ability to bypass the P-gp efflux transport system.

In the present study, paclitaxel was selected as an unambiguous P-gp substrate drug with low water solubility. Paclitaxel is a chemotherapeutic agent and belongs to a new class of antimicrotubule anticancer drugs (143). It promotes microtubule polymerisation which disrupts the normal tubule dynamics essential in cellular division, leading to cell death by apoptosis (154). Despite of its clinical efficacy, pharmaceutical applications of paclitaxel are limited by its low water solubility. Paclitaxel permeability across the intestinal barrier is also significantly limited by the P-gp efflux transport system, resulting in low oral bioavailability.

Novel drug carrier systems based on PAMAM dendrimer, consisting G3 PAMAM dendrimer, the permeability enhancer moieties – lauryl chains, the linker – glutaric anhydride, and the drug – paclitaxel, were biologically evaluated in the present study. Cytotoxicity of G3 PAMAM dendrimer and conjugates was determined using Caco-2 cells. Caco-2 cells is a widely used *in vitro* cell culture model for studies of intestinal drug absorption (131). Lactate dehydrogenase (LDH) release assay was used to determine dendrimer and conjugates toxicity towards the Caco-2 cells. The permeation of dendrimer and conjugates across the cell monolayers was conducted using non-toxic concentrations of the dendrimer and conjugates as determined from cytotoxicity study. Integrity of the cell monolayers was also evaluated by measuring the transepithelial electrical resistance (TEER) across the cell monolayers.

## 3.2 Materials and methods

### 3.2.1 Materials

Triton X-100, trypan blue, Corning Transwell® polycarbonate membrane inserts (pore size 3.0µm, membrane diameter 12mm), Corning® Costar® 96 well flat bottom cell culture plates, phosphate buffer saline (PBS), and dimethylsulfoxide (DMSO) were purchased from Sigma-Aldrich Co. Ltd. (Gillingham, Dorset, UK). Dulbecco's Modified Eagles Medium (DMEM) high glucose, foetal bovine serum (FBS), L-glutamine, non-essential amino acid, 50 IU/ml penicillin and 50mg/ml streptomycin, trypsin-ethylenediaminetetraacetic acid (EDTA) 0.25%, (4-(2-hydroxyethyl)-1-piperazineethanesulfonic acid) buffer solution (HEPES), and Hank's Balanced Salt Solution (HBSS) were purchased from Gibco BRL, Invitrogen (Paisley, UK). Cytotoxicity detection kit (LDH) was purchased from Roche Applied Science (Mannheim, Germany). Caco-2 cells were kindly provided by Dr. Jeff Penny at The University of Manchester. G3 PAMAM dendrimers with ethylenediamine cores in methanol (20% w/w) were purchased from Dendritech Inc. Paclitaxel was purchased from Advance Tech. & Ind. Co., Ltd. (Kln, Hong Kong). G3 PAMAM-lauryl conjugates (G3-Lx), 2' glutaryl-paclitaxel (pac-glu), G3-glutarate-paclitaxel (G3-glu-pac) and lauryl-G3-glutarate-paclitaxel (Lx-G3-glu-pac), and FITC-labelled G3 PAMAM conjugates were synthesised and characterised as described in chapter 2.

### 3.2.2 Caco-2 cell culture techniques

#### 3.2.2.1 Maintenance and optimisation of growth conditions

Caco-2 cells (passage 54-68) were maintained in 75 cm<sup>2</sup> flasks containing growth medium (DMEM supplemented with 10% v/v FBS, 1% v/v non-essential amino acids, 2 mM glutamine, 50 IU/ml penicillin and 50 µg/ml streptomycin) at 37°C in an atmosphere of 5% CO<sub>2</sub> and 95% relative humidity.

### 3.2.2.2 Reviving cell stocks

A vial of Caco-2 cell lines stock stored in a liquid nitrogen tank was retrieved and thawed rapidly in a 37°C warm water bath. Contents of the vials were quickly transferred to a universal tube containing 4 ml growth medium. Cells were centrifuged at  $1000 \times g$  for 5 min and a cell pellet was formed. After removing the medium carefully, the cell pellet was resuspended in 10 ml growth medium in a T75 flask and incubated at 37°C in an atmosphere of 5% CO<sub>2</sub> and 95% relative humidity. Growth medium was changed on alternate days until the cells achieved 80 – 90% confluency for passaging.

### 3.2.2.3 Passaging cells

Upon achieving 80 – 90% cell confluency, growth medium was removed and cells were washed with 5 ml sterile PBS. After removing the PBS, cells incubated with 3 ml trypsin-EDTA solution (0.25% v/v) at 37°C in an atmosphere of 5% CO<sub>2</sub> and 95% relative humidity for 3-5 min to allow cell detachment. The trypsin solution was inactivated by adding the same amount (3 ml) of growth medium. The cells suspension was transferred to a universal tube and centrifuged at 1000 rpm for 5 min. After removing the supernatant, the cell pellet was resuspended and transferred as a 1:6 split to T75 flasks containing 10 ml growth medium.

### 3.2.2.4 Viable cell number counting by trypan blue assay

The number of viable cells was assessed by 0.4% (w/v) trypan blue exclusion analyses with a haemocytometer. The principle behind the assay was that viable cell with an intact membrane would exclude the dye and would appear to be stain free. In contrast, non-viable cells without an intact membrane would take up the dye and would appear to be stain blue.

The cell pellet was resuspended in growth medium as described in section 3.2.2.3. 0.2 ml cell suspension was added to a 1.5 ml microfuge tube containing 0.5 ml trypan blue

and 0.3 ml HBSS with 25mM HEPES, mixed well and incubated for 5-15 min, allowing the dye uptake by the non-viable cells. A volume of 20  $\mu$ l of the trypan blue cell suspension mixture was placed in each chamber of the haemocytometer and the number of viable cells was counted. Cell count was expressed as cells per ml or total cells.

### 3.2.2.5 Cryopreserving cells

After passaging, the cell pellet was resuspended in freezing medium (growth medium with 10% v/v DMSO). Cell suspension (1 ml) was transferred to a cryogenic vial and maintained at -80°C overnight prior to long term storage in liquid nitrogen.

### 3.2.3 Measurement of *in vitro* cytotoxicity of G3 PAMAM dendrimers and paclitaxel conjugates using Caco-2 cells

The *in vitro* cytotoxicity of G3 PAMAM dendrimer and paclitaxel conjugates was determined using the lactate dehydrogenase release (LDH) assay. Cell seeding density was obtained by optimal cell concentration determination and cytotoxicity tests on Caco-2 cells were conducted by quantification of lactate dehydrogenase release using a LDH detection kit (Roche Diagnostics).

#### 3.2.3.1 Lactate dehydrogenase release assay

Lactate dehydrogenase (LDH) is a stable cytoplasmic enzyme found in all cells. Upon damage of the plasma membrane, LDH is rapidly released. The released LDH from damaged cells when reacted with the reaction mixture of the assay, reduces  $\text{NAD}^+$  (Nicotinamide adenine dinucleotide) to  $\text{NADH} + \text{H}^+$  by the oxidation of lactate to pyruvate. This oxidation process then reduces the yellow tetrazolium salt INT (2-[4-iodophenyl]-3-4-nitrophenyl)-5-phenyltetrazolium chloride) by diaphorase catalyst to a red formazan salt. Figure 3-1 showed the reaction scheme of the enzyme release activity. The amount of red formazan formed was directly proportional to the number of lysed cells. Based on this principle, the assay measured the LDH release activity of damaged cells to determine the cytotoxicity of a substance.

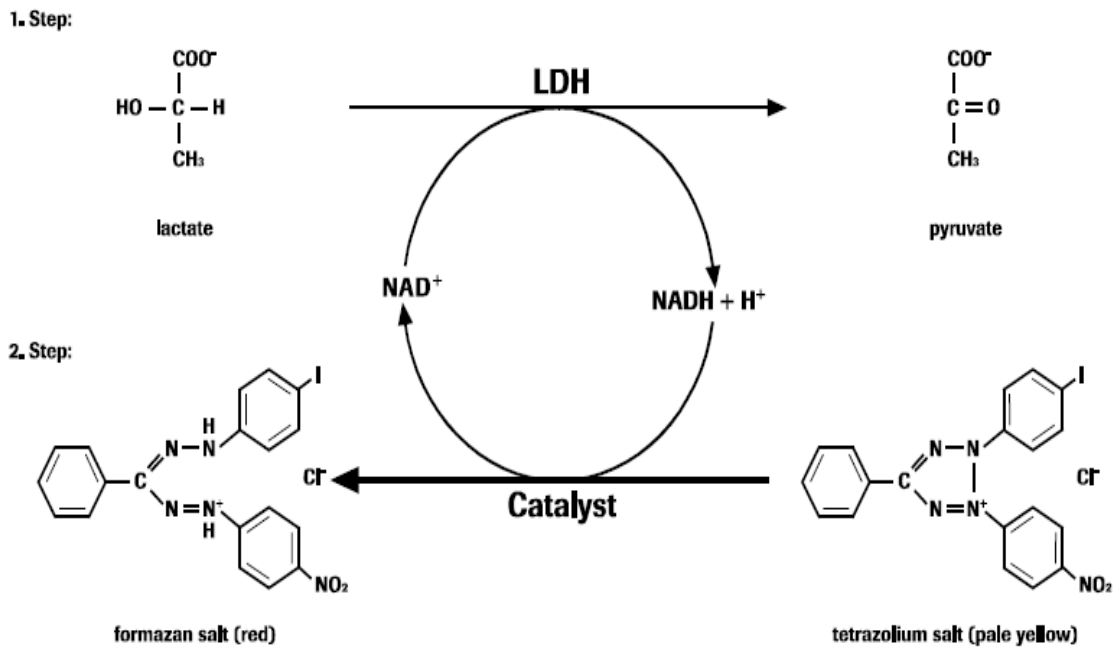


**Figure 3-1: Reaction scheme of LDH assay enzyme activity, taken from (155).**

### 3.2.3.2 Optimal cell concentration determination

After passaging cells as in section 3.2.2.3, the cell pellet was resuspended in growth medium (DMEM supplemented with 1% v/v FBS, 1% v/v non-essential amino acids, 50 IU/ml penicillin and 50  $\mu\text{g/ml}$  streptomycin) and cell number was assessed by trypan blue assay described in section 3.2.2.4. Cell suspension concentration was adjusted to  $1 \times 10^6$  cells/ml and followed by two-fold serial dilutions (up to 7 dilutions) with growth medium across the 96-well plate. The cells were incubated overnight at  $37^\circ\text{C}$  in an atmosphere of 5%  $\text{CO}_2$  and 95% relative humidity to allow cells adherence. After 24 h, the growth medium was removed and the cells were washed with sterile PBS. The removed growth medium was replaced with 200  $\mu\text{l}$  of low control (i.e. spontaneous LDH release, assay medium HBSS with 25 mM HEPES) or 200  $\mu\text{l}$  of the high control (i.e. maximum LDH release, 1% Triton X-100 in assay medium). A volume of 200  $\mu\text{l}$  of assay medium was also added to triplicate wells without cells as background control.

After 3 h of incubation at 37°C and 5% CO<sub>2</sub>, a 100 µl sample of the supernatant medium was removed from each well and placed into the corresponding wells of another 96-well plate. 100 µl of freshly prepared reaction mixture was added to each sample and then incubated for 30 min at room temperature, protected from light. The sample absorbance was then measured at 492 nm (reference wavelength of 612 nm) by a multiplate reader (TECAN GENios Pro, Grödig, Austria). A curve of the absorbance vs. cell seeding density was plotted for both low and high controls. The seeding density that produced the greatest difference between the high and low control absorbances with a value of less than or equivalent to 1 was identified as the optimal cell concentration.

### 3.2.3.3 Cytotoxicity studies

Caco-2 cells (Passage 54-62) in 100 µl growth medium (DMEM supplemented with 1% v/v FBS, 1% v/v non-essential amino acids, 50 IU/ml penicillin and 50 µg/ml streptomycin) were seeded into a 96-well plate at the optimal cell density determined in section 3.2.3.2. The cells were then incubated overnight at 37°C in an atmosphere of 5% CO<sub>2</sub> and 95% relative humidity to allow adherence of cells. After 24 h, the growth medium was removed and the cells were washed with sterile PBS. 200 µl of assay medium (HBSS with 25 mM HEPES) containing different concentrations of G3 PAMAM dendrimer, surface modified-G3 PAMAM, paclitaxel and conjugates were added to each well. Cells were also treated with low control (blank assay medium HBSS) and high control (1% Triton X-100 in assay medium). 200 µl of blank assay medium in the well without cells was used as background control. After 3 h of incubation, a 100 µl of the supernatant medium was removed from each well and placed into the corresponding wells of another 96-well plate to react with 100 µl of freshly prepared reaction mixture for 30 min at room temperature, protected from light. The sample absorbance was then measured at 492 nm (reference wavelength of 612 nm) by a multiplate reader. The percentage of cytotoxicity was calculated using equation below:

$$\% \text{ Cytotoxicity} = [(exp. - \text{low control}) / (\text{high control} - \text{low control})] \times 100\%$$

### 3.2.4 Transepithelial transport studies across Caco-2 cell monolayers

A well established method was used to investigate the transport of compounds across a monolayer of cells grown on a Transwell® insert. Figure 3-2 showed a sketch of the Transwell® insert. The upper chamber or apical side represented the luminal side of the intestinal epithelium while the lower chamber or the basolateral side represented the serosal side of the epithelium. Cell culture models were grown on the insert semi-permeable membrane and the permeability across the cell monolayers was measured as apparent permeability coefficient ( $P_{app}$ ). The transepithelial transport and permeability of a compound could be determined across the cell monolayers in two directions, apical to the basolateral ( $A \rightarrow B$ ) and basolateral to the apical ( $B \rightarrow A$ ) directions. Permeation in the  $A \rightarrow B$  direction indicates the quantitative intestinal absorption of a test compound across the cell culture model, while permeation in the  $B \rightarrow A$  direction suggested mediated transport by efflux transporters (e.g. P-gp) when a relatively higher apparent permeability coefficient of  $B \rightarrow A$  than  $A \rightarrow B$  is observed.

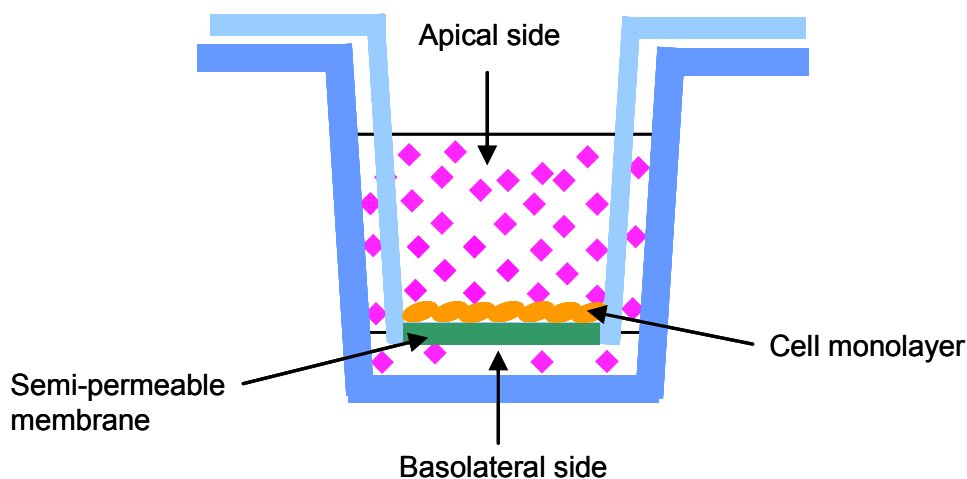


**Figure 3-2: A diagram of cell monolayer cultured on a Transwell® insert (108).**

#### 3.2.4.1 Caco-2 cell monolayer integrity

Measurement of transepithelial electrical resistance (TEER) of cells grown on Transwell® insert was conducted using a Voltohmmeter (EVOM, World Precision

Instruments, Sarasota, FL, USA) to assess the cell monolayers integrity. In general, the electrical resistance was measured using the chopstick electrodes with the shorter electrode placed in the inner Transwell® chamber whilst the longer electrode placed in the external bath solution. Reading of the background resistance of the filter membrane was taken as the blank control and the TEER for the monolayer was determined as the following equation:

$$\text{TEER } (\Omega \cdot \text{cm}^2) = (R_{\text{total}} - R_{\text{blank}}) \times A$$

$R_{\text{total}}$  = measured resistance of solution, membrane, and tissue

$R_{\text{blank}}$  = measured resistance of solution and membrane

$A$  = the surface area of filter (1 cm<sup>2</sup>)

#### 3.2.4.2 Permeability studies

Caco-2 cells (passage 54-62) with a density of  $1.2 \times 10^5$  cells/cm<sup>2</sup> were seeded onto a polycarbonate 12-well Transwell® insert (pore size 3.0µm). Cells were grown and maintained in growth medium (DMEM supplemented with 10% v/v FBS, 1% v/v non-essential amino acids, 50 IU/ml penicillin and 50 µg/ml streptomycin) at 37°C in an atmosphere of 5% CO<sub>2</sub> and 95% relative humidity, with medium change on alternative days for 21-23 days. The integrity and tight junction formation of the Caco-2 cells monolayers were tested on alternative days (during medium change, 21-23 days), before and after experiments by measuring the TEER.

Before conducting the permeability experiments, cells were washed twice with PBS and subsequently equilibrated with transport medium (HBSS with 25 mM HEPES) for 20 min at 37°C in an atmosphere of 5% CO<sub>2</sub> and 95% relative humidity, and the TEER was measured. Only confluent monolayers with TEER values (corrected against the blank filter resistance) in a range of 800-1000 Ωcm<sup>2</sup>, were used in studies. Transport of FITC-labelled G3 PAMAM dendrimer and surface-modified dendrimers (Lx-G3, Lx-G3-glu-pac and G3-glu-pac), free paclitaxel and pac-glu was determined in both A→B and B→A directions. Dendrimers and conjugates solutions (each equivalent to 50 nM of

paclitaxel) in transport medium were placed in the donor compartment and were incubated at 37°C in an atmosphere of 5% CO<sub>2</sub> and 95% relative humidity for 3 h.

During the permeability experiment, TEER values were recorded every 30 min. Samples (100 µl) were collected from the receiver compartment at 0, 60, 120, 180 min and from the donor compartment at 180 min. Fluorescence of FITC labelled conjugates samples were determined using a multiplate reader at excitation/ emission of 485 nm/ 535 nm. FITC and conjugates standard curves (Figure 6-9 to Figure 6-14, Appendix III) were constructed to quantify the conjugates concentration. Free paclitaxel and pac-glu were analysed by HPLC. The solvent system used was same as described in section 2.2.5.

The apparent permeability coefficient ( $P_{app}$ ) was calculated using the equation below (130):

$$P_{app} \text{ (cm/sec)} = dc/dt \times V/AC_0$$

- dc/dt = the change in donor concentration over time (mol/l.sec)
- V = the volume in the reservoir of receiver side (cm<sup>3</sup>)
- A = the surface area of membrane (1 cm<sup>2</sup>)
- C<sub>0</sub> = the initial concentration in donor side (mol/l)

### 3.2.5 Statistical analysis of data

All data were expressed as mean values ± standard deviation (mean ± SD) with n = 3 – 4 of triplicate experiments. Statistical analysis was carried out using the Student's t-test. Probability values of  $p < 0.05$  were considered to be statistically significant.

### **3.3 Results and discussion**

#### **3.3.1 Cytotoxicity studies of G3 PAMAM dendrimer and drug conjugates using Caco-2 cells**

In the present study, optimal cell concentration of the Caco-2 cells was first determined to obtain cell density for use in cytotoxicity studies. The influence of G3 PAMAM dendrimer and conjugates (possessing lauryl and/or pac-glu moieties) on the viability of Caco-2 cells was evaluated using the LDH release assay. The cytotoxicity studies were conducted to determine the non-cytotoxic concentration of dendrimer and conjugates to be used later in permeability studies across the Caco-2 cell monolayers.

##### **3.3.1.1 Optimal cell concentration determination using LDH assay**

Preliminary experiments were conducted to determine the optimal seeding density for Caco-2 cells. Figure 3-3 shows LDH absorbance measured at 492 nm with a reference wavelength of 612 nm. The maximum amount of releasable LDH enzyme activity was determined by lysing the cells with Triton X-100 (as high control) while the spontaneous release of LDH activity was determined by incubating the cells with assay medium (as low control). The seeding density that produced the largest difference between the high and low controls with absorbance less or equivalent to 1 was  $0.6 \times 10^4$  cells per well, which was identified as the optimal cell concentration for Caco-2 cells. It is important to determine the optimal seeding density as different cell types may contain different amounts of LDH and have different sensitivities to cytotoxic compounds (156). The optimal cell concentration determined was used in cytotoxicity studies of G3 PAMAM dendrimers and conjugates on the Caco-2 cells.

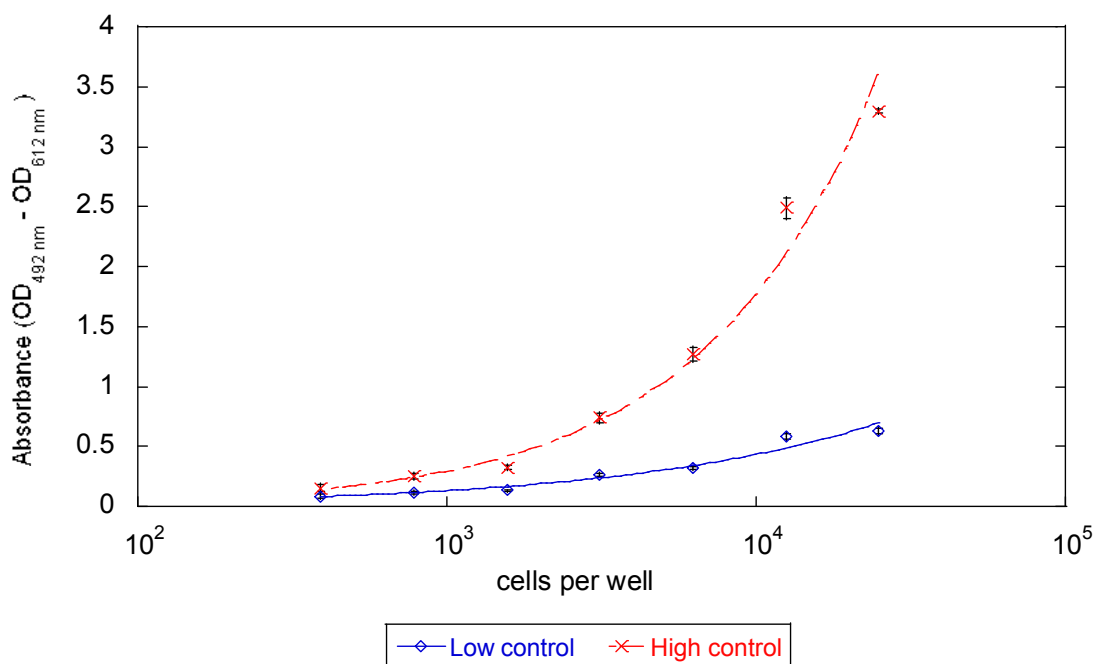


**Figure 3-3: The absorbance of Caco-2 cell seeding densities incubated with assay medium (low control) or Triton X-100 1% (high control) for optimal concentration determination, (mean  $\pm$  SD, n = 3 of triplicate experiments).**

### 3.3.1.2 The effect of G3 PAMAM dendrimer and drug conjugates on Caco-2 cell viability

The cytotoxicity effect of G3 PAMAM dendrimer and conjugates towards Caco-2 cells was determined using the LDH assay with the cell seeding density obtained from the optimal cell concentration determination. G3 PAMAM dendrimer was relatively non-toxic to Caco-2 cells compared to all the G3 PAMAM conjugates at the test concentrations (0.05 – 50  $\mu$ M) (Figure 3-4). A comparison of  $IC_{50}$  of G3 PAMAM dendrimer and other conjugates as illustrated in Table 3-1 and shows that G3 PAMAM dendrimer with an  $IC_{50}$  value of  $279.38 \pm 13.60 \mu$ M is significantly ( $p < 0.05$ ) less toxic. After the addition of lauryl chains, G3L3 and G3L6 were found to be relatively more toxic than G3 PAMAM dendrimer, with significantly reduced  $IC_{50}$  values of  $2.53 \pm 0.58$  and  $3.32 \pm 0.75 \mu$ M, respectively. These results are in contrast to those by Jevprasesphant *et al.* (103, 106) who reported surface modified cationic PAMAM

dendrimers (e.g. G2, G3 and G4) with lauroyl chloride chains were less toxic toward Caco-2 cells. However, later studies carried out by our research group showed increased cytotoxicity of PAMAM dendrimers conjugated with lauryl alcohol moieties, which supported the finding in the present study (157-160). PAMAM dendrimer conjugated with lauroyl chloride has an amide bond between the dendrimer and lauroyl chains (103, 106) whilst PAMAM dendrimer conjugated with lauryl alcohol has a carbamate bond (157-160). The different cytotoxicity profiles might due to the different linkages between the lauroyl/ lauryl moieties and the dendrimer.

Dendrimer	IC <sub>50</sub> (μM)
G3	279.38 ± 13.60*
G3L3	2.53 ± 0.58
G3L6	3.32 ± 0.75
G3glu-pac	18.58 ± 4.68
L3-G3-glu-pac	14.40 ± 0.84
L6-G3-glu-pac	8.60 ± 0.46

**Table 3-1: The cytotoxicity effect of G3 PAMAM dendrimer and drug conjugates on the Caco-2 cells as determined by IC<sub>50</sub> (mean ± SD, n = 3 of triplicate experiments). \* indicates a significant difference ( $p < 0.05$ ) from other conjugates.**

After conjugation of paclitaxel via a glutaric anhydride linker to G3 PAMAM dendrimer, cytotoxicity of the conjugate (G3-glu-pac) was also significantly increased. The IC<sub>50</sub> of G3-glu-pac was decreased to 18.58 ± 4.68 μM compared to that of parent G3 PAMAM dendrimer. The IC<sub>50</sub> values of G3L3-glu-pac and G3L6-glu-pac were found to be 14.40 ± 0.84 and 8.60 ± 0.46 μM, respectively. These results indicate that the addition of paclitaxel to G3 PAMAM dendrimer caused significant ( $p < 0.05$ ) increase in cytotoxicity towards Caco-2 cells. Nonetheless, decreased cytotoxicity of G3L3-glu-pac and G3L6-glu-pac was observed when compared to G3L3 and G3L6 conjugates. Decreased cytotoxicity of G3L3-glu-pac and G3L6-glu-pac

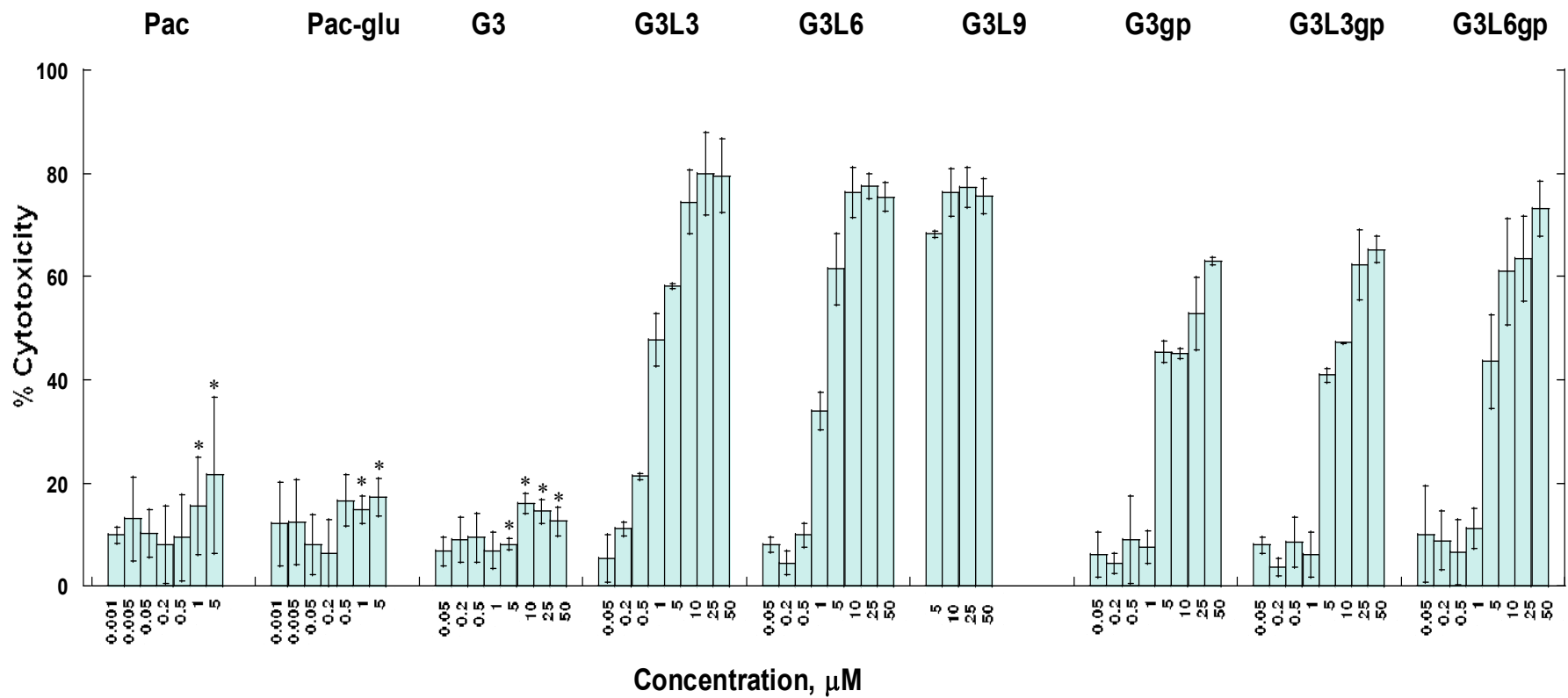


Figure 3-4: The cytotoxicity effect of G3 PAMAM dendrimer, free paclitaxel and conjugates on the Caco-2 cells (mean ± SD, n = 4 of triplicate experiments). \* indicates a significant difference ( $p < 0.05$ ) from other conjugates.

was observed when compared to G3L3 and G3L6 conjugates. Studies of the cellular internalisation mechanism using surface modified PAMAM dendrimers by Saovaprakhiran *et al.* (157) showed that the surface properties of PAMAM dendrimer have significant influences on cell internalisation. The addition of pac-glu molecules to the lauryl modified G3 PAMAM dendrimers changes the surface properties of the conjugates, which is likely to modify the interaction and internalisation of the conjugates into the cells, thus changing the cytotoxicity profile.

As shown in Figure 3-4, pac and pac-glu were relatively non-toxic at the test concentrations of 0.001 – 5  $\mu$ M after 3 h incubation time. No significant difference of cytotoxicity in Caco-2 cells was observed after the addition of linker to paclitaxel. Previous work has reported that the cytotoxicity of paclitaxel was shown to be time dependent with incubation time of 5 h or more (152, 161).

When conducting cytotoxicity test using LDH release assay, cell growth medium such as DMEM was not used as an assay medium. This is due to pyruvate (an inhibitor of the LDH reaction) contents in some formulations of DMEM.

### 3.3.2 Permeability studies of G3 PAMAM and conjugates on Caco-2 cells

#### 3.3.2.1 Permeation of G3 PAMAM dendrimer and drug conjugates across Caco-2 cell monolayers

The permeation of paclitaxel, G3 PAMAM dendrimer and conjugates across Caco-2 cell monolayers was evaluated in both the A $\rightarrow$ B and B $\rightarrow$ A directions at the non-toxic concentrations as determined in the cytotoxicity studies using the LDH release assay. The results of the permeability studies are summarised in Figure 3-5. Paclitaxel, a known unambiguous P-gp efflux transporter substrate, showed a significantly ( $p < 0.05$ ) higher B $\rightarrow$ A  $P_{app}$  than A $\rightarrow$ B  $P_{app}$ , consistent with the previous finding of paclitaxel transport profile across cell lines with functionally active P-gp efflux transporters (162). After attaching the linker (glu) to the drug, no significant difference in permeability was observed suggesting that the conjugation of the glutaric anhydride linker to paclitaxel did not affect the permeability of the drug.

The A→B  $P_{app}$  of G3 PAMAM dendrimer was approximately  $1.26 \times 10^{-6}$  cm/s. After adding lauryl chains, the A→B  $P_{app}$  values of G3L3 (approximately  $2.63 \times 10^{-6}$  cm/s) and G3L6 (approximately  $3.18 \times 10^{-6}$  cm/s) were significantly ( $p < 0.05$ ) greater than that of unmodified G3 PAMAM dendrimer. It has been reported that surface modified dendrimers with medium chain fatty acids significantly enhanced permeation across Caco-2 cell monolayers (103). Lauryl alcohol was also reported to function as a permeability enhancer (28). The addition of the permeability enhancer, lauryl moieties to G3 PAMAM dendrimer might facilitate the interaction with the cell membrane, thus increased the permeation across cell monolayers.

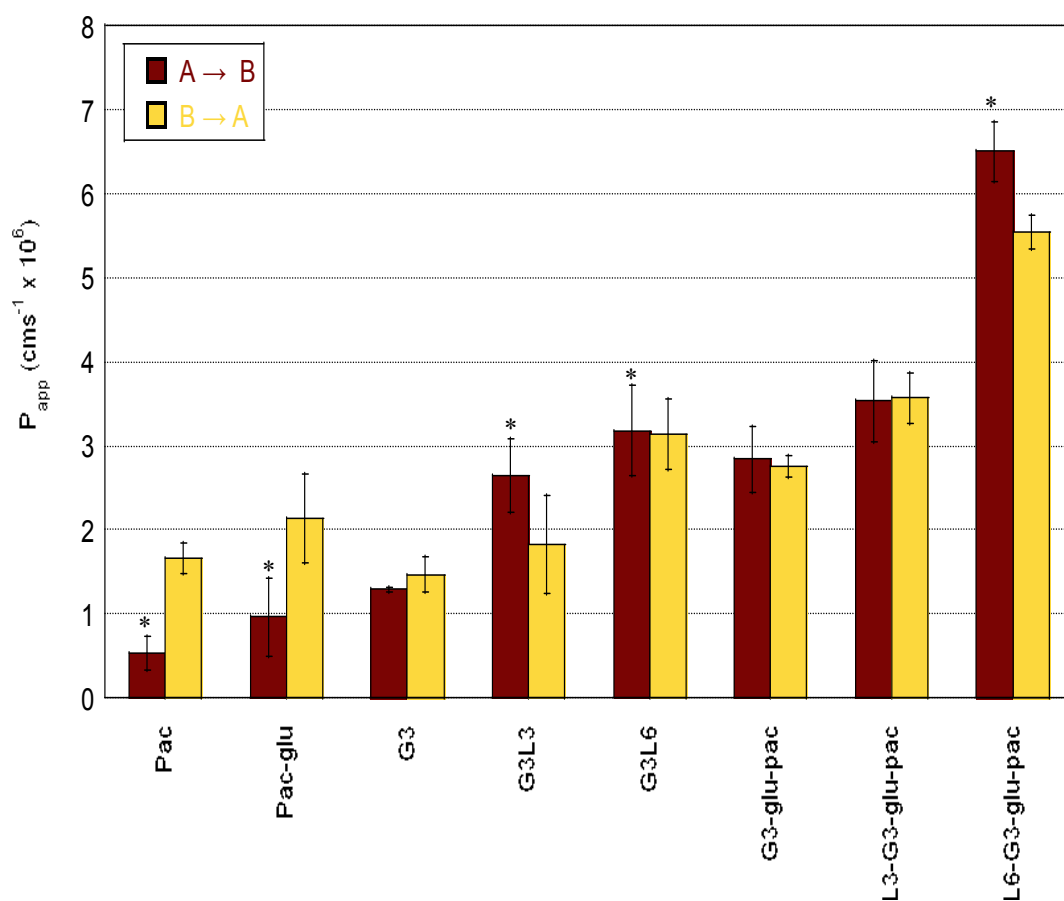


**Figure 3-5:** The A→B (■) and B→A (■) permeability of G3 PAMAM dendrimer, free paclitaxel and conjugates across the Caco-2 cell monolayers after 3 h incubation at 37°C (mean ± SD, n = 3 of triplicate experiments). \*  $p < 0.05$ .

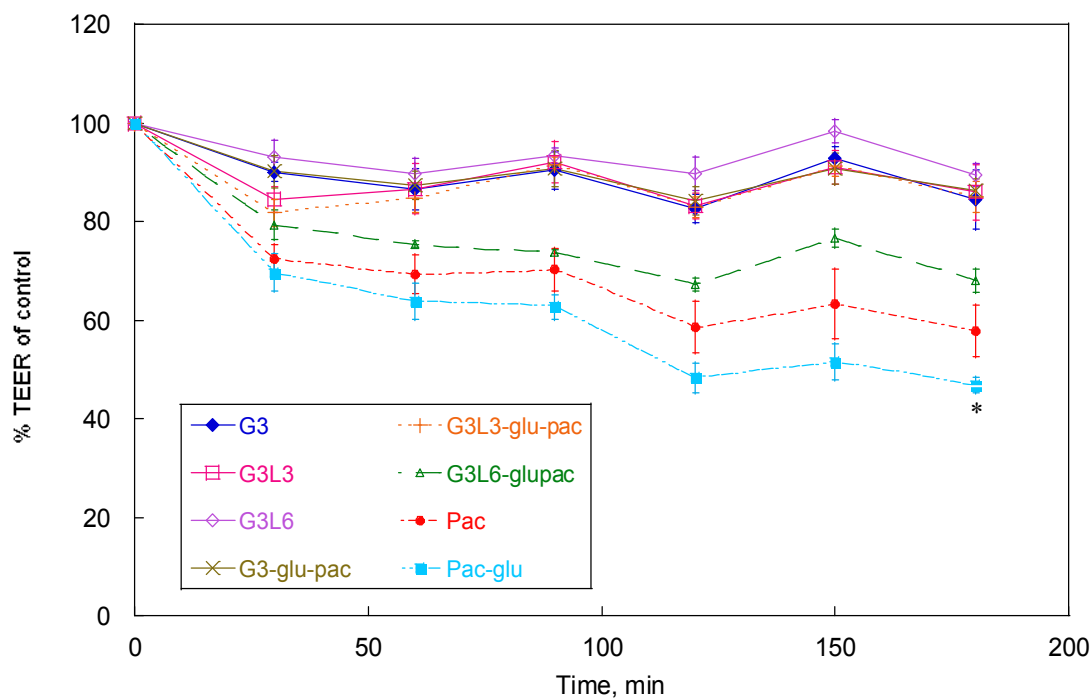
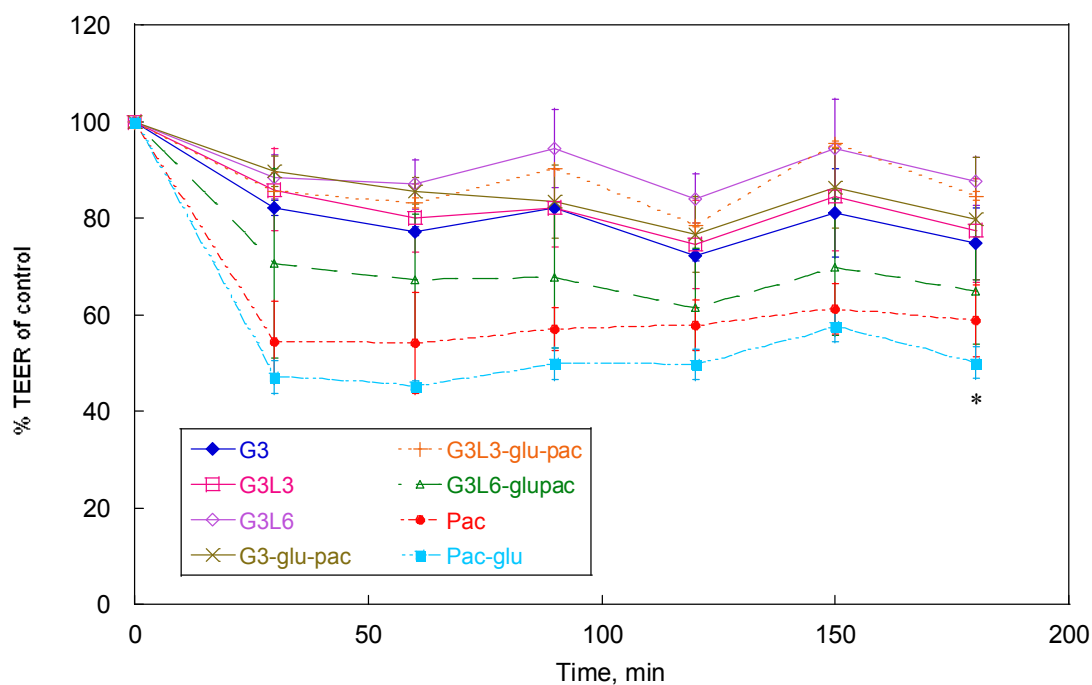
As shown in Figure 3-5, conjugation of paclitaxel via glu linker to G3 PAMAM dendrimer (G3-glu-pac) increased the  $A \rightarrow B$   $P_{app}$  by approximately 5.4 fold compared to that of the free drug. Permeability of L3-G3-glu-pac and L6-G3-glu-pac were further increased.  $A \rightarrow B$   $P_{app}$  of L6-G3-glu-pac was 12.4 fold greater than that of paclitaxel. The  $A \rightarrow B$   $P_{app}$  values of G3 and lauryl-G3 were not significantly ( $p > 0.05$ ) different from the  $B \rightarrow A$   $P_{app}$  values, suggesting that these molecules are not substrates for the intestinal efflux transporter. Thus, it is proposed that G3 PAMAM dendrimer and surface modified G3 with lauryl chains can act as carriers to enhance the permeability of paclitaxel, and can bypass the P-gp efflux transporters which are functionally active in Caco-2 cell monolayers. These findings are supported by previous research which showed that PAMAM dendrimer is able to enhance permeability of drugs which are P-gp substrates (83, 86, 162).

### 3.3.2.2 The effect of G3 PAMAM dendrimer and drug conjugates on Caco-2 cell monolayers integrity

Transepithelial electrical resistance (TEER) measurements were conducted during the 3 h incubation with test substances at 37°C to examine the effect of G3 PAMAM dendrimer and conjugates on the monolayer integrity. Figure 3-6A shows the changes in the TEER values of Caco-2 cell monolayers following the apical incubation with G3 PAMAM dendrimer and conjugates. After incubation with G3 PAMAM dendrimer, the average TEER value of the Caco-2 cell monolayers was decreased by approximately 15% ( $84.5 \pm 5.9\%$ ) with slight fluctuation over 3 h. Apical incubation with G3L3, G3L6, G3-glu-pac and L3-G3-glu-pac resulted in a decrease in TEER ( $86.0 \pm 5.6\%$ ,  $89.5 \pm 2.4\%$ ,  $86.4 \pm 2.4\%$  and  $85.0 \pm 3.1\%$  respectively), similar to that of G3 PAMAM dendrimer. A noticeable 32% (approximately) drop of TEER was observed when cells were exposed to L6-G3-glu-pac at the apical side after 3 h. Permeability of L6-G3-glu-pac was significantly ( $p < 0.05$ ) higher than those of other conjugates, suggesting that the decrease of TEER might be due to modulation of tight junctions, hence enhancing the permeability. PAMAM dendrimer was previously reported to demonstrate transepithelial transport via both transcellular and paracellular pathways across Caco-2 cell monolayers (11, 103, 162, 163).

The TEER measurement following 3 h incubation with pac and pac-glu showed a significant ( $p < 0.05$ ) decrease of TEER, for pac (approximately 42%) and pac-glu (approximately 53%). However, the permeability of pac and pac-glu was lowest among all conjugates tested. Previous work by D'Emanuele group (103) showed that G3 PAMAM dendrimers enhance paracellular transport by opening up tight junctions. D'Emanuele *et al.* (83) reported that the transport of propranolol across the Caco-2 cell monolayers was not enhanced in the presence of G3 PAMAM dendrimers. This suggests that the route of propranolol transport is mainly via transcellular even when G3 PAMAM dendrimer with the ability of opening up tight junctions was in presence. El-sayed *et al.* (162) also reported that PAMAM dendrimers demonstrated modulation of tight junctions of Caco-2 cell monolayers, leading to an increase in the paracellular permeability. However, transport study of paclitaxel by El-sayed *et al.* (162) demonstrated no difference in the permeation of drug in the presence or absence of G2 PAMAM dendrimers. Their finding indicated transport of paclitaxel across the epithelia was solely via transcellular route and was not influenced by PAMAM dendrimers (162). This could explain the low permeability of pac and pac-glu even though pronounced decreases of TEER of Caco-2 cell monolayers were observed in the present study. TEER has been described as the measure of for paracellular permeability (164).

There was no significant ( $p > 0.05$ ) difference in TEER values when dendrimer and conjugates were incubated on the apical side compared with the basolateral side. The recovery of TEER to approximately 100% was observed following the removal of G3 PAMAM dendrimer and conjugates from the cells after experiments (data not shown).

**A****B**

**Figure 3-6: The effect of G3 PAMAM dendrimer, free paclitaxel and conjugates on the TEER of Caco-2 cell monolayers after (A) apical and (B) basolateral incubation at 37°C (mean  $\pm$  SD, n = 3 of triplicate experiments). \* $p < 0.05$ .**

### 3.4 Conclusions

Biological evaluation of PAMAM dendrimer and conjugates using Caco-2 cells showed that the cytotoxicity was dependent on the surface properties of dendrimer and conjugates. G3 PAMAM dendrimer was found to be relatively non-toxic compared to all the other conjugates at all the test concentrations. Conjugation of lauryl chains and paclitaxel molecules on the surface of G3 PAMAM dendrimer significantly ( $p < 0.05$ ) increased the cytotoxicity in Caco-2 cells. Surface modification of G3 PAMAM dendrimers has also influenced the permeation of dendrimer and drug conjugates, and the integrity of Caco-2 cells monolayers. The B→A  $P_{app}$  of paclitaxel was found to be significantly ( $p < 0.05$ ) higher than the A→B  $P_{app}$ , indicating active function of P-gp efflux transporter system in the cell model. Covalent conjugation of paclitaxel to G3 PAMAM dendrimer via glutaric anhydride as a linker significantly ( $p < 0.05$ ) increased its A→B  $P_{app}$  across Caco-2 cell monolayers. A more pronounced increase of paclitaxel permeation was observed when surface modified G3 PAMAM dendrimer with six lauryl chains was used as a carrier. L6-G3-glu-pac showed the highest permeability across the Caco-2 cells monolayers where lauryl chains were acting as permeability enhancer. The transport of G3-paclitaxel conjugates across the cells is thought to occur via both paracellular and transcellular routes. The results suggest that G3 PAMAM dendrimer-based drug delivery systems can be used as potential nanocarriers for low water soluble and P-gp substrate drug (e.g. paclitaxel) to enhance solubility and permeability, furthermore to bypass P-gp efflux transporter system in cellular barriers.

**CHAPTER 4: BIOLOGICAL EVALUATION OF G3 PAMAM  
DENDRIMER AND DRUG CONJUGATES WITH  
PORCINE BRAIN ENDOTHELIAL CELLS**

---

---

## 4.1 Introduction

The blood-brain barrier (BBB) has long been described as an important barrier to most drugs which are efflux transporters (e.g. P-gp) substrate and have poor aqueous solubility. Various *in vitro* cell models have been developed and used to investigate the permeability of this barrier, but an 'industrial standard' has not been well established. Caco-2 and Mardin-Darby Carnine Kidney (MDCK) cells have been commonly applied as 'BBB surrogates' models in permeability studies across the barrier layer to estimate entry of drugs to brain. Despite their gastrointestinal origin, these models can still provide reasonable prediction for compounds that penetrate the brain by passive partition into brain endothelial membranes without involving interaction with transporters (165). However, it has recently been described that the lipid membrane nature between the gastrointestinal (GI) tract and the BBB is different. Furthermore, the profile of transporter expression in the GI and the BBB is certainly different (58). Therefore, a real BBB-based model will give a better prediction for CNS targeted drugs that are substrates for efflux transporters. During the selection of BBB-based cell model, two major features are important, namely, tightness of the tight junctions and polarised expression of transporters. Effective tight junctions of a fully differentiated BBB represent the physical barrier and defining roles of the BBB. Polarisation of transporter to apical and basolateral membrane domains also largely depends on effective tight junctions. Possessing these two major features, porcine brain endothelial cells (PBECS) are among the *in vitro* BBB cell models that are commonly used in pharmaceutical assays (58, 135, 166).

The results from biological evaluation of G3 PAMAM dendrimers and drug conjugates using Caco-2 cells indicated that G3 PAMAM dendrimers and prodrugs can bypass the P-gp efflux transporter with significantly enhanced permeation across the Caco-2 cell monolayers. Thus, further biological evaluation was carried out using PBECS as the blood-brain barrier cell model to examine the potential of G3 PAMAM dendrimer as a carrier for paclitaxel (P-gp substrate) to bypass the blood-brain barrier.

In this present study, PBECS were selected as the cell model to assess the permeability of G3 PAMAM dendrimer and prodrugs across the blood-brain barrier. Effects of cell

culture conditions were investigated to establish optimal conditions for cell growth. Cell growth and cell morphology were monitored until desired confluency was achieved. G3 PAMAM dendrimer conjugates that were successfully synthesised (chapter 2) were biologically evaluated using the PBECs. Cytotoxicity of G3 PAMAM dendrimer and its drug conjugates towards the PBECs was determined using lactate dehydrogenase (LDH) release assay. Permeability studies of dendrimer and drug conjugates across the cell monolayers was conducted using non-toxic concentrations of the dendrimer and conjugates determined from cytotoxicity studies. This was to ensure that the dendrimer and conjugates treatment induced no toxicity in endothelial cells. TEER measurements were performed on PBEC monolayers that were grown and maintained in Transwell® filter inserts until the cell monolayers achieved the desired TEER values and were ready to be used for permeability studies. Integrity of the cell monolayers was also evaluated by measuring the TEER across the cell monolayers.

## 4.2 Materials and methods

### 4.2.1 Materials

Triton X-100, trypan blue, fibronectin, Dulbecco's Modified Eagles Medium (DMEM) low glucose, 10 KU/ml penicillin and 10 mg/ml streptomycin, L-glutamine, 100 KU Heparin, puromycin, 8-(4-Chlorophenylthio)adenosine 3',5'-cyclic monophosphate sodium salt (cAMP), hydrocortisone, Hank's Balanced Salt Solution (HBSS) without calcium ions and magnesium ions, trypsin-EDTA, dimethylsulfoxide (DMSO) and Corning® Costar® 96 well flat bottom cell culture plate were purchased from Sigma-Aldrich Co. Ltd. (Gillingham, Dorset, UK). Dulbecco's Modified Eagles Medium (DMEM) without phenol red and (4-(2-hydroxyethyl)-1-piperazineethanesulfonic acid) buffer solution (HEPES) were purchased from Gibco BRL, Invitrogen (Paisley, UK). Bovine plasma derived serum was purchased from First Link Ltd. (Birmingham, UK). 4-(3-Butoxy-4-methoxybenzyl)-2-imidazolidinone (RO-20-1724) was purchased from Merck-Calbiochem Chemicals Ltd. (Beeston, Nottingham, UK). BD type 1 rat tail collagen was purchased from Scientific Laboratory Supplies Ltd. (Wilford, Nottingham, UK). Tissue culture flask EasYFlask angled neck polystyrene radiation sterilised filter cap 75 cm<sup>2</sup> growth area, Costar Transwell-Clear 12 well tissue culture-treated sterile polyester membrane inserts (pore size 0.4 µm, membrane diameter 12 mm), syringe filter Millex GP PES (33 mm 0.22 µm pore size) Millipore, bottle top Nalgene filter unit MF75 series disposable SFCA membrane 50 mm (fits 45 mm neck, 150 ml 0.2 µm pore size) were purchased from Fisher Scientific UK Ltd (Loughborough, UK). Cytotoxicity detection kit (LDH) was obtained from Roche Applied Science (Mannheim, Germany). Solution of G3 PAMAM dendrimer with an ethylenediamine core in methanol (20% w/w) were purchased from Dendritech Inc. Paclitaxel (pac) was purchased from Advance Tech. & Ind. Co., Ltd. (Kln, Hong Kong). G3 PAMAM-lauryl conjugates (G3-Lx), 2'-glutaryl-paclitaxel (pac-glu), G3-glutarate-paclitaxel (G3-glu-pac) and lauryl-G3-glutarate-paclitaxel (Lx-G3-glu-pac), FITC-labelled G3 PAMAM conjugates were synthesised and characterised as described in chapter 2. Primary porcine brain endothelial cells (PBECs) were acquired from Professor Joan N. Abbott, Blood-Brain Barrier Group in King's College London.

## 4.2.2 PBECs cell culture techniques

### 4.2.2.1 Preparation of lab-made rat tail collagen

#### *Removal of collagen fibres*

Rat tails were removed and collected from experimental rats. The rat tails can be kept frozen at  $-20^{\circ}\text{C}$  with storage of more than one year without appreciable loss of solubility of collagen fibres. Approximately 2 h before preparation, the tails were allowed to thaw slowly at room temperature. Once the tails were thawed, a longitudinal incision was made along the length of the tail from the base to the tip of tail. The skin was then pulled off from the tail. The distal three or four vertebrae at the tip of the tail were then broken off and pulled away slowly to remove the collagen fibres/muscle tendons that were attached to the vertebrae. This procedure was repeated with every two or three vertebrae going from the tip to the base of the tail to collect the removed vertebrae and collagen fibres. The collagen fibres were severed from the points of attachment on the vertebra and left to dry at room temperature for approximately 3 h. The dried fibres were then weighed.

#### *Sterilisation and dilution of collagen fibres*

The dry fibres were sterilised by exposing to UV light generated by a germicidal UV lamp for 48 h. The UV sterilised collagen fibres were transferred into an 0.1% acetic acid solution (1 g of collagen fibres in 300 ml solution) and stirred with a pre-sterilised magnetic stirrer bar at low speed for approximately 48 h. Undissolved crude fibres were removed by filtering the solution through a sterile triple gauze filter to obtain a collagen solution free of non-dissolved fibres.

This project had the relevant ethical clearance from the Annual Project Ethics Committee of UCLan.

#### 4.2.2.2 Plating cell culture medium

Cell culture medium with different compositions were prepared freshly and filtered through 0.22 µm pore size Millipore filter prior to use.

*Plating cell growth medium with puromycin:* DMEM was supplemented with 10% v/v bovine plasma-derived serum, 100 U/ml penicillin and 100 µg/ml streptomycin, 2 mM L-glutamine, 125 µg/ml heparin and 45 µg/ml puromycin.

*Plating cell growth medium without puromycin:* DMEM was supplemented with 10% v/v bovine plasma-derived serum, 100 U/ml penicillin and 100 µg/ml streptomycin, 2 mM L-glutamine and 125 µg/ml heparin.

*Plating serum-free medium:* DMEM was supplemented with 100 U/ml penicillin and 100 µg/ml streptomycin, 2 mM L-glutamine, 125 µg/ml heparin and 550 nM hydrocortisone.

#### 4.2.2.3 Maintenance and optimisation of growth conditions

PBECs (passage 1) were maintained in 75 cm<sup>3</sup> (T75) flasks containing cell growth medium with or without puromycin at 37°C in an atmosphere of 5% CO<sub>2</sub> and 95% relative humidity.

#### 4.2.2.4 Thawing cells

Vial of PBECs stocks stored in a liquid nitrogen tank was retrieved and defrosted rapidly by immersing in a 37°C warm water bath for 1 – 2 min. Contents of the vials were quickly transferred to a universal tube containing 16 ml growth medium with puromycin and added into two T75 flasks ( 8 ml each). Cells were incubated at 37°C in an atmosphere of 5% CO<sub>2</sub> and 95% relative humidity. The growth medium with puromycin was replaced by growth medium without puromycin on the third or fourth

day of cell growth until the cells achieved 70 – 80% confluency within 5 – 7 days for passaging.

#### 4.2.2.5 Coating with rat tail collagen and fibronectin

Before passaging cells, 4 ml of BD type 1 rat tail collagen (dilution to 100 µg/ml with 0.02 M acetic acid) or 4 ml of lab-made rat tail collagen with 1:10 dilution was added into a T75 flask for 2 h at room temperature to coat the cell growth surface. After 2 h, rat tail collagen was removed and the flask was washed twice with HBSS without phenol red. The cell growth surface was then coated with fibronectin by adding 4 ml of 7.5 µg/ml fibronectin into the flask and left for another 2 h at room temperature. Fibronectin was removed from the flask and washed twice with HBSS without phenol red. The T75 flask coated with rat tail collagen and fibronectin was now ready for the use in cell passaging. When coating the 96-well plate and the Transwell® insert, the same coating procedures were applied by using 100 µl of rat tail and fibronectin for each well; and 0.5 ml for each insert.

#### 4.2.2.6 Passaging cells

At 70 – 80% confluency, growth medium was removed and cells were washed twice with 8 ml HBSS without Ca<sup>2+</sup> and Mg<sup>2+</sup>. After removing the HBSS, cells were detached by incubating with 2 ml trypsin-EDTA (1x) per flask at 37°C in an atmosphere of 5% CO<sub>2</sub> and 95% relative humidity for 3-5 min. The flasks were continually observed under the microscope, gently tapped to recover any adherent cells. When the majority of the endothelial cells were observed to be detached, 8 ml of plating growth medium without puromycin was added to each flask to inactivate the trypsin solution. The cell suspension was transferred to a universal tube and centrifuged at 1500 rpm for 5 min. After removing the supernatant, the cell pellet was resuspended in 1 ml growth medium without puromycin. The number of viable cells was counted as described in section 3.2.2.4 and cells were seeded onto collagen/fibronectin coated 96-well plate or Transwell® inserts for further studies.

### 4.2.3 Examination of PBECs morphology

The morphology of PBECs grown and maintained on collagen-coated and fibronectin treated T75 flask was examined using Leica DM IL Inverted light microscope (Bucks, United Kingdom). Photomicrographs of the cultures were taken using Cannon DS6041 EOS Digital Rebel camera on different culture days to observe the changes of the cells morphology until 100% confluency was achieved.

### 4.2.4 Measurement of *in vitro* cytotoxicity of G3 PAMAM dendrimer and paclitaxel conjugates using PBECs

Cytotoxicity studies were performed using the LDH assay as described previously in section 3.2.3.1.

#### 4.2.4.1 Optimal cell concentration determination

Prior to passaging of PBECs, 96-wells plates were coated with 100 µl/well of rat tail collagen following with 100 µl/well of fibronectin (section 4.2.2.5). After passaging cells (section 4.2.2.6), the cell pellet was resuspended in growth medium with 1% bovine plasma-derived serum and without puromycin (DMEM supplemented with 1% v/v bovine plasma-derived serum, 100 U/ml penicillin and 100 µg/ml streptomycin, 2 mM L-glutamine and 125 µg/ml heparin). The cell suspension concentration was adjusted to  $2 \times 10^5$  cells/ml and followed by two-fold serial dilutions (up to 7 dilutions) with growth medium across the rat tail collagen/fibronectin coated-96-well plate. The cells were incubated overnight at 37°C in an atmosphere of 5% CO<sub>2</sub> and 95% relative humidity to allow cells adherence. After 24 h, the growth medium was removed and the cells were washed with assay medium (HBSS with 25 mM HEPES). The removed growth medium was replaced with 200 µl of low control (i.e. spontaneous LDH release, assay medium HBSS with 25 mM HEPES) or 200 µl of the high control (i.e. maximum LDH release, 1% Triton X-100 in assay medium). A volume of 200 µl of assay medium was also added to triplicate wells without cells as background control. After 3 h of incubation at 37°C and 5% CO<sub>2</sub>, a 100 µl sample of the supernatant medium was

removed from each well and placed into corresponding wells of another 96-well plate. A volume of 100  $\mu$ l of freshly prepared reaction mixture was added to each sample and then incubated for 30 min at room temperature, protected from light. The sample absorbance was then measured at 492 nm (reference wavelength of 612 nm) on a multiplate reader. A curve of the absorbance vs. cell seeding density was plotted for both low and high controls. The seeding density that produced the greatest difference between low and high control absorbances with a value less than or equivalent to 1 was identified as the optimal cell concentration.

#### 4.2.4.2 Cytotoxicity studies

PBECs (Passage 1) in 100  $\mu$ l growth medium without puromycin (DMEM supplemented with 1% v/v bovine plasma-derived serum, 100 U/ml penicillin and 100  $\mu$ g/ml streptomycin, 2 mM L-glutamine and 125  $\mu$ g/ml heparin) were seeded onto a 96-well plate at the optimal cell density determined in section 4.2.4.1. The cells were then incubated overnight at 37°C in an atmosphere of 5% CO<sub>2</sub> and 95% relative humidity to allow adherence of cells. After 24 h, the growth medium was removed and the cells were washed with assay medium (HBSS with 25mM HEPES). 200  $\mu$ l of assay medium (HBSS with 25 mM HEPES) containing different concentrations of G3 PAMAM dendrimer, surface modified-G3 PAMAM and drug conjugates was added to each well. The cells were also treated with low control (blank assay medium HBSS) and high control (1% Triton X-100 in assay medium). A volume of 200  $\mu$ l of blank assay medium in the well without cells was used as background control. After 3 h of incubation, a 100  $\mu$ l sample of the supernatant medium was removed from each well and placed into corresponding wells of another 96-well plate to react with 100  $\mu$ l of freshly prepared reaction mixture for 30 min at room temperature, protected from light. The sample absorbance was then measured at 492 nm (reference wavelength of 612 nm) on a multiplate reader. The percentage of cytotoxicity was calculated using equation in section 3.2.3.3.

## 4.2.5 Transendothelial transport studies across PBEC monolayers

The transport studies across the PBECs were carried out by a similar method used to investigate the transport of compound across monolayers of Caco-2 cells grown on a Transwell® insert described in section 3.2.4. The apical side represents the luminal side of the brain endothelium whilst the basolateral side represent the abluminal side (blood) of the endothelium. PBECs are grown on the insert semi-permeable membrane and the permeability across the cell monolayers was measured as apparent permeability ( $P_{app}$ ). The  $P_{app}$  of the tested compound was determined across the cell monolayers in both  $A \rightarrow B$  and  $B \rightarrow A$  directions.

### 4.2.5.1 Passaging cells onto a Transwell® insert

Prior to passaging of PBECs onto the Transwell® inserts, inserts were coated with 0.5 ml rat tail collagen and fibronectin. After the number of viable cells was assessed, PBECs (passage 1) with a density of  $1.0 \times 10^5$  cells/  $\text{cm}^2$  were seeded onto polyester 12-well Transwell® insert (pore size 0.4  $\mu\text{m}$ ). Cells were grown and maintained in growth medium without puromycin (DMEM supplemented with 10% v/v bovine plasma-derived serum, 100 U/ml penicillin and 100  $\mu\text{g}/\text{ml}$  streptomycin, 2 mM L-glutamine and 125  $\mu\text{g}/\text{ml}$  heparin) at 37°C in an atmosphere of 5%  $\text{CO}_2$  and 95% relative humidity.

### 4.2.5.2 Treatment with cAMP and RO-20-1724

PBECs became 100% confluent within 3 – 4 days and the growth medium was replaced by a serum-free medium (DMEM supplemented with 100 U/ml penicillin and 100  $\mu\text{g}/\text{ml}$  streptomycin, 2 mM L-glutamine, 125  $\mu\text{g}/\text{ml}$  heparin and 550 nM hydrocortisone). Cells were then treated with 3',5'-cyclic monophosphate sodium salt (cAMP) and 4-(3-Butoxy-4-methoxybenzyl)-2-imidazolidinone (the cAMP phosphodiesterase-4-specific inhibitor, RO-20-1724) for 24 h before permeability studies. A mixture solution of 250  $\mu\text{M}$  of cAMP and 17.5  $\mu\text{M}$  of RO-20-1724 in a proportion of 20:1 (cAMP: RO-20-1724) was freshly prepared. To the filter insert, 5.3

$\mu\text{l}$  of the mixture solution was added; and 15.7  $\mu\text{l}$  was added to the well. After a 24 h treatment, PBECs were ready for experiments.

#### 4.2.5.3 Transendothelial electrical resistance (TEER) measurement with PBECs

Transepithelial electrical resistance (TEER) of cells grown on Transwell® insert was measured according to the procedures described in section 3.2.4.1 to assess the cell monolayer integrity. TEER values were measured and compared under various cultured conditions to ensure that cells with ideal tight junction formation were used in permeability studies. Monitoring of TEER values from day 2 to day 10 for PBECs culture was conducted.

#### 4.2.5.4 Permeability studies

PBECs were seeded onto the Transwell® insert (pore size 0.4  $\mu\text{m}$ ) and treated with cAMP and RO-20-1724 for permeability studies as described in section 4.2.5.2. The integrity and the measure of tight junction formation of the PBEC monolayers were tested before and after experiments by conducting the TEER measurement using a Voltohmmeter. Before experiments, cells were washed twice with HBSS without  $\text{Ca}^{2+}$  and  $\text{Mg}^{2+}$ , and subsequently equilibrated with transport medium (HBSS with 25 mM HEPES) for 20 min at 37°C in an atmosphere of 5%  $\text{CO}_2$  and 95% relative humidity, and the TEER was measured. Only confluent monolayers with TEER value corrected for the blank filter resistance above 200  $\Omega\cdot\text{cm}^2$  were selected for use in transport studies. Transport of FITC-labelled PAMAM dendrimers and surface-modified dendrimers (Lx-G3, Lx-G3-glu-pac and G3-glu-pac), free pac and pac-glu was analysed in both  $\text{A}\rightarrow\text{B}$  and  $\text{B}\rightarrow\text{A}$  directions. Solutions containing dendrimers and conjugates (each equivalent to 50 nM of paclitaxel) in the transport medium were added to the donor compartment. The cells were placed on a speed and temperature controlled shaker at 200 rpm and incubated at 37°C for 3 h. During the experiment, TEER was recorded every 30 min. Samples (100  $\mu\text{l}$ ) were collected from the receiver compartment at 0, 60, 120, 180 min and from the donor compartment at 180 min. The

fluorescence of FITC labelled conjugates samples were determined by using a multiplate reader at excitation/ emission of 485 nm/535 nm. FITC and conjugates standard curves (Figure 6-9 to Figure 6-14, Appendix III) were constructed to quantify conjugate concentration. Free paclitaxel was analysed by HPLC. Permeation of G3 PAMAM dendrimer and conjugates across the PBEC monolayers was calculated and expressed as an apparent permeability coefficient ( $P_{app}$ ).

Prior to the permeability studies, the stability of dendrimer conjugates across the PBEC monolayers was examined. Samples (100  $\mu$ l) of dendrimer conjugates were collected from the apical site at 0 min, and basolateral site at 180 min. The samples were analysed by HPLC to observe the release of paclitaxel from the conjugates after transport across the monolayers. It was found that no significant release of paclitaxel was observed after the conjugates were transported across the cell monolayers with 3 h incubation at 37°C (Figure 6-6, Appendix I).

#### 4.2.6 Statistical analysis of data

All data were expressed as mean values  $\pm$  standard deviation (mean  $\pm$  SD) with  $n = 3 - 4$  of triplicate experiments. Statistical analysis was carried out using the Student's t-test. Probability values of  $p < 0.05$  were considered to be statistically significant.

## 4.3 Results and discussion

### 4.3.1 Morphology of the PBEC monolayer

Porcine brain endothelial cells were grown on collagen-coated and fibronectin-treated T75 flask. The cells were observed to retain the characteristic morphology of capillary endothelial cells with elongated and spindle-shape, forming a continuous monolayer across the growth surface. (Figure 4-1). On day 1, cells were thawed and passaged on the collagen-coated and fibronectin-treated T75 flask. Adhesion of cells on the growth surface was within 24 h after passaging and cells preferentially grew in clusters. On day 3 in culture, the cells with cobblestone-shaped morphology growing in clusters were observed (Figure 4-1a1 and a2). PBECs reached 80-90% confluency on day 7 with the morphology of typical differentiated capillary endothelial cells (139, 140) (Figure 4-1b1 and b2).

### 4.3.2 Effect of cell culture conditions on PBECs growth

#### 4.3.2.1 Rat tail collagen and fibronectin

Extracellular matrices are used in a wide range of applications in cell culture techniques. They enable cell attachment and promote cell differentiation in an environment that is close to that of *in vivo*. It has been reported that cell differentiation could be influenced by the nature of extracellular matrix on which the cells are grown (167). During the culture of PBECs, self-prepared and commercial rat tail collagens were used for coating the cell growth surface. Improvement of cell growth rate to confluency was observed when commercial rat tail collagen was used compared to self-prepared source. The cells were observed to achieve approximately 80-90% confluency in 7 days of culture with commercial rat tail collagen (data not shown). Conversely, less than 50% confluency of cells was observed after more than 14 days of culture using self-prepared rat tail collagen (data not shown). Cell growth surface was also coated with fibronectin which is a major adhesive glycoprotein that was found to involve in cell interaction with collagen (167).

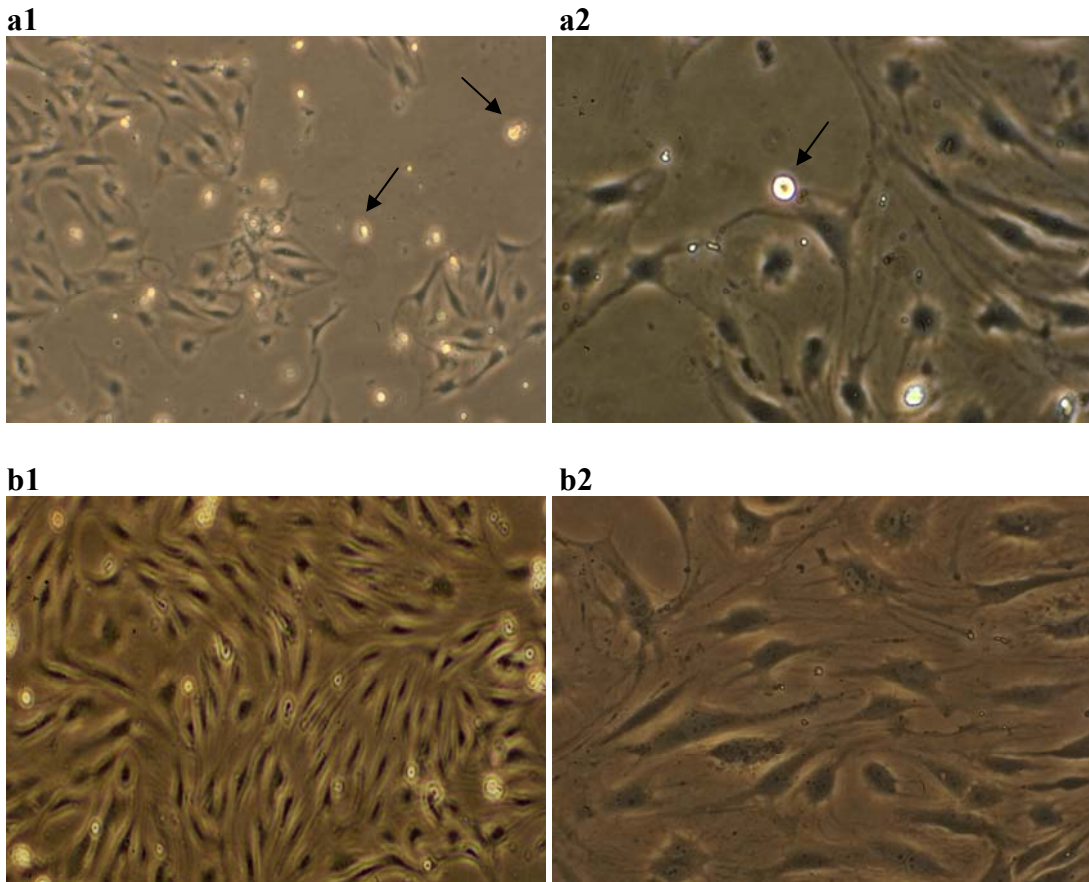


**Figure 4-1: Phase contract microscopy of primary cultured PBECs on culture day 3 (a1 and a2) and day 7 (b1 and b2). Arrows indicating cells undergoing proliferation and differentiation (a1 and b1 original magnification 10x, a2 and b2 original magnification 40x).**

#### 4.3.2.2 Growth medium

Cultures of PBECs were grown and maintained in T75 flasks containing cell growth medium at 37°C in an atmosphere of 5% CO<sub>2</sub> and 95% relative humidity. The main aim to generate primary culture of brain capillary endothelial cells was to achieve maximum yield and purity of the cells. Thus, methods were explored and applied to minimise or eliminate fast-growing contaminating cells, e.g. pericytes, fibroblasts and smooth muscle cells.

Growth media with and without puromycin were used during the culture of PBECs. When cells were freshly thawed onto the T75 flask, growth medium with puromycin was used for the culture. Puromycin is a cytotoxic P-gp substrate. It was introduced into growth medium to eliminate contaminating cells from endothelial cell cultures. The principle is based on non-cytotoxic effect to brain endothelial cells which express P-gp efflux transporter; therefore the endothelial cells will survive. On the other hand, the application of puromycin will cause a cytotoxic effect to the contaminating cells which lack P-gp, thus eliminating the unwanted contaminating cells (139). Figure 4-2 shows the PBECs on culture day 3. Dark spots indicated by the arrows are dead contaminating cells due to the application of puromycin.

On culture day 4, the medium was replaced with growth medium without puromycin. On culture day 7 post-seeding, the cells were confluent and were observed with a characteristic elongated spindle-like morphology (Figure 4-3). No contaminant cells were observed in the culture. It was found that the volume of growth medium played an important role in cell growth. At the early stage of culture, 80% confluency of cells was only achieved after 12-14 days of culture when 8-10 ml of growth medium was used (data not shown). However, when the volume of medium was increased to 20-25 ml/ T75 flask, 80-90% of cell confluency was able to be achieved in 7 days of culture as shown in Figure 4-1.

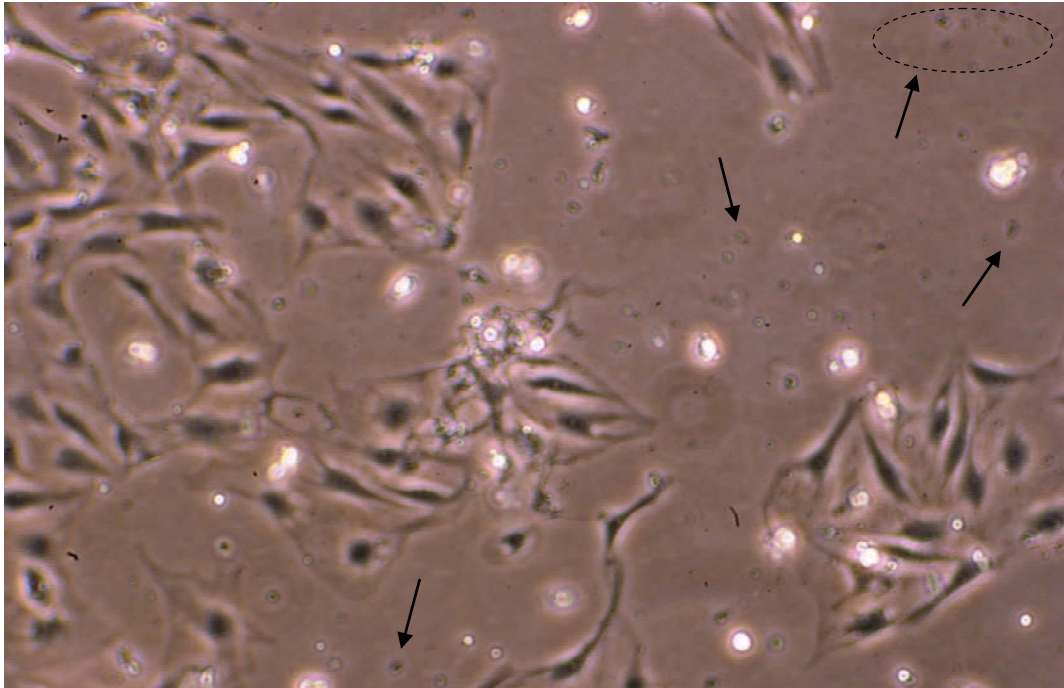


**Figure 4-2: Phase contrast microscopy of primary cultured PBECs on culture day 3. Arrows indicating dead contaminant cells (original magnification 10x).**

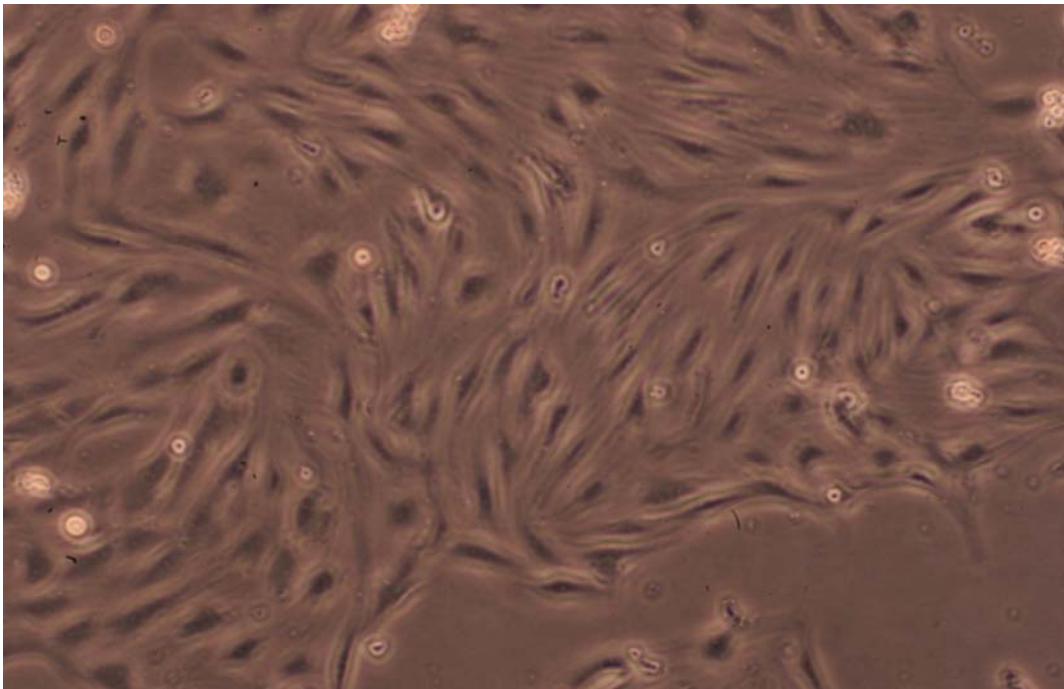


**Figure 4-3: Phase contrast microscopy of primary cultured PBECs on culture day 7 (original magnification 10x).**

### 4.3.3 Cytotoxicity studies of G3 PAMAM dendrimer and drug conjugates on PBECs

In this present study, optimal cell concentration of the PBECs was first determined to obtain the cell density for use in cytotoxicity studies. LDH assay was used to evaluate the influence of G3 PAMAM dendrimer and conjugates (possessing lauryl and/or pac-glu moieties) on the viability of PBECs. The cytotoxicity studies were conducted to determine the non-cytotoxic concentration of dendrimer and conjugates to be used later in permeability studies across the PBEC monolayers.

#### 4.3.3.1 Optimal cell concentration

The optimal seeding density for PBECs culture was determined by preliminary experiments. Figure 4-4 shows LDH absorbance measured at 492 nm with reference wavelength of 612 nm. High control was obtained by lysing the cells with Triton X-100 1% which gives the maximum amount of releasable LDH enzyme activity, while low control was obtained by incubating the cells with assay medium which gives the spontaneous release of LDH activity. The seeding density that produced the greatest difference between the high and low control absorbances with a value less than or equivalent to 1, indicating the optimal cell concentration was  $2 \times 10^4$  cells per well for PBECs. This optimal cell concentration was used as PBECs seeding density to conduct cytotoxicity studies for G3 PAMAM dendrimer and conjugates.

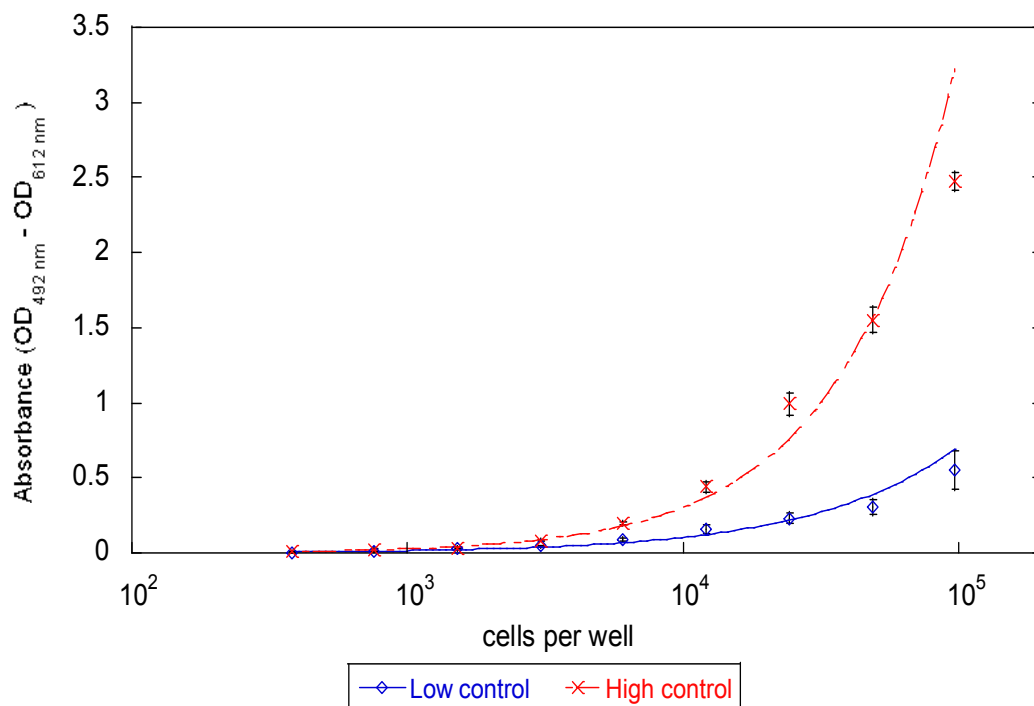


**Figure 4-4: The absorbance of PBECs seeding densities incubated with assay medium (low control) or Triton X-100 1% (high control) for optimal concentration determination (mean  $\pm$  SD, n = 3 of triplicate experiments).**

#### 4.3.3.2 The effect of G3 PAMAM and drug conjugates on PBECs viability

The cytotoxicity of G3 PAMAM dendrimer and drug conjugates towards the PBECs was determined using the LDH assay with the cell seeding density obtained from optimal cell concentration determination. The results from Figure 4-5 show that G3 PAMAM dendrimer was relatively non-toxic to PBECs compared to all the conjugates at the test concentrations. A comparison of IC<sub>50</sub> values of G3 PAMAM dendrimer and the other conjugates are illustrated in Table 4-1 shows that G3 PAMAM dendrimer with an IC<sub>50</sub> value of  $186.38 \pm 7.95 \mu\text{M}$  is significantly ( $p < 0.05$ ) less toxic than the other conjugates. After addition of lauryl chains, G3L6 was found to be relatively more toxic than G3 PAMAM dendrimer, with a significantly ( $p < 0.05$ ) reduced IC<sub>50</sub> value of  $1.21 \pm 0.57 \mu\text{M}$ . These cytotoxicity results using PBECs were consistent with our previous finding when Caco-2 cells were used in chapter 3. PAMAM dendrimers conjugated with lauryl alcohol via a carbamate bond were found to increase the cytotoxicity of conjugates (157-160). On the other hand, dendrimers conjugated with

lauroyl chloride via an amide bond were reported to decrease the conjugate cytotoxicity toward Caco-2 cells (103, 106). These different cytotoxicity profiles are possibly due to the different linkages between the lauroyl/ lauryl moieties and the dendrimers. Carbamates are used in pesticides (168) and the carbamate linkage in the conjugates may contribute to the increased cytotoxicity in the present study. Anhydrovinblastine (AVLB) derivatives synthesised with carbamate group was reported with potent increased cytotoxicity. The IC<sub>50</sub> of the carbamate derivative on A549 and HeLa cell lines at 38nM and 9nM was found to be significantly lower compared to the IC<sub>50</sub> values of AVLB at 49nM and 26nM (169).

Dendrimer	IC <sub>50</sub> (μM)
G3	186.38 ± 7.95*
G3L6	1.21 ± 0.57
G3-glu-pac	9.98 ± 2.14
L6-G3-glu-pac	6.55 ± 0.57

**Table 4-1: The cytotoxicity effect of G3 PAMAM dendrimer and conjugates on the PBECs as determined by IC<sub>50</sub> (mean ± SD, n = 3 of triplicate experiments). \* indicates a significant difference (*p* < 0.05) from other conjugates.**

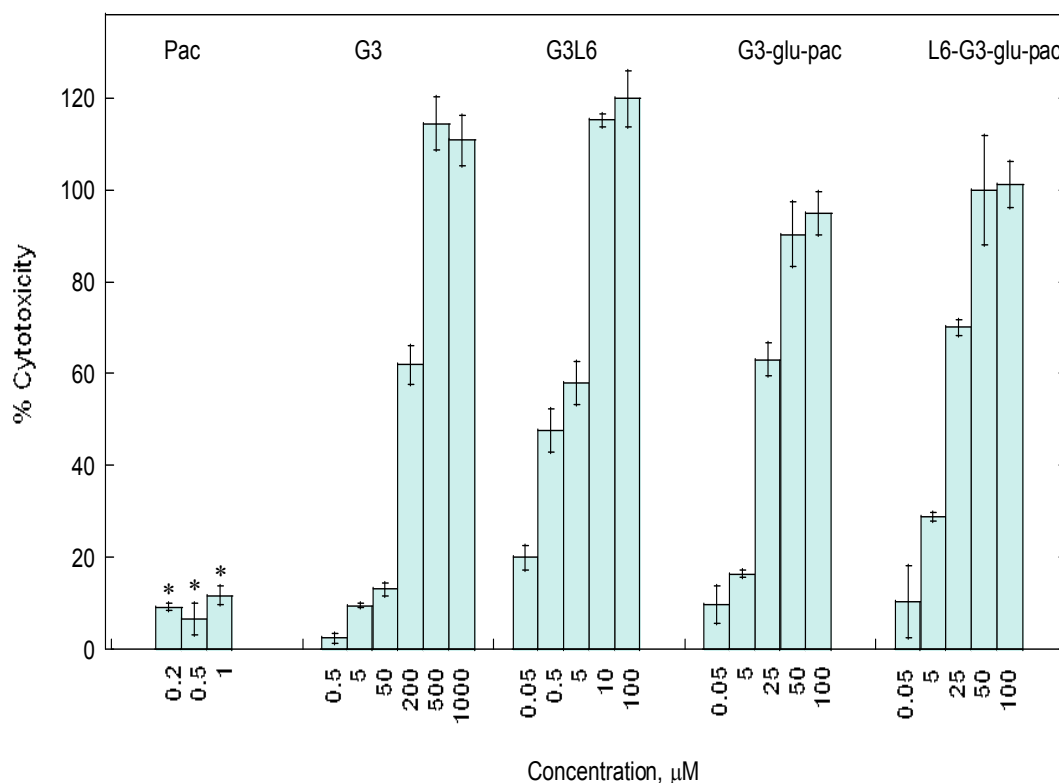


**Figure 4-5: The cytotoxicity effect of G3 PAMAM dendrimer, free paclitaxel and conjugates on the PBECS (mean  $\pm$  SD, n = 3 of triplicate experiments). \* indicates a significant difference ( $p < 0.05$ ) from other conjugates.**

After conjugation with a molecule of paclitaxel via a glutaric anhydride, the  $IC_{50}$  value of G3-glu-pac was decreased to  $9.98 \pm 2.14 \mu\text{M}$  compared to that of G3 PAMAM dendrimer. The  $IC_{50}$  value of G3L6-glu-pac was found to be  $6.55 \pm 0.57 \mu\text{M}$ . These results indicate that the addition of paclitaxel via glu linker to G3 PAMAM dendrimer caused significant ( $p < 0.05$ ) increase in cytotoxicity in PBECS. The enhanced cytotoxicity could be associated with increased solubility and cellular uptake of the conjugates. PAMAM dendrimers have been reported to enhance solubility of low water soluble drugs (85, 86). Najlah *et al.* (85, 86) reported increased solubility and permeability of naproxen and terfenadine when the drugs were covalently conjugated to PAMAM dendrimers via biodegradable linkers. Increased paclitaxel solubility by conjugation to polyglycerol was demonstrated by Ooya *et al.* (170, 171). Devarakonda *et al.* (117) investigated the influence of G4 PAMAM-OH dendrimer and PEG

polymer on the delivery and anticancer effect of paclitaxel. Significantly increased solubility and a 10-fold increase in the cytotoxicity of paclitaxel toward human ovarian carcinoma A2780 cells was reported when the drug was covalently conjugated to the dendrimer via a succinic acid linker compared to those of free drug. Conjugation of a low-solubility drug to high-solubility polymers form a prodrug with enhanced solubility, subsequently increasing the bioavailability that lead to increased cytotoxicity or anticancer activity.

Comparison of the  $IC_{50}$  values between G3L6 and G3L6-glu-pac shows that the addition of paclitaxel molecule to lauryl modified G3 PAMAM dendrimer decreased the cytotoxicity of the conjugates towards PBECs, similar to the findings for Caco-2 cells in chapter 3. As shown in Figure 4-5, free paclitaxel was relatively non-toxic at the test concentration of 0.2 – 1.0  $\mu$ M after 3 h incubation time. As demonstrated by Saovaprakhiran *et al.* (157) studies on the cellular internalisation mechanism using surface modified PAMAM dendrimers, the surface properties of PAMAM dendrimer have significant influences on cell internalisation. The addition of pac-glu molecules to the lauryl modified G3 PAMAM dendrimers changes the surface properties of the conjugates, which is likely to modify the interaction and internalisation of the conjugates into cells, thus resulting in a different toxicity profile.

#### 4.3.4 Permeability studies of G3 and drug conjugates on PBECs

##### 4.3.4.1 TEER measurement of PBEC monolayers

Transendothelial electrical resistance (TEER) values of PBEC monolayers were measured for the duration of culture. Figure 4-6 shows the changes of TEER from less than 50  $\Omega$ .cm<sup>2</sup> on day 3 to approximately 300  $\Omega$ .cm<sup>2</sup> on day 7 post-seeding on filter insert. The TEER values were observed to decrease pronouncedly after 9 days in culture. Various methods were developed and reported to improve the barrier properties for efficient drug permeability studies using *in vitro* blood-brain barrier cell models. TEER measurements of the cell monolayers was used to assess the integrity as well as the paracellular permeability (141).

Upon achieving 100% confluency on the day 4 post-seeding and culture of PBECs in Transwell® filter insert, growth medium without serum and with hydrocortisone (DMEM supplemented with 100 U/ml penicillin and 100 µg/ml streptomycin, 2 mM L-glutamine, 125 µg/ml heparin and 550 nM hydrocortisone) was used. Replacement of serum-free medium with hydrocortisone shows a pronounced increase of TEER from day 4 post-seeding (Figure 4-6). Serum withdrawal has been reported to result in reinforcement of the blood-brain barrier properties of cultured endothelial cells. PBECs with low TEER (less than 200 Ω.cm<sup>2</sup>) were reported in the presence of serum. The absence of serum was found to strongly inhibit cells proliferation, promoting cell differentiation which forms tighter tight junctions, and significantly increase TEER values. Addition of hydrocortisone has also been reported to increase TEER values by 150% (172) as well as significantly lower sucrose permeability (135).

Cells were then treated with supplements of cAMP in combination with the cAMP-specific phosphodiesterase inhibitor RO-20-1724 (cAMP/RO-20-1724). Elevated tight junctions resistance has been previously reported after treatment with supplements e.g. cAMP/RO-20-1724 (137, 138). However, the TEER values of the PBEC monolayers (Figure 4-6) were not elevated to the desired level (above 200 Ω.cm<sup>2</sup>) after 24 h of cAMP/RO-20-1724 treatment. Growth medium without serum and with hydrocortisone was changed daily for the culture. PBEC monolayers were treated with freshly prepared cAMP/RO-20-1724 mixture everyday until the TEER values were increased to approximately 300 Ω.cm<sup>2</sup> on day 7 post-seeding where the monolayers were ready for permeability studies. Only PBEC monolayers with TEER value above 200 Ω.cm<sup>2</sup> were used for experiments. The TEER values were observed to gradually decrease after 9 days in culture.

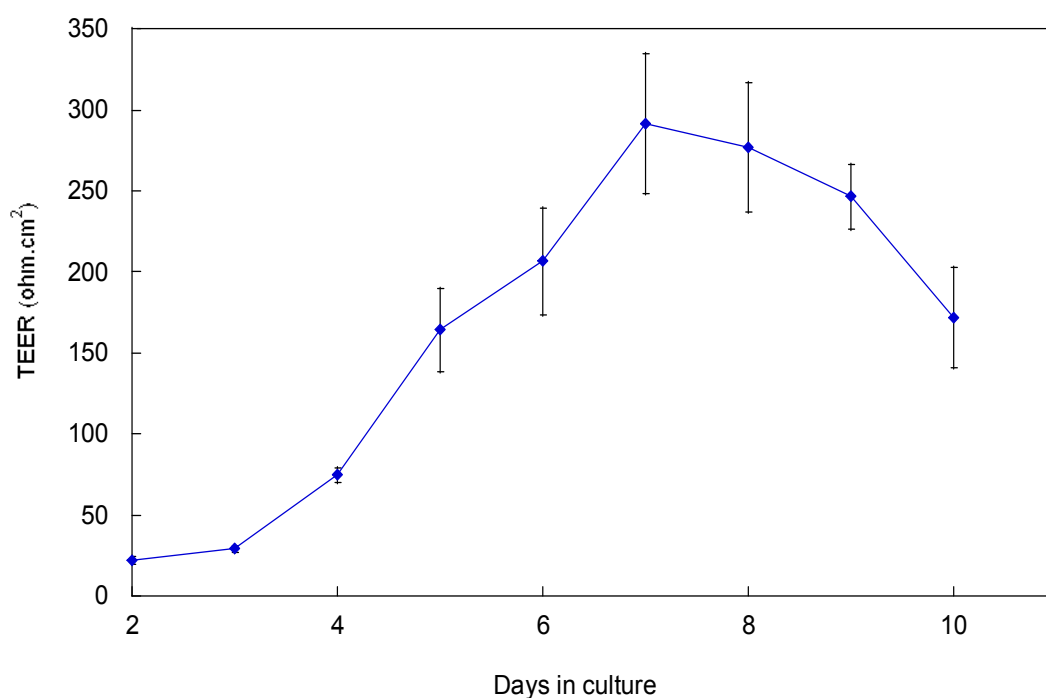


**Figure 4-6: Transendothelial electrical resistance values of PBEC monolayers on various days in culture (mean  $\pm$  SD, n = 3 of triplicate experiments).**

#### 4.3.4.2 Permeation of G3 PAMAM dendrimer and drug conjugates across PBEC monolayers

**The permeation of paclitaxel, G3 PAMAM dendrimer and conjugates across the PBEC monolayers was evaluated in both A $\rightarrow$ B and B $\rightarrow$ A direction at a non-toxic concentration as determined in the cytotoxicity studies using the LDH release assay. Results of the permeability studies were summarised in**

Figure 4-7. Paclitaxel, a known unambiguous P-gp efflux transporter substrate, was found to have a significant ( $p < 0.05$ ) higher B $\rightarrow$ A  $P_{app}$  than the A $\rightarrow$ B  $P_{app}$ . This finding is consistent with the previous results of paclitaxel transport profile across Caco-2 cell monolayers in chapter 3. The significant higher B $\rightarrow$ A  $P_{app}$  indicated that functionally active P-gp efflux transporters existed on the PBEC monolayers.

It was noted that the overall  $P_{app}$  values of G3 PAMAM dendrimer, paclitaxel and conjugates were higher for PBECs compared to Caco-2 cells. It might be due to lower

TEER values (200-350  $\Omega\cdot\text{cm}^2$ ) of PBEC monolayers compared to the TEER values ( $> 500 \Omega\cdot\text{cm}^2$ ) of Caco-2 cells. Another possible factor may be due to the influence of stirred condition during permeability study using PBEC monolayers. The stirred condition minimised the effect of unstirred water layer (UWL) which better mimics the *in vivo* BBB environment. It has been reported that the UWL in Caco-2 under unstirred conditions presents an artificial and rate-limiting barrier to passive diffusion across the cell monolayers (132).

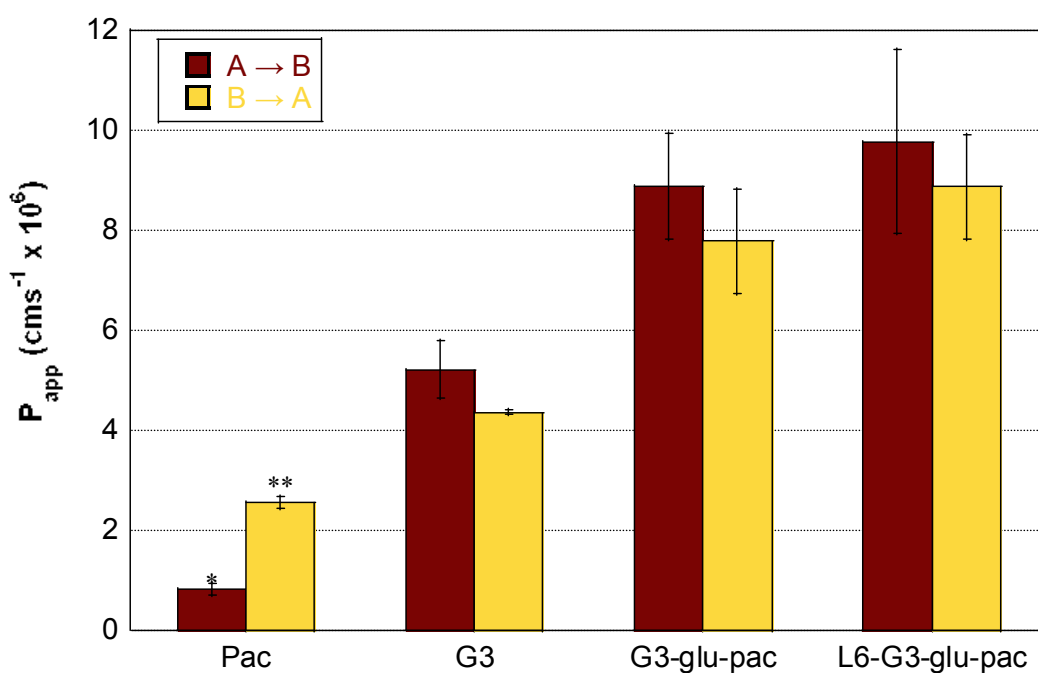
**The A $\rightarrow$ B  $P_{\text{app}}$  of G3 PAMAM dendrimer was approximately  $5.22 \times 10^{-6}$  cm/s. The A $\rightarrow$ B  $P_{\text{app}}$  of G3 was not significantly different from B $\rightarrow$ A  $P_{\text{app}}$ , suggesting that G3 PAMAM dendrimer is not a substrate for the efflux transporter in the blood-brain barrier. Conjugating paclitaxel to G3 PAMAM dendrimer (G3-glu-pac) increased the A $\rightarrow$ B  $P_{\text{app}}$  by approximately 10 fold compare to that of free paclitaxel (**

Figure 4-7). Permeability of L6-G3-glu-pac was further increased, with the A $\rightarrow$ B  $P_{\text{app}}$  approximately 12 fold greater than that of free paclitaxel. By conjugating paclitaxel to G3 and surface-modified G3 PAMAM dendrimers with lauryl chains as permeation enhancer (28, 103), the permeation of paclitaxel across the PBEC monolayers was significantly improved. These findings were similar to the permeability profile using Caco-2 cells in Chapter 3. BBB-impermeable polypeptide, horseradish peroxidase (HRP) modified with stearoyl acid chloride was synthesised by Batrakova *et al.* (173). Addition of lipophilic (stearoyl) moieties demonstrated enhanced transport across the BBB and increased accumulation in the brain *in vitro* and *in vivo*.

Limited transport of paclitaxel across cellular barriers is largely due to exclusion by the P-gp efflux transporter system. Enhanced permeation of paclitaxel across the blood-brain barrier has been reported by inhibiting the P-gp efflux. Analogues of cyclosporine A (P-gp inhibitors) were found to enhance brain paclitaxel levels by 3-fold in mice and rats (24, 174). However, long-term use of inhibitors is not advisable as down regulation of efflux transporter activity may occur; which allow free trafficking of potentially toxic substrates (5). Chemical modification of the drug offered an alternative approach to enhance permeation of drugs across the BBB. A specific binding site for taxoids on the P-gp efflux transporter was reported by Ojima *et al.* (175). It has been shown that selected chemical modification of paclitaxel molecules at the C-10 position can reduced the drug interaction with P-gp, thus enhance the permeability across the BBB (176-178). In the present study, paclitaxel

molecules were conjugated to G3 PAMAM dendrimer at the C'2 position and significantly enhanced permeability of the conjugates was observed. This suggests that C'2 may be an alternative site for chemical modification to improve drug permeability across the BBB.

From the results of the present study, it is proposed that G3 PAMAM dendrimer and surface modified G3 with lauryl chains can act as carriers to enhance the permeability of paclitaxel and can bypass the P-gp efflux transporters which are functionally active in PBEC monolayers. These findings were in good agreement with the results of Caco-2 cells (Chapter 3) as well as previous reports that showed PAMAM dendrimer as carriers to enhance permeability of drugs which are P-gp substrate (83, 86, 162).



**Figure 4-7: The A→B (■) and B→ A (■) permeability of G3 PAMAM dendrimer, free paclitaxel and conjugates across the PBEC monolayers after 3 h incubation at 37°C (mean ± SD, n = 3 of triplicate experiments). \* indicates a significant difference ( $p < 0.05$ ) from other conjugates. \*\* indicates a significant difference ( $p < 0.05$ ) for B→A compared to A→B.**

#### 4.3.4.3 The effect of G3 PAMAM dendrimer and drug conjugates on PBEC monolayers integrity

Transepithelial electrical resistance (TEER) measurements were conducted during the 3 h incubation with test substances at 37°C to examine the effect of G3 PAMAM dendrimer and conjugates on the monolayer integrity. Figure 4-8A shows the changes in TEER values of PBEC monolayers following apical incubation with G3 PAMAM dendrimer and drug conjugates. After incubation of PBECs with G3 PAMAM dendrimer, the TEER value was decreased by approximately 20% over 3 h. Apical incubation with G3-glu-pac and L6-G3-glu-pac showed a decrease in TEER ( $81.5 \pm 3.0\%$  and  $73.3 \pm 1.4\%$  respectively). PAMAM dendrimers have been reported to demonstrate transepithelial transport via both transcellular and paracellular pathways across Caco-2 cell monolayers (11, 103, 162, 163). The internalisation of G3 PAMAM dendrimer has been shown to occur via both caveolae-dependent endocytosis and macropinocytosis pathway, while the surface modified G3 PAMAM dendrimer with two lauryl chains was internalised via caveolae-dependent, clathrin-dependent, and macropinocytosis pathway into HT-29 cells. The internalisation mechanism was described to be influenced by the surface properties G3 PAMAM dendrimer (157). The significantly increased permeability, together with the decreased TEER value of G3-glu-pac and G3L6-flu-pac therefore suggests that the transport is via both transcellular and paracellular pathway across the PBEC monolayers.

The TEER measurement following 3 h incubation with pac showed a significant decrease of TEER by approximately 43% with PBECs. The permeability of pac was lowest among all compounds tested. The findings are similar to the TEER measurements of Caco-2 cell monolayers (chapter 3). It has been shown that PAMAM dendrimers can enhance paracellular permeation by modulating and opening tight junctions (84, 103, 162). D'Emanuele *et al.* (83) reported that the transport of propranolol was not enhanced by the presence of G3 PAMAM dendrimers, which suggests that the transport was mainly via transcellular pathway. Previous work reported by El-sayed *et al.* (162) indicated that paclitaxel transport was solely via the transcellular route and was not influenced by PAMAM dendrimer that modulates the tight junctions. TEER has been described as a measure of paracellular permeability

(164). This could explain the low permeability of paclitaxel even though pronounced decreases of TEER were observed with PBEC monolayers. In addition, anti-microtubule drugs (vinblastine, colchicine and paclitaxel) have been reported to demonstrate disruptive effect on cell monolayers integrity and decreased TEER after exposure to the drugs (141). However, the permeability and transport profile were not reported.

No significant difference in TEER values was observed when dendrimer and conjugates were incubated on the apical side compared with the basolateral side. The recovery of TEER to approximately 100% was observed following removal of G3 PAMAM dendrimer and conjugates from the cells after experiments (data not shown).

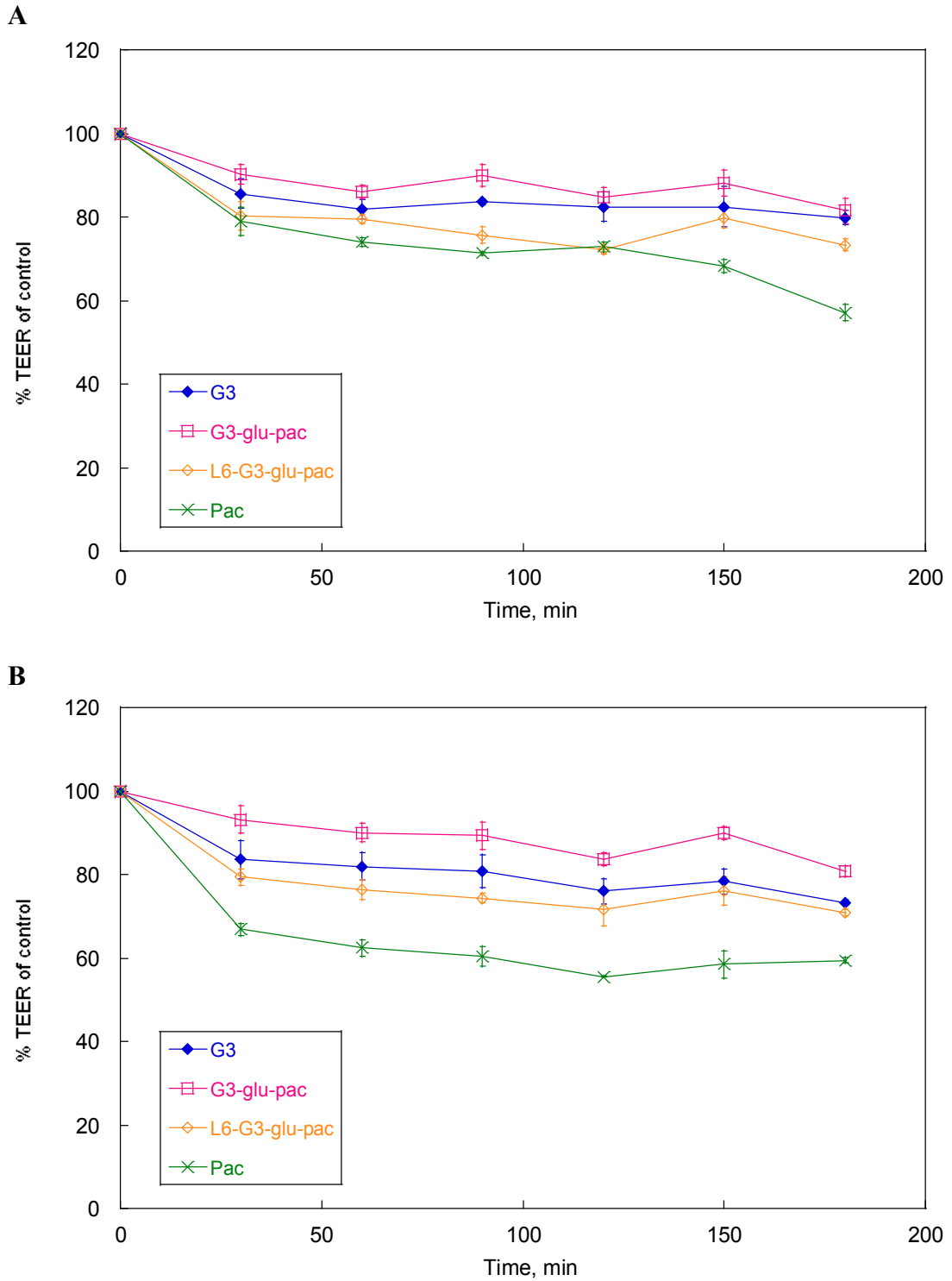


**Figure 4-8: The effect of free G3 PAMAM dendrimer, free paclitaxel and conjugates on the TEER of PBEC monolayers after (A) apical and (B) basolateral incubation (mean  $\pm$  SD, n = 3 of triplicate experiments).**

## 4.4 Conclusions

In this present study, PBECs were successfully cultured with characteristic elongated spindle-like morphology observed under the microscope. 100% confluency was achieved within 7 days of culture with the growth medium volume increased to 20-25 ml per T75 flask. TEER measurements were determined for PBEC monolayers that were grown and maintained on filter inserts. Only cell monolayers that achieved TEER values higher than  $200 \Omega \cdot \text{cm}^2$  were used for permeability studies. The elevation of TEER values was observed with PBEC monolayers cultured in serum-free medium and treated with cAMP/RO-20-1724 mixture.

Biological evaluation of G3 PAMAM dendrimer and conjugates using PBECs showed that the cytotoxicity was dependent on the surface properties of dendrimer and conjugates, supporting the findings in the cytotoxicity study of Caco-2 cells. G3 PAMAM dendrimer was found to be relatively non-toxic compared to all other conjugates at all test concentrations. Conjugation of lauryl chains and paclitaxel molecules on G3 PAMAM dendrimer significantly increased the cytotoxicity in PBECs. Surface modification of G3 PAMAM dendrimers has also influenced the permeation and integrity of PBEC monolayers. The B $\rightarrow$ A  $P_{\text{app}}$  of paclitaxel was found to be significantly higher than the A $\rightarrow$ B  $P_{\text{app}}$ , indicating active function of P-gp efflux transporter system in the cell model. Covalent conjugation of paclitaxel to G3 PAMAM dendrimer via a glutaric anhydride linker significantly increased its A $\rightarrow$ B  $P_{\text{app}}$  through PBEC monolayers. The A $\rightarrow$ B  $P_{\text{app}}$  of L6-G3-glu-pac was found to be 12 fold greater than that of free paclitaxel across the PBEC monolayers, where lauryl chains were acting as permeability enhancer. The transport of G3-paclitaxel conjugates across the cells is thought to occur via both paracellular and transcellular routes.

The cytotoxicity and permeability results using PBECs are found to be in good agreement with the findings when Caco-2 cells were used as the cellular barrier cell model. Thus, it can be concluded that G3 and surface modified G3 PAMAM dendrimers can act as potential nanocarriers for low solubility and P-gp substrate drug (e.g. paclitaxel) to enhance solubility and permeability, and to bypass the P-gp efflux transporter system in both intestinal and blood-brain barriers.

## **CHAPTER 5: CONCLUSIONS AND FUTURE WORK**

---

## 5.1 Conclusions

The development of effective drug delivery systems to cross cellular barriers has always remained a major challenge in pharmaceutical research. In the recent years, dendrimers, a novel class of polymers with well-defined structure and amenable functional surface groups, have emerged as a candidate drug carrier. The potential use of dendrimer-based drug delivery system was explored and investigated to overcome cellular barriers (e.g. intestinal and blood-brain barriers).

In this study, novel dendrimer based drug delivery systems consisting of G3 PAMAM dendrimer, the permeability enhancer moieties – lauryl chains, the linker – glutaric anhydride and the drug – paclitaxel were successfully synthesised and characterised. Chemical stability studies demonstrated that the dendrimer conjugates have good stability at all pHs (1.2, 7.4, and 8.5) after 48 h of incubation. Ester bonds of the conjugates are stable under physiological conditions with 10 days of incubation.

Biological evaluation of G3 PAMAM dendrimer and conjugates was first conducted using Caco-2 cells as the intestinal barrier cell model. Free G3 PAMAM dendrimer was found to be relatively non-toxic while conjugation of lauryl chains and paclitaxel molecule on the surface of G3 PAMAM dendrimer significantly increased the cytotoxicity in Caco-2 cells. G3 PAMAM dendrimers conjugated with lauryl chains and pac-glu has also demonstrated significant enhanced permeation across the Caco-2 cells monolayers. L6-G3-glu-pac was found with the highest permeability, with the  $A \rightarrow B P_{app}$  12.4 fold greater than that of free paclitaxel. These results suggest that the dendrimer-based drug delivery systems can bypass the P-gp efflux transporter and overcome the intestinal barrier.

Further biological evaluation of the dendrimer conjugates was carried out using PBECs as a cell model to assess the ability of the dendrimer-based drug delivery systems to overcome the blood-brain barrier. The cytotoxicity and permeability results for PBECs are found to be in good agreement with the findings for Caco-2 cells. G3 PAMAM dendrimer significantly increased the cytotoxicity in PBECs. Similar to the transport profile observed in Caco-2, L6-G3-glu-pac was found with the highest permeability

(approximately 12 fold greater than that of free paclitaxel) across the PBEC monolayers. These results showed that the conjugation of lauryl chains and pac-glu molecules to the dendrimer efficiently enhanced the permeability. This is possibly due to the permeation enhancing properties of lauryl chains, and the addition of hydrophobic moieties that aids the interaction with plasma membrane.

The present results suggest that G3 and surface modified G3 PAMAM dendrimers are able to act as potential nanocarriers to enhance permeability of drugs (e.g. paclitaxel) that are poor water soluble and are P-gp efflux transporter substrate. It was concluded that the dendrimer-based drug delivery systems could bypass the P-gp efflux transporter and overcome both the intestinal and the blood-brain barriers.

## **5.2 Future work**

The present study extends the potential of dendrimer-based drug delivery system to overcome the intestinal barrier and also the blood-brain barrier. However, numerous challenges still remain in drug delivery to the central nervous system. Future work in this area could involve surface modification of dendrimer with targeting moieties (e.g. transferrin, insulin or angiopeps for LRP-1 receptor) for drug delivery to the blood-brain barrier. Given the complexity of blood-brain barrier functions, further studies could investigate the mechanism of the internalisation pathway of dendrimer and drug conjugates across the PBEC monolayers to provide a better understanding in designing the dendrimer-based drug delivery systems. In addition, *in vivo* and *in situ* studies could be conducted in order to provide quantitative correlation between the *in vitro* and *in vivo/ in situ* transports of the dendrimer-drug conjugates tested. With a more complete understanding of the therapeutic profile, dendrimer-based drug delivery systems are to be expected to have great potential in not only oral drug delivery, but also in CNS therapeutics delivery.

## CHAPTER 6: APPENDICES

---

## Appendix I: HPLC chromatograms of paclitaxel, pac-glu, G3 PAMAM dendrimers and conjugates

*Methods:* The appearance of pac, pac-glu, G3 PAMAM dendrimer and conjugates was detected using Agilent 1100 Series HPLC system (UK) equipped with a Luna 5  $\mu$ m, C18 column (250 mm x 4.6 mm) (Phenomenex, Cheshire, UK), with phenanthrene as an internal standard. Solvent system used: MeOH: TFA (0.05% w/v) (80:20). The flow rate was 1.0 ml/min and the UV detection wavelength was 230 nm.

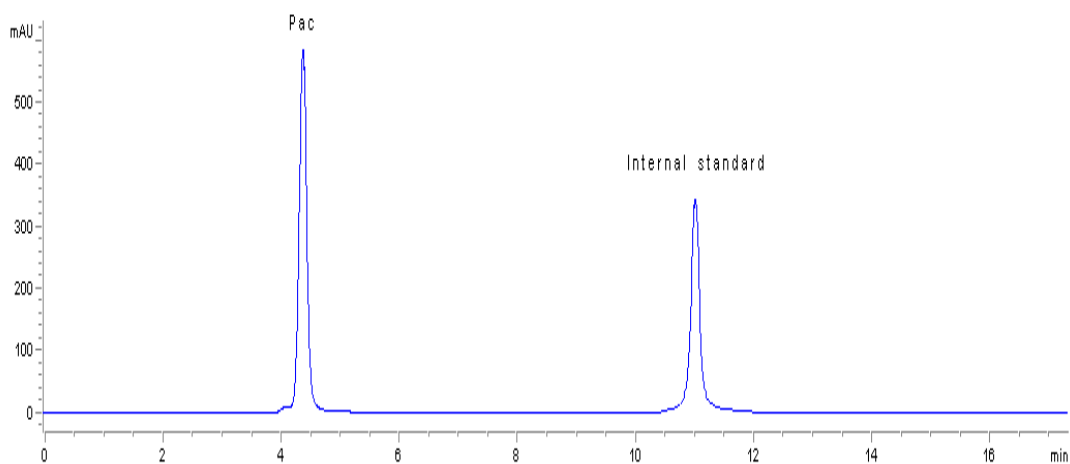


**Figure 6-1: HPLC chromatogram of pac and internal standard.**

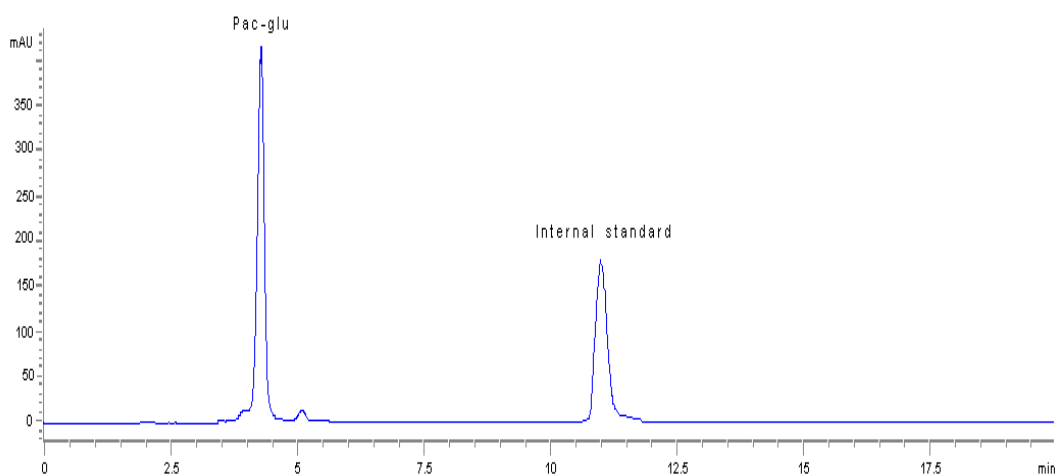


**Figure 6-2: HPLC chromatogram of pac-glu and internal standard.**

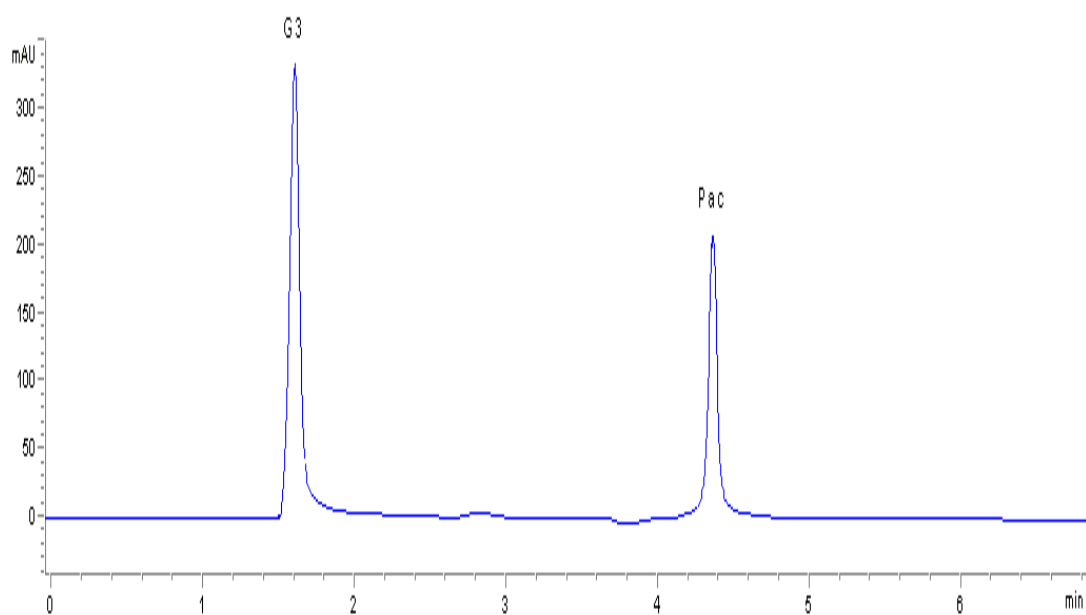


**Figure 6-3: HPLC chromatogram of G3 PAMAM dendrimer and paclitaxel.**

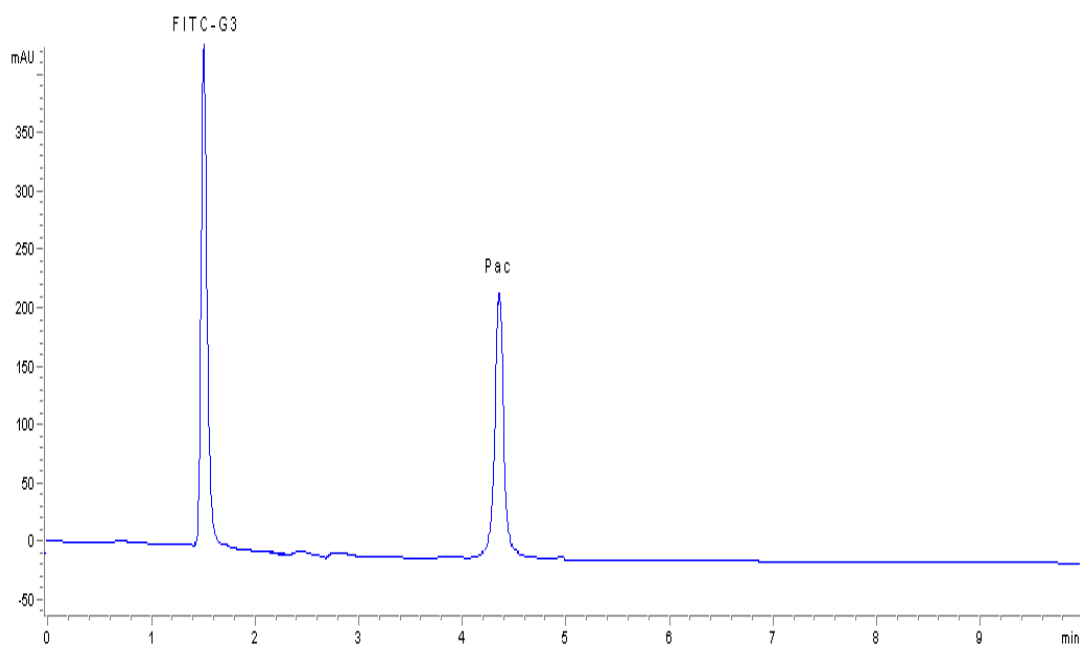


**Figure 6-4: HPLC chromatogram of FITC-G3 and paclitaxel.**

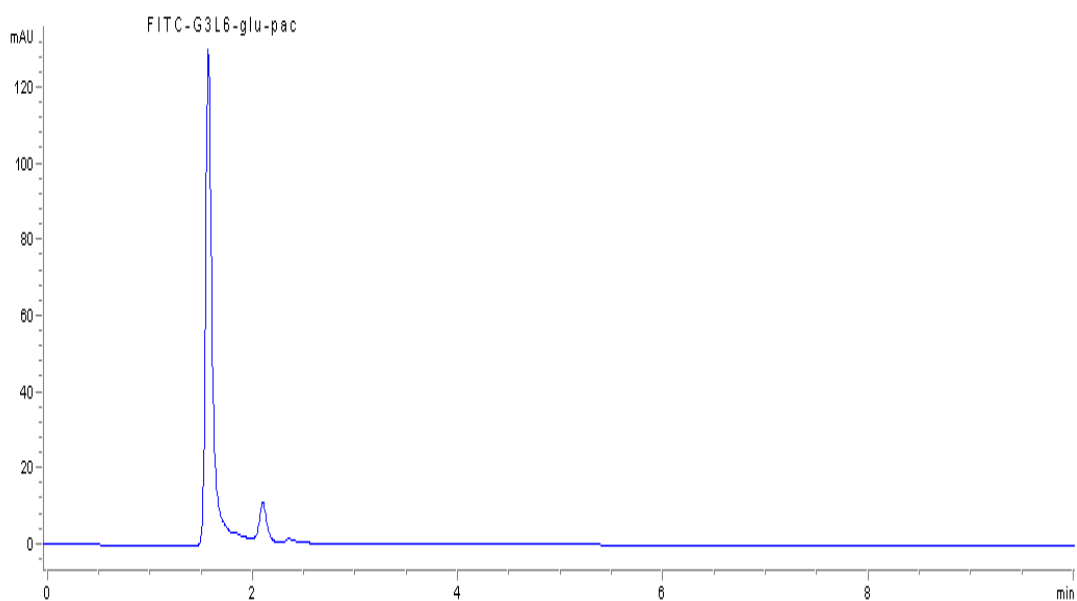


**Figure 6-5: HPLC chromatogram of FITC-G3L6-glu-pac.**

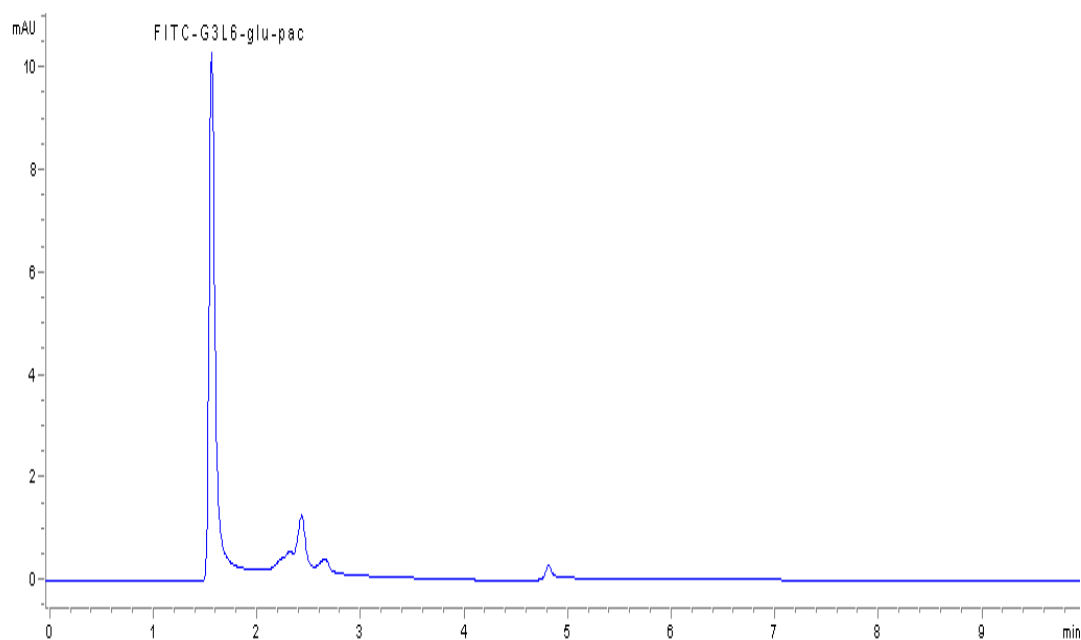


**Figure 6-6: HPLC chromatogram of FITC-G3L6-glu-pac collected after crossing PBEC monolayers during permeability studies.**

## Appendix II: HPLC assay calibration curves of paclitaxel and pac-glu

*Methods:* HPLC analyses were performed using Agilent 1100 Series HPLC system (UK) equipped with a Luna 5  $\mu\text{m}$ , C18 column (250 mm x 4.6 mm) (Phenomenex, Cheshire, UK). The UV detection wavelength was 230 nm.

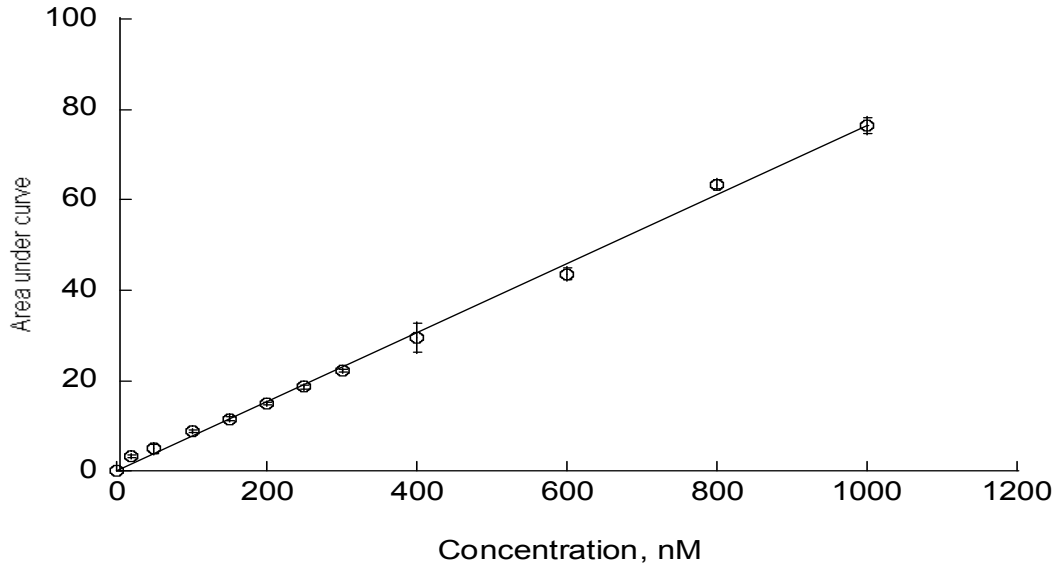


**Figure 6-7: Calibration curve of paclitaxel in methanol,  $R^2 = 0.9974$  (mean  $\pm$  SD, n = 3).**

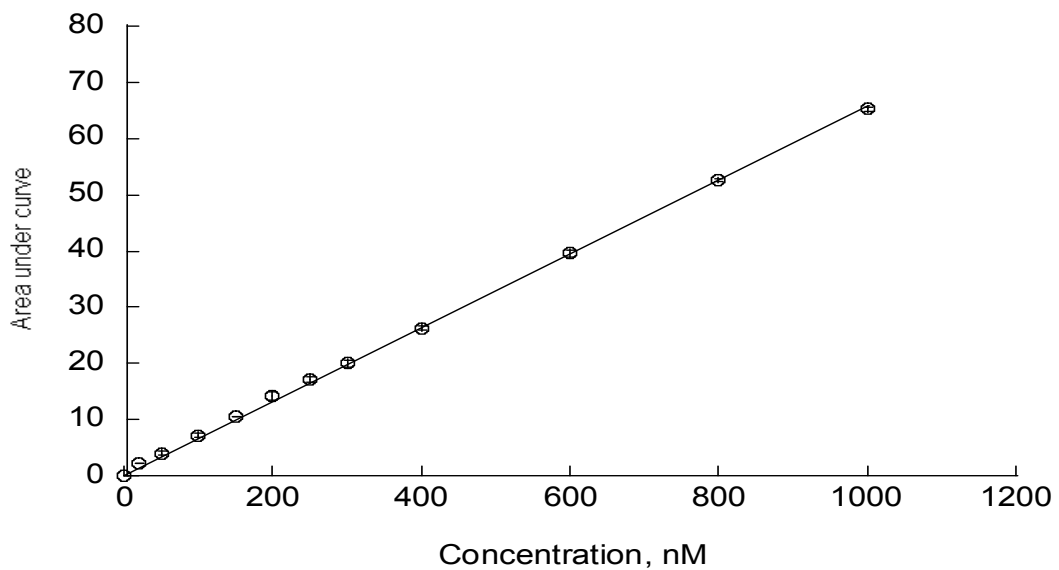


**Figure 6-8: Calibration curve of pac-glu in methanol,  $R^2 = 0.9991$  (mean  $\pm$  SD, n = 3).**

### Appendix III: Spectrofluorometric assay calibration curves of FITC-labelled G3 PAMAM dendrimers and conjugates

*Method:* Measurements were carried out at excitation/ emission wavelength of 485 nm/ 535 nm using TECAN GENios Pro multiplate reader (Grödig, Austria).

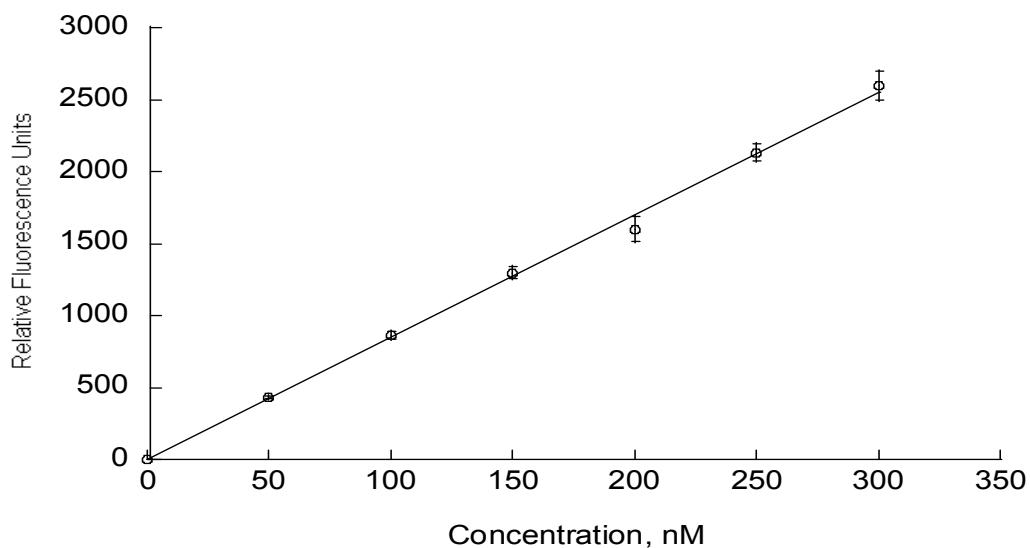


**Figure 6-9: Calibration curve of FITC-G3 in transport medium,  $R^2 = 0.9974$  (mean  $\pm$  SD, n = 3).**

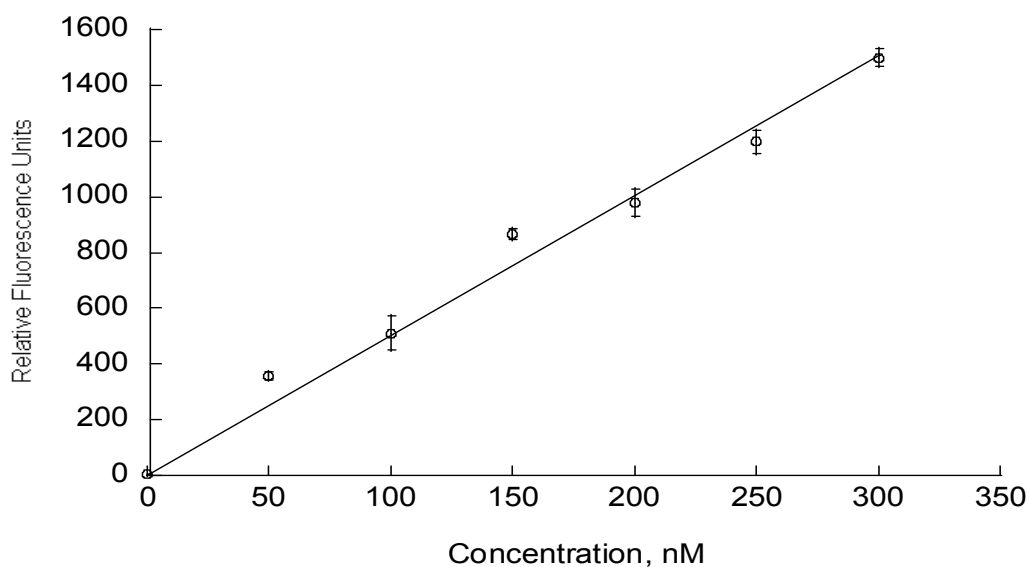


**Figure 6-10: Calibration curve of FITC-G3L3 in transport medium,  $R^2 = 0.9824$  (mean  $\pm$  SD, n = 3).**

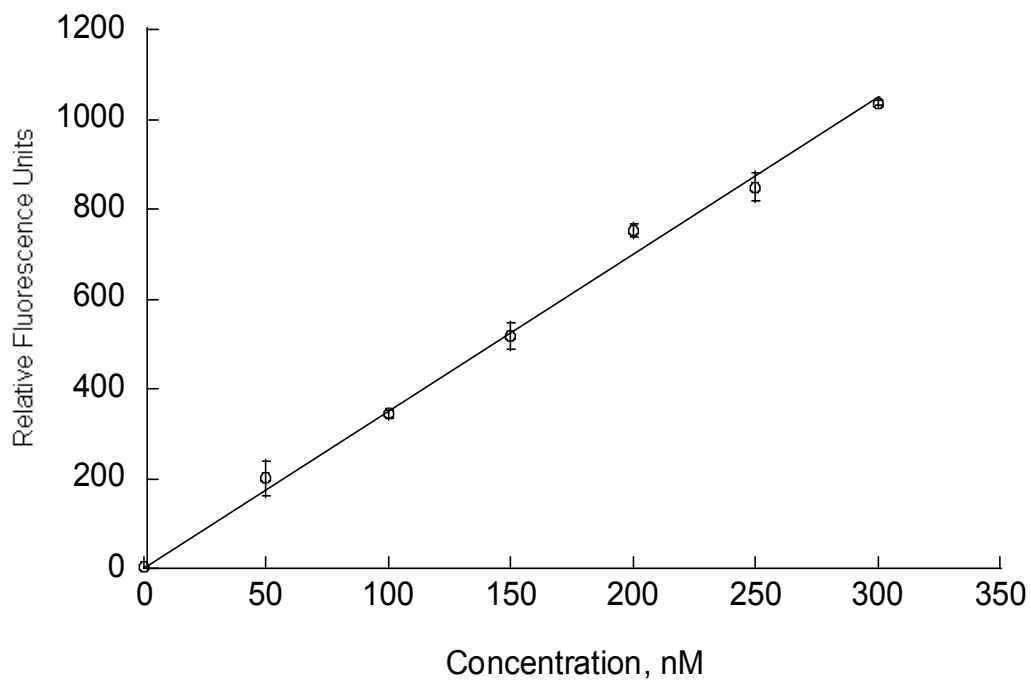


**Figure 6-11: Calibration curve of FITC-G3L6 in transport medium,  $R^2 = 0.9947$  (mean  $\pm$  SD, n = 3).**

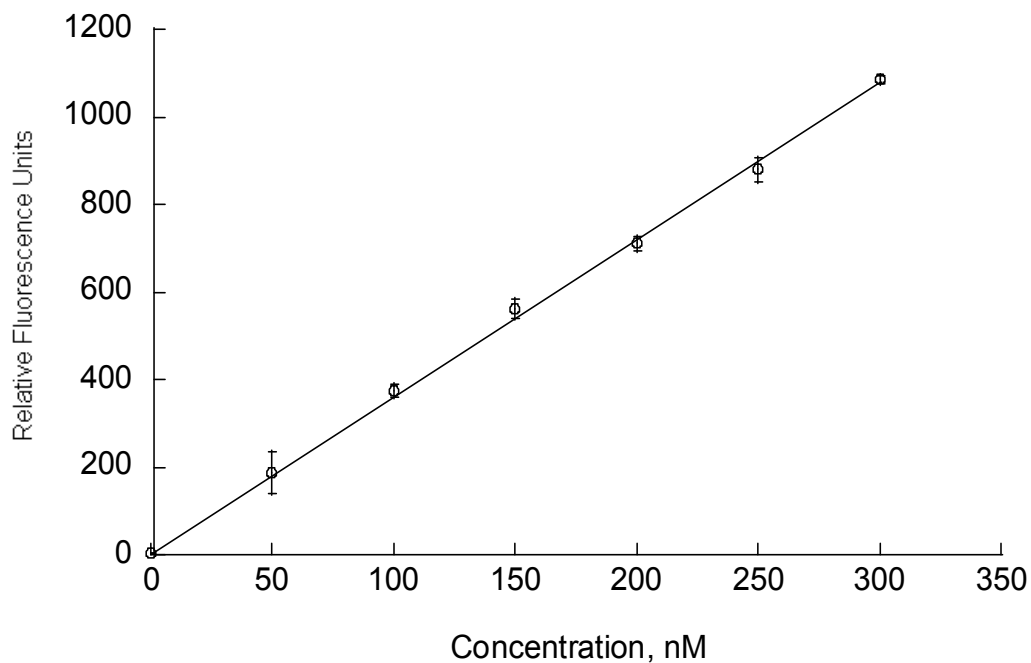


**Figure 6-12: Calibration curve of FITC-G3-glu-pac in transport medium,  $R^2 = 0.9986$  (mean  $\pm$  SD, n = 3).**

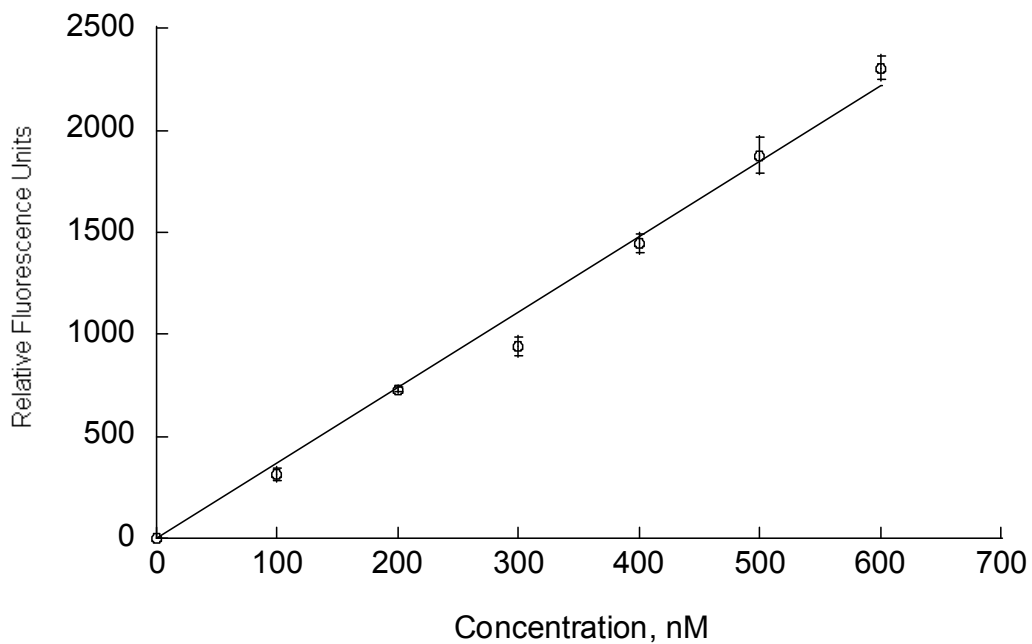


**Figure 6-13: Calibration curve of FITC-G3L3-glu-pac in transport medium,  $R^2 = 0.9904$  (mean  $\pm$  SD, n = 3).**

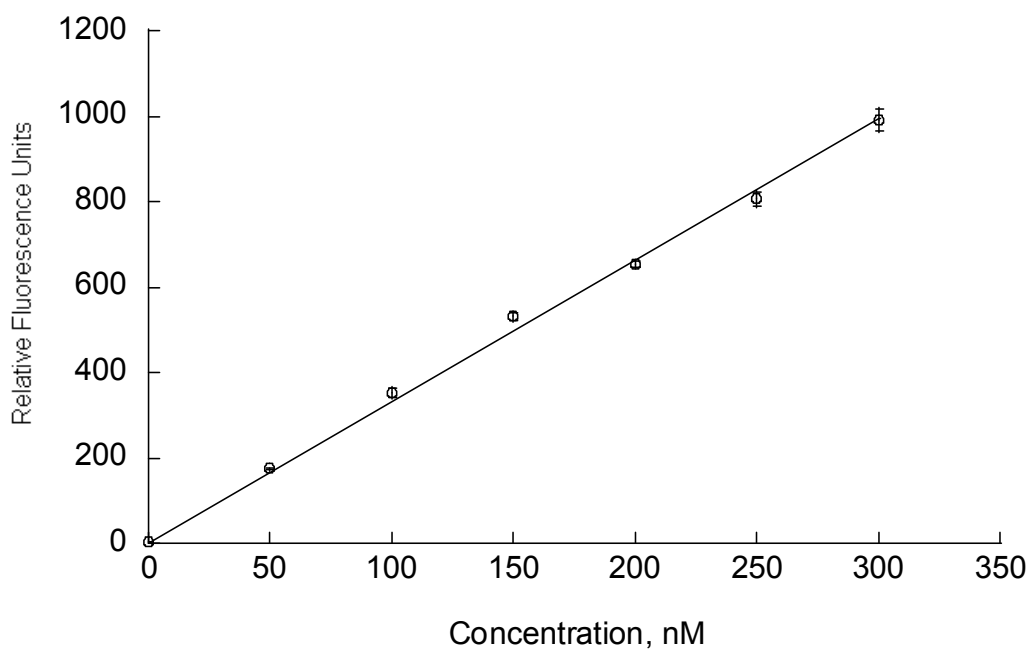


**Figure 6-14: Calibration curve of FITC-G3L6-glu-pac in transport medium,  $R^2 = 0.9969$  (mean  $\pm$  SD, n = 3).**

## **Appendix IV: Publications, conference presentations and awards**

### **PUBLICATIONS**

H.M. Teow, Z. Zhou, M. Najlah and A. D'Emanuele. The use of a dendrimer carrier to enhance paclitaxel delivery and bypass the P-glycoprotein efflux transporter. 2009, J. Pharm. Pharmacol., 34 (Supplement 1), 75-76.

### **CONFERENCES PRESENTATIONS**

The British Pharmaceutical Conference 2009, Manchester, UK (poster presentation).

United Kingdom International Controlled Release Society Symposium 2008, London, UK (poster presentation).

Science and Technology Annual Graduate School Conference in 2009, 2008 and 2007, UCLan, UK (poster and oral presentation).

### **AWARDS**

Commendation for Poster Presentation, The British Pharmaceutical Conference 2009, Manchester.

## CHAPTER 7: REFERENCES

---

1. H. Lennernäs and E. Lundgren. Intestinal and blood-brain drug transport: beyond involvement of a single transport function. *Drug Disc. Today: Tech.* **1**: 417-422 (2004).
2. N. J. Abbott. Astrocyte-endothelial interactions and blood-brain barrier permeability. *J. Anat.* **200**: 523-534 (2002).
3. S. Dauchy, F. Dutheil, R. Weaver, J. , F. Chassoux, C. Dumas-Duport, P.-O. Couraud, J.-M. Scherrmann, I. De Wazier, and X. Declèves. ABC transporters, cytochromes P450 and their main transcription factors: expression at the human blood-brain barrier. *J. Neurochem.* **107**: 1518-1528 (2008).
4. N. J. Abbott and I. A. Romero. Transporting therapeutics across the blood-brain barrier. *Mol. Med. Today* **2**: 106-113 (1996).
5. D. J. Begley. Delivery of therapeutic agents to the central nervous system: the problems and the possibilities. *Pharmacol. Therapeut.* **104**: 29-45 (2004).
6. M. Goldberg and I. Gomez-Orellana. Challenges for the oral delivery of macromolecules. *Nat. Rev. Drug. Discov.* **2**: 289-295 (2003).
7. U. Bickel, Y. S. Kang, T. Yoshikawa, and W. M. Pardridge. In vivo demonstration of subcellular localization of anti-transferrin receptor monoclonal antibody-colloidal gold conjugate in brain capillary endothelium. *J. Histochem. Cytochem.* **42**: 1493-1497 (1994).
8. C. C. Visser, S. Stevanovic, L. H. Voorwinden, L. v. Bloois, P. J. Gaillard, M. Danhof, D. J. A. Crommelin, and A. G. d. Boer. Targeting liposomes with protein drugs to the blood-brain barrier in vitro. *Eur. J. Pharm. Sci.* **25**: 299-305 (2005).
9. J. Kreuter, R. N. Alyautdin, D. A. Kharkevich, and A. A. Ivanov. Passage of peptides through the blood-brain barrier with colloidal polymer particles (nanoparticles). *Brain Res.* **674**: 171-174 (1995).
10. A. D'Emanuele and D. Attwood. Dendrimer-drug interactions. *Adv. Drug Deliv. Rev.* **57**: 2147-2162 (2005).
11. M. Najlah and A. D'Emanuele. Crossing cellular barriers using dendrimer nanotechnologies. *Curr. Opin. Pharmacol.* **6**: 522-527 (2006).
12. M. E. Aulton. *Pharmaceutics, the Science of Dosage Form Design*, 2<sup>nd</sup> edition, Elsevier Limited, Edinburgh, 2002.

13. V. W. Tang and D. A. Goodenough. Paracellular ion channel at the tight junction. *Biophys. J.* **84**: 1660-1673 (2003).
14. URL: [http://cellbiology.med.unsw.edu.au/units/images/Cell\\_membrane.png](http://cellbiology.med.unsw.edu.au/units/images/Cell_membrane.png) (accessed 16/04/2010).
15. G. Camenisch, J. Alsenz, H. van de Waterbeemd, and G. Folkers. Estimation of permeability by passive diffusion through Caco-2 cell monolayers using the drugs' lipophilicity and molecular weight. *Eur. J. Pharm. Sci.* **6**: 313-319 (1998).
16. P. Anderle, Y. Huang, and W. Sadée. Intestinal membrane transport of drugs and nutrients: genomics of membrane transporters using expression microarrays. *Eur. J. Pharm. Sci.* **21**: 17-24 (2004).
17. G. M. Friedrichsen, W. Chen, M. Begtrup, C.-P. Lee, P. L. Smith, and R. T. Borchardt. Synthesis of analogs of L-valacyclovir and determination of their substrate activity for the oligopeptide transporter in Caco-2 cells. *Eur. J. Pharm. Sci.* **16**: 1-13 (2002).
18. H.-k. Han, R. L. A. de Vruhe, J. K. Rhie, K.-M. Y. Covitz, P. L. Smith, C.-P. Lee, D.-M. Oh, W. Sadee, and G. L. Amidon. 5' -Amino acid esters of antiviral nucleosides, acyclovir, and AZT are absorbed by the intestinal PEPT1 peptide transporter. *Pharm. Res.* **15**: 1154-1159 (1998).
19. M. E. Ganapathy, M. Brandsch, P. D. Prasad, V. Ganapathy, and F. H. Leibach. Differential recognition of  $\beta$ -lactam antibiotics by intestinal and renal peptide transporters, PEPT 1 and PEPT 2. *J. Biol. Chem.* **270**: 25672-25677 (1995).
20. J. Hunter, B. H. Hirst, and N. L. Simmons. Drug absorption limited by P-glycoprotein-mediated secretory drug transport in human intestinal epithelial Caco-2 cell layers. *Pharm. Res.* **10**: 743-749 (1993).
21. B.-L. Leu and J.-d. Huang. Inhibition of intestinal P-glycoprotein and effects on etoposide absorption. *Cancer Chemother. Pharmacol.* **35**: 432-436 (1995).
22. P. Anderle, E. Niederer, W. Rubas, C. Hilgendorf, H. Spahn-Langguth, H. Wunderli-Allenspach, H. P. Merkle, and P. Langguth. P-glycoprotein (P-gp) mediated efflux in Caco-2 cell monolayers: the influence of culturing conditions and drug exposure on P-gp expression levels. *J. Pharm. Sci.* **87**: 757-762 (1998).
23. U. K. Walle and T. Walle. Taxol transport by human intestinal epithelial caco-2 cells. *Drug Metab. Dispos.* **26**: 343-346 (1998).
24. S. Fellner, B. Bauer, D. S. Miller, M. Schaffrik, M. Fankhanel, T. Spruss, G. Bernhardt, C. Graeff, L. Farber, H. Gschaidmeier, A. Buschauer, and G. Fricker.

- Transport of paclitaxel (Taxol) across the blood-brain barrier in vitro and in vivo. *J. Clin. Invest.* **110**: 1309-1318 (2002).
25. M. M. Gottesman, T. Fojo, and S. E. Bates. Multidrug resistance in cancer: role of ATP-dependent transporters. *Nat. Rev. Cancer* **2**: 48-58 (2002).
  26. A. L. Daugherty and R. J. Mistry. Transcellular uptake mechanisms of the intestinal epithelial barrier Part one. *Pharm. Sci. Technol. Today* **2**: 144-151 (1999).
  27. M. J. Cano-Cebrián, T. Zornoza, L. Granero, and A. Polache. Intestinal absorption enhancement via the paracellular route by fatty acids, chitosans and others: a target for drug delivery. *Curr. Drug Delivery* **2**: 9-22 (2005).
  28. B. J. Aungst. Intestinal permeation enhancers. *J. Pharm. Sci.* **89**: 429-442 (2000).
  29. M. Sakai, A. B. J. Noach, M. C. M. Blom-Roosemalen, A. G. De Boer, and D. D. Breimer. Absorption enhancement of hydrophilic compounds by verapamil in Caco-2 cell monolayers. *Biochem. Pharmacol.* **48**: 1199-1210 (1994).
  30. H. N. Nellans. (B) Mechanisms of peptide and protein absorption: (1) Paracellular intestinal transport: modulation of absorption. *Adv. Drug Deliv. Rev.* **7**: 339-364 (1991).
  31. A. Fasano. Modulation of intestinal permeability: an innovative method of oral drug delivery for the treatment of inherited and acquired human diseases. *Mol. Genet. Metab.* **64**: 12-18 (1998).
  32. N. J. Abbott. Prediction of blood-brain barrier permeation in drug discovery from in vivo, in vitro and in silico models. *Drug Disc. Today: Tech.* **1**: 407-416 (2004).
  33. J. Bernacki, A. Dobrowolska, K. Nierwinska, and A. Malecki. Physiology and pharmacological role of the blood-brain barrier. *Pharmacol. Rep.* **60**: 600-622 (2008).
  34. E. P. Das. *Sauerstoff-bedürfniss des organismus : eine farbenanalytische studie.*, Berlin : Hirschwald, 1885.
  35. P. Ballabh, A. Braun, and M. Nedergaard. The blood-brain barrier: an overview: structure, regulation, and clinical implications. *Neurobiol. Dis.* **16**: 1-13 (2004).
  36. N. J. Abbott, L. Rönnbäck, and E. Hansson. Astrocyte endothelial interactions at the blood-brain barrier. *Nat. Rev. Neurosci.* **7**: 41-53 (2006).

37. P. Grieb, R. E. Forster, D. Strome, C. W. Goodwin, and P. C. Pape. O<sub>2</sub> exchange between blood and brain tissues studied with 18O<sub>2</sub> indicator-dilution technique. *J. Appl. Physiol.* **58**: 1929-1941 (1985).
38. P. J. Gaillard, I. C. J. van der Sandt, L. H. Voorwinden, D. Vu, J. L. Nielsen, A. G. de Boer, and D. D. Breimer. Astrocytes increase the functional expression of P-glycoprotein in an in vitro model of the blood-brain barrier. *Pharm. Res.* **17**: 1198-1205 (2000).
39. Y. Hayashi, M. Nomura, S.-I. Yamagishi, S.-I. Harada, J. Yamashita, and H. Yamamoto. Induction of various blood-brain barrier properties in non-neural endothelial cells by close apposition to co-cultured astrocytes. *Glia* **19**: 13-26 (1997).
40. R. Haseloff, I. Blasig, H. Bauer, and H. Bauer. In search of the astrocytic factor(s) modulating blood-brain barrier functions in brain capillary endothelial cells in vitro. *Cell. Mol. Neurobiol.* **25**: 25-39 (2005).
41. K. Sobue, N. Yamamoto, K. Yoneda, M. E. Hodgson, K. Yamashiro, N. Tsuruoka, T. Tsuda, H. Katsuya, Y. Miura, K. Asai, and T. Kato. Induction of blood-brain barrier properties in immortalized bovine brain endothelial cells by astrocytic factors. *Neurosci. Res.* **35**: 155-164 (1999).
42. G. Miller. Drug targeting: breaking down barriers. *Science* **297**: 1116-1118 (2002).
43. A. G. de Boer and P. J. Gaillard. Strategies to improve drug delivery across the blood-brain barrier. *Clin. Pharmacokinet.* **46**: 553 (2007).
44. C. Crone and S. P. Olesen. Electrical resistance of brain microvascular endothelium. *Brain. Res.* **241**: 49-55 (1982).
45. R. Cecchelli, V. Berezowski, S. Lundquist, M. Culot, M. Renftel, M.-P. Dehouck, and L. Fenart. Modelling of the blood brain barrier in drug discovery and development. *Nat. Rev. Drug. Discov.* **6**: 650-661 (2007).
46. K. Matter and M. S. Balda. Signalling to and from tight junctions. *Nat. Rev. Mol. Cell. Biol.* **4**: 225-237 (2003).
47. N. J. Abbott, A. A. K. Patabendige, D. E. M. Dolman, S. R. Yusof, and D. J. Begley. Structure and function of the blood-brain barrier. *Neurobiol. Dis.* **37**: 13-25 (2010).
48. A. Tsujii and I. Tamai. Carrier-mediated intestinal transport of drugs. *Pharm. Res.* **13**: 963-977 (1996).

49. Q. R. Smith. Carrier-mediated transport to enhance drug delivery to brain. *Int. Congr. Series* **1277**: 63-74 (2005).
50. I. A. Simpson, S. J. Vannucci, M. R. DeJoseph, and R. A. Hawkins. Glucose transporter asymmetries in the bovine blood-brain barrier. *J. Biol. Chem.* **276**: 12725-12729 (2001).
51. J. B. M. M. van Bree, C. D. Heijligers-Feijen, A. G. de Boer, M. Danhof, and D. D. Breimer. Stereoselective transport of baclofen across the blood-brain barrier in rats as determined by the unit impulse response methodology. *Pharm. Res.* **8**: 259-262 (1991).
52. D. F. Welty, G. P. Schielke, M. G. Vartanian, and C. P. Taylor. Gabapentin anticonvulsant action in rats: disequilibrium with peak drug concentrations in plasma and brain microdialysate. *Epilepsy Res.* **16**: 175-181 (1993).
53. S. I. Rapoport. Drug delivery to the brain: barrier modification and drug modification methodologies. *NiDA Res. Monogr.* **120**: 121-137 (1992).
54. A. H. Schinkel. P-Glycoprotein, a gatekeeper in the blood-brain barrier. *Adv. Drug Deliv. Rev.* **36**: 179-194 (1999).
55. A. Tsuji and I. Tamai. Carrier-mediated or specialized transport of drugs across the blood-brain barrier. *Adv. Drug Deliv. Rev.* **36**: 277-290 (1999).
56. B. F. Pan, A. Dutt, and J. A. Nelson. Enhanced transepithelial flux of cimetidine by Madin-Darby canine kidney cells overexpressing human P-glycoprotein. *J. Pharmacol. Exp. Ther.* **270**: 1-7 (1994).
57. T. R. Stouch and O. Gudmundsson. Progress in understanding the structure-activity relationships of P-glycoprotein. *Adv. Drug Deliv. Rev.* **54**: 315-328 (2002).
58. N. J. Abbott, B. T. John, and J. T. David. In vitro models for examining and predicting brain uptake of drugs, *Compr. Med. Chem. II*, Elsevier, Oxford, 2007, pp. 301-320.
59. G. Fricker. Overcoming MDR at the blood-brain barrier. *Int. Congr. Ser.* **1277**: 131-143 (2005).
60. J. Huwyler, A. Cerletti, G. Fricker, A. N. Eberle, and J. Drewe. By-passing of P-glycoprotein using immunoliposomes. *J. Drug Targeting* **10**: 73-79 (2002).
61. A. Cerletti, J. Drewe, G. Fricker, A. Eberle, and J. Huwyler. Endocytosis and transcytosis of an immunoliposome-based brain drug delivery system. *J. Drug Targeting* **8**: 435-446 (2000).

62. M. Thöle, S. Nobmann, J. Huwyler, A. Bartmann, and G. Fricker. Uptake of cationized albumin coupled liposomes by cultured porcine brain microvessel endothelial cells and intact brain capillaries. *J. Drug Targeting* **10**: 337-344 (2002).
63. J. Kreuter. Nanoparticulate systems for brain delivery of drugs. *Adv. Drug Deliv. Rev.* **47**: 65-81 (2001).
64. C. F. Higgins and M. M. Gottesman. Is the multidrug transporter a flippase? *Trends Biochem. Sci.* **17**: 18-21 (1992).
65. A. H. Schinkel and J. W. Jonker. Mammalian drug efflux transporters of the ATP binding cassette (ABC) family: an overview. *Adv. Drug Deliv. Rev.* **55**: 3-29 (2003).
66. W. Löscher and H. Potschka. Blood-brain barrier active efflux transporters: ATP-binding cassette gene family. *NeuroRx* **2**: 86-98 (2005).
67. G. Rappa, R. A. Finch, A. C. Sartorelli, and A. Lorico. New insights into the biology and pharmacology of the multidrug resistance protein (MRP) from gene knockout models. *Biochem. Pharmacol.* **58**: 557-562 (1999).
68. W. Löscher and H. Potschka. Role of multidrug transporters in pharmacoresistance to antiepileptic drugs. *J. Pharmacol. Exp. Ther.* **301**: 7-14 (2002).
69. M. Leggas, M. Adachi, G. L. Scheffer, D. Sun, P. Wielinga, G. Du, K. E. Mercer, Y. Zhuang, J. C. Panetta, B. Johnston, R. J. Scheper, C. F. Stewart, and J. D. Schuetz. Mrp4 confers resistance to topotecan and protects the brain from chemotherapy. *Mol. Cell. Biol.* **24**: 7612-7621 (2004).
70. W. Zhang, J. Mojsilovic-Petrovic, M. F. Andrade, H. Zhang, M. Ball, and D. B. Stanimirovic. Expression and functional characterization of ABCG2 in brain endothelial cells and vessels. *FASEB J.* 02-1131fje (2003).
71. T. Eisenblätter, S. Hüwel, and H.-J. Galla. Characterisation of the brain multidrug resistance protein (BMDP/ABCG2/BCRP) expressed at the blood-brain barrier. *Brain. Res.* **971**: 221-231 (2003).
72. T. Moos and E. Morgan. Transferrin and transferrin receptor function in brain barrier systems. *Cell. Mol. Neurobiol.* **20**: 77-95 (2000).
73. W. M. Pardridge. Drug and gene targeting to the brain via blood-brain barrier receptor-mediated transport systems. *Int. Congr. Ser.* **1277**: 49-62 (2005).

74. P. J. Gaillard, C. C. Visser, and A. G. de Boer. Targeted delivery across the blood-brain barrier. *Expert Opin. Drug Deliv.* **2**: 299-309 (2005).
75. Y. Saito, J. Buciak, J. Yang, and W. M. Pardridge. Vector-mediated delivery of  $^{125}\text{I}$ -labeled  $\beta$ -amyloid peptide  $\text{A}\beta^{1-40}$  through the blood-brain barrier and binding to Alzheimer disease amyloid of the  $\text{A}\beta^{1-40}$ /vector complex. *Proc. Natl. Acad. Sci. U. S. A.* **92**: 10227-10231 (1995).
76. M. Demeule, J. Poirier, J. Jodoin, Y. Bertrand, R. R. Desrosiers, C. Dagenais, T. Nguyen, J. Lanthier, R. Gabathuler, M. Kennard, W. A. Jefferies, D. Karkan, S. Tsai, L. Fenart, R. Cecchelli, and R. Béliveau. High transcytosis of melanotransferrin (P97) across the blood-brain barrier. *J. Neurochem.* **83**: 924-933 (2002).
77. R. Gabathuler, G. Arthur, M. Kennard, Q. Chen, S. Tsai, J. Yang, W. Schoorl, T. Z. Vitalis, and W. A. Jefferies. Development of a potential protein vector (NeuroTrans) to deliver drugs across the blood-brain barrier. *Int. Congr. Ser.* **1277**: 171-184 (2005).
78. W. Pan, A. J. Kastin, T. C. Zankel, P. van Kerkhof, T. Terasaki, and G. Bu. Efficient transfer of receptor-associated protein (RAP) across the blood-brain barrier. *J. Cell. Sci.* **117**: 5071-5078 (2004).
79. M. Demeule, J.-C. Currie, Y. Bertrand, C. Ché, T. Nguyen, A. Régina, R. Gabathuler, J.-P. Castaigne, and R. Béliveau. Involvement of the low-density lipoprotein receptor-related protein in the transcytosis of the brain delivery vector Angiopep-2. *J. Neurochem.* **106**: 1534-1544 (2008).
80. M. Demeule, A. Régina, C. Ché, J. Poirier, T. Nguyen, R. Gabathuler, J.-P. Castaigne, and R. Béliveau. Identification and design of peptides as a new drug delivery system for the brain. *J. Pharmacol. Exp. Ther.* **324**: 1064-1072 (2008).
81. A. Régina, M. Demeule, C. Ch, I. Lavallée, J. Poirier, R. Gabathuler, R. Béliveau, and J. P. Castaigne. Antitumour activity of ANG1005, a conjugate between paclitaxel and the new brain delivery vector Angiopep-2. *Br. J. Pharmacol.* **155**: 185-197 (2008).
82. F. Thomas, K. Taskar, V. Rudraraju, S. Goda, H. Thorsheim, J. Gaasch, R. Mittapalli, D. Palmieri, P. Steeg, P. Lockman, and Q. Smith. Uptake of ANG1005, a novel paclitaxel derivative, through the blood-brain barrier into brain and experimental brain metastases of breast cancer. *Pharm. Res.* **26**: 2486-2494 (2009).
83. A. D'Emanuele, R. Jevprasesphant, J. Penny, and D. Attwood. The use of a dendrimer-propranolol prodrug to bypass efflux transporters and enhance oral bioavailability. *J. Control. Rel.* **95**: 447-453 (2004).

84. R. Jevprasesphant, J. Penny, D. Attwood, and A. D'Emanuele. Transport of dendrimer nanocarriers through epithelial cells via the transcellular route. *J. Control. Rel.* **97**: 259-267 (2004).
85. M. Najlah, S. Freeman, D. Attwood, and A. D'Emanuele. Synthesis, characterization and stability of dendrimer prodrugs. *Int. J. Pharm.* **308**: 175-182 (2006).
86. M. Najlah, S. Freeman, D. Attwood, and A. D'Emanuele. Synthesis and assessment of first-generation polyamidoamine dendrimer prodrugs to enhance the cellular permeability of P-gp substrates. *Bioconjugate Chem.* **18**: 937-946 (2007).
87. M. Najlah, S. Freeman, D. Attwood, and A. D'Emanuele. In vitro evaluation of dendrimer prodrugs for oral drug delivery. *Int. J. Pharm.* **336**: 183-190 (2007).
88. D. A. Tomalia, H. Baker, J. Dewald, M. Hall, G. Kallos, S. Martin, J. Roeck, J. Ryder, and P. Smith. A new class of polymers: starburst-dendritic macromolecules. *Polym. J.* **17**: 117-132 (1985).
89. M. Murat and G. S. Grest. Molecular dynamics study of dendrimer molecules in solvents of varying quality. *Macromolecules* **29**: 1278-1285 (1996).
90. U. Boas, J. B. Christensen, and P. M. H. Heeaard. *Dendrimers in medicine and biotechnology: new molecular tools*, The Royal Society of Chemistry, Cambridge, 2006.
91. D. A. Tomalia, A. M. Naylor, and W. A. I. Goddard. Starburst dendrimers: molecular-level control of size, shape, surface chemistry, topology, and flexibility from atoms to macroscopic matter. *Angew. Chem. Int. Ed.* **29**: 138-175 (1990).
92. A. Shipway. URL: <http://www.ninger.com/dendrimer/> (accessed 21/08/2008).
93. G. R. Newkome, Z. Yao, G. R. Baker, and V. K. Gupta. Micelles. Part 1. Cascade molecules: a new approach to micelles. A [27]-arborol. *J. Org. Chem.* **50**: 2003-2004 (1985).
94. C. Dufès, I. F. Uchegbu, and A. G. Schätzlein. Dendrimers in gene delivery. *Adv. Drug Deliv. Rev.* **57**: 2177-2202 (2005).
95. J. C. Hummelen, J. L. J. Van Dongen, and E. W. Meijer. Electrospray mass spectrometry of poly(propylene imine) dendrimers - the issue of dendritic purity or polydispersity. *Chem. Eur. J.* **3**: 1489-1493 (1997).

96. G. M. Dykes. Dendrimers: a review of their appeal and applications. *J. Chem. Tech. Biotechnol.* **76**: 903-918 (2001).
97. C. J. Hawker and J. M. J. Frechet. Preparation of polymers with controlled molecular architecture. A new convergent approach to dendritic macromolecules. *J. Am. Chem. Soc.* **112**: 7638-7647 (1990).
98. R. Arshady. Dendrimers assemblies nanocomposites. In dendrimers assemblies and nanocomposites concept, criteria, definitions, volume 5, R. Arshady, ed. (London: Citrus Books). 1-29 (2003).
99. O. M. Milhem, C. Myles, N. B. McKeown, D. Attwood, and A. D'Emanuele. Polyamidoamine Starburst® dendrimers as solubility enhancers. *Int. J. Pharm.* **197**: 239-241 (2000).
100. Y. Cheng, H. Qu, M. Ma, Z. Xu, P. Xu, Y. Fang, and T. Xu. Polyamidoamine (PAMAM) dendrimers as biocompatible carriers of quinolone antimicrobials: An in vitro study. *Eur. J. Med. Chem.* **42**: 1032-1038 (2007).
101. J. D. Eichman, A. U. Bielinska, J. F. Kukowska-Latallo, and J. R. Baker. The use of PAMAM dendrimers in the efficient transfer of genetic material into cells. *Pharm. Sci. Technol. Today* **3**: 232-245 (2000).
102. S.-E. Stiriba, H. Frey, and R. Haag. Dendritic polymers in biomedical applications: from potential to clinical use in diagnostics and therapy. *Angew. Chem. Int. Ed.* **41**: 1329-1334 (2002).
103. R. Jevprasesphant, J. Penny, D. Attwood, N. B. McKeown, and A. D'Emanuele. Engineering of dendrimer surfaces to enhance transepithelial transport and reduce cytotoxicity. *Pharm. Res.* **20**: 1543-1550 (2003).
104. K. Kono, M. Liu, and J. M. J. Frechet. Design of dendritic macromolecules containing folate or methotrexate residues. *Bioconjugate Chem.* **10**: 1115-1121 (1999).
105. I. J. Majoros, A. Myc, T. Thomas, C. B. Mehta, and J. R. Baker. PAMAM dendrimer-based multifunctional conjugate for cancer therapy: synthesis, characterization, and functionality. *Biomacromolecules* **7**: 572-579 (2006).
106. R. Jevprasesphant, J. Penny, R. Jalal, D. Attwood, N. B. McKeown, and A. D'Emanuele. The influence of surface modification on the cytotoxicity of PAMAM dendrimers. *Int. J. Pharm.* **252**: 263-266 (2003).
107. A. D'Emanuele, D. Attwood, and R. Abu-Rmaileh. Dendrimers. *Encyc. Pharm. Tech.* 872 - 890 (2006).

108. R. Esfand and D. A. Tomalia. Poly(amidoamine) (PAMAM) dendrimers: from biomimicry to drug delivery and biomedical applications. *Drug Disc. Today* **6**: 427-436 (2001).
109. I. Lee, B. D. Athey, A. W. Wetzel, W. Meixner, and J. R. Baker. Structural molecular dynamics studies on polyamidoamine dendrimers for a therapeutic application: effects of pH and generation. *Macromolecules* **35**: 4510-4520 (2002).
110. A. W. Bosman, H. M. Janssen, and E. W. Meijer. About dendrimers: structure, physical properties, and applications. *Chem. Rev.* **99**: 1665-1688 (1999).
111. B. Devarakonda, R. A. Hill, and M. M. de Villiers. The effect of PAMAM dendrimer generation size and surface functional group on the aqueous solubility of nifedipine. *Int. J. Pharm.* **284**: 133-140 (2004).
112. B. Devarakonda, A. Judefeind, S. Chigurupati, S. Thomas, G. V. Shah, D. P. Otto, and M. M. de Villiers. The Effect of Polyamidoamine Dendrimers on the In Vitro Cytotoxicity of Paclitaxel in Cultured Prostate Cancer (PC-3M) Cells. *J. Biomed. Nanotechnol.* **3**: 384-393 (2007).
113. P. Kolhe, E. Misra, R. M. Kannan, S. Kannan, and M. Lieh-Lai. Drug complexation, in vitro release and cellular entry of dendrimers and hyperbranched polymers. *Int. J. Pharm.* **259**: 143-160 (2003).
114. S. Kannan, P. Kolhe, V. Raykova, M. Glibatec, R. M. Kannan, M. Lieh-Lai, and D. Bassett. Dynamics of cellular entry and drug delivery by dendritic polymers into human lung epithelial carcinoma cells. *J. Biomater. Sci. Polymer Edn.* **15**: 311-330 (2004).
115. W. Ke, Y. Zhao, R. Huang, C. Jiang, and Y. Pei. Enhanced oral bioavailability of doxorubicin in a dendrimer drug delivery system. *J. Pharm. Sci.* **97**: 2208-2216 (2008).
116. J. Khandare, P. Kolhe, O. Pillai, S. Kannan, M. Lieh-Lai, and R. M. Kannan. Synthesis, cellular transport, and activity of polyamidoamine dendrimer-methylprednisolone conjugates. *Bioconjugate Chem.* **16**: 330-337 (2005).
117. J. J. Khandare, S. Jayant, A. Singh, P. Chandna, Y. Wang, N. Vorsa, and T. Minko. Dendrimer versus linear conjugate: influence of polymeric architecture on the delivery and anticancer effect of paclitaxel. *Bioconjugate Chem.* **17**: 1464-1472 (2006).
118. X. Bi, X. Shi, I. J. Majoros, R. Shukla, and J. R. Baker. Multifunctional poly(amidoamine) dendrimer-taxol conjugates: synthesis, characterization and stability. *J. Comput. Theor. Nanosci.* **4**: 1179-1187 (2007).

119. R.-Q. Huang, Y.-H. Qu, W.-L. Ke, J.-H. Zhu, Y.-Y. Pei, and C. Jiang. Efficient gene delivery targeted to the brain using a transferrin-conjugated polyethyleneglycol-modified polyamidoamine dendrimer. *FASEB J.* **21**: 1117-1125 (2007).
120. R. Huang, W. Ke, Y. Liu, C. Jiang, and Y. Pei. The use of lactoferrin as a ligand for targeting the polyamidoamine-based gene delivery system to the brain. *Biomaterials* **29**: 238-246 (2008).
121. T. H. Gouw. *Guide to Modern Methods of Instrument Analysis*, Wiley & Sons, Inc., New York, NY, 1972.
122. D. H. Williams and I. Fleming. *Spectroscopy Methods in Organic Chemistry*, 5th edition, The McGraw-Hill Companies, Berkshire, UK, 1995.
123. S. Lindsay. *High Performance Liquid Chromatography*, Wiley & Sons, Great Britain, 1987.
124. E. Prichard. *Practical Laboratory Skills Training Guides: High Performance Liquid Chromatography*, LGC Limited, Teddington, Middlesex, England, 2003.
125. URL: [http://www1.waters.com/waters/nav.htm?locale=de\\_DE&cid=10049055](http://www1.waters.com/waters/nav.htm?locale=de_DE&cid=10049055) (accessed 23/08/2010).
126. I. Hidalgo, J., T. Raub, J., and R. Borchardt, T. Characterization of the human colon carcinoma cell line (Caco-2) as a model system for intestinal epithelial permeability. *Gastroenterology* **96**: 736-749 (1989).
127. M. Pinto, S. Robine-Leon, M.-D. Appay, M. Kedinger, N. Triadou, E. Dussaulx, B. Lacroix, P. Simon-Assmann, K. Haffen, J. Fogh, and A. Zweibaum. Enterocyte-like differentiation and polarization of the human colon carcinoma cell line Caco-2 in culture. *Biol. Cell* **47**: 323-330 (1983).
128. I. J. Hidalgo and R. T. Borchardt. Transport of bile acids in a human intestinal epithelial cell line, Caco-2. *BBA-Gen Subjects* **1035**: 97-103 (1990).
129. L.-S. L. Gan and D. R. Thakker. Applications of the Caco-2 model in the design and development of orally active drugs: elucidation of biochemical and physical barriers posed by the intestinal epithelium. *Adv. Drug Deliv. Rev.* **23**: 77-98 (1997).
130. P. Artursson. Epithelial transport of drugs in cell culture. I: a model for studying the passive diffusion of drugs over intestinal absorptive (Caco-2) cells. *J. Pharm. Sci.* **79**: 476-482 (1990).

131. P. Artursson and J. Karlsson. Correlation between oral drug absorption in humans and apparent drug permeability coefficients in human intestinal epithelial (caco-2) cells. *Biochem. Biophys. Res. Commun.* **175**: 880-885 (1991).
132. Y. Zhang, C. S. W. Li, Y. Ye, K. Johnson, J. Poe, S. Johnson, W. Bobrowski, R. Garrido, and C. Madhu. Porcine brain microvessel endothelial cells as an *in vitro* model to predict *in vivo* blood-brain barrier permeability. *Drug Metab. Dispos.* **34**: 1935-1943 (2006).
133. F. Roux and P.-O. Couraud. Rat brain endothelial cell lines for the study of blood-brain barrier permeability and transport functions. *Cell. Mol. Neurobiol.* **25**: 41-57 (2005).
134. T. Terasaki and K.-i. Hosoya. Conditionally immortalized cell Lines as a new *in vitro* model for the study of barrier functions. *Biol. Pharm. Bull.* **24**: 111-118 (2001).
135. H. Franke, H.-J. Galla, and C. T. Beuckmann. Primary cultures of brain microvessel endothelial cells: a valid and flexible model to study drug transport through the blood-brain barrier *in vitro*. *Brain Res. Protoc.* **5**: 248-256 (2000).
136. V. V. Jeliaskova-Mecheva and D. J. Bobilya. A porcine astrocyte/endothelial cell co-culture model of the blood-brain barrier. *Brain Res. Protoc.* **12**: 91-98 (2003).
137. M. Török, J. Huwyler, H. Gutmann, G. Fricker, and J. Drewe. Modulation of transendothelial permeability and expression of ATP-binding cassette transporters in cultured brain capillary endothelial cells by astrocytic factors and cell-culture conditions. *Exp. Brain Res.* **153**: 356-365 (2003).
138. L. L. Rubin, D. E. Hall, S. Porter, K. Barbu, C. Cannon, H. C. Horner, M. Janatpour, C. W. Liaw, K. Manning, and J. Morales. A cell culture model of the blood-brain barrier. *J. Cell Biol.* **115**: 1725-1735 (1991).
139. N. Perrière, P. H. Demeuse, E. Garcia, A. Regina, M. Debray, J. P. Andreux, P. Couvreur, J. M. Scherrmann, J. Temsamani, P. O. Couraud, M. A. Deli, and F. Roux. Puromycin-based purification of rat brain capillary endothelial cell cultures. Effect on the expression of blood-brain barrier-specific properties. *J. Neurochem.* **93**: 279-289 (2005).
140. P. J. Gaillard, L. H. Voorwinden, J. L. Nielsen, A. Ivanov, R. Atsumi, H. Engman, C. Ringbom, A. G. de Boer, and D. D. Breimer. Establishment and functional characterization of an *in vitro* model of the blood-brain barrier, comprising a co-culture of brain capillary endothelial cells and astrocytes. *Eur. J. Pharm. Sci.* **12**: 215-222 (2001).

141. I. C. J. van der Sandt, P. J. Gaillard, H. H. Voorwinden, A. G. de Boer, and D. D. Breimer. P-glycoprotein inhibition leads to enhanced disruptive effects by anti-microtubule cytotostatics at the *in vitro* blood-brain barrier. *Pharm. Res.* **18**: 587-592 (2001).
142. M. C. Wani, H. L. Taylor, M. E. Wall, P. Coggon, and A. T. McPhail. Plant antitumor agents. VI. Isolation and structure of taxol, a novel antileukemic and antitumor agent from *Taxus brevifolia*. *J. Am. Chem. Soc.* **93**: 2325-2327 (1971).
143. E. K. Rowinsky, L. A. Cazenave, and R. C. Donehower. Taxol: a novel investigational antimicrotubule agent. *J. Natl. Cancer Inst.* **82**: 1247-1259 (1990).
144. I. J. Majoros, T. P. Thomas, C. B. Mehta, and J. R. Baker. Poly(amidoamine) dendrimer-based multifunctional engineered nanodevice for cancer therapy. *J. Med. Chem.* **48**: 5892-5899 (2005).
145. Q. Shi, H.-K. Wang, K. F. Bastow, Y. Tachibana, K. Chen, F.-Y. Lee, and K.-H. Lee. Antitumor agents 210. synthesis and evaluation of taxoid-epipodophyllotoxin conjugates as novel cytotoxic agents. *Bioorg. Med. Chem.* **9**: 2999-3004 (2001).
146. H. M. Deutsch, J. A. Glinski, M. Hernandez, R. D. Haugwitz, V. L. Narayanan, M. Suffness, and L. H. Zalkow. Synthesis of congeners and prodrugs. 3. Water-soluble prodrugs of taxol with potent antitumor activity. *J. Med. Chem.* **32**: 788-792 (1989).
147. N. F. Magri and D. G. I. Kingston. Modified taxols. 2. Oxidation products of taxol. *J. Org. Chem.* **51**: 797-802 (1986).
148. W. Mellado, N. F. Magri, D. G. I. Kingston, R. Garcia-Arenas, G. A. Orr, and S. B. Horwitz. Preparation and biological activity of taxol acetates. *Biochem. Biophys. Res. Commun.* **124**: 329-336 (1984).
149. H. Ogura, S. Nagai, and K. Takeda. A novel reagent (N-succinimidyl diphenylphosphate) for synthesis of active ester and peptide. *Tetrahedron Lett.* **21**: 1467-1468 (1980).
150. J. Cowley, J. Penny, N. Day, D. Attwood, and A. D'Emanuele. Gastrointestinal mucus and its effect on the transepithelial transport of PAMAM dendrimers. *J. Pharm. Pharmacol.* **59 (Supplement)**: 157 (2007).
151. A. Safavy, G. I. Georg, D. V. Velde, K. P. Raisch, K. Safavy, M. Carpenter, W. Wang, J. A. Bonner, M. B. Khazaeli, and D. J. Buchsbaum. Site-specifically traced drug release and biodistribution of a paclitaxel-antibody conjugate

- toward improvement of the linker structure. *Bioconjugate Chem.* **15**: 1264-1274 (2004).
152. F. Dosio, P. Brusa, P. Crosasso, S. Arpicco, and L. Cattel. Preparation, characterization and properties in vitro and in vivo of a paclitaxel-albumin conjugate. *J. Control. Rel.* **47**: 293-304 (1997).
  153. T. Y. Zakharian, A. Seryshev, B. Sitharaman, B. E. Gilbert, V. Knight, and L. J. Wilson. A Fullerene-paclitaxel chemotherapeutic: synthesis, characterization, and study of biological activity in tissue culture. *J. Am. Chem. Soc.* **127**: 12508-12509 (2005).
  154. V. Guillemard and H. U. Saragovi. Taxane-antibody conjugates afford potent cytotoxicity, enhanced solubility, and tumor target selectivity. *Cancer Res.* **61**: 694-699 (2001).
  155. Cytotoxicity Detection Kit (LDH), *Cat. No. 11644793001*, Roche Applied Science, July 2005.
  156. T. Decker and M.-L. Lohmann-Matthes. A quick and simple method for the quantitation of lactate dehydrogenase release in measurements of cellular cytotoxicity and tumor necrosis factor (TNF) activity. *J. Immunol. Methods* **115**: 61-69 (1988).
  157. A. Saovapakhiran, A. D'Emanuele, D. Attwood, and J. Penny. Surface modification of PAMAM dendrimers modulates the mechanism of cellular internalization. *Bioconjugate Chem.* **20**: 693-701 (2009).
  158. J. R. Cowley. Dendrimer Carriers: The Effect of Gastrointestinal Mucus on the Transepithelial Transport of PAMAM dendrimers, *School of Pharmacy and Pharmaceutical Sciences*, The University of Manchester, Manchester, 2007, pp. 174.
  159. M. Najlah. Dendrimer Prodrugs to Enhance Drug Bioavailability, *School of Pharmacy and Pharmaceutical Sciences*, The University of Manchester, Manchester, 2006, pp. 127-130.
  160. A. Saovapakhiran. Development of Novel Dendrimer Carriers for Drug Delivery, *School of Pharmacy and Pharmaceutical Sciences*, The University of Manchester, Manchester, 2008, pp. 99-101.
  161. J. M. Koziara, P. R. Lockman, D. D. Allen, and R. J. Mumper. Paclitaxel nanoparticles for the potential treatment of brain tumors. *J. Control. Rel.* **99**: 259-269 (2004).

162. M. El-Sayed, C. A. Rhodes, M. Ginski, and H. Ghandehari. Transport mechanism(s) of poly (amidoamine) dendrimers across Caco-2 cell monolayers. *Int. J. Pharm.* **265**: 151-157 (2003).
163. M. El-Sayed, M. Ginski, C. Rhodes, and H. Ghandehari. Transepithelial transport of poly(amidoamine) dendrimers across Caco-2 cell monolayers. *J. of Control. Rel.* **81**: 355-365 (2002).
164. P. J. Gaillard and A. G. de Boer. Relationship between permeability status of the blood-brain barrier and in vitro permeability coefficient of a drug. *Eur. J. Pharm. Sci.* **12**: 95-102 (2000).
165. P. Garberg, M. Ball, N. Borg, R. Cecchelli, L. Fenart, R. D. Hurst, T. Lindmark, A. Mabondzo, J. E. Nilsson, T. J. Raub, D. Stanimirovic, T. Terasaki, J. O. Öberg, and T. Österberg. In vitro models for the blood-brain barrier. *Toxicol. In Vitro* **19**: 299-334 (2005).
166. M. Smith, Y. Omid, and M. Gumbleton. Primary porcine brain microvascular endothelial cells: Biochemical and functional characterisation as a model for drug transport and targeting. *J. Drug Targeting* **15**: 253 - 268 (2007).
167. T. Tilling, D. Korte, and D. Hoheisel. Basement membrane proteins influence brain capillary endothelial barrier function in vitro. *J. Neurochem.* **71**: 1151-1157 (1998).
168. R. K. Locke, V. B. Bastone, and R. L. Baron. Studies of carbamate pesticide metabolism utilizing plant and mammalian cells in culture. *J. Agric. Food Chem.* **19**: 1205-1209 (1971).
169. Y. Shao, H. Ding, W. Tang, L. Lou, and L. Hu. Synthesis and structure-activity relationships study of novel anti-tumor carbamate anhydrovinblastine analogues. *Bioorg. Med. Chem.* **15**: 5061-5075 (2007).
170. T. Ooya, J. Lee, and K. Park. Effects of ethylene glycol-based graft, star-shaped, and dendritic polymers on solubilization and controlled release of paclitaxel. *J. Control. Rel.* **93**: 121-127 (2003).
171. T. Ooya, J. Lee, and K. Park. Hydrotropic dendrimers of generations 4 and 5: synthesis, characterization, and hydrotropic solubilization of paclitaxel. *Bioconjugate Chem.* **15**: 1221-1229 (2004).
172. D. J. Begley, M. W. Bradbury, and J. Kreuter. *The Blood-Brain Barrier and Drug Delivery to the CNS*, Marcel Dekker, Inc., New York. Basel, 2000.
173. E. V. Batrakova, S. V. Vinogradov, S. M. Robinson, M. L. Niehoff, W. A. Banks, and A. V. Kabanov. Polypeptide point modifications with fatty acid and

amphiphilic block copolymers for enhanced brain delivery. *Bioconjugate Chem.* **16**: 793-802 (2005).

174. E. M. Kemper, A. E. van Zandbergen, C. Cleypool, H. A. Mos, W. Boogerd, J. H. Beijnen, and O. van Tellingen. Increased penetration of paclitaxel into the brain by inhibition of P-glycoprotein. *Clin. Cancer Res.* **9**: 2849-2855 (2003).
175. I. Ojima, O. Duclos, G. Dorman, B. Simonot, G. D. Prestwich, S. Rao, K. A. Lerro, and S. B. Horwitz. A New paclitaxel photoaffinity analog with a 3-(4-benzoylphenyl)propanoyl probe for characterization of drug-binding sites on tubulin and P-glycoprotein. *J. Med. Chem.* **38**: 3891-3894 (1995).
176. A. Rice, Y. Liu, M. L. Michaelis, R. H. Himes, G. I. Georg, and K. L. Audus. Chemical modification of paclitaxel (Taxol) reduces P-glycoprotein interactions and increases permeation across the blood-brain barrier *in vitro* and *in situ*. *J. Med. Chem.* **48**: 832-838 (2005).
177. C. Ballatore, B. Zhang, J. Q. Trojanowski, V. M. Y. Lee, and A. B. Smith Iii. In situ blood-brain barrier permeability of a C-10 paclitaxel carbamate. *Bioorg. Med. Chem. Lett.* **18**: 6119-6121 (2008).
178. B. J. Turunen, H. Ge, J. Oyetunji, K. E. Desino, V. Vasandani, S. Güthe, R. H. Himes, K. L. Audus, A. Seelig, and G. I. Georg. Paclitaxel succinate analogs: Anionic and amide introduction as a strategy to impart blood-brain barrier permeability. *Bioorg. Med. Chem. Lett.* **18**: 5971-5974 (2008).